Papers presented to the

EIGHTEENTH SYMPOSIUM

ON ANTARCTIC METEORITES

May 31- June 2, 1993

NATIONAL INSTITUTE OF POLAR RESEARCH, 国立極地研究所

TOKYO

Papers presented to the

EIGHTEENTH SYMPOSIUM

ON ANTARCTIC METEORITES

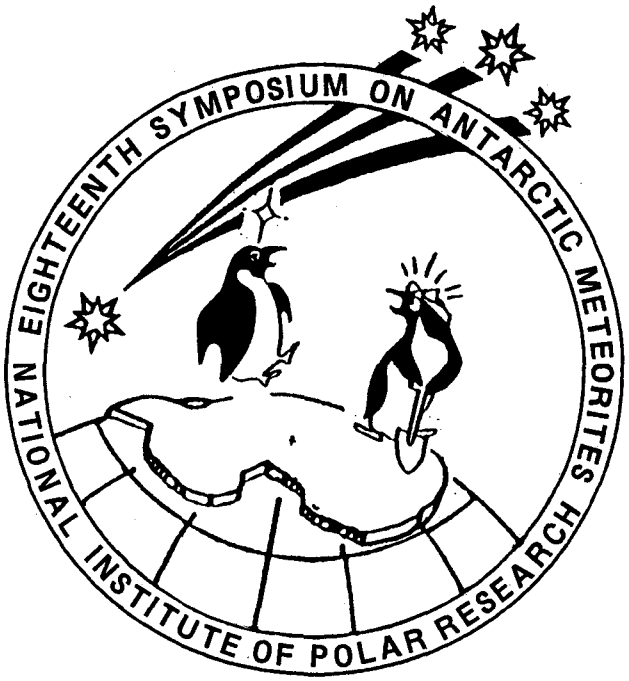

May 31- June 2, 1993

NATIONAL INSTITUTE OF POLAR RESEARCH, 国立極地研究所
TOKYO

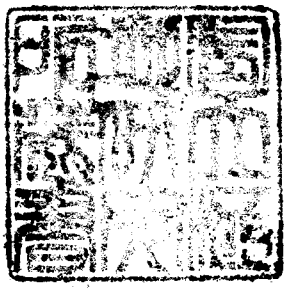

Monday, May 31, 1993

08:30 - 12:00 Registration Auditorium (6th Floor)

09:25 - 09:30 Opening Address **Takao Hoshiai**
Director-General
National Institute of Polar Research

* Designates Speaker

Chairmen: Takeda H. and Tomeoka K.

1 09:30 - 09:45 **Yanai K.*, Shiraishi K. and Kojima H.**
Asuka-90 meteorites collection: Preliminary report of discovery, initial processing and identification

2 09:45 - 10:00 **Takeda H.*, Yamaguchi A., Bogard D.D. and Nyquist L.E.**
Mineralogical records of Ar-Ar age resetting of eucrites Y-792769 and Y-793164 by cratering events

3 10:00 - 10:15 **Yanai K.* and Haramura H.**
Achondrite Binda: Re-examination as a common type eucrite

4 10:15 - 10:30 **Miyamoto M.* and Takeda H.**
Cooling history of cumulate eucrites as inferred from exsolution lamellae of pyroxene

5 10:30 - 10:45 **Kojima T.* and Tomeoka K.**
An unusual dark clast in Allende: Product of parent body process

6 10:45 - 11:00 **Fujita T.* and Kitamura M.**
Origin of a lithic fragment in the Moorabie (L3) chondrite

7 11:00 - 11:15 **Tomeoka K.***
Plagioclase-rich chondrules in the Yamato-791717 CO carbonaceous chondrite

8 11:15 - 11:30 **Nakamura T.*, Tomeoka K., Sekine T. and Takeda H.**
High-temperature, multiple shock experiments on the Allende CV3 chondrite: An attempt to reproduce the Leoville CV3 chondrite

9 11:30 - 11:45 **Takeda H., Arai T.* and Mori H.**
Mineralogy of Asuka-881757 lunar meteorite, a new type of mare rock

10 11:45 - 12:00 **Taylor S.R.***
The origin of the Mg-suite in the lunar highland crust

12:00 - 13:00 Lunch Time

Chairmen: Takaoka N. and Nakamura N.

11 13:00 - 13:15 **Wang D.* and Lin Y.-T.**
Petrographic and compositional features of the intermediate group chondrites

12	13:15 - 13:30	**Yugami K.*, Miyamoto M., Takeda H. and Hiroi T.** Mineralogy of ALH81187: A partly reduced acapulcoite
13	13:30 - 13:45	**Morikawa N.* and Nakamura N.** Trace element abundances in five primitive achondrites
14	13:45 - 14:00	**Takaoka N.*, Motomura Y. and Ozaki K.** Where are noble gases trapped in Y-74063 (unique) ?
15	14:00 - 14:15	**Ikeda Y.* and Prinz M.** Origin of ureilites based on Allende dark inclusions
16	14:15 - 14:30	**Shimaoka T.* and Ebihara M.** Chemical composition of six aubrites
17	14:30 - 14:45	**Miura Yasunori, Noma Y., Okamoto M.* and Iancu O.G.** Two major dynamic formation processes of shocked graphite and quarts
18	14:45 - 15:00	**Murae T.*** Shock formation of kerogen-like organic matter in carbonaceous chondrites from graphite
	15:00 - 15:15	Tea Time

Special Session: Unique Inclusions in Ordinary Chondrites (19 - 24)

19	15:15 - 15:30	**Yanai K.* and Kojima H.** General features of unique inclusions in Yamato ordinary chondrites
20	15:30 - 15:45	**Nakamura N.*, Hutchison R., Yanai K., Morikawa N. and Okano O.** Consortium study of three inclusions in Yamato ordinary chondrites: A progress report
21	15:45 - 16:00	**Sack R.O. and Lipschutz M.E.*** Mineral chemistry and formation of igneous inclusions from consortium samples Y-75097, Y-793241, and Y-794046
22	16:00 - 16:15	**Wang M-S, Michlovich E., Vogt S., Lindstrom M.M., Mittlefehldt D.W. and Lipschutz M.E.*** Contents of trace elements and cosmogenic radionuclides in consortium samples Y-75097, Y-793241 and Y-794046
23	16:15 - 16:30	**Fukuoka T.*** Chemistry of the lithic inclusions in Yamato-793241 and -794046 meteorites
24	16:30 - 16:45	**Fujimaki H.*, Ishikawa K. and Aoki K.** Rb-Sr isotopic study of Yamato-794046 and its inclusion
25	16:45 - 17:00	**Miura Yasunori*, Haramura H., Yanai K., Okamoto M. and Iancu O.G.** Bulk composition and classification of the Tahara chondrite
26	17:00 - 17:15	**Nakai I.* and Tsuchiyama A.** Existence of divalent chromium in Yamato-691 determined by micro X-ray absorption near edge structure analysis

27	17:15 - 17:30	**Lin Y.-T.*, El Goresy A., Wang D. and Ouyan Z.** Preliminary comparison between Qingzhen (EH3) and MAC88136(EL3)	
	17:45 - 20:00	Reception	Lecture Room (2F)

Tuesday, June 1, 1993

Chairmen: Ikeda Y. and Kimura M.

28	09:00 - 09:15	**Kimura M.*, Noguchi T. and Wang D.** Petrology and mineralogy of an anomalous Ningqiang carbonaceous chondrite (CV3)
29	09:15 - 09:30	**Noguchi T.*** Petrology and mineralogy of the Coolidge meteorite (C4) and its comparison to the CV and CK chondrites
30	09:30 - 09:45	**Kallemeyn G.W.*** A carbonaceous chondrite grouplet from MacAlpine Hills, Antarctica
31	09:45 - 10:00	**Hiroi T., Pieters C.M., Zolensky M.E. and Lipschutz M.E.*** Similarity of reflectance spectra between C, G, B, F asteroids and thermally metamorphosed carbonaceous chondrites
32	10:00 - 10:15	**Shibata Y.* and Matsueda H.** Primitive Fe-Ni metal and phosphate minerals in Yamato-82094 carbonaceous chondrite
33	10:15 - 10:30	**Noguchi T.*, Fujino K. and Momoi H.** Phyllosilicates in chondrules and matrix in the Murchison CM2 chondrite
34	10:30 - 10:45	**Kojima H.* and Yanai K.** Where has the CM Chondrite altered ?
35	10:45 - 11:00	**Krot A.N.* and Wasson J.T.** Silica-fayalite-bearing chondrules in ordinary chondrites: Evidence of oxidation in the solar nebula
36	11:00 - 11:15	**Krot A.N.*, Rubin A.E. and Wasson J.T.** Glassy chondrules in ordinary chondrites: Evidence of fine-grained precursor materials rich in refractory (Ca, Al, Ti) and moderately volatile (Na, K) elements
37	11:15 - 11:30	**Maruyama S.*, Yurimoto H., Sueno S. and Kurita K.** Fe-Mg zoning in olivines of Allende chondrules
38	11:30 - 11:45	**Misawa K.*, Fujita T., Kitamura M., Nakamura N. and Yurimoto H.** A relict spinel grain in an Allende ferromagnesian chondrule
39	11:45 - 12:00	**El Goresy A., Matsunami S.*, Zinner E., Palme H., Lin Y.-T. and Nazarov M.** A CAI from Efremovka with superrefractory REE patterns and enormous enrichments in Sc, Zr, and Y in fassaite and perovskite
	12:00 - 13:00	Lunch Time

Chairmen: Matsuda J. and Fukuoka T.

40	13:00 - 13:15	**Yurimoto H.*, Nagasawa H. and Mori Y.** *In-situ* oxygen isotope analysis in Allende CAI
41	13:15 - 13:30	**Nagahara H.*, Young E.D. and Hoering T.C.** Evaporation rate and oxygen-isotopic fractionation of SiO_2 in equilibrium, in vacuum, and in hydrogen gas
42	13:30 - 13:45	**Tsuchiyama A.*, Uyeda C. and Makoshi Y.** An experimental study of evaporation kinetics of FeS, and its cosmochemical significance
43	13:45 - 14:00	**Uyeda C.* and Tsuchiyama A.** Isotope line analysis on primitive meteorites using ion microprobe II: Measurement of sulfur
44	14:00 - 14:15	**Imae N.* and Kitamura M.** FeS formation reaction between metallic iron and H_2S gas in the primordial solar nebula
45	14:15 - 14:30	**Kagi H.*, Tsuchida I., Wakatsuki M., Takahashi K., Kamimura N. and Wada H.** Down-shifted Raman spectra observed in interstellar graphite grains
46	14:30 - 14:45	**Amari S.*, Zinner E. and Lewis R.S.** Interstellar graphite from the Murchison meteorite: Morphologies correlate with carbon isotopic ratios
47	14:45 - 15:00	**Kiyota K.*, Sugiura N. and Hashizume K.** Isotopically light nitrogen in UOCs which is not due to presolar diamonds nor SiC
48	15:00 - 15:15	**Ozima M.* and Mochizuki K.** Nano-diamonds in primitive chondrites: (1) Theory
49	15:15 - 15:30	**Mochizuki K.*, Ozima M., Tsuchiyama A., Kitamura M. and Shimobayashi N.** Nano-diamonds in primitive chondrites: Radiation-induced origin ? (2) Experiment
	15:30 - 15:45	Tea Time
50	15:45 - 16:00	**Nakamura A.*, Ebihara M., Kobayashi K., Ito Y., Yonezawa C. and Hoshi M.** Neutron induced prompt gamma-ray analysis of chondrites in conjunction with isotopic analysis of iron
51	16:00 - 16:15	**Tazaki H., Ejiri H. and Ohsumi H.*** The measurement of ^{26}Al in meteorites by using ultra-low background γ-ray detector
52	16:15 - 16:30	**Fukuoka T.*, Yamakoshi K. and Nishio F.** ^{26}Al in Yamato-86009 and -86770 and Asuka-8603 meteorites: Determination of ^{26}Al in small samples using extremely low background γ-ray counting system

—— Special Lecture (I) ——

Chairman: Matsuda J.

53 16:30 - 17:30 **Prof. Gero Kurat* (Naturhistoriches Museum, Vienna, Austria),** Koeberl C., Presper Y., Brandstätter, F. and Maurette M.

Micrometeorites from the Antarctic blue ice

Wednesday, June 2, 1993

Chairmen: Sugiura N. and Fujimaki H.

54	09:00 - 09:15	**Sugiura N.* and Kiyota K.** A search for solar nitrogen in gas-rich chondrites
55	09:15 - 09:30	**Hashizume K.* and Sugiura N.** A nitrogen concentrated phase in IA iron meteorite Canyon Diablo
56	09:30 - 09:45	**Matsuda J.*, Nagao K. and Kurat G.** Noble gases in Acuna iron meteorite
57	09:45 - 10:00	**Matsubara K.*, Matsuda J. and Koeberl C.** Noble gas compositions in Muong Nong-type tektites
58	10:00 - 10:15	**Wada N.* and Ozima M.** Noble gas elemental abundance systematics in terrestrial planets
59	10:15 - 10:30	**Kaneoka I.*, Nagao K. and Pellas P.** ^{40}Ar-^{39}Ar analyses of equilibrated LL chondrites from Antarctica
60	10:30 - 10:45	**Kano N.*, Yamakoshi K. and Matsuzaki H.** Isotopic, chemical and textural properties of acid residues from various meteorites
61	10:45 - 11:00	**Miono S.*** Comparison between carbonaceous chondrite and microspherule in Paleozoic-Mesozoic bedded chert – II
62	11:00 - 11:15	**Honda M.*, Nagai H., Nishiizumi K. and Ebihara M.** Weathering of a chondrite, Tsarev, L5
63	11:15 - 11:30	**Miono S. and Nakanishi A.*** Terrestrial ages of Antarctic meteorites measured by thermoluminescence of the fusion crust II
64	11:30 - 11:45	**Miura Yayoi*, Sugiura N. and Nagao K.** ^{81}Kr-Kr exposure ages and noble gas isotopic compositions of three non-Antarctic eucrites Millbillillie, Camel Donga and Juvinas
	11:45 - 13:00	Lunch Time

Chairman: Ebihara M.

65	13:00 - 13:15	**Scorzelli R.B.*, Souza Azevedo I., Pereira R.A., Perez C.A.C. and Fernandes A.A.R.** Mössbauer spectroscopy study of the metallic particles of the Antarctic L6 chondrite Allan Hills-769
66	13:15 - 13:30	**Scorzelli R.B.* and Fernandes A.A.R.** Fe-Ni alloys in a unique Antarctic meteorite Yamato-791694

67 13:30 - 13:45 **Ohsumi K.*, Miyamoto M. and Takase T.**
Diffraction study of olivines in thin sections by micro-region Laue method using synchrotron radiation

68 13:45 - 14:00 **Ninagawa K.*, Nakagawa M., Matoba A., Yamaguchi H., Yamamoto I., Wada T., Yamashita Y., Huang S., Sears D.W.G., Matsunami S. and Nishimura H.**
Red thermoluminescence from enstatite

69 14:00 - 14:15 **Akai J.* and Sekine T.**
Shock effects experiments of serpentine, and thermal metamorphic conditions in Antarctic carbonaceous chondrite

—— Special Lecture (II) ——

Chairman: Ebihara M.

70 14:30 - 15:30 **Prof. Stuart Ross Taylor* (ANU, Canberra, Australia)**

The planetesimal hypothesis and the Early Solar System

Abstract Only

Monday, May 31, 1993

08:30 - 12:00	*Registration, 6th Floor*
09:25 - 09:30	*Opening address, Auditorium*
09:30 - 17:30	*Symposium,Auditorium*
17:45 - 20:00	*Reception, Lecture Room, 2nd Floor*

ASUKA-90 METEORITES COLLECTION: PREMINARY REPORT OF DISCOVERY, INITIAL PROCESSING AND IDENTIFICATION; **Keizo Yanai, Kazuyuki Shiraishi** and **Hideyasu Kojima**, National Institute of Polar Research (NIPR), 9-10, Kaga 1-chome, Itabashi-ku, Tokyo 173 Japan

Over 2,500 specimens of the Asuka meteorites have been recovered from the bare icefield around the Sör Rondane Mountains, Queen Maud Land, East Antarctica by the Japanese Antarctic Research Expedition (JARE) since 1986. Almost 50 meteorites have newly been collected on the bare icefield around the mountains by the Asuka Wintering Party (led by Dr. K. Shiraishi, 1989-1991). The meteorites search was carried out on the bare ice areas at the eastern end of the Sör Rondane Mountains in November 1990 (Fig. 1).

The Asuka party carried out the search for meteorite as a part of geological survey on the main bare icefield, at the eastern part of Mt. Balchen. Searching was very difficult at more eastern bare icefield for numerous large crevasses and heavy moraine cover in places at the mountain side. The party collected 48 individual specimens consisting completely fusion-crusted and fragmented one. Most of the meteorites were distributed around the location RY175-KY182(Flag Number's) on the traverse route (Fig. 1), at elevations higher than 1,500 m, but some specimens were found on the ice below 1,500 m altitude. Most meteorites are highly weathered, covered by brown limonitic stains, and fragmented in to tiny pieces with sand-like grains. They might have been exposed on the bare ice surface for a long time, compared with the complete fusion-crusted meteorites.

The specimens were named officially as the **Asuka-90** meteorites, and named individually as **Asuka(A)-9001** to **A-9048**, in order of discovery. Table shows the preliminary data of meteorite specimens including total number, types and weight together with the previous collected Asuka meteorites (Table 1). According to the initial processing, the Asuka-90 meteorites comprise one achondrite (eucrite breccia) and ordinary chondrites, including no iron, no stony-iron and no carbonaceous chondrite.

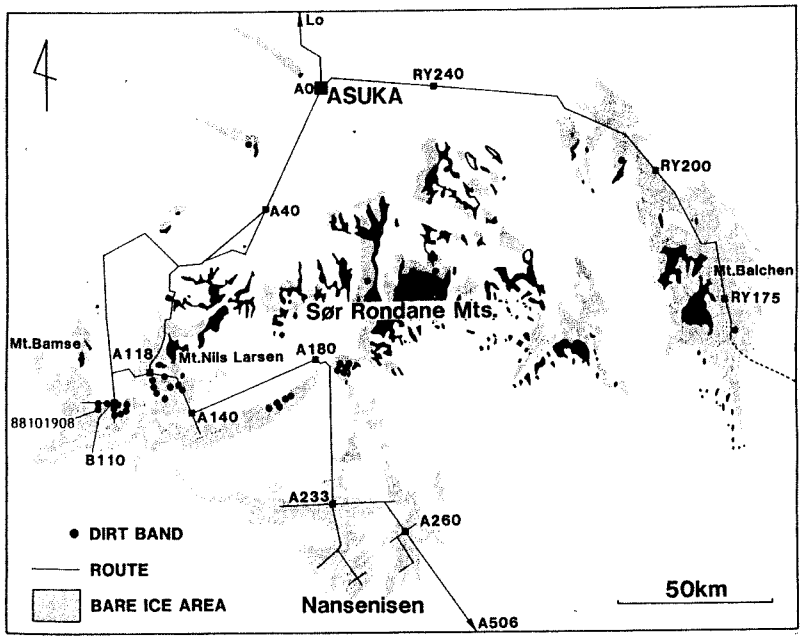

Fig. 1
Field locations of the bare ice and meteorite search area aroud the Sör Rondane Mountains, Queen Maud Land, East Antarctica.

Table 1 Asuka meteorites collections

Name (year)	Asuka-86 (1986/87)	Asuka-87 (1988)	Asuka-88 (1988/89)	Asuka-90 (1990/91)
Total	3	352	2,124	48
The largest(kg)	1.5(L)	46(LL)	43(H)	8.27(L)
Irons	-	1	7	-
Stony-Irons	-	1	5	-
Achondrites	-	9	53	1
C. chondrites	-	2	31	-
Chondrites	3	326	] 2,028	] 47
Doubtful	-	13		
Total weight	2.20kg	120.13g	394.08kg	11.48kg

MINERALOGICAL RECORDS OF Ar-Ar AGE RESETTING OF EUCRITES Y-792769 AND Y-793164 BY CRATERING EVENTS. Hiroshi Takeda[1], Akira Yamaguchi[1], D. D. Bogard[2] and L. E. Nyquist[2]. [1]Mineralogical Institute, Faculty of Science, University of Tokyo, Hongo, Tokyo 113, Japan; [2]Mail Code SN, NASA Johnson Space Center, Houston, Texas 77058, U.S.A.

Introduction Comparison of mineralogy of Yamato(Y-) 792769 and Y-793164 has been performed to confirm a proposed pairing for these two specimens [1] and to correlate their common shock compaction textures with the resetting of their ^{39}Ar-^{40}Ar ages. ^{39}Ar-^{40}Ar studies of Y-792769 have been complete [2] whereas those for Y-793164 are in progress. Y-792769 is a polymict breccia containing pyroxenes of a limited range in chemical compositions and is one of the largest eucrite in the Yamato collection. Compared to other Yamato polymict eucrites, Y-792769 includes fewer and smaller eucritic clasts having homogenized pyroxenes [2]. Its fine-grained matrix is shock-compacted and sintered. The terrestrial ages of Y-792769 and Y-793164 reported by Miura et al. [1] suggest their pairing, but a thin section photograph of Y-793164,65-1 (Photo 292) in the Photographic Catalog of Antarctic Meteorites [3] is quite different from that of Y-792769 [2]. We investigated both Y-793164,65-1 and a new polished thin section to search for common textural features.

The parent body of howardites, eucrites, and diogenites (HED achondrites) experienced large scale melting and differentiation in the earliest history of the solar system [4]. The isotopic investigations of the HED achondrites point to prolonged cratering records on the HED parent body and suggest that it survived the cataclysm affecting the Moon ~3.8-4.0 Ga ago [5, 2]. The youngest record of impact melting is 3.04 Ga [6]. Thermal histories of monomict eucrites have been discussed in the context of the geological setting on the HED parent body [7]. Because the pyroxenes in Y-792769 are individually homogenized, this breccia probably came from a cratered region with a limited range in cooling history. The event which formed Y-792769 and Y-793164 also may have been a secondary event which occurred after the pyroxenes in constituent fragments of monomict eucrites were homogenized in prior cratering events. To deduce the cratering history, it is important that chronological information be obtained from various isotopic systems; thus ^{39}Ar-^{40}Ar, Rb-Sr and Sm-Nd isotopic studies of Y-792769 were undertaken in collaboration with the mineralogical and petrographical investigations.

Samples and Methods Polished thin sections (PTS) Y-793164,65-1, 63-1 and Y-792769,62-2 [8] were supplied from NIPR. PTS ,65-1 was made from a clast and ,63-1 represents a matrix portion. Two samples, Y792769,68 and Y-792769,82 supplied from NIPR were taken from locations separated by about 10 cm and not far from the surface of the meteorite. PTSs were prepared from these samples and a part of lithic clast ,68 B1. Sub-samples for isotopic analysis were prepared from these parent samples. Preparation of a PTS and samples used for ^{39}Ar-^{40}Ar analyses and for Rb-Sr and Sm-Nd isotopic analyses and their analytical procedures are described in Bogard et al. [2].

Results The PTS Y-793164,65-1 shows that this is a part of a sub-ophitic clast with a few lath-shaped plagioclase crystals up to 1.1 X 0.34 mm in size. The most noteworthy textural feature is that large parts of

pyroxene are replaced by aggregate of fine acicular plagioclase. The sizes of the acicular crystals (up to 0.15 X 0.05 mm) are far less than the plagioclase in the original crystalline portion. This texture is similar to that observed in a recrystallized portion of Juvinas [9]. Irregular aggregates of ilmenite 0.1 mm in diameter are present at the recrystallized mesostases.

PTS Y-793164,63-1 is quite different from ,65-1 and represents a matrix portion of this meteorite. Subrounded fragments of lithic and mineral clasts are set in a compact, dark yellowish brown matrix of much comminuted materials. The sizes of the fragments are finer than those in common polymict eucrites and the finest grains look like sintered glassy materials. The clast types include fragments of a lithic clast represented by PTS ,65-1, a pyroxene fragment 0.72 X 0.42 mm in size with fine exsolution lamellae and quickly cooled dark matrix-rich clast with acicular plagioclase crystals, and dark devitrified impact melts. The matrix texture is similar to that of Y-792769 described below [2].

The pyroxene compositions of Y-793164 distribute on the more Fe-rich side of the pyroxene quadrilaterals, similar to ordinary eucrites of type 4 to 5 [7], but show spreading of mg numbers[=(MgX100)/(Mg+Fe)] (Fig. 1). The pyroxene compositions of the clasts (e.g. BS3) show a small range in mg numbers (Fig. 1). This is similar to a clast represented by PTS ,65-1, which shows a homogenized trend (Fig. 1). The recrystallized portions with acicular plagioclase show more a Ca-rich trend.

The plagioclase compositions of lath-shaped crystals in PTS Y-793164,65-1 range from An_{80} to An_{90} (Fig. 2), representing a crystallization trend from the original magma. The acicular crystals in PTS ,65-1 show a much wider range towards the Ca-rich direction. The plagioclase compositions in clast BS3 in PTS ,63-1 have the same trend as in the lath crystals in PTS ,65-1. However those of fragments in the matrix show a wider range towards the Na-rich side.

PTSs of Y-792769 consist mostly of fine-grained, compact matrix and a few lithic clasts. The largest basaltic clast shows a subophitic texture of pigeonite and plagioclase. The pyroxenes have one of the most Fe-rich trends found for eucrites, similar to the trend for the Lakangaon eucrite [10]. Other types of lithic clasts are present, but their abundances are lower than in common polymict eucrites. Their pyroxenes also show exsolution and the homogenized Mg/Fe distribution trends of ordinary eucrites, but the mg numbers often differ slightly from one clast to the other.

The matrix (e.g., PTS Y-792769,84) shows dark, yellowish fine-grained sintered textures lacking very fine fragments. Small, subrounded fragments of pyroxene and plagioclase are occasionally scattered in the matrix, but the size distribution is different from that of mineral fragments in normal polymict eucrites such as Y-75011. The fine-grained, sintered material gives the impression that the matrix has a continuous, glassy appearance. Compositions of pyroxene in the matrix distribute to the more Fe-rich side of the clast pyroxenes.

The argon data indicate that clast Y-792769,68 was almost completely degassed of its radiogenic ^{40}Ar 3.99 ± 0.04 Ga ago and has not been substantially heated since that time. This dated event is probably also the cause of the sintered texture observed in the matrix and inferred to be the result of shock compaction during formation of the breccia. The detailed results on the isotopic age determination is given by Bogard et al. [2]. Isotopic studies for samples of Y-793164 are in progress at the NASA/JSC.

Discussion Comparisons of mineralogical data obtained for both Y-792769 [2] and Y-793164 indicate that both eucrites are distinct from other groups recovered from Antarctica [8] and support the proposal of their pairing by Miura et al. [1]. The shock sintered texture of these two meteorites is a very characteristic feature not known previously in polymict eucrites. Textural variations of the clasts suggest the polymict nature of the breccia, but their compositional variations of pyroxenes are smaller than for other polymict eucrites [8]. The compositional ranges are smaller for Y-793164 than for Y-792769, but the difference may be due to local heterogeneity. It appears that these breccias contain originally homogenized monomict eucrites with small compositional ranges in pyroxenes.

The last thermal event, which produced this texture and formed the Y-792769 breccia, is determined by the well-defined ^{39}Ar-^{40}Ar age of 3.99±0.04 Ga. The complete resetting of the ^{39}Ar-^{40}Ar age is consistent with textures viewed in the transmission electron microscope (TEM) which suggest shock compaction converted part of the matrix to maskelynite [2]. Sm-Nd data define an apparent isochron corresponding to an age of 4.23±0.12 Ga. This apparent age probably reflects partial resetting of the Sm-Nd system during breccia formation. The ~3.99 Ga ^{39}Ar-^{40}Ar age predates the accepted age of formation of the lunar Imbrium and Serenitatis basins, but probably stems from the same period of intense meteoroid bombardment in which the entire inner solar system was affected.

Shock-induced breciation and sintering of Y-792769 and Y-793164 presumably resulted from impact of a large meteoroid on the HED parent body. The nearly homogeneous distribution of the matrix within the entire meteorite and the presence of the TEM-scale exsolution in the matrix pyroxenes and of maskelynitized plagioclases in the matrix suggest that the breccia was produced in a single cratering event. The nearly uniform compositions of the matrix pyroxene also indicate some degree of subsolidus annealing, but this annealing would not have reset the age. Alternatively, the pyroxene in the original lithologies had limited composition ranges.

According to the geological setting suggested for the HED parent body [4, 7], the original components of Y-792769 may have been derived from the floor or wall of a crater, where the original monomict eucrites of some clasts were thermally metamorphosed. Then, components with different pyroxene chemistries were mixed by the last major impact event, which reset the ^{39}Ar-^{40}Ar age. The ^{39}Ar-^{40}Ar age of the impact event in which Y-792769 was formed is similar to the ^{39}Ar-^{40}Ar ages of many lunar highland rocks which had their isotopic systematics reset by large cratering events in early lunar history. The ^{39}Ar-^{40}Ar age determined for Y-792769, however, is slightly older than the usually accepted times of formation of the large Imbrium and Serenitatis basins on the moon.

We thank NIPR for the consortium samples, and Mr. K. Saiki, O. Tachikawa, H. Mori and K. Hashimoto for technical assistance.

References [1] Miura Y. et al. (1993) Geochim. Cosmochim. Acta (in press). [2] Bogard D. D., Takeda H., Nyquist L. E., Mori H., Aoyama T., Bansal B. and Wiesmann H. (1993) Geochim. Cosmochim. Acta (in press). [3] Yanai K. and Kojima H. (1987) Photographic Catalog of Antarctic Meteorites, 216p. [4] Nyquist L. E., Takeda H., Bansal B. M., Shih C. -Y, Wiesmann H. and Wooden J. L. (1986) J. Geophys. Res. 91, B8,8137-8150. [5] Nyquist L. E., Bogard D. D., Wiesmann H., Bansal B. M., Shih C-Y. and Morris R. M. (1990) Geochim. Cosmochim. Acta 54, 2195-2206. [6] Bogard D. D., Taylor G. J., Keil K., Smith M. R. and Schmitt R. A. (1985) Geochim.

Cosmochim. Acta 49, 941-946. [7] Takeda H. and Graham A. L. (1991) Meteoritics 26, 129-134. [8] Takeda H. (1991) Geochim. Cosmochim. Acta 55, 35-47. [9] Takeda H. and Yamaguchi A. (1991) Meteoritics 26, 400-401. [10] Mason B., Jarosewich E. and Nelen J. A. (1979) Smithsonian Contrib. Earth Sci. 22, 27-45..

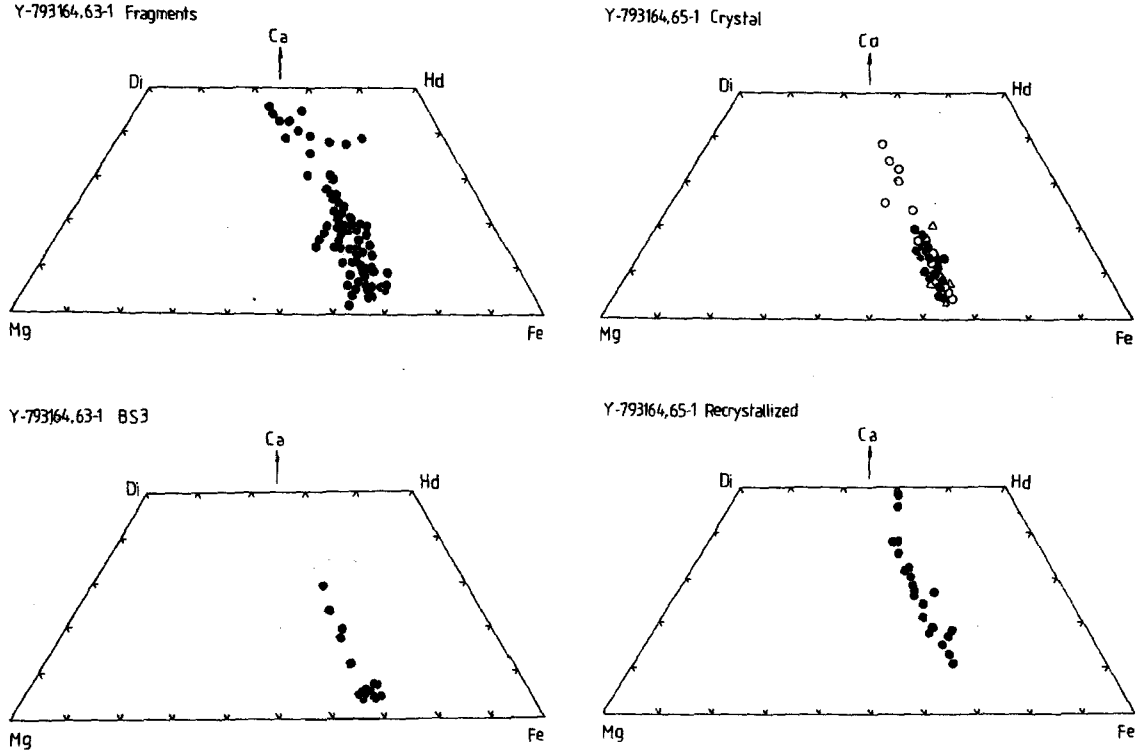

Fig. 1. Pyroxene compositions of Y-793164. (a) Closed circles in Y-793164,63-1 Fragments: pyroxene fragments in matrix. (b) Closed circles in BS3: exsolution trends of basalt BS3. (c) Open triangles, open and closed circles in ,65-1 crystal: pyroxenes in different crystals of a clast ,65-1. (d) Closed circles in ,65-1 Recrystallized: pyroxenes in matrix with acicular plagioclases.

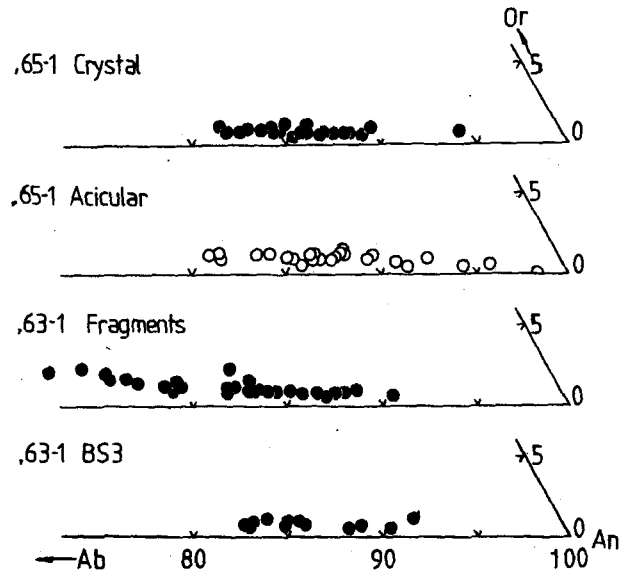

Fig. 2. A part of Or-Ab-An diagrams of plagioclases in fragments and clasts of Y-793164. Numbers are An values.

ACHONDRITE BINDA; RE-EXAMINATION AS A COMMON TYPE OF EUCRITE.

Keizo Yanai and **Hiroshi Haramura**, National Institute of Polar Research, 9-10, Kaga 1-chome, Itabashi-ku, Tokyo 173 Japan

The Binda meteorite have been originally identified as an unique achondrite with an almost crystalline texture and classified as only one unbrecciated and most Mg-rich eucrite. Previously, the Binda meteorite is designated one of howardites (Graham et al., 1985), or Ca-rich(Mg-poor) diogenites or Mg-rich(Ca-poor) eucrites. The specimen has also been recognizing an intermediate type of diogenites-eucrites for a long time. Excepting the Binda meteorite there were not an unbrecciated achondrites belong to the intermediate type between diogenites and eucrites.

We carried out re-examination based on the results of electron microprobe analysis, polarization-microscope studies and wet chemical analyses for this unique achondrite. The Binda meteorite should be classified as one of an unbrecciated and common type of eucrite by the re-examination.

Megascopically, the Binda meteorites provided to us from the Australian Museum, has a lot of thin black veinlets probably produced by shock, in relatively coarse-grained and light grey-fresh interior. The thin section shows a crystalline texture of slightly brecciated with shocked veins and consists mostly of pyroxene and plagioclase with traced opaques(Fig. 1). The compositional ranges of pyroxene are limited on the line of orthpyroxene (ca, $Fn_{37}Fs_{60}Wo_3$) and clinopyroxene (ca, $En_{30}Fs_{26}Wo_{44}$)(Fig. 2). This texture and mineral compositions indicate that the Binda meteorite is a common(usual) type of eucrite. It belongs neither intermediate type of diogenites-eucrites, nor howardites.

Previous analytical chemical data was given by Anderson and Mingaye (1913) as following: 8.8% Al_2O_3 and 6.2% CaO. The new chemical data for balk sample of the Binda containing 14.02% Al_2O_3 and 11.90% CaO, are given by our recent analytical work by wet method (Table). The results of the new wet chemical analysis also strongly indicated that the Binda meteorite is into the one of common type of eucrite.

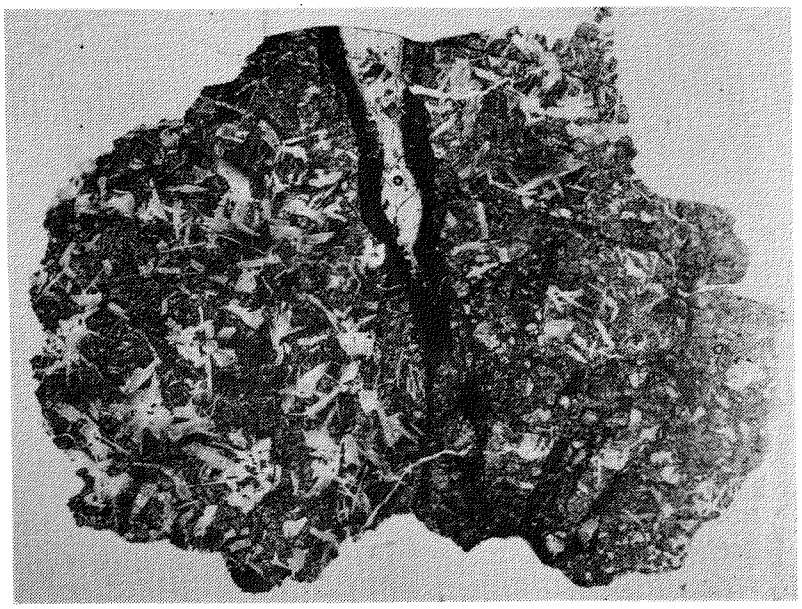

Fig. 1
Photomicrograph of the Binda meteorite showing almost crystalline texture with brecciated parts and black veins. Width 15mm

References:
Anderson C. A. and Mingaye J. C. H.(1913) Description and analysis of the Binda meteorite. Rec. Aust. Mus. **10**, 49-52.
Graham A. L., Bevan A. W. R. and Hutchison R. (1985) Catalog of Meteorites. British Museum (Natural History), p460.

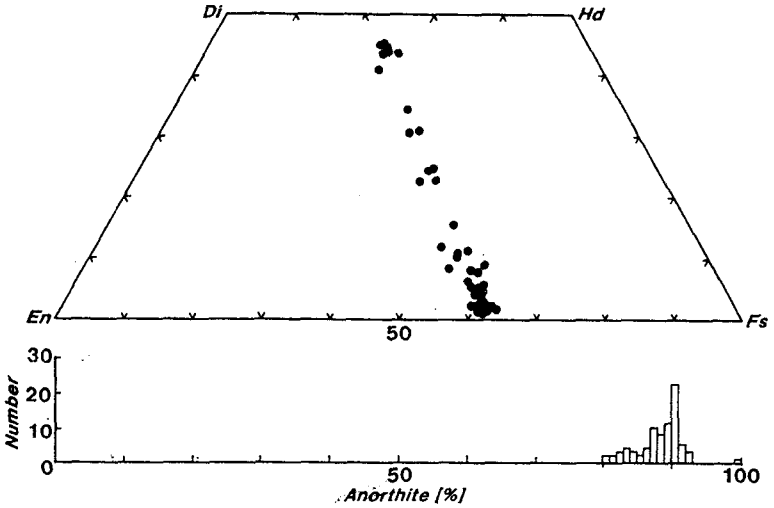

Fig. 2
Pyroxene compositions on the pyroxene quadrilateral and distribution of plagioclase feldspar compositions.

Table 1 Major-element chemical analyses of the Binda meteorite in weight percent.

	1	2
SiO_2	50.41	47.28
TiO_2	0.23	0.75
Al_2O_3	6.95	14.02
Fe_2O_3	—	0
FeO	16.83	17.50
MnO	0.54	0.48
MgO	17.75	7.31
CaO	5.82	11.90
Na_2O	0.20	0.06
K_2O	—	0.04
$H_2O(-)$	—	0.00
$H_2O(+)$	—	0.0
P_2O_5	0.04	0.15
Cr_2O_3	0.75	0.18
FeS	—	0.95
Ni (ppm)	—	22
Co (ppm)	—	<30
Total	99.52	100.62

1: Anderson and Mingaye(1913)
2: Analyst: H. Haramura

COOLING HISTORY OF CUMULATE EUCRITES AS INFERRED FROM EXSOLUTION LAMELLAE OF PYROXENE

Miyamoto, M. and Takeda, H.
Mineralogical Institute, Graduate School of Science, University of Tokyo, Hongo, Tokyo 113

Introduction We estimated the burial depth and cooling rate of cumulate eucrite Serra de Magé on the basis of the width of augite lamellae and compositional gradients of Ca in pyroxenes by numerically solving the diffusion equation [1]. According to the layered clast model of the HED parent body [2], cumulate eucrites are located at the lower part in a eucritic crust on a diogenitic mantle. Therefore, the burial depths of cumulate eucrites give the minimum thickness of the eucritic crust of the HED parent body.

Method and Samples Pyroxene in Serra de Magé contains coarse (001) augite lamellae up to about 35 μm in width in the host orthopyroxene. The host phase of the Serra de Magé pyroxene is inverted to orthopyroxene from initially crystallized pigeonite during slow subsolidus cooling history [3] and includes augite blebs produced by decomposition at the pigeonite eutectoid reaction line. The chemical composition of the augite lamellae is $Ca_{45.1}Mg_{38.3}Fe_{16.6}$ and that of the host orthopyroxene is $Ca_{1.9}Mg_{54.6}Fe_{43.5}$. The bulk chemical composition of the Serra de Magé pyroxene is $Ca_8Mg_{52}Fe_{40}$. We determined the bulk chemical composition of pyroxene including exsolution lamellae by spot analyses with a few μm intervals along lines which traverse several augite lamellae with an electron microprobe.

For augite lamellae in orthopyroxene in the Serra de Magé eucrite, we computed both the width of the lamellae and compositional gradients between the augite and host orthopyroxene for various cooling conditions and compared them to profiles measured by electron microprobe. The method is similar to that in our previous studies [1,4]. As the temperature goes down, pyroxene begins to exsolve augite when the bulk pyroxene content meets the solvus function. Augite lamellae grow as time passes and temperature falls. We used the solvus function reported by Lindsley [5] to calculate the chemical compositions of augite and pigeonite at the interface between the lamella and host phase as a function of temperature during a cooling. We used the Ca diffusion coefficient in pyroxene parallel to the c direction which is experimentally determined by Fujino et al. [6], because Serra de Magé pyroxene contains (001) augite lamellae.

Results and Discussion For the Serra de Magé pyroxene, pyroxene having the bulk Ca content of 8 mol% begins to exsolve at 970 °C when the bulk Ca content meets the solvus, and cools down to 600 °C at a rate of 0.0002 °C /yr to form a coarse (001) augite lamella of 32 μm in width (Fig. 1). This cooling rate corresponds to a burial depth of about 7 km by assuming a rock-like thermal diffusivity (0.004 cm^2/s). The result of Serra de Magé gives a good

agreement of compositional gradients near the interface between the computed and observed profiles without the assumption of a reheating event, unlike pyroxene in the Moore County cumulate eucrite [1]. The slow cooling rate of Serra de Magé is in agreement with an earlier proposal by Harlow et al. [3].

Figure 2 compares the observed Ca profile with model profiles for two cooling rates above and below the best-fit cooling rate, and provides an indication of how well our fitting method constrains the cooling rate. The best-fit rate (0.0002 °C/yr; Fig. 1) gives an obviously better fit to the observed data than rates twice or half as fast (Fig. 2). The width of augite lamella computed for the 1/2x rate is not so different from that for the best-fit rate. This result is due to the 'exhaustion' of Ca atoms to grow augite lamellae because of low Ca content of Serra de Magé pyroxene. The observed compositional gradient in augite and orthopyroxene is clearly a better match to the model profile for the best-fit rate than to that for the 1/2x rate. The observed compositional gradient in orthopyroxene is clearly a better match to the model profile for the best-fit rate than to that for the 2x rate.

Roughly speaking, the width of lamella is inverse to the square root of a cooling rate on the assumption of diffusion-controlled lamella growth, that is, a slow cooling yields a wide lamella. Although the width of augite lamellae of the Serra de Magé pyroxene (about 32 μm) is much narrower than that of Moore County pyroxene (about 100 μm), the cooling rate obtained for the Serra de Magé pyroxene (0.0002 °C/yr) is a small value similar to that for the Moore County pyroxene (0.00016 °C/yr)[1]. This slow cooling of Serra de Magé despite thin augite lamella compared with Moore County is mainly due to the bulk Ca content of the Serra de Magé pyroxene (8 mol%) lower than that of the Moore County pyroxene (10 mol%)[7].

According to the results of our calculations of the Serra de Magé and Moore County cumulate eucrites which have relatively wide augite lamellae among eucrites [1], we estimated the thickness of a eucritic crust in the HED parent body to be thicker than 8 km.

We thank Drs. M. Prinz and G. E. Harlow for the meteorite samples.

References

[1] Miyamoto M. and Takeda H. (1992) *Lunar Planet. Sci.* XXIII, 921-922.

[2] Takeda H. (1979) *Icarus*, 40, 455-470.

[3] Harlow G. E., Nehru C. E., Prinz M., Taylor G. J. and Keil K. (1979) *Earth Planet. Sci. Lett.*, 43, 173-181.

[4] McKay G., Ogawa T., Miyamoto M., and Takeda H. (1993) *Lunar Planet. Sci.* XXIV, 967-968.

[5] Lindsley D. H. (1983) *Amer. Mineral.*, 68, 477-493.

[6] Fujino K., Naohara H., and Momoi H. (1990) *EOS*, 71, 943.

[7] Hess H. H. and Henderson E. P. (1949) *Amer. Mineral.*, 34, 494-507.

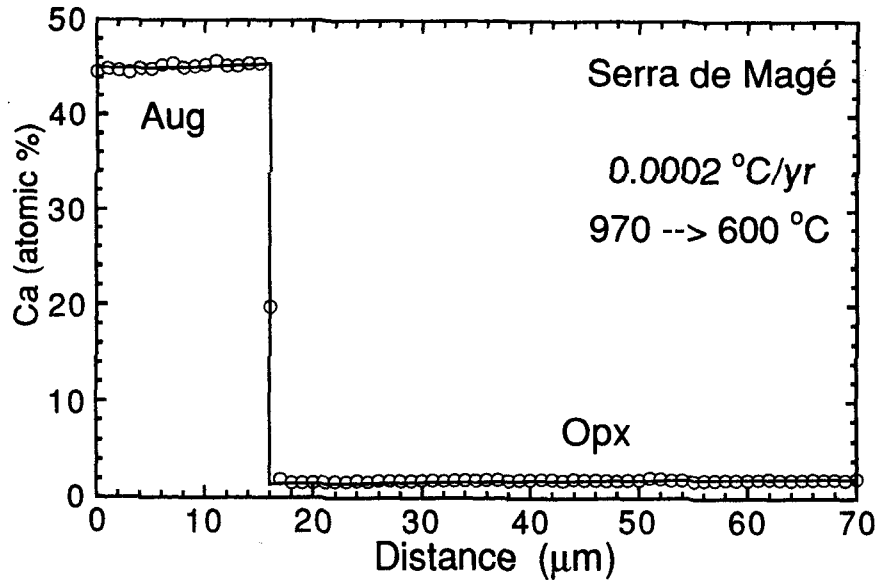

Fig. 1. Observed and computed Ca zoning profiles in orthopyroxene adjacent to augite lamella in the Serra de Magé eucrite. Open circles show an observed profile at the interval of 1 μm. The origin is the center of the augite lamella. Solid line shows the computed profile for the best-fit cooling (0.0002 oC/yr) from 970 °C to 600 °C

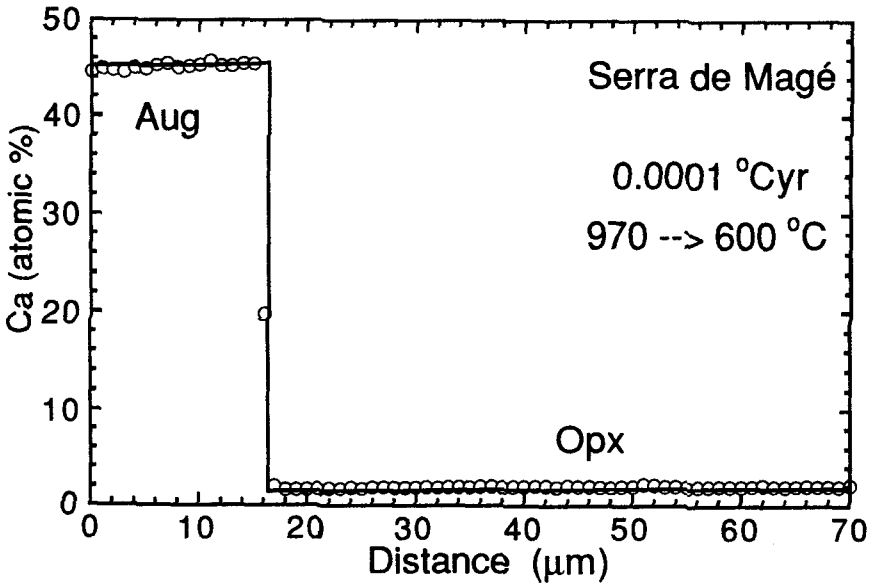

Fig. 2. Observed and computed Ca zoning profiles. Profiles are computed for cooling rates of 1/2x (0.0001 oC/yr) and 2x (0.0004 °C/yr) the bets-fit rate (0.0002 °C/yr).

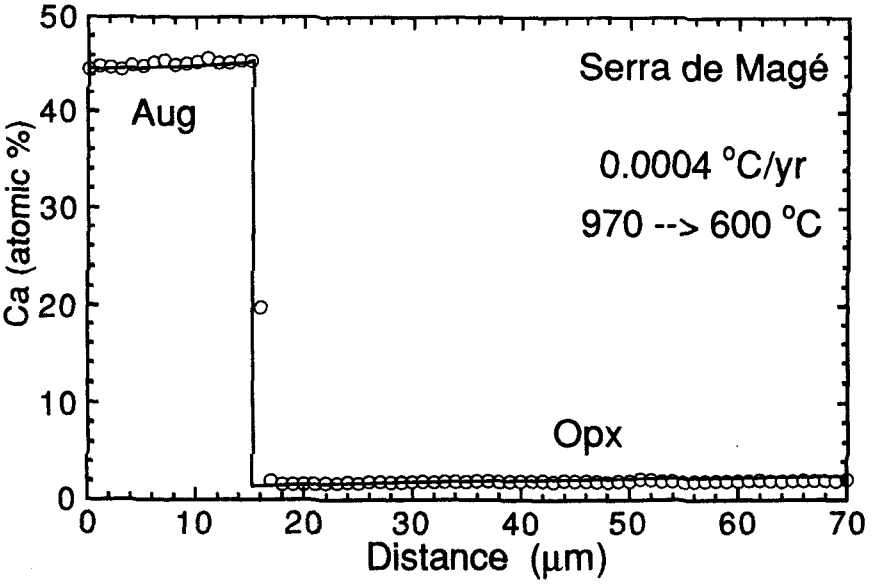

AN UNUSUAL DARK CLAST IN ALLENDE: POSSIBLE PRODUCT OF PARENT BODY PROCESS

Tomoko Kojima[1), 2)] and Kazushige Tomeoka[1)]

1) Department of Earth and Planetary Sciences, Faculty of Science, Kobe University, Nada, Kobe 657

2) Mineralogical Institute, Faculty of Science, University of Tokyo, Hongo, Tokyo 113

INTRODUCTION

Dark inclusions or clasts commonly occur in Allende and, less commonly, in some of other CV3 carbonaceous chondrites [e.g. 1-4]. They widely range in texture from chondritic one with chondrules and CAIs embedded in a fine-grained matrix, to the fine-grained aggregates of Fe-rich olivine free of coarse-grained components [1,4]. It has been controversial whether such dark inclusions or clasts are primary aggregates of materials formed in the solar nebula [3] or products of secondary process on the meteorite parent body [2]. Kojima et al. [5,6] recently studied two unusual clasts in the Vigarano CV3 chondrite that resemble the fine-grained variety of dark inclusions, and found evidence that they probably experienced thermal heating after intense aqueous alteration on the meteorite parent body.

Kurat et al. [7] and Palme et al. [8] have described an unusual dark clast in Allende (termed All-AF by them) composed mostly of fine-grained Fe-rich olivine, and interpreted it to be primary aggregates of condensates in the solar nebula. The texture and mineralogy of All-AF in their descriptions appear to have some similarities to the unusual clasts in Vigarano [5,6]. Dr. G. Kurat generously provided us with one of their thin sections of All-AF complying with our request. We here present the preliminary results of our petrographic and scanning electron microscope (SEM) study of All-AF. We found evidence supporting that All-AF has experienced aqueous alteration and thermal dehydration on the meteorite parent body.

TEXTURE AND MINERALOGY

The unusual clast in Allende, All-AF, has a rectangular shape of about 1x2 cm in size. Under an optical microscope, it appears to consist of densely packed round, oval to irregular shaped objects embedded in a dark matrix. Most of the objects are brownish translucent in transmitted light, and appear to be similar in size and shape to chondrules in the Allende host. Some also resemble CAIs. However, these objects consist mainly of fine-grains (<10 μm in diameter) of Fe-rich (24~30 FeO wt %) olivine, closely similar to "chondrule-like inclusions" in the Vigarano clasts [5,6]. Some objects are composed of assemblies of smaller sections, each consisting of fine-grained Fe-rich olivine. Some of them contain bars (<30 μm in thickness, <500 μm in length) of aggregates of Fe-rich olivine that are oriented parallel to each

other. Within each section, olivine grains and bars have basically a common crystal orientation i.e. extinct simultaneously in crossed polarized light. The textures and optical characteristics suggest that these objects may be pseudomorphs after porphyritic or barred olivine chondrules.

Another remarkable feature in All-AF is that veins of various thicknesses occur all over the clast. There are two kinds of veins in All-AF; type I veins widely range in width from several to 100 μm. They are densely filled with fine-grained fibrous olivine most of which occur nearly vertical to the walls of the veins. Type II veins, which are narrower (<30 μm in width) and more uniform in width than type I veins, differ from type I veins in that they have a distinct layered structure; the outer layers consist of nepheline grains (<5 μm in diameter), and inner layers consist of anhedral grains of Fe-rich olivine (<10 μm in diameter) which resemble those in the matrix of All-AF. The central portions of the type II veins are commonly pore space occasionally filled by salitic pyroxene, exhibiting a pipe-like appearance. In a portion particularly abundant in both types of veins, a vein of type I was found to crosscut a vein of type II suggesting that the type I veins were formed after the type II veins.

DISCUSSION

All-AF is composed mostly of fine-grains of homogeneous Fe-rich olivine and contains a number of objects that appear to be altered chondrules; thus it texturally and mineralogically resemble the unusual clasts in Vigarano [5,6]. Veins in All-AF are much larger and more widely distributed than those in the Vigarano clasts, suggesting that All-AF was once involved in extensive aqueous alteration. Some of the round or oval objects in All-AF well preserve the internal textures of precursor chondrules and are apparently not the random aggregates of fine grains of olivine.

Both All-AF and Vigarano clasts contain no hydrous phases such as phyllosilicate; they consist entirely of anhydrous minerals. In the case of Vigarano clasts, olivine grains show characteristic fibrous texture suggesting that they were produced by dehydration and transformation of phyllosilicate [6]. Serpentine is known to transform to olivine at >300°C [9]. Olivines in All-AF were presumably also formed through the heating process. Fibrous morphologies of olivine grains observed in many places in All-AF, particularly in type I veins, supports the interpretation. The presence of two different kinds of veins suggests that the aqueous alteration occurred in two stages.

Similarity in size between chondrule-like objects in All-AF and chondrules in the Allende host suggests that the precursor of All-AF may be a CV3 type chondrite, possibly Allende itself. Oxygen isotopic data support this view [8]. If that is the case, the existence of All-AF provides strong evidence that water once existed in the CV3 chondrite parent body and aqueous alteration took place on a large scale somewhere on the parent body. However, some problems

including high abundances of leachable elements (Na, K etc.) [7] and an anomalous REE pattern [8] of All-AF remain to be explained.

ACKNOWLEDGMENT

We thank Dr. G. Kurat , Naturhistorisches Museum, for providing a polished thin section of All-AF.

REFERENCES

[1] Fruland R.M., King E.A. and McKay D.S. (1978) Proc. Lunar Planet. Sci. Conf. 9th, 1305-1329.

[2] Bunch T.E. and Chang S. (1983) Lunar Planet. Sci. XIV (Abstr), 75-76.

[3] Bischoff A., Palme H., Spettel B., Clayton R.N. and Mayeda T.K. (1988) Lunar Planet. Sci. XIX (Abstr.), 88-89.

[4] Johnson C.A., Prinz M., Weisberg M.K., Clayton R.N. and Mayeda T.K. (1989) Geochim. Cosmochim. Acta 54, 819-830.

[5] Kojima T., Tomeoka K. and Takeda H. (1992) 17th Symp. Antarct. Meteorites (Abstr.), 24-26.

[6] Kojima T., Tomeoka K. and Takeda H. (1993) Submitted to Meteoritics.

[7] Kurat G., Palme H., Brandstätter F. and Huth J. (1989) Z. Naturforsch. 44a, 988-1004.

[8] Palme H., Kurat G., Spettel B. and Burghele A. (1989) Z. Naturforsch. 44a, 1005-1014.

[9] Akai J. (1992) Proc. NIPR Symp. Antarct. Meteorites 5, 120-135.

Origin of a lithic fragment in the Moorabie (L3) chondrite.

Takashi Fujita and Masao Kitamura

Department of Geology and Mineralogy, Faculty of Science, Kyoto University, Sakyo Kyoto 606.

A lithic fragment mainly consisting of olivines and pyroxenes was found in the Moorabie (L3) chondrite. The common origin of the fragment and the precursors of chondrules was suggested.

Moorabie (L3) chondrite shows the shock induced texture such as wavy extinction of olivine grains, preferred orientation of ellipsoidal chondrules, and melting texture of metal-sulfide grains. Based on the study of the sulfide-rich fragment in the Moorabie, Fujita and Kitamura (1992) reported that the chondrite experienced the shock reheating process after the accretion to the parent body. Although the metal sulfide textures are severely affected by the shock event, the compositions of the silicate components still remains the unequilibrated characteristics of the L3 chondrites.

<silicate rich lithic fragment> A silicate rich lithic fragment (1x3mm) in the Moorabie (Fig.1) is mainly composed of olivine and pyroxene. The fragment also includes a small amount of plagioclase, feldsparthic glass (or maskerynite) and two large chromite grains. Olivines are euhedral and show reverse zoning textures (Fo82-85). The pyroxenes have anhedral morphology and the chemical zoning from enstatite to augite. Large chromite grains (larger one: 100μm) are in euhedral shapes. The almost holocrystalline texture and the large sizes of Ca-rich pyroxene and euhedral chromite dislike the texture of the chondrules in the same chondrite.

<Olivines> The texture and compositions of olivine grains in various constituents of the Moorabie were compared with those of the olivines in the fragment. Occurrences of the large (>several tens μms) olivine grains in the Moorabie can be classified to the following five types;

A) isolated fragments of the large olivine grains (several 100μms),
B) large olivine grains included in chondrules,
C) olivines in normal chondrules (porphyritic olivines, barred olivines etc.),
D) relict olivine with dusty core and clear rim,
E) olivine grains in the lithic fragment.

Figures (2a-d) show the back-scattered electron micrographs of the olivine grains of each types. Compositions of the olivines are plotted in Figure 3. Isolated olivine grains (type A) have almost homogeneous compositions or reverse zoning, except for one grain which shows normal zoning. Some chondrules in the chondrite include large olivine grains (type B). The grains have the composition around Fo85 and anhedral morphology. On the other hand, the olivines in the porphyritic and barred olivine chondrules (type C) are in euhedral shapes

and have the larger variation of compositions. In the porphyritic chondrules, the olivine grains often show the normal zoning textures. An typical relict olivine grain (type D) with the dusty core and clear rim has the composition around (Fo85) in its core.

The compositions of olivines in the chondrite may have been affected by the accretion and shock reheating process. However, the type C olivines which have smaller sizes than types, A,B,D, and E show larger compositional variety than the latter four types. Thus, the compositional similarity in the four types (A,B,D,E) can not be explained only by the secondary equilibration process. The similarities of the composition, texture, and grain size among the types, A,B,D and E suggest that the four types of olivines are genetically related with each other. The dusty core in the type D olivine has been interpreted as the relict texture of the precursor material of the chondrules (e.g.,Nagahara,1981). The similarities between types B and D in shape, size and composition suggest that the type B olivines are also the relict of the precursor. The similarity between the three types, B, D, and E, then, suggests the possible precursor origin of the lithic fragment common to the precursor of the chondrules. Isolated olivine fragments (type A) may have been formed by the fragmentation of such lithic precursor.

<Pyroxene>

Pyroxenes in the lithic fragment also have the large grain size (several 100 μms) and are enriched in Ca. The crystallization trend of the grains show more ferrous content than the chondrule pyroxene in the same chondrites. These textures are consistent with the possible precursor material proposed by Fujita and Kitamura (1992) based on the study of the origin of fine pyroxene fragments in the UOC's. Therefore, the texture of the pyroxene also implies the precursor origin of the silicate rich fragment.

As a result, it can be suggested that the silicate rich fragment is a fragment of the precursor material of the chondrite. Then, the texture of the fragment implies that the precursor was formed from liquids in the grand-parent body.

References

Fujita,T. and Kitamura,M. (1992): Papers presented for the 17th symposium on Antarctic meteorites,34-35.
Fujita,T. and Kitamura,M. (1992): Proc. NIPR Symp. Antarct. Meteorites,5,258-269.
Nagahara,H. (1981): Nature,292,135-136.

Figure 1
Back-scattered electron image of the lithic fragment
ol:olivine,
px: enstatite-augite,
pl:plagioclase,
c:chromite.

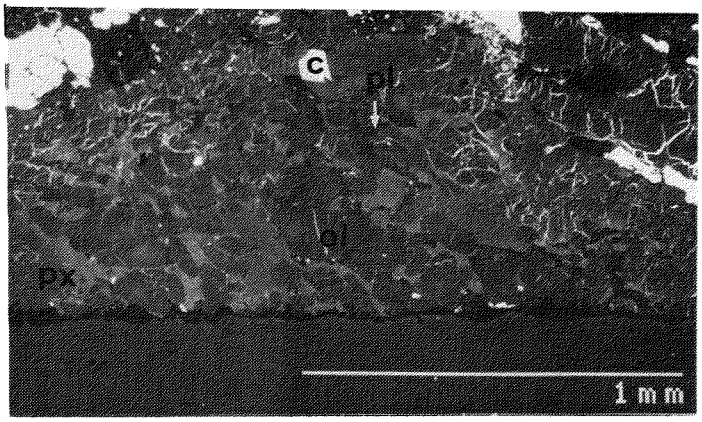

Figure 2
Back-scattered electron images of the olivine of a)isolated fragment, b) large grain in the chondrule, c) porphyritic chondrule, and d) dusty relict grain. ol: olivine. Length of the each scale bar is 100μm.

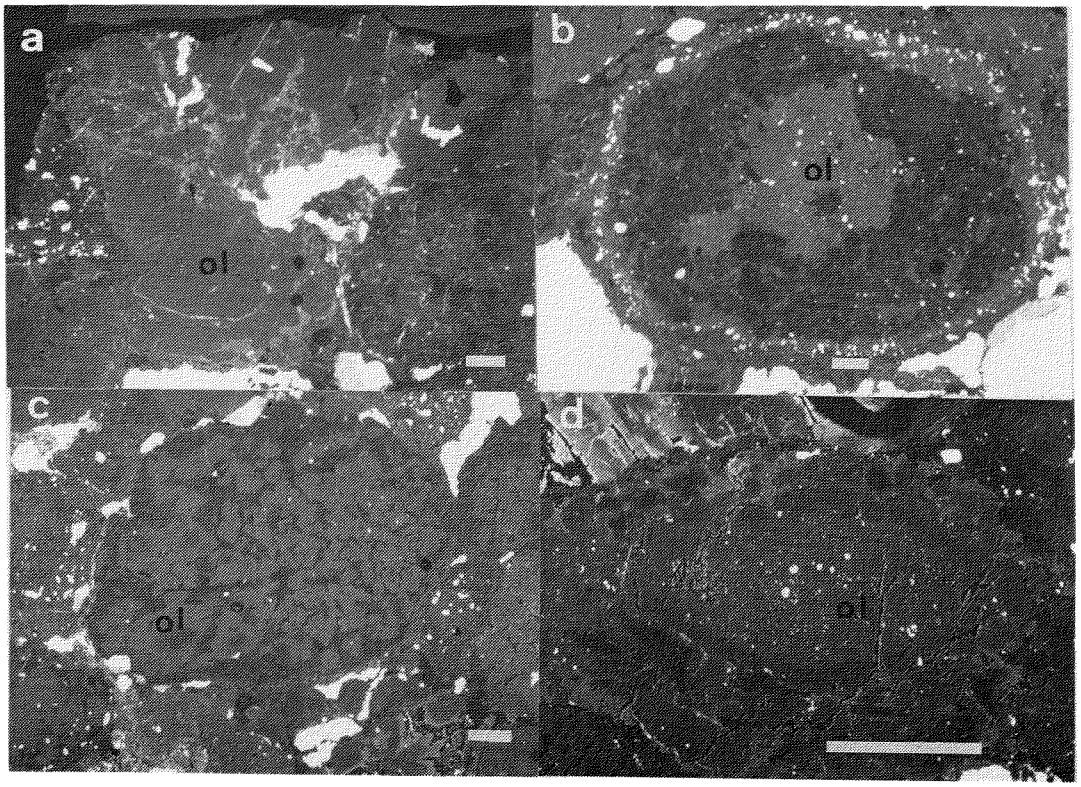

Figure 3
MgO/(MgO+FeO) content of olivines of the four types.
a) isolated fragment, b) large olivine in the chondrule, c) chondrule olivines, d) dusty core of the relict olivine, and e) olivines in the lithic fragment.

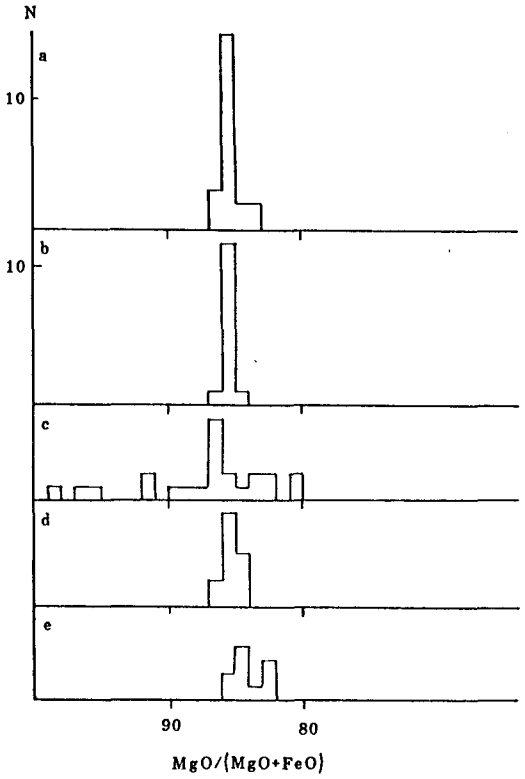

PLAGIOCLASE-RICH CHONDRULES IN THE YAMATO-791717 CO CARBONACEOUS CHONDRITE

Kazushige Tomeoka, Department of Earth and Planetary Sciences, Faculty of Science, Kobe University, Nada, Kobe 657

INTRODUCTION

Tomeoka et al. [1] have showed that Ca-Al-rich inclusions (CAIs) in the Yamato-791717 CO chondrite contain major amounts of nepheline and provided evidence that nepheline was formed by alteration of primary phases such as melilite, fassaite and spinel. I here present the results of detailed mineralogical and petrographic studies of chondrules in Y791717. It has been found that many chondrules in Y791717 contain major amounts of Na-rich plagioclase; nepheline occurs but is rare. Textures and mineralogy of chondrules suggest that the plagioclase was formed by alteration of mesostasis glass. The high abundances of nepheline in CAIs and Na-rich plagioclase in chondrules in this meteorite can not be just a coincidence. The nepheline and the plagioclase in Y791717 were probably formed by similar alteration porcesses in the similar Na-rich environments.

RESULTS

26 chondrules containing plagioclase have been selected and studied by an optical microscope and a scanning electron microscope (SEM) equipped with an energy dispersive X-ray spectrometer. They are mostly rounded, porphyritic olivine chondrules with few barred olivine chondrules and range in apparent diameter from 300 to 800μ m. They can be mainly divided into two types. The first, the high-FeO type, contains olivine with a large range in composition (Fa_{25}-Fa_{58}) and corresponds to type II chondrules defined by McSween [2]. The second, the low-FeO type, contains olivine with Fa_3-Fa_{25} and corresponds to type I chondrules.

The high-FeO chondrules contain euhedral olivines with a large range in diameter from 10 to 200 μ m. The olivine grains, particularly large ones (>100μ m), are commonly strongly zoned, with increasing Fe contents towards the edges of grains. Some chondrules contain minor amounts of Fe-rich Ca-pyroxene ($(Ca_{0.3}Mg_{0.3}Fe_{0.4})SiO_3$) and low-Ca pyroxene ($(Mg_{0.6}\ Fe_{0.4})SiO_3$) and Al-Ti-rich fassaitic pyroxene. Mesostases in the chondrules consist of plagioclase with abundant microcrystallites of Ca-pyroxene (mostly augite). Plagioclase occurs where glass is normally found in the mesostases. It has a large range of compositions (Ab_{53}-Ab_{92}) but is commonly very Na-rich (>Ab_{50}). The microcrystallites of Ca-pyroxene occurs as parallel-grown, fine needles with width of <1 to 10 μ m; their textures are closely similar to the "chain" or "lattice" textures, which are commonly seen in chondrules in unequilibrated ordinary chondrites [e.g., 3]. These textures are known to be indicative of rapid cooling [4]. In most places, plagioclase and Ca-pyroxene are intimately intergrown on a submicron scale. Many of the chondrules contain small, euhedral grains of chromite and Fe-Cr-Al spinel. Tiny grains of troilite and kamacite are present. No detectable amount of glass was present in the mesostases.

The low-FeO chondrules contain smaller (<50 μm) and more rounded olivines than those in the high-FeO chondrules. The olivines are also commonly zoned, but the zoning is not so pronounced as that in the high-FeO chondrules. The low-FeO chondrules contain low-Ca pyroxene which is commonly elongated and concentrated on the chondrule rims. Like in the high-FeO chondrules, plagioclase occurs in the mesostases where it coexists with microcrystallites of Ca-pyroxene. But, the plagioclase has much higher Ca-contents (Ab_{12}-Ab_{37}) than those in the high-FeO chondrules. Nepheline was found only in very minor amounts in the mesostases of some chondrules.

DISCUSSION AND CONCLUSIONS

The present study reveals that Na-rich plagioclase is abundant in the mesostases of many chondrules in the Y791717 CO chondrite. Chondrules containing such a high abundance of Na-rich plagioclase have not been known previously. I believe that this should be related to the high abundance of nepheline in the CAIs in this meteorite [1]. The textures suggest that the plagioclase in the chondrules was formed by alteration of mesostasis glass. Glass is known to be among the most reactive to alteration by the solar nebula and aqueous solutions [5,6].

Plagioclase in the high-FeO (type II) chondrules in Y791717 has high Na-contents close to albite, whereas plagioclase in the low-FeO (type I) chondrules consistently has much lower Na-contents. The compositional differences can be explained by the distinctions in composition of precursor glasses. It is known that the mesostasis glass in type II chondrules in unequilibrated ordinary chondrites are distinctly poorer in Ca and richer in Si and Al than those in type I chondrules [3].

Tomeoka et al. [1] suggested that the alteration in the Y791717 CAIs presumably occurred before accretion with reaction of primary phases with the low-temperature nebular gas rich in Na, Fe and Cl. I believe that plagioclase in the Y791717 chondrules was also formed secondarily by reaction with the solar nebular gas in the same environment as for the CAIs at relatively low temperatures (<1000 K). The silica-rich precursor glass in chondrules probably favored the formation of plagioclase, whereas the relatively silica-poor precursor minerals in CAIs such as melilite, fassaite and spinel favored the formation of nepheline. The degree of the alteration appears to be very high compared to CAIs and chondrules in other reported meteorites. Recently, Kimura and Ikeda [7] reported that some chondrules in Allende (CV) and ALH-77003 (CO) contain considerable amounts of nepheline, sodalite and plagioclase, and they interpreted that these minerals were produced by reaction with the solar nebula. Therefore, the low-temperature alteration reactions involving chondrules and CAIs may have been a more common process in the early solar nebula than previously thought.

References:

[1] Tomeoka, K., Nomura, K. and Takeda, H. (1992) Meteoritics 27, 136-143.
[2] McSween, H. Y. (1977) Geochim. Cosmochim. Acta 41, 1843-1860.

[3] Jones, R. H. (1990) Geochim. Cosmochim. Acta 54, 1785-1802.
[4] Donaldson, C. H. (1976) Contrib. Mineral. Petrol. 57, 187-213.
[5] Hashimoto, A. and Grossman, L. (1987) Geochim. Cosmochim. Acta 51, 1685-1704.
[6] Tomeoka, K. and Buseck, P. R. (1990) Geochim. Cosmochim. Acta 54, 1745-1754.
[7] Kimura, M and Ikeda, Y. (1992) Papers presented to the 17th Symposium on Antarctic Meteorites, 31-33.

HIGH-TEMPERATURE, MULTIPLE SHOCK EXPERIMENTS ON THE ALLENDE CV3 CHONDRITE: AN ATTEMPT TO REPRODUCE THE LEOVILLE CV3 CHONDRITE

Tomoki Nakamura[1], Kazushige Tomeoka[2], Toshimori Sekine[3] and Hiroshi Takeda[1].

1. Mineralogical Institute, Faculty of Science, University of Tokyo, Hongo, Tokyo 113
2. Department of Earth and Planetary Sciences, Faculty of Science, Kobe university, Nada, Kobe 657
3. National Institute for Research in Inorganic Materials, 1-1 Namiki, Tsukuba 305

INTRODUCTION

Carbonaceous chondrites are believed to have been part of early planetesimals. Recently, it comes to be known that shock effects are recorded in many carbonaceous chondrites (e. g. [1, 2]), suggesting that impact events are a common process in the early evolution of planetesimals. Therefore, it is expected that some effects of multiple impacts and impacts under high temperature would remain in the carbonaceous chondrites.

There are some previous studies on shock recovery experiments of chondritic materials (e. g. [3] ~ [5]). However, no attempt has been made to elucidate the effects of repeated impacts and pre-existing heat on the carbonaceous chondrites. In order to understand textural and mineralogical characteristics of carbonaceous chondrites affected by multiple impacts and also by impacts under high temperature, we carried out high-temperature, multiple shock experiments using the Allende CV3 chondrite.

One of our goals is to reproduce the texture of Leoville CV3 chondrite which shows a strong preferred orientation of the flattened chondrules with high aspect ratios (1.9 in average) [6]. Leoville shows much evidence of deformation by moderate shock pressures (~ 20 GPa) in both chondrules and matrix, indicating that it has experienced shock pressures after accretion [1]. However, it remains to be known whether such moderate shock pressures can flatten round chondrules to such high aspect ratios as observed in the chondrules in Leoville. There was an unsuccessful attempt to reproduce the texture of Leoville by a single shock pressure [7]. Our new results support the idea that multiple impacts by relatively mild shock pressures (~ 20 GPa) were mainly responsible to produce the texture of Leoville [1].

METHODS OF SHOCK EXPERIMENTS

Shock experiments were conducted by using a 30-mm bore propellant gun equipped with a system that can control temperature of the target assembly up to about 1000 °C [8]. The projectile is a 12-mm thick stainless steel plate bedded at the front of a high density polyethylene sabot. The target is a disk of Allende CV chondrite 12 mm in diameter and 3~4 mm in thickness. The peak pressure in the target was estimated as an equilibrated value with that of target container, because the Hugoniot for carbonaceous chondrites is unknown.

Shock experiments were carried out at pressures of about 21 GPa at the following three different conditions; (1) shocked once (singly shocked) initially at room temperature, (2) shocked twice (doubly shocked) initially at room temperature and (3) shocked once initially at 607 °C . The duration of a shock stress pulse is estimated to be approximately 4.5 μ sec. for each shock.

RESULTS

Shocked once at room temperature

All chondrules are flattened with an average axial ratio (long axis / short axis) 1.4 and show a moderate preferred orientation nearly perpendicular to the compacting axis. Almost all olivine and low-Ca pyroxene in chondrules exhibit high densities of fractures and show wavy extinction. Matrix is strongly compacted but each olivine grain can be distinguished in SEM images. Kamacite, troilite and pentlandite grains in the matrix show irregular shapes, but they do not appear to have melted. There are many open cracks going through matrix and chondrules.

Shocked twice at room temperature

Chondrules are clearly more flattened with an average axial ratio 1.9 and show a more pronounced preferred orientation. Olivine and low-Ca pyroxene in chondrules show extremely fine fractures and exhibit wavy extinction. Like singly shocked Allende, many open cracks are also produced.

Distinct differences from the singly shocked Allende are seen in the texture of matrix. The matrix is so strongly compacted that each olivine grain can hardly be distinguished in SEM images. Kamacite, troilite and pentlandite grains in the matrix are strongly elongated along surfaces of chondrules. All of these characteristics closely resemble those in the matrix of Leoville CV chondrite [1].

Shocked once at 607 °C

Chondrules are flattened with an average axial ratio 1.8 and show a strong preferred orientation. Olivine grains in the matrix appear to be compressed by shock and sintered by heat, so that they look very smooth in SEM images. Si- and Ca-rich glassy grains ranging 10 - 50 μm in diameter occur in many places in the matrix. Kamacite, troilite and pentlandite are apparently melted to form network-like veins in the matrix. In places, the Fe-Ni-S melt is segregated in areas ~ 400 μ m across. Olivine grains around the Fe-Ni-S melt show Fe - Mg zoning along their fractures.

DISCUSSION AND CONCLUSIONS

The doubly shocked Allende sample is most similar in texture of both chondrules and matrix to the Leoville CV3 chondrite. The singly shocked Allende samples at room temperature and 607 °C also show chondrule flattening and preferred orientation, but differ considerably in texture of matrix from Leoville. This appears to indicate that the deformation texture of Leoville resulted from repeated impacts under low temperature. Repeated impacts of relatively mild shock pressure apparently facilitate mechanical compaction of chondrite without intensive

heat generation. It is known that interior thermal energy due to shock increases in proportion to the square of shock pressures. Therefore, a single strong shock pressure might melt sulfide and metal in the matrix due to post shock heating such as those observed in the matrix of Allende shocked at 607 °C.

Based on the observations of the singly and doubly shocked Allende samples at room temperature, we can evaluate differences in effects between the first shock and the second shock. The first shock produced numerous fractures (thus finely divided domains) in olivine and pyroxene in chondrules and matrix. At the second shock, the olivine and pyroxene presumably behaved like a mosaic, rather than a single crystal. Therefore, we think that the deformation (flattening and elongation) of chondrules and matrix proceeded more efficiently at the second shock.

The present study also reveals that the effects of shock at high temperature (607 °C) are quite different from those at room temperature. The flattening of chondrules and the compaction of matrix are clearly more pronounced at 607 °C than at room temperature. This can be explained by an increase of plasticity of components constituting chondrules and matrix at 607 °C. Melting of metal, sulfides and silicates and cation diffusion in olivine are also significantly facilitated at the high temperature.

Our study reveals that three experimentally shocked materials, all of which have experienced the similar peak shock pressures (21GPa), exhibit considerably different textures due to differences of conditions, i. e., double impacts and / or heating. Therefore, we think that it is very difficult to estimate a peak pressure only from textures of shocked chondrites.

REFERENCES

[1] Nakamura, T., Tomeoka, K. and Takeda, H., *Earth Planet. Sci. Lett. 114,* 159-170, 1992. [2] Scott, E. R. D., Keil, K. and Stöffler, D., *Lunar and Planet. Sci. Lett. 22,* 1205-1206, 1991. [3] Sears, D. W., Ashworth, J. R. and Broadbent, C. P. and Bevan, A. W. R., *Geochim. Cosmochim. Acta 48,* 343-360, 1984. [4] Arakawa, M., Sawamoto, H., Urakawa, S., Kato, M., Mizutani, H. and Kumazawa, M., *Abstract in Koatu-toronkai,* 3C-13, 1987. [5] Kitamura, M., Tsuchiyama, A., Watanabe, S., Syono, Y. and Fukuoka, K., in *High-pressure Research: Applications to Earth and Planetary Sciences.* edited by Y. Syono and M. H. Manghnami, 333-340, 1992. [6] Cain, P. M., McSween, H. Y., Woodward, N. B., *Earth Planet. Sci. Lett. 77,* 165-175, 1986. [7] King, E. A., King, T. V. V., Arndt, J. and Hornemann, U., *Meteoritics 13,* 549, 1978. [8] Sekine, T., *J. of Matr. Sci. Lett. 8,* 872-874, 1989.

MINERALOGY OF ASUKA-881757 LUNAR METEORITE, A NEW TYPE OF MARE ROCK.
Hiroshi Takeda, Tomoko Arai and Hiroshi Mori. Mineralogical Institute, Faculty of Science, University of Tokyo, Hongo, Tokyo 113, Japan

Introduction. Consortium studies on lunar meteorites, Yamato(Y-) 793169 and Asuka(A-) 881757 (formerly Asuka-31) have been performed to characterize these new samples from unknown locations in the lunar mare. Consortium reports were presented both at 17th Symp. Antarctic Meteorites at NIPR in 1992 [1-6] and 24th Lunar and Planetary Science Conference in 1993 [7-10]. Their conclusions are summarized as follows. Both meteorites are coarse-grained mare rocks having low Mg/Fe ratios (bulk mg'=30-35) and low TiO_2 (1.5-2.5 % in homogenized bulk samples). They are intermediate between VLT and low-Ti mare basalts. Although these meteorites are not identical to each other, their mineral and bulk compositions, isotopic systematic and crystallization ages are remarkably similar and distinct from those of all other mare basalts [7]. They appear to represent a new type of low-Ti mare basalt that crystallized at about 3.9 Ga [9, 10]. These meteorites are inconsistent with the canonical correlation between the TiO_2 contents and ages of mare basalts and suggest that our knowledge of lunar volcanism is far from complete. This paper reports further mineralogical studies of A-881757, including its microtextures in comparison with Y-793169 observed by Transmission electron microscopy (TEM).

Samples and experimental techniques. We investigated polished thin sections (PTS) A-881757,51-4 supplied by NIPR for the consortium studies. Mineral chemistries and textures of the PTSs were examined by an electron probe microanalyzer (EPMA) and scanning electron microscope (SEM), JEOL 840A with X-ray chemical map analysis (CMA) utilities of Kevex Super 8000. Chemical analyses were made with JEOL EPMA (8600 Super Probe) at the Geological Inst., and with a JEOL EPMA (JCXA-733) at Ocean Res. Inst., Univ. of Tokyo. We measured pyroxene and spinel compositions selected by the CMA system [11].

We also investigated small fragments of pyroxene and plagioclase with JEOL 100CX and 2010 TEMs. The method is the same as that for ALHA81005 [12]. Because of their small grain sizes, powdered specimens were used for the TEM. Examination of microtextures of the samples was carried out by the above TEMs.

Results. Mineralogy of A-881757 has been described previously in detail [13, 1, 2]. The rock is coarse-grained and equigranular with crystal sizes between 2-4 mm. The pyroxene cores are more Fe-rich than that of Y-793169 [1] and are similar to those in the large basaltic clasts of EET87521 [14] among trends of mare basalts [15]. The zoning range of A-881757 is smaller than that of Y-793169 and is more Fe-rich than that of Y-793169 [1]. Plagioclase is milky white and completely converted into maskelynite. The An histogram range from 82 to 98 with maximum value at 94. Although this sample was originally classified as a VLT basalt, it was reported that abundant opaque mineral portions contain fair amounts of ilmenite (6 vol. %) [13].

Modal abundance of the opaque minerals in PTS A-881757,51-4 are: ulvöspinel 11 %, ilmenite 1 %, troilite 3 %, fayalite 1 %. The amount of ulvöspinel is larger than previously reported. Our PTS is enriched in the opaque minerals and includes one symplectite region [13]. The Cr_2O_3

contents of ulvöspinel are uniform within the crystal but vary from 5 to 16 wt % from grain to grain. In the Cr/(Cr+Al) and Ti/(Ti+Al+Cr) versus Fe/(Fe+Mg) diagram (Fig. 1), the A-881757 data are compared with those of other mare basalts [15].

The microtextures of a pyroxene in A-881757 observed by TEM show alternating lamellae of pigeonite and augite with common (001). The thickness of the lamellae are 100~200 nm. Because of almost equal thickness of the two kinds of lamellae, the original pyroxene may be subcalcic augite. Plagioclase is completely converted into amorphous material in the TEM scale. The exsolution lamellae of the Y-793169 pyroxene is much thinner than those of A-881757. The thickness ranges from 20 to 30 nm. The thickness of pigeonite and augite is nearly identical and shares common (001). Dense stacking faults are observed parallel to (100). The plagioclase shows abundant albite twinning with 20 nm thick individual lamella over the entire region of the TEM view.

Discussion. Our study of all opaque minerals in PTS A-881757,51-4 indicates that ulvöspinel is far more abundant than ilmenite. The higher bulk TiO_2 contents are consistent with the presence of fair amounts of ulvöspinel in this rock but the TiO_2 concentration is not as high as we expected from the appearance since the TiO_2 concentration of ulvöspinel (32 wt%) is lower than that of ilmenite (53 %). The presence of Ti-rich phases in the mesostasis of all these two lunar basaltic meteorites indicates that precipitation of the Ti-rich phases will take place even for such low Ti basalts at the last stage of the small-scale differentiation. The mode of occurrence of the coexisting ulvöspinel, chromite and ilmenite is different from that of common low Ti basalts in the Apollo 12 and 15 samples [15].

The Ti/(Ti+Cr+Al) versus Fe/(Fe+Mg) variation of spinels (Fig. 1) in Y-793169 shows that spinel trends represent only very last stage of the local differentiation of the mare basalt. The Cr/(Cr+Al) versus Fe/(Fe+Mg) trend (Fig. 1) shows some resemblance to the Apollo 12 ilmenite basalts and feldspathic basalts [15], but the Cr/(Cr+Al) ratios of Y-793169 are a little lower than those of the Apollo 12 low-Ti basalt, and the Y-793169 trend represents only for that of the Fe-rich end. It is to be noted that the low-Ti basalt trends represent core-to-rim variation during crystal growth in fairly early stage, while the Y-793169 trend is shown by the coexisting three Ti-bearing phases, indicating that the precipitation of Ti-bearing spinels took place at the last stage of the small-scale differentiation. The differences in compositional variation of Cr_2O_3 contents among ulvöspinel grains in A-881757 (Fig. 1) suggest that this rock is not plutonic one.

The microtextures of pyroxene in A-881757 and Y-793169 suggest that their crystallization conditions are in line with a hypothesis that Y-793169 may have crystallized near the surface in disequilibrium growth condition, whereas A-881757 cooled at depth under conditions slower than that of Y-793169 in similar lava unit. The cooling rate of A-881757 is still faster than those of true plutonic gabbroes in spite of their coarse-grained texture [13]. The mode of occurrence of the spinels in these lunar meteorites is consistent with our proposal that they represent a new type of mare rock. The preservation of maskelynite in A-881757 supports a model of direct excavation of the original mass from the depth.

We are indebted to NIPR for the samples. We thank T. Ishii, E. Yoshida, M. Otsuki and O. Tachikawa for their help in microanalyses, and K. Hashimoto, C. Akiyama for their technical assistance. This work was

supported by funds from Cooperative Program (No. 84134) provided by Ocean Research Institute, University of Tokyo.

References [1] Takeda H., Arai T. and Saiki K. (1993) Proc. NIPR Symp. Antarct. Meteorites, 6, (in press). [2] Koeberl C., Kurat G. and Brandstätter F. (1993) Ibid. (in press). [3] Warren P. H. and Kallemeyn G. W. (1993) Ibid. (in press). [4] Torigoye N., Misawa K. and Tatsumoto M. (1993) Ibid. (in press). [5] Nagao K. and Miura Y. (1993) Ibid. (in press). [6] Nishiizumi K., Arnold J. R., Caffee M. W., Finkel R. C., Southon J. and Reedy R. C. (1992) Abstr. 17th Symp. Antarctic Meteorites, p. 129-132, NIPR. [7] Yanai K., Takeda H., Lindstrom M. M., Tatsumoto M., Torigoye N., Misawa K., Warren P. H., Kallemeyn G. W., Koeberl C., Kojima H., Takahashi K., Masuda A. and Nishiizumi K. (1993) Lunar Planet. Sci. (LPS) XXIV, 1555-1556. [8] Takeda H., Arai T. and Saiki K. (1993) Ibid. 1393-1394. [9] Torigoye N., Misawa K., Dalrymple G. B. and Tatsumoto M. (1993) Ibid. 1437-1438. [10] Warren P. H. and Lindstrom M. M. (1993) Ibid. 1483-1484. [11] Saiki K., Yamaguchi A., and Takeda H. (1992) LPS XXIII, 1201-1202. [12] Takeda H., Mori H. and Tagai T. (1986) Mem. Natl. Inst. Polar Res. Spec. Issue, 41, 45-57. [13] Yanai K. (1991) Proc. Lunar Planet. Sci. Conf. 21, 317-324. [14] Takeda H., Mori H., Saito J. and Miyamoto M. (1992) Proc. Lunar Planet. Sci. Conf. 22, 355-364. [15] Papike J. J., Hodges F. N., Bence A. E., Cameron, M. and Rhodes J. M. (1976) Rev. Geophys. Space Phys. 14, 475-540.

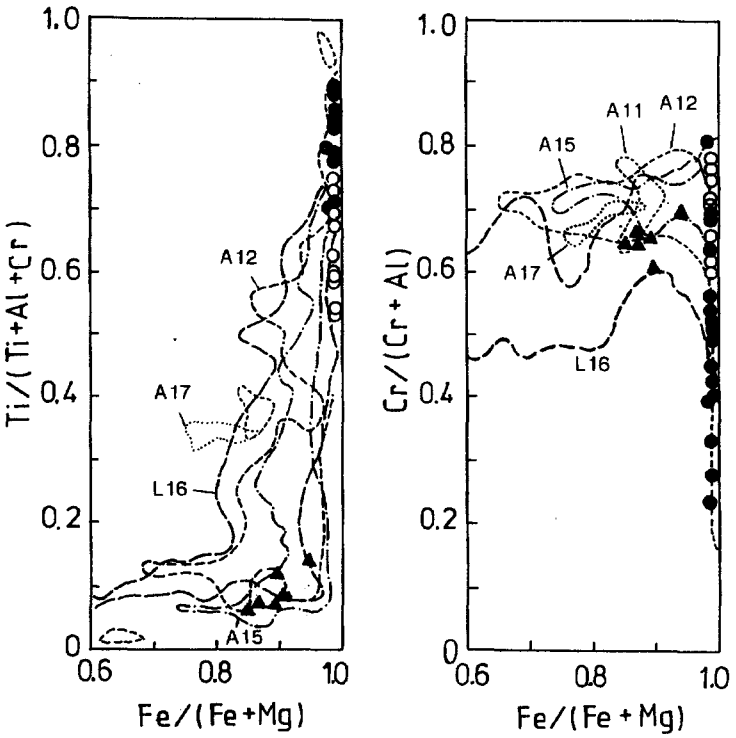

Fig. 1 Cr/(Cr+Al) and Ti/(Ti+Cr+Al) versus Fe/(Fe+Mg) diagrams for spinel in lunar mare basalts. Open symbols: A-881757, Solid symbols: Y-793169, Lines: Ranges taken from the Apollo and Luna data [15].

THE ORIGIN OF THE Mg-SUITE IN THE LUNAR HIGHLAND CRUST

Stuart Ross Taylor
Australian National University, Canberra, Australia

Three principal constituents make up the lunar highland crust: ferroan anorthosites, the Mg-suite and KREEP. Most of the rocks returned from the highlands are polymict breccias, formed by the massive bombardment. Some monomict breccias with low siderophile element contents are thought to be "pristine" rocks representing the original igneous components making up the highland crust.

Ferroan anorthosite, typically coarsely crystalline with cumulate textures, is the single most common pristine highland rock type, making up probably 80% of the highland crust. Most of the pristine clasts in lunar meteorites are ferroan anorthosites. Calcic plagioclase, typically An_{95-97} with a pronounced enrichment in Eu (Eu/Eu* ~50) is the major component (95%). The next most abundant mineral is low-Mg and low-Ca pyroxene, but these mafic minerals are usually minor constituents in this essentially monomineralic feldspathic rock.

The crystallization of ferroan anorthosites from the lunar magma ocean and the flotation of the feldspathic highland crust as "rockbergs" is dated at 4440 ± 20 m.y. from the Sm-Nd age for the Apollo 16 anorthosite 60025 [1] Their primitive $^{87}Sr/^{86}Sr$ ratios, Eu enrichment, uniform composition, old age, global extent and the presence of large massifs of pure (<3% mafics) anorthosite [2] all suggest that the ferroan anorthosites crystallized from a magma ocean.

KREEP is strongly enriched in those "incompatible" trace elements excluded from the major mineral phases (olivine, orthopyroxene, clinopyroxene, plagioclase, ilmenite) and originated as the final 2% or so melt phase from the crystallization of the magma ocean [3]. This residual phase crystallized at about 4360 m.y. and was intimately mixed with the feldspathic crust by cratering. The KREEP component tends to dominate the trace element chemistry of the highland crust. REE enrichments up to 1000 times the chondritic abundances are known.

A wide variety of more basic rocks, including norites, troctolites, dunites, spinel troctolites and gabbro-norites, form the Mg-suite [4]. Granulites from deep within the crust are present. These rock types have more primitive Mg/Mg+Fe ratios than the ferroan anorthosites. Their ages range from about 4.43 b.y. down to about 4.17 b.y. A crucial point is that the ages are typically 100-200 m.y. younger than those of the ferroan anorthosites.

The Mg-suite does not appear to be directly related to the crystallization from the magma ocean and is petrographically distinct from

the older ferroan anorthosites. It makes up a significant proportion (perhaps 20%) of the highland crust. It is Mg-rich, commonly with Mg#>90 and so primitive in terms of igneous differentiation, but also contains high concentrations of incompatible elements, typical of highly evolved or differentiated igneous systems. Thus it has two distinct and contradictory components in terms of conventional petrology. REE contents are typicallly 15 to 100 times chondritic and the REE patterns are parallel to those of KREEP and ferroan anorthosites [5]. This KREEP signature was present in the magma from which the Mg-suite crystallized and does not represent post-crystallization contamination by KREEP.

An origin by mixing of these two distinct components, one primitive to account for the major elements (particularly the high Mg/Fe), and the other evolved to account for the trace element characteristics, is suggested by the contradictory characteristics of the Mg-suite. The source of the highly evolved trace element component is clearly KREEP. The source of the "primitive" Mg-rich component is less clear. Many theories propose that the Mg-suite rocks are deived from different plutons that intruded the crust as separate igneous intrusions. However, all Mg-suite rocks have parallel REE patterns [5]. This characteristic is compatible with mixing, but should not be expected to occur in many separate igneous intrusions.

Another significant point is that the Mg-suite also contains Mg-rich orthopyroxene, a mineral that is lacking in most mare basalts, so that clearly the source regions of the mare basalts were distinct from those of the Mg-suite. During crystallization of the lunar magma ocean, Mg-rich minerals, (e.g. olivine and orthopyroxene) are the first to crystallize. They accumulate on the bottom of the magma chamber at depths of over 400 km. It has been suggested that massive overturning of the crystal pile has occurred to bring these Mg-rich minerals close to the surface [6]. The source regions of the mare basalts were solid by 4400 m.y. as shown by the isotopic systematics.Thus the magma ocean had completed crystallization by 4400 m.y. with only the minor KREEP component remaining liquid until about 4360 m.y. Thus the lunar interior was effectively solid, although still hot, at the time of the formation of the Mg-suite. Arguments have been advanced for only localized overturning during crystallization of the magma ocean [7] and it seems difficult to envisage a massive overturning of the upper 400 km of the lunar interior after 4400 m.y.

Remelting of such early refractory Mg-rich cumulates would be difficult in the absence of an obvious internal source of energy. Subsequent melting deep in the lunar interior to produce mare basalts took place in differentiated cumulates. It produced mare basalt lavas that do not have the primitive and evolved characteristics of the Mg-suite. The total amount of mare basalt melt was very small, probably about 0.1% of lunar volume. The melting occurred over a period exceeding 1 b.y. in over 20 separate

locations and was essentially trivial on a Moon-wide scale. It was fueled by variable amounts of K, U and Th trapped in the cumulates,

The Mg-suite, has a volume about 20 times that of the mare basalts, and was produced much more quickly, in less than 20% of the time that the Moon took to produce the mare basalts. The formation of the Mg-suite thus requires a major source of energy and a large volume of a primitive component, assuming the evolved component is derived from KREEP.

Large-scale overturning of the lunar mantle seems unlikely to produce the compositionally distinct and voluminous Mg-suite magmas. If the primitive compositions cannot be derived from the interior, then they may have come from above.

The giant impact hypothesis for lunar origin spins out the silicate mantle of the impactor into Earth orbit. It thus provides a ring of debris of primitive lunar composition from which the Moon accreted. If accretion of this material into the Moon is not 100% efficient, sweep-up of some left-over bodies at relatively low velocities could occur following the formation of the lunar crust as suggested by the lunar cratering record. The impact of such bodies could result in mixing of whole Moon compositions with some remelted ferroan anorthosite and with the residual KREEP liquid. Such early impacts at about 4.3 b.y. into hot crust might differ significantly from later basin-forming events in cold crust (e.g. Imbrium, Orientale). In this context it is significant that gravity anomalies are confined to young basins and that the old highlands are in isostatic equilibrium. The magmas so formed could then pond beneath the ferroan anorthositic crust and subsequently intrude the crust. Such a model can account for the mineralogy of the Mg-suite, with orthopyroxene and plagioclase, for the old ages (but younger than the accretion of most of the Moon) and provide both the primitive "whole Moon" component and a sufficient energy source. The amount of material added to the Moon need amount only to about 2% of lunar volume.

[1] Carlson, R. W. and Lugmair, G. W. (1988) *Earth Planet. Sci. Lett.* **90**, 119.

[2] Belton, M. J. S. et al. (1992) *Science* **255**, 570.

[3] Taylor, S. R. and Jakes, P. (1974) PLC 5,1287.

[4] see Warren, P.H. *Amer. Mineral.* (in press) for a review of pristine samples.

[5] Taylor, S. R. and Koeberl, C. (1992) *Meteoritics*, **27**, 295.

[6] Ryder, G. (1991) *Geophys. Res. Lett.* **18**, 2065.

[7] Snyder, G. A. and Taylor, L. A. (1992) *Antarctic Meteorites Symposium* **17**, 114.

PETROGRAPHIC AND COMPOSITIONAL FEATURES OF THE INTERMEDIATE GROUP CHONDRITES

WANG Daode and LIN Yangting
(Institute of Geochemistry, Guangzhou Branch,
Chinese Academy of Sciences, Guangzhou 510640)

INTRODUCTION

In term of taxonomic parameters, a few of chondrites can not be classified into any one of the 11 well known chemical groups including H, L, LL, EH, EL, CI, CM, CO, CV, CR and CK. This study demonstrated that some of them displayed intermediate properties of two neighbouring groups, hence classification of E/H, H/L, L/LL and LL/C intermediate groups were respectively proposed, based on Fa-content of olivine, Fs-content of low-Ca pyroxene, Co-content of kamacite, bulk concentrations of refractory siderophile elements (Ir, Os) in metal phase and petrographic features.

PROPERTIES OF THE INTERMEDIATE GROUP CHONDRITES

E/H intermediate group chondrites The most representative sample was Yamato74063, which was recognized as the first E/H intermediate group chondrite in term of Fa-content of olivine (10.9 mol%) and Fs-content of low-Ca pyroxene (10.7 mol%)[1]. Furthermore, bulk composition of Fe-Ni metal in Yamato74063 varied from range of E-group to ordinary chondrites, with Os-content (3.2 ppm) in range of E-group, Ir-content (4.64 ppm) close to H-group and Co-content (7.8 mg/g) dropping between H- and L-groups. In addition, abundance of troilite (9.39 wt%) was in range between ordinary chondrites and enstatite chondrites. Abundance of Fe-Ni metal in Yamato74063 (5.90 wt%) was extremely low. Although Acapulco meteorite showed texture of achondrites, its bulk composition was in range of H-group chondrites with more enrichments of siderophile elements and metal[2]. Fa-content of olivine(10.5 mol%) and Fs-content of low-Ca pyroxene (10.5 mol%) in Acapulco meteorite was in range between H- and E-group chondrites too. However, refractory siderophile elements was more enriched in the Fe-Ni metal of Acapulco meteorite (Ir 6.22 ppm, Os 7.1 ppm, Co 5.34 mg/g) than H-group chondrites.

H/L intermediate group chondrites Bremervorde and Tieschitz were reclassified into H/L intermediate group[3]. Though Fa-content of olivine (18.6) and Co-content of kamacite (4.5 mg/g) of Bremervorde were in range of H-group chondrites, its bulk $\Delta^{17}O$ value of 1.01‰ [4] was similar to L-group and the abundance of metal (135 mg/g) was in range between H-group (172-222 mg/g) and L-group (30-94 mg/g)[5]. [6]reported that abundance of siderophile elements of Bremervorder fell in range between H- and L-groups too, which was late confirmed by [3]. In the Tieschitz meteorite, concentration of Siderophile elements was close to the low extreme of H-group chondrites, but Co-content of kamacite (7.6 mg/g) was in range of L-group. Moreover, both abundance of Fe-Ni metal (9.9 wt%) and bulk $\Delta^{17}O$ value (0.8 ‰ [4]) fell between H and L groups. Krymka was also suggested a H/L intermediate group

chondrite with concentration of Ir, Os and Co in Fe-Ni metal plotted between H- and L-groups. The abundance of Fe-Ni metal was in range of L-group, while Fa-content of olivine was about 15.5 lower than H-group, however its Fa value was very scatter due to low petrographic type of 3.1.

L/LL intermediate group chondrites Since recognizance of Qidong as a L/LL intermediate group chondrite[7,8], two another chondrites former classified into L4 type (Bjurbole and Cynthiana) were reclassified as the L/LL intermediate group chondrites as well. Model composition of the Qidong meteorite was 90.2 wt% silicates, 4.7 wt% Fe-Ni metal, 4.3 wt% troilite and 0.7 wt% chromite. The abundance of Fe-Ni metal was near low extreme of the L-chondrites (4.4-11.7 wt%) and at middle of the LL-chondrites (3.0-6.0 wt%) [9]. Concentrations of Ir, Os and Co of Fe-Ni metal were plotted between L- and LL-groups, but more close to the former. Olivine ($Fa_{25.7}$) and low-Ca pyroxene ($Fs_{21.5}Wo_{1.6}$) were homogeneous and near upper extreme of the L-chondrites. 150 Analyses of Fe-Ni metal grains by electron microprobe revealed that most Fe-Ni metal were taenite with taenite/kamacite ratio of 60. Kamacite contained an average Co-content of 15 mg/g at the lower extreme of the LL-chondrites, which was clear beyond range of L-chondrites. In the Cynthiana meteorite, concentrations of Ir, Os and Co of Fe-Ni metal, Co-content of kamacite (10.9 mg/g) and Fa-value of olivine (26.5 mol%) were all plotted between L- and LL-groups. Although Co-content of kamacite (8.0 mg/g) and concentrations of Ir, Os and Co of Fe-Ni metal of the Xi Ujimgin meteorite were in range of H-group, its olivine contained unusually high Fa-content (26.4 mol%). Abundances of siderophile elements of the above all 4 L/LL intermediate group chondrites fell between L- and LL-groups.

LL/C intermediate group chondrites The Carlisle Lakes meteorite and ALHA85151 were in detail studied by[4,10,11,12]. Below properties suggested that they were intermediate chemical group chondrites lying between ordinary chondrites and carbonaceous chondrites: (a). Concentrations of Ir, Os, and Co of Fe-Ni metal dropped between LL- and CV-groups; (c). Abundance of lithophile elements was in range of ordinary chondrites, while abundance of refractory and common siderophiles were about 1 X CI, Ga and As somewhat lower (0.6-0.9 X CI) but Au much lower (0.17 X CI for Carlisle Lakes, 0.36 X CI for ALH85151) different from ordinary chondrites. (d). In comparison with LL-group chondrites, the LL/C intermediate group was more oxidized ($Fa_{39.3}$) and contained more abundant olivine but less pyroxenes and Fe-Ni metal, which mainly occurred as awaruite (Ni 64 wt%, Co 2 wt%) and coexisted with sulfides (pyrrhotite and pentlandite). In addition, magnetite was very rare or absent. This was similar to model composition of carbonaceous chondrites.

DISCUSSION AND CONCLUSIONS

The identification of intermediate groups of E/H, H/L, L/LL and LL/C demonstrated that beside chemical and isotopic heterogeneities in the solar nebula, the variation of chemical composition was continuous. Taking assumption that as increasing formation distance from the sun, chondrites

became more oxidized[13], our result suggested that chemical composition in the solar nebula continuously varied along the radius. This became much clearer in term of variation of redox, which was not only revealed by Fa-content of olivine and Fs-content of low-Ca pyroxene but also by concentration of refractory siderophile elements in Fe-Ni metal. In fact, most chondrites exhibited a well positive relationship between Fa-content of olivine (or Fs-content of low-Ca pyroxene) and the concentration of refractory siderophile elements in Fe-Ni metal. Both of FeO-content of silicates and composition of Fe-Ni metal were controlled by Oxygen fugacity (fo_2). At more oxidized condition, more proportion of Fe existed in form of FeO, hence condensed silicates with higher FeO-content and Fe-Ni metal with more refractory siderophile elements since Fe is much readier to be oxidized than the other siderophile elements.

In spite of well defined relationship between Fa-content of olivine (or Fs-content of low-Ca pyroxene) and concentration of refractory siderophile elements in Fe-Ni metal for the most of chondrites, a few deviation were also recognized. Two explanations were proposed for the deviation of redox between silicates and Fe-Ni metal: First, a few of chondrites probably experienced significant fractionation between silicates and Fe-Ni metal during condensation in the solar nebula, since silicates and Fe-Ni metal were very different in gravity, magnetism and electricity etc. Moving out part of silicates could change its average composition, because composition of silicates varied during condensation as indicated by heterogeneity of unequilibrated chondrites. Second, part of Fe-Ni metal and silicates probably formed at separative location with different oxygen fugacities. They were transported and accreted onto a same parent body later by some mechanism. Anyhow, discovery of deviation between silicates and Fe-Ni metal supplied a hint to understand fractionation between silicates and Fe-Ni metal.

SUPPORTED BY the State Antarctic Committee and Chinese Academy of Sciences

REFERENCES [1]Yanai K. and Kojima H. (1991) **Proc. NIPR, Symp. Antarct. Met.** 4, 118-130. [2]Palme H., Schultz L., Weber H.W., Waenke H., Michel-Levy M.C. and Lorin J. C. (1981) GCA 45, 727-752. [3]Wang D. and Chen Y. (1991) **Geochem.** vol.1(in Chinese), 13-26. [4]Weisberg M.K., Prinz M., Kojima H., Yanai K., Clayton R.N. and Mayeda T.K. (1991) GCA 55, 2657-2669. [5]Chou C-L., Baedecker P.A. and Wasson J.T. (1973) GCA 37, 2159-2171. [6]Sears D.W. and Weeks k.S. (1986) GCA 50, 2815-2832. [7]Wang D. and Rubin A.E. (1987a) **Geochem.** vol.4(in Chinese), 295-302. [8]Wang D. and Rubin A.E. (1987b) **Meteoritics** 22, 97-104. [9]Gomes C.B. and Keil K. (1980) **Brazilian stone meteorites.** University of New Mexico Press, Albuquerque 161. [10]Binns R.A. and Pooley G.D. (1979) **Meteoritics** 14, 349-350. [11]Mason B. (1987) **Antarctic Met. News.** 10, 21. [12]Rubin A.E. and kallemeyn G.W. (1989) GCA 53, 3035-3044. [13]Wasson J.T. (1985) **Meteorites: Their record of early solar-system history.** Freeman.

MINERALOGY OF ALH81187: A PARTLY REDUCED ACAPULCOITE

Keiko Yugami[1)], Masamichi Miyamoto[1)], Hiroshi Takeda [1)] and Takahiro Hiroi [2)]
[1)]Mineralogical Institute, Faculty of Science, University of Tokyo, Hongo, Tokyo 113
[2)]SN3, NASA/Johnson Space Center, Houston, TX 77058, U.S.A.

Introduction Primitive achondrites is a term for the unique meteorites that have achondritic texture and chondrite-related chemistry proposed by Prinz et al. [1]. They show recrystallized texture and have no chondrule, but their mineral and bulk chemical compositions are related to chondritic materials. Their main minerals are pyroxene, olivine and Fe-Ni metal with minor plagioclase, troilite and chromite. Acapulco and Winona are representative primitive achondrites for two groups, acapulcoites and winonaites [1,2]. They differ from each other in chemical compositions of minerals and oxygen isotope compositions. Mafic silicates in winonaites are more reduced than in those of acapulcoites [3,4]. The oxygen isotope compositions of ALH81187 indicate that it is a primitive achondrite of the acapulcoite group [5]. The reflectance spectrum of ALH81187 has been measured to explain the spectra of S asteroids by Hiroi et al. [8]. It is interesting to see why this meteorite shows a better fit for some S asteroids in spectra. ALH81187 contains olivine with compositions comparable to those of winonaites. We performed a mineralogical study on ALH81187 in comparison with ALH81261 using electron-probe microanalyzers(EPMA) on an assumption that it was originally an acapulcoite and subsequently reduced to a state similar to winonaite in mineral chummiest by some processes.

Samples and Methods The polished thin sections(PTSs) of ALH81187 and ALH81261 was supplied from the Meteorite Working Group of U.S.A. We have studied these PTSs by electron probe microanalyzer(EPMA) JEOL 733 at Ocean Research Institute and Geological Institute, University of Tokyo and scanning electron microscope(SEM) JEOL840A. The modal abundances of minerals were obtained by processing the back scattered electron image(BEI) of SEM acquired by the Kevex Super 8000 System.

Results ALH81187: The modal abundances of minerals obtained by processing BEI data are approximately: olivine 30%, orthopyroxene 37%, augite 13% and nickel-iron, troilite, etc. 20%. The recrystallized texture which is typical of the primitive achondrites is disturbed at grain boundaries and minute dusty inclusions are present within these crystals. The silicate minerals have medium grain size (0.05-0.6mm across) and brownish small fragments that fill the space between them, and the silicate grains do not show curved grain boundaries common in acapulcoites such as ALH81261. Brown veinlets and small areas are limonite [6]. EPMA analyses of silicates show the average of *mg* number=[Mgx100/(Fe+Mg)] of pyroxene is 94.3 and that of olivine is 95.8. They are not much different from those of winonaites [3], but most Fe rich core value (mg=90) is rather close to those of acapulcaites. The profile of *mg* number of olivine from core to rim of a crystal is flat, but mg number of some pyroxene grains varies from 6.4-6.9 (core) to 2.0-4.3 (rim) (the core to rim distance is about 35 μm) (Fig.1,2).

ALH81261: The modal abundances of minerals are approximately: olivine+orthopyroxene 60%, augite 6%, plagioclase 20% and nickel-iron, troilite, chromite, etc. 13%. The BEIs of olivine and pyroxene are indistinguishable. The proportion of pyroxene to olivine is about 1:1

[7]. The EPMA analyses show the average of *mg* number of pyroxene is 90.1 and that of olivine is 89.9. They are in the range of acapulcoites. The silicate grains have rounded, complex boundaries. The opaque-silicate boundaries are also show similar shapes. Some opaque grains include iron, troilite and chromite within the same curved boundaries but those between them are rather straight. The silicate grains have inclusions generally in regions near cores, and some inclusions are in lines that look like grain boundaries. However, the density of overall inclusions is smaller than that of ALH81187. The *mg* numbers are larger at the rim (10.2) than at the core (10.7) in some olivine grains. The analyses of chromite give the average of Fe/(Mg+Fe) atomic ratio=0.63 and Cr/(Al+Cr)=0.62, ZnO in chromite is 1.2 wt%.

Discussion: ALH81187 is similar to ALH81261 in their grain size of silicates and Fe Ni metals which look like to be disseminated into the space between silicate grains. Although both meteorites are acapulcoites, ALH81187 is richer in pyroxene and metal than ALH81261, and *mg* numbers of pyroxene and olivine of ALH81187 are larger than those of ALH81261, especially those at rims of pyroxene grains. Olivine is more likely to be reduced than pyroxene because of smaller diffusion coefficient of Mg than that of Fe, and olivine decomposes to pyroxene, metallic iron and silica by reduction if it is exposed to a low oxygen fugacity environment. The dusty inclusions in the central region of grains of both meteorites may indicate that they were partly but not completely melted but it is also likely that the especially inclusions in outer part of the grains of ALH81187 were produced by reduction in solid state, if we correlate the disturbed grain boundaries were produced by a shock event. The texture of ALH81187 indicates that the precursor material before shock may be similar to ALH81261.

The Y-74357 lodranite shows similar dusty inclusions in olivine, which is completely reduced to give Mg-rich composition closer to winonaites, but the pyroxene crystal shows reduction at only outer region (about 30μm) (Fig.1 (a)). Miyamoto and Takeda[8] attributed this phenomenon to the difference in diffusion of Mg/Fe between pyroxene and olivine and the reduction that took place when the parent body was exposed to vacuum after being broken up and while the interior is still hot. They reported that the cooling rate of 1.5°C/year from 1000 to 600°C gives the best fit for the observed Fe-Mg profile at rims of orthopyroxene grains of Y-74357. Because of similar diffusion profiles observed in the ALH81187 orthopyroxene to those of Y-74357 and entirely reduced olivine in both meteorites, we can envision similar thermal histories for these two meteorites. The ranges of reverse zoning at the rims of orthopyroxene grains of ALH81187 are wider than those of Y-74357. It suggests that the cooling rate of ALH81187 may be slightly slower than that of Y-74357. Then it may have been shocked and exposed in vacuum while it is hot. The chemical compositions of ALH81187 show that it was apparently reduced. So it is provable that ALH81187 was originally an acapulcoite like ALH81261 and was partly reduced to be in present state by shock.

The reflectance spectrum of this meteorite mixed with other components resembles to those of S asteroids [9]. It has been already suggested that the spectra of reduced and nickel-iron-rich primitive achondrites such as Y-74357 will give better fit for those of S asteroids [10]. ALH81187 is much fine grained and their grain boundaries are filled with opaque materials. The reduction process related to shock events such as observed for ALH81187 may have relationship to what is called as "space weathering" [10,11,12].

We thank Meteorite working Group of U.S.A. for providing PTSs of ALH81187 and ALH81261. We also thank the Ocean Research Institute and Geological Institute, University of Tokyo for permitting the use of EPMA.

References [1] Prinz, M., Waggoner, D. G., and Hamilton, P. J. (1980): Lunar Planet. Sci., XI, 902-904. [2] Palme, H., Schultz, L, Spettel, B., Webber, H. W., Wänke, Christophe Michel-Levy, M. and Lorion, J. C. (1981): Geochim. Cosmochim. Acta, 45 727-752. [3] Kimura, M., Tsuchiya, A., Fukuoka, T., Iimura, Y. (1992): Proc. NIPR Symp. Antarct. Meteorites, 5, 165-190. [4] Clayton, R. N., Mayeda, K. and Nagahara, H. (1992): Lunar Planet. Sci., XI, 231-232. [5] Macoy, T. J., Keil, K., Clayton, R. N. and Mayeda, T. K. (1993): Lunar Planet. Sci., XXIV, 945-946. [6] Mason (1984): Antarctic Meteorite Newsletter, 7(2),8 [7] Mason (1985): Antarctic Meteorite Newsletter, 8(1),9 [8] Miyamoto, M. and Takeda, H. (1991): 16th Symp. Antarct. Meteorites, 165-167. [9] Hiroi, T., Bell, J. F., Takeda, H., and Peters, C. M.: Icarus, in press. [10] Hiroi, T. and Takeda, H. (1991): Proc. NIPR Symp. Antarct. Meteorites, 4, 163-177. [11] Bell (1991): Lunar Planet. Sci., XXII, 81-82. [10] Hiroi, T. and Takeda, H. (1991): Proc. NIPR Symp. Antarct. Meteorites, 4,163-177. [12] Takeda, H., Saito, J. and Hiroi, T. (1992): Proc. Japan Academy, 68, Se B. NO. 8 115-120.

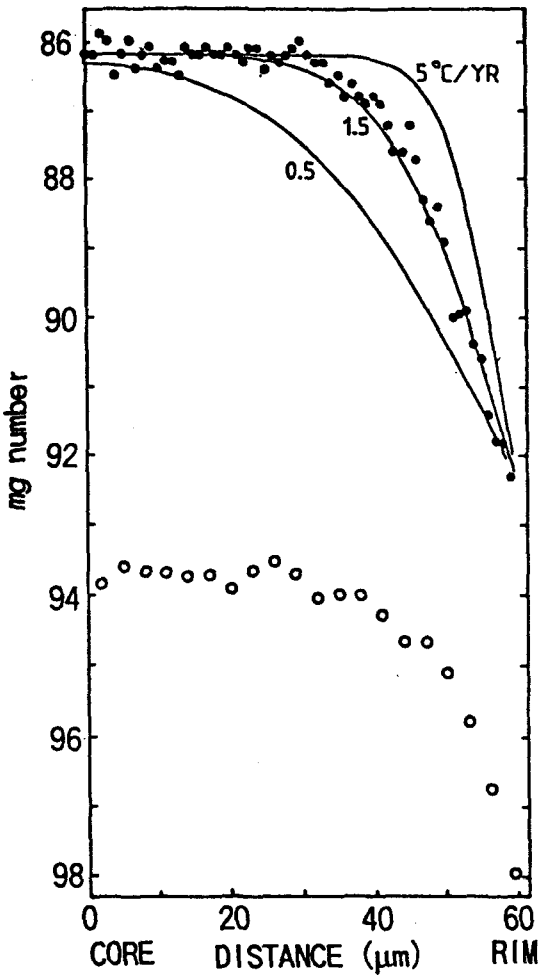

Fig. 1 (a). Chemical zoning profiles of orthopyroxyne grains in ALH81187 and Y-74357. Open circles indicate *mg* numbers of an orhopyroxene grain in ALH81187. Solid circles indicate *mg* numbers of an orthopyroxene grain in Y-74357 and curves show calculated diffusion profiles[8].

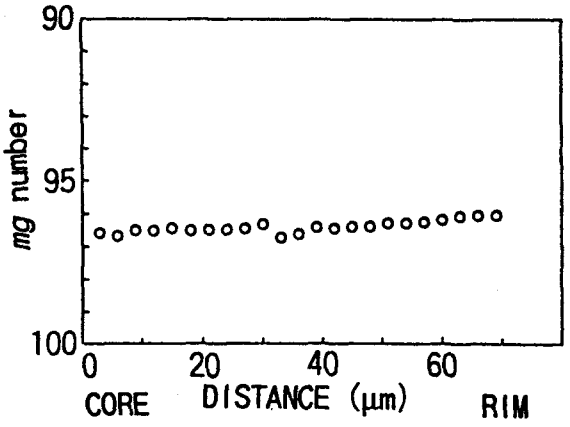

Fig. 1 (b). Chemical zoning profile of an olivine grain in ALH81187. Open circles indicate *mg* numbers.

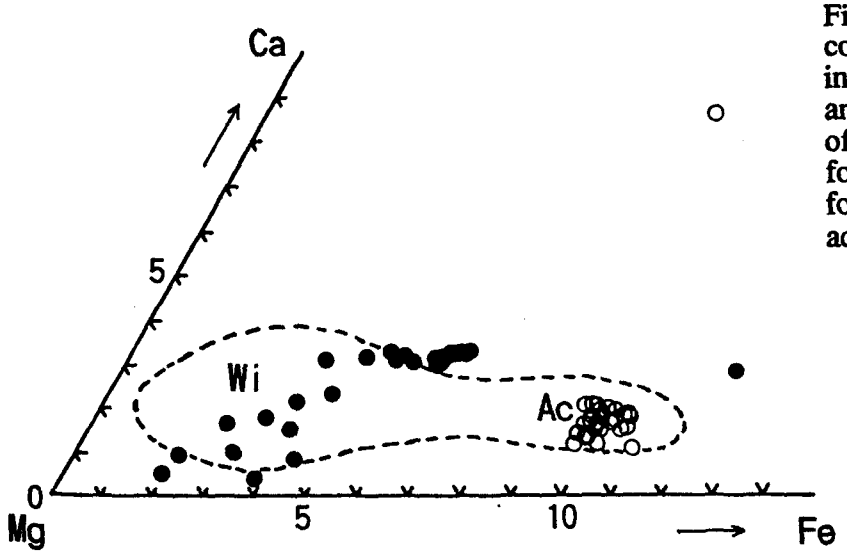

Fig. 2. Orthopyroxyne compositions. Solid circles indicate those of ALH81187, and open circles indicate those of ALH81261. Dotted area is for primitive achondrites. Wi is for winonaites, and Ac is for acapulcoites.

Trace Element Abundances in Five Primitive Achondrites.

Noritoshi Morikawa and Noboru Nakamura Department of Earth Science, Faculty of Science, Kobe University, Nada, Kobe 657, Japan.

Many petrological and chemical studies suggest that "primitive achondrites" suffered extensive thermal metamorphism and/or partial melting. Rare earth, alkali metal and alkaline earth elements are known to be a sensitive indicator of igneous fractionation processes.

In order to investigate petrogenesis of primitive achondrites, the abundances of Fe, Mg, Ca, Li, K, Rb, Sr, Ba and rare earth elements (REE) in five primitive achondrites (LEW88280, MAC88177 ; lodranites, Acapulco ; acapulcoite, LEW88763 ; brachinite and Yamato74025; winonaite) are determined by isotope dilution mass spectrometry. We also analyzed Na by atomic absorption spectrometry and some major and minor elements (Al, Ni, Co, Cr, Mn and Zn) by inductively coupled plasma atomic emission spectrometry (ICP-AES).

LEW 88280 , MAC 88177

Results for both meteorites together with Acapulco are shown in fig.1-a. Although absolute abundances are different for two lodranites, REE patterns are essentially identical, i.e. light-REE(LREE) depleted (La/Lu= 0.196 for LEW88280, 0.183 for MAC88177) and large negative Eu anomaly {(Eu/Eu*)n = 0.26 for LEW88280, 0.31 for MAC88177, Eu* is interpolated between Sm and Gd}. These two meteorites have also quite similar patterns of other lithophiles. The high abundances of all lithophile elements for MAC88177 are due to the less content of metal/sulfide phase. Much lower abundances of siderophile elements (Co, Ni) in MAC88177 than those in LEW88280 support this interpretation.

Lodran (1) and Yamato 74357 (2) , lodranite, have similar elemental patterns. The depletion of plagiophiles such as Al, Eu, Sr and alkalis suggests the extraction of plagioclase from a chondritic source.

Modal abundances of lodranites (e.g. Lodran, Yamato74357 and MAC88177) lack plagioclase and phosphates. Although no modal data have been reported for LEW88280, our results of Al concentration (0.15xCI) indicate the lack of plagioclase.

Using the mineral/liquid partition coefficients, we performed the model caluculation. We applied non-modal partial melting model assuming that plagioclase and phosphate were melted and extracted. It was found that calculated REE pattern is very similar to our analytical data.

Acapulco

Acapulco has an exceptionally LREE enriched pattern (La/Lu=2.72). In particular, La and Ce have somewhat higher values (La=4.86xCI, Ce=4.42xCI). Our data mostly agree with previously reported data by INAA (3). This suggesting that highly fractionated REE is not due to sample heterogeneity but may be an intrinsic property.

LEW 88763

LEW88763 is classified as a brachinite (4). Fig.1-b shows the elemental abundances in LEW88763 and Brachina (data from Nehru et al.(5)). Although sample size used for analysis in this work was quite small (~25mg), the major element (Fe, Mg, Ca and Al) abundances for both meteorites are very similar. LEW88763 has almost chondritic REE pattern. On the contrary, REE pattern of Brachina is slightly LREE-depleted. These two brachinites contain more alkalies than any other groupes of primitive achondrites. However, it is noteworthy that Rb is most depleted among alkalies and that the Rb depletion is commonly noted for other primitive achondrites.

The most clear difference between LEW88763 and Brachina is the abundance of Zn. Zn in LEW88763 is extremely low (0.10xCI), although Brachina has almost chondritic (0.99xCI). It could be possible that this was caused by small sample size used in this work, though it seems suspectable that such a large difference is caused by sampling problem.

Yamato 74025

Yamato74025 is classified as a winonaite. Fig.1-c shows the alkali and REE pattern of Yamato74025. REE is almost chondritic but slight LREE-depletion is noticeable. Excepting Li, alkali metals are delpeted with increasing of ionic radi. Such an extreme depletion of Li is not found in any other primitive achondrites, although Li data are reported only for several primitive achondrites so far. This feature is found for some acapulcoites ,e.g. Yamato74063 and ALH78230 (2). These two acapulcoites are interpreted as residue of a few % of partial melting from chondritic source material. Yamato74025 may be also formed through similar processes. Kimura et al.(6) found heterogeneous distributions of elements among two 100mg-sized samples. So it is possible that our results may not represent the whole rock of Yamato74025. In any case, we suggest that very low Rb is the results of small degree of partial melting and extraction of liquids.

Reference

(1) Bild and Wasson (1976) Min. Mag. **40**, 721-735
(2) Torigoye et al. (1993) Proc. NIPR Symp. Antarct. Meteorites, **6** (accepted)
(3) Palme et al. (1981) Geochim. Cosmochim. Acta, **45**, 727-752
(4) Antarctic Meteorite NEWSLETTER (ed. by Lindstorm) vol.14,No.2 (1991)
(5) Nehru et al. (1983) Proc. Lunar. Planet. Sci. Conf., **14**, 237-244
(6) Kimura et al. (1992) Proc. NIPR Symp. Antarct. Meteorites, **5**, 165-190

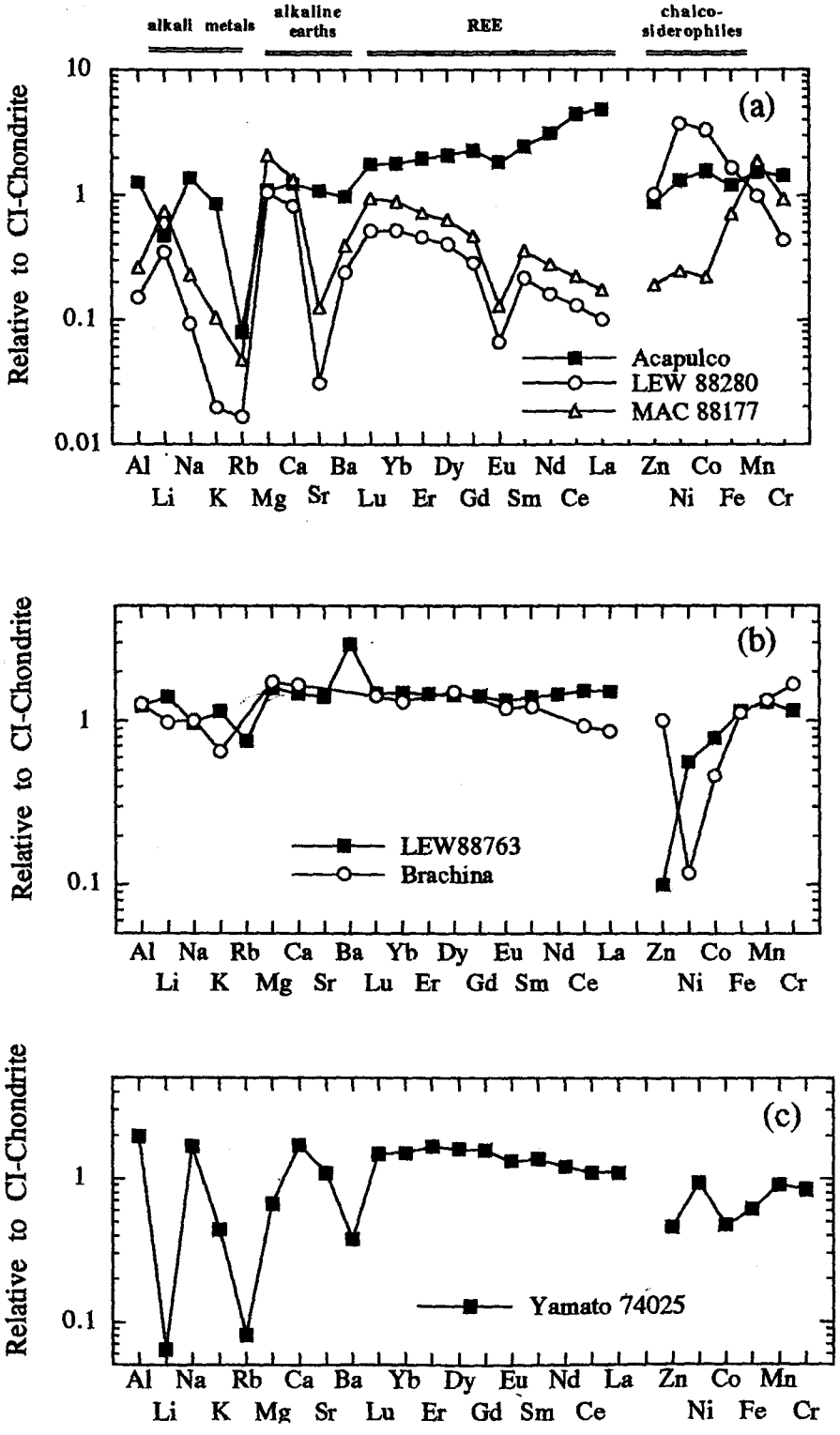

Fig.1 CI-normalized abundances of elements in primitive achondrites. Elements are arranged in the order of increasing ionic radii from the left to the right for each groups of elements.

WHERE ARE NOBLE GASES TRAPPED IN Y-74063 (UNIQUE)?

N.Takaoka, Y.Motomura and K.Ozaki (Dept. Earth & Planet.Sci., Kyushu Univ., Fukuoka) and K.Nagao (Inst.Study Earth Interior, Okayama Univ., Misasa, Tottori)

Y-74063 is a unique meteorite with affinities to Acapulco in texture, mineralogy and chemistry. It contains large amounts of trapped heavy noble gases [1]. The Xe concentration is even higher than that of ureilites with a few exceptions. The isotopic ratios of trapped Kr and Xe from bulk, silicate and metal fractions are homogeneous and identical with those of Q-gases [2], but the trapped $^{36}Ar/^{132}Xe$ ratio is different for bulk, silicate and metal, i.e., 22, 17 and 72, respectively [3]. With laser ablation, Takaoka et al. [3] have measured abundances and isotopic ratios of noble gases released from mineral grains. Most grains released large amounts of trapped gases, which suggests that the trapped gases are not concentrated in specific carrier phases but in many major minerals.

In this work, we measure trapped noble gases by laser ablation mass spectrometry (with laser beam of 50 μm in diameter and 25 mJ/pulse), and examine mineral grains by optical microscope and EPMA observations. The noble gas abundance is normalized by using cosmogenic ^{3}He released on laser ablation and the respective concentration of cosmogenic ^{3}He in silicate and metal [3].

Result of laser probe analysis is given in Table 1. Several grains such as pit 18, 19, 24, 27 and 28 release large amounts of trapped gases. In particular, pit 19 that represents a silicate (opx) grain including many tiny inclusions, releases extraordinarily large amounts of trapped ^{132}Xe. The ^{36}Ar release is also high ($^{36}Ar/^{132}Xe$ = 11), but the release of ^{40}Ar that is radiogenic, is lower than background. Pit 28 that also represents silicate (opx) including tiny inclusions, also releases large amounts of trapped gases with $^{36}Ar/^{132}Xe$ = 170. Pit 18 (FeS) releases large amounts of ^{132}Xe with negligible ^{36}Ar ($^{36}Ar/^{132}Xe$ = 2). In contrast, some grains such as pit 16, 17, 21 and 22 release negligible amounts of trapped gases. They are silicate (opx), Fe-Ni, FeS and silicate (opx), respectively. Although these observations confirm the previous result that the silicate grains including tiny metal inclusions are gas-rich [3], no additional evidence indicating obvious relationships between the trapped gas abundance and the mineral phase is found.

Mineralogical study of PTS's, prepared from a remaining portion (3 mm acoss) of the same chip as was analysed for noble gases, indicates that some silicate grains, mainly of orthopyroxene, contain abundant tiny inclusions of various shapes. The shape of inclusions is ovoid to amevoid. From BSE images, a considerable portion of the inclusions is of voids, sometimes with opaque daughter minerals on walls, while the overwhelming portion is metallic. Size of voids is 1 to several μm in diameter. No glass inclusions are found. It is not obvious if the gas-rich grain of troilite is porous or not.

The void is not artifact on preparation of PTS's, but intrinsic because the inclusions with opaque daughter minerals on walls are found on both the inside and the surface of PTS's with transmitted light. Originally such voids must have been filled with gas and/or fluid, but no inclusions having typical features of fluids are found.

A possible origin of voids is to trap ambient gases along cracks or cleavages of minerals and to enclose them therein. The voids can be containers of the trapped noble gases. In this case, the noble gases must be concentrated preferentially. The total volume of voids, estimated to be 10^{-3+-1} cm^3 per gram of mineral and ^{132}Xe (8.5×10^{-7} cm^3/g) for orthopyroxene containing tiny inclusions give 10^{-3} atm for partial pressure of Xe in voids. This is nine orders of magnitude higher than that for solar nebula gas of $p_o = 6 \times 10^{-3}$ atm. In addition, the fractionated elemental abundance requires some medium intervening in enriching heavy noble gases and transmitting them into the meteorites.

Adsorption on carbon [e.g, 4] and implantation [e.g., 5] have been proposed for trapping preferentially heavy noble gases in the early solar system. The abundance of ^{132}Xe for orthopyroxene with dusty inclusions is approximately identical with that for C-residues of C-chondrites [2] and ureilites [6]. Since carbon has not been found in Y-74063, if carbon was the medium which enriched and carried heavy noble gases into the meteorite, it should be removed by exhausting it, for instance, for reduction of silicates and oxides. It is supposed that CO_2 occurring by oxidation of C could be a carrier of noble gases released from C and must have played an importnat role to produce voids and to occlude noble gases in mineral grains.

References [1] Takaoka,N. and Yoshida,Y.(1991) Proc. NIPR Symp. Ant. Met. 4, 178-186 [2] Wieler,R. et al.(1992) GCA 56, 2907-2921 [3] Takaoka,N. et al.(1993) Proc. NIPR Symp. Ant. Met. 6 (in press) [4] Wacker,J.F. et al.(1985) GCA 49, 1035-1048; Zadnik,M. G. et al.(1985) GCA 49, 1049-1059 [5] Matsuda et al.(1991) GCA 55, 2011-2023 [6] Gobel, R. et al.(1978) JGR 83, 855-866.

Table 1 Normalized releases, and isotopic and elemental ratios of noble gases from Y-74063 (unique). Data for bulk are given for comparison.

Pit No.	^{4}He[1]	^{36}Ar[1]	^{84}Kr[1]	^{132}Xe[1]	$^{3}He/^{4}He$	$^{40}Ar/^{36}Ar$	$^{36}Ar/^{132}Xe$	comments
14	57	4	44	140	0.002	9	30	silicate. 50 mg/p.
15	10	2	8	20	0.013	53	100	silicate(dusty)
16	6	0.1	b.b.[2]	4	0.022	0	20	silicate
17	3	b.b.	14	4	0.026	0	0	Fe-Ni
18	13	0.3	5	170	0.007	20	2	FeS
19	6	9	87	850	0.021	0	11	silicate(dusty)
20	6	1	18	21	0.016	140	50	FeS
21	5	0.2	6	4	0.020	250	50	FeS
22	10	1	b.b.	3	0.013	35	300	silicate
23	3	0.1	12	62	0.021	91	2	Fe-Ni
24	40	14	25	72	0.003	15	190	silic.boundary
25	19	0.2	b.b.	50	0.007	1080	4	reshot of pit 14
26	10	2	8	14	0.012	110	160	silicate
27	15	2	b.b.	12	0.008	140	130	silic.boundary
28	17	16	31	96	0.010	7.8	170	silicate(dusty)
29	5	0.2	2	15	0.017	500	13	FeS
bulk	27.0	1.46	55.3	66.5	0.00475	33.9	22	ref.[3]

1) Normalized release is defined by $NR(X)_j = C(^{3}He)[X]_j/[^{3}He]_j$, where $C(^{3}He)$, $[X]_j$ and $[^{3}He]_j$ are concentration of ^{3}He for silicate, metal and troilite, and amounts of noble gas X and ^{3}He released from pit j, respectively. The abundances are given in units of 10^{-6} and 10^{-9} cm^3/g for ^{4}He and ^{36}Ar, and ^{84}Kr and ^{132}Xe, respectively.

2) Below blank.

ORIGIN OF UREILITES BASED ON ALLENDE DARK INCLUSIONS

Yukio Ikeda, Department of Earth Sciences, Ibaraki University, Mito 310, JAPAN, and Martin Prinz, Department of Mineral Sciences, American Museum of Natural History, New York, NY, USA.

Introduction Ureilites are coarse-grained primitive achondrites with igneous textures consisting mainly of olivine, pigeonite, and carbonaceous materials (mainly graphite) with minor amounts of Fe-metal, cohenite, sulfide, augite, low-Ca pyroxene, and Si-Al-alkali glass. The oxygen isotopic compositions of ureilites overlap with those of the Allende dark inclusions, indicating that the ureilite parent body (UPB) accreted with isotopic and chemical heterogeneities which were not much modified by subsequent parent-body processes [1]. This favors models involving partial melting of primitive precursors.

Results Our model for the origin of ureilites is based on the assumption that the original precursors of ureilites were very-fine-grained materials similar to the dark inclusions and matrix in Allende. The precursors experienced varying degrees of reduction and partial melting by impact shock heating of the accretional bombardment near the surface of the UPB.

The average composition of several Allende dark inclusions (Table 1) was used as the original precursor. The compositions of the silicate residues were calculated using a phase diagram of the olivine-silica-plagioclase system with an MgO/(MgO+FeO) mole ratio of 0.7 and $An_{75}Ab_{25}$. Normative components of ilmenite, chromite, and phosphate were assumed to go into the silicate melts. The partition coefficients of MgO and FeO between silicate melts and silicate residues (olivine and pigeonite) was taken as 0.35, and the MnO/FeO ratio was assumed to be constant for the silicate melts and residues. The CaO molecules were partitioned between the normative pyroxene of the silicate melts and residual pigeonite using a coefficient of 0.25.

The results obtained by these calculations are shown in Fig. 1, where monomict ureilites are also plotted. As shown in Table 2, the ferroan group of ureilites (Haverö, Novo Urei, Kenna, etc.) were produced by 50-70% reduction of the FeO in the original precursor, the intermediate group (Dyalpur, Dingo Pup Donga, etc.) by 65-75% reduction, and the magnesian group (ALH82130, Y-74659, etc.) by 80-90% reduction. The partial melting degrees of the silicate portions range mainly from 35-60%, except for PCA82506 (20-30%) and ALH82130 (70-75%). Most of the carbon (about 1 wt%) of the original precursor remained as a graphite residue during the partial melting of the silicates. The total weights of the residues (including silicates, Fe-metal, and graphite) are about 40-50% of the original precursor, indicating that about half or more of the original material was lost as silicate and Fe-Ni-S melts during the formation of the ureilites. The missing silicate-melt components occur in some of the polymict ureilites, and the missing Fe-Ni-S-melt components may be IIC irons.

Discussion Several hypotheses for the origin of ureilites have been presented by numerous authors [2,3,4,5,6,7], although none can fully explain all of characteristics of ureilites [8]. The Mg/(Mg+Fe) ratios of ureilites range from 0.74-0.95, and the MnO contents are reversely correlated with the FeO contents, suggesting that ureilites were produced by reduction of ferroan precursors. The main argument is the nature of the reducing agent. If carbon was the reducing agent, the original precursors should have contained more than 5 wt%, because a large amount of CO gas species must have been lost from the source region during reduction. Such high-C precursors are not realistic. Therefore, we present a model, based on Allende dark inclusions, that the original ferroan precursors were reduced by an oxidized nebular gas which was trapped in the porous precursors and supplied from the UPB interior by a degassing process due to the UPB compaction. This model is able to explain most of the characteristics of ureilites.

References 1. Clayton R.N. and Mayeda T.K. (1988) GCA 52, 1313-1318. 2. Berkley J.L., Taylor G.J., Keil K., Harlow G.E., and Prinz M., GCA 44, 1579-1597. 3. Goodrich C.A., Jones J.H., and Berkley J.L., GCA 51, 2255-2273. 4. Takeda H. (1987), EPSL 81, 358-370. 5. Rubin A.E. (1988), Meteoritics 23, 333-337. 6. Warren P.H. and Kallemeyn G.W. (1989), Meteoritics 24, 233-246. 7. Scott E.R.D., Keil K., and Taylor G.J. (1992), LPS 23, 1253-1254. 8. Goodrich C.A. (1992), Meteoritics 27, 327-352.

Table 1. Chemical compositions of dark inclusions and matrix in Allende. "NiFe" is the taenite component containing Ni and Fe in equal amounts. "C", for the averages, is the carbon content. "Average" is normalized to 100% and has a normative composition of $An_{75}Ab_{25}$.

	Dark inclusions					Matrix			
	A	D	L	O	Average	B	F	K	Average
SiO_2	29.29	29.66	29.21	29.64	33.62	28.51	29.61	31.86	33.58
TiO_2	0.02	0.03	0.04	0.00	0.02	0.03	0.03	0.01	0.02
Al_2O_3	1.64	1.83	1.71	1.77	1.99	2.95	2.23	1.91	2.64
Cr_2O_3	0.34	0.24	0.43	0.31	0.38	0.32	0.33	0.34	0.37
FeO	30.13	30.45	26.55	27.27	32.65	32.44	27.98	28.16	33.07
MnO	0.22	0.25	0.22	0.22	0.26	0.16	0.20	0.21	0.21
MgO	16.88	19.14	17.23	17.30	20.14	18.59	16.61	17.09	19.52
CaO	2.84	2.17	3.16	3.40	3.30	0.67	3.31	4.50	3.17
Na_2O	0.10	0.29	0.12	0.10	0.17	0.58	0.24	0.27	0.40
K_2O	0.01	0.02	0.00	0.00	0.01	0.03	0.00	0.00	0.01
P_2O_5	0.25	0.27	0.34	0.43	0.36	0.14	0.23	0.31	0.26
FeS	3.71	1.90	3.82	3.35	3.65	2.17	3.53	2.96	3.24
NiFe	2.39	1.47	2.53	2.19	2.45	2.05	2.70	1.98	2.51
C					~1				~1
Total	87.82	87.72	85.36	85.98	100.00	88.64	87.00	89.60	100.00

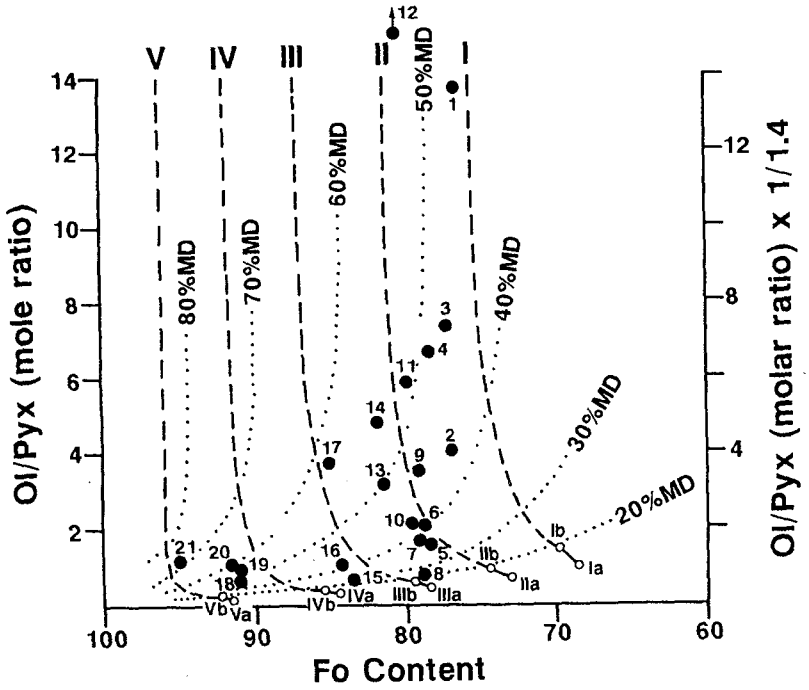

Fig. 1. Relationships between the residual olivine-pyroxene (Ol-Pyx) ratios and the forsterite (Fo) of residual olivine (dash-curves) are shown for five reduced precursors (cases I, II, III, IV, and V are 50, 60, 70, 80, and 90% reduction of the FeO content of the original precursor, respectively). Dotted curves show the partial melting degrees (MD) of the silicates. Filled circles with numbers are ureilites, and the numbers correspond to those in Table 2. Most of ureilites are plotted using the modal ratios (Goodrich, 1992) except for a ureilite with number 4 (Y-74123), which is the normative ratio calculated from the bulk composition (Takeda, 1987).

Table 2. Reduction degrees (Red.Deg.) and partial melting degrees (Mel.Deg.) of silicates estimated from Fig. 1 for monomict ureilites. Three subgroups (Berkley et al., 1980) are shown; subgroup 1 (high FeO, Fo_{74-81}), 2 (intermediate FeO, Fo_{83-86}), and 3 (low FeO, Fo_{91-95}). Ureilites with * have poikilitic textures (Goodrich, 1992).

No.	Ureilite	Red.Deg.	Mel.Deg.	FeO-subgroup
1	ALHA78019	50-55	45-50	1
2	Y-74130*	~55	40-45	1
3	META78008*	50-55	45-50	1
4	Y-74123	55-60	45-50	1
5	Goalpara	60-65	35-40	1
6	Kenna	~60	~40	1
7	Novo Urei	60-65	35-40	1
8	PCA82506	65-70	20-30	1
9	Havero	55-60	45-50	1
10	RC027	60-65	40-45	1
11	Y-790981	55-60	50-55	1
12	LEW86216	55-60	50-55	1
13	Y-82100	60-65	~50	1-2
14	ALH83014	60-65	50-55	1-2
15	Dingo Pup Donga	70-75	~30	2
16	Dyalpur	70-75	40-45	2
17	ALHA77257	65-70	55-60	2
18	Y-74659	~85	~50	3
19	Y-791538	80-85	~55	3
20	LEW88201	80-85	~60	3
21	ALH82130*	85-90	70-75	3

CHEMICAL COMPOSITION OF SIX AUBRITES.

Taro SHIMAOKA and Mitsuru EBIHARA
Department of Chemistry, Faculty of Science, Tokyo Metropolitan University, Hachioji, Tokyo 192-03, Japan.

Introduction

Aubrites (enstatite achondrite) are heterogeneous assemblages of nearly iron-free enstatite and a variety of rare minerals formed under highly reducing conditions (e.g. [1]). Based on mineralogical and chemical compositions (e.g. [1]) and oxygen isotope ratios ([1]), a number of authors suggested that aubrites were derived from known enstatite chondrites by igneous processes on the same parent bodies. In contrast, some authors suspected that aubrites were not produced from known enstatite chondrites on the same parent bodies and that they represent samples from a third enstatite chondrite-like parent body, mainly based on titanium fractionation in sulfides ([2,3]).

In order to contribute to the understanding of the origin of aubrites, we examined six aubrites (Bishopville, Cumberland Falls, Khor Temiki, Mayo Belwa, Norton County and Pena Blanca Spring), two enstatite chondrites (Happy Canyon and Ilafegh 004) and a mesosiderite (Mount Egerton). We report here the preliminary results of major, minor and trace elements determined by instrumental neutron activation analyses (INAA) for aubrites.

Experimental

The block samples were broken into fragments. A few fragments were used for preparation of polished sections and the residual fragments (~200 mg) were further pulverized. A part of each powdered sample (~40 mg) was used for INAA to determine the bulk chemical composition. Chemical compositions of major constituent minerals were determined with a scanning electron microscope equipped with an energy dispersive spectrometer (SEM-EDS).

Results and Discussion

Bulk chemical compositions of six aubrites are shown in Fig. 1. In this figure, lithophile elements are plotted at the left part, while siderophile and other non-lithophile elements are at the right. Elements in each part are ordered from left to right according to decreasing nebular condensation temperatures. Overall, lithophile elements in aubrites are almost comparable to CI-chondrite abundances, whereas siderophile and other non-lithophile elements except for Se in Khor Temiki are poor compared with those in CI-chondrites. These features are consistent with those for bulk compositions calculated with mineral compositions and modal compositions ([1]).

Bishopville, Mayo Belwa and Khor Temiki show relatively high abundances of Na and Al. These aubrites commonly have a positive Eu anomaly (Fig. 2). Such an anomaly can be explained by relatively high abundances of plagioclase (albite) in these aubrites. As shown in Fig. 2, Bishopville has a light rare earths (LREE) -enriched pattern while LREE in other aubrites are only slightly enriched or rather depleted. As shown in Fig. 3, aubrites are mineral assemblages of enstatite and other rare minerals (e.g. albite, Fe-Ni metal, pentlandite and oldhamite). Although oldhamite, the major REE host in enstatite chondrite ([4]), can be a good candidate for the aubrites as well ([5]), some other phases enriched in heavy REE must be exist.

Our data suggest that Fe-Ni metal and oldhamite had been removed from the enstatite chondrite-like materials by various degree of melting through igneous processes and that various REE patterns were produced rather locally. REE analyses on both oldhamites and silicate fractions separated from aubrites seem to be promising to obtain more conclusive results and are now in progress.

References

1. WATTERS, T. R. and PRINZ, M. (1979) *Proc. LPSC* **10**, 1073-1093.
2. BRETT, R. and KEIL, K. (1986/87) *EPSL* **81**, 1-6.
3. KEIL, K. (1989) *Meteoritics* **24**, 195-208.

4. LUNDBERG, L. and CROZAZ, C. (1988) *Meteoritics* **23**, 285-286.
5. STRAIT, M. M. (1985) *LPSC* **16**, 830-831.

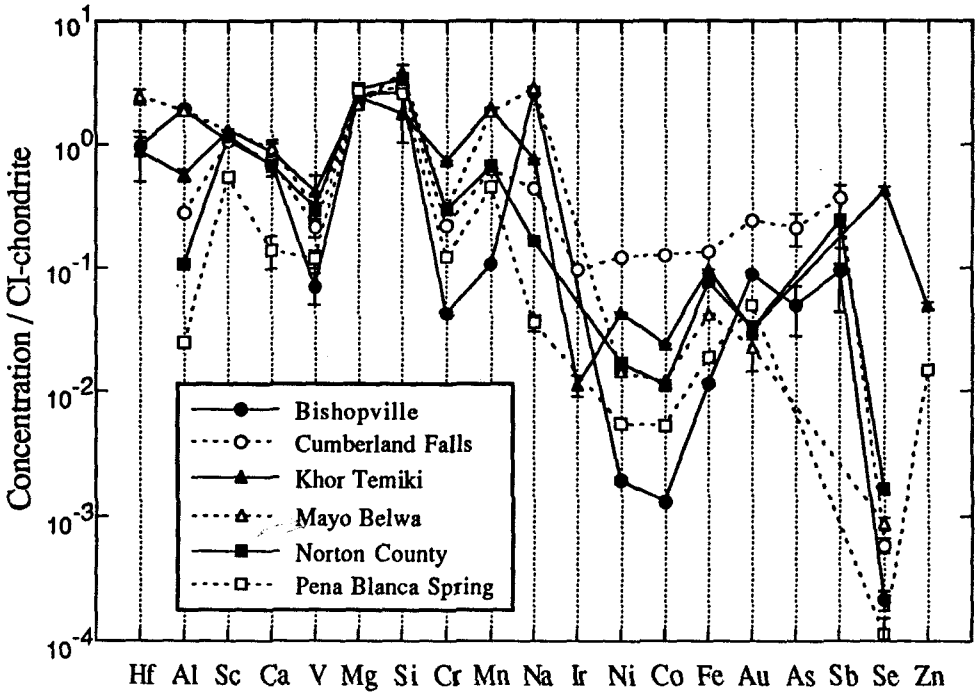

Fig. 1. Elemental abundances of six aubrites relative to CI-chondrite abundances.

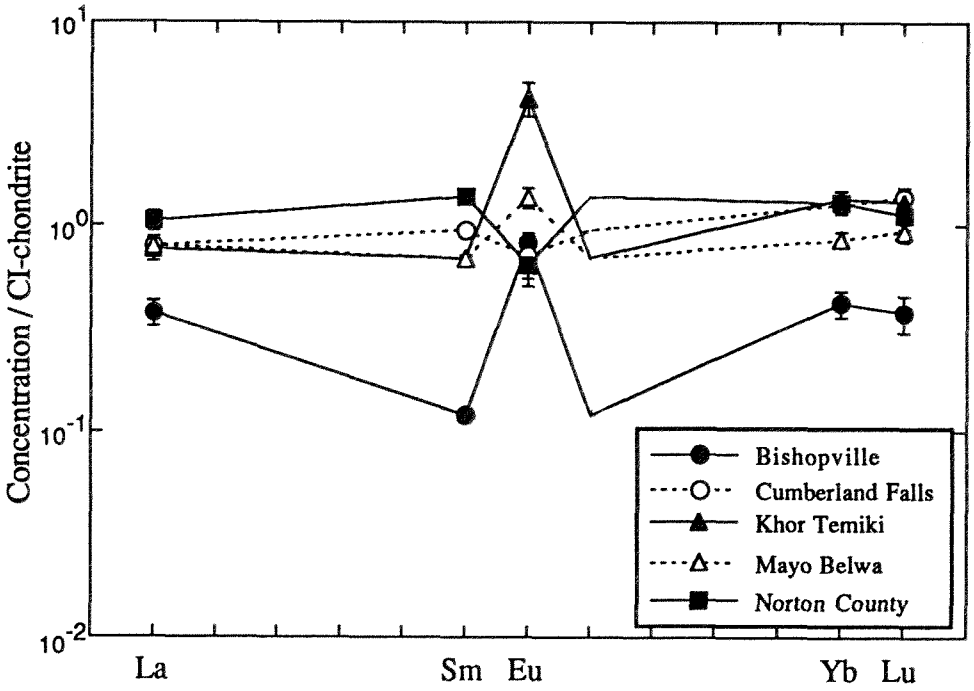

Fig.2. REE concentration in six aubrites relative to CI-chondrite.

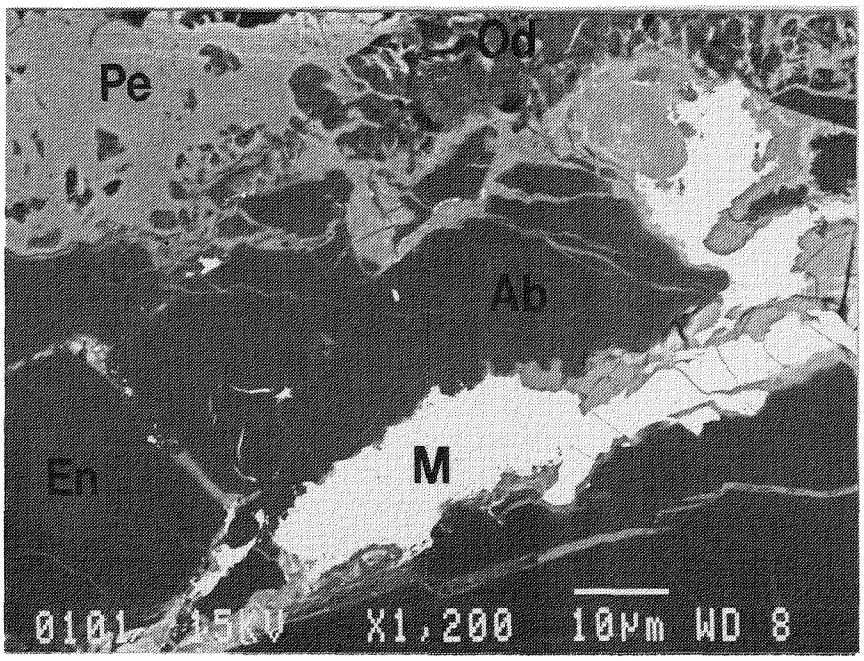

Fig. 3. SEM back scattered electron image (BEI) of mineral assemblage in Bishopville. (En : enstatite ; Ab : albite ; M : Fe-Ni metal ; Pe : pentlandite ; Od : oldhamite)

TWO MAJOR DYNAMIC FORMATION PROCESSES OF SHOCKED GRAPHITE AND QUARTZ

Yasunori MIURA[1], Yuichiro NOMA[1], Makoto OKAMOTO[2] and O.G.IANCU[1]
[1]Faculty of Science, Yamaguchi University, Yoshida, Yamaguchi 753, Japan.
[2]Faculty of Science, Okayama University, Tsushimanaka, Okayama 700, Japan.

High-pressure type carbon and silica minerals are considered to be formed by solid (liquid)-solid transformation under static or dynamic (impact) high-pressure. But it is difficult to explain static recrystallization process in shocked texture and materials of meteoritic craters and meteorites. Miura (1992) reported that shocked quartz aggregates of impact craters, meteorites and the K/T boundary samples are formed by quenched accretion of various aggregates by dynamic impact process. But two major differences in composition are observed in shocked carbon or shocked silica minerals; that is, only carbon (or silica) or mixture of Fe-Ni metals from iron meteorite. The main purpose of the present study is to elucidate the two major dynamic formation processes of shock metamorphism from compositional, structural and textural data.

I. New shocked graphites from the Barringer crater

Diamond has been reported from the Barringer crater as cliftonite (Foote, 1891) and hexagonal diamond (lonsdaleite, by Hannemann et al., 1967), though these data are based mainly on optical or powder (camera) data. Recently shocked quartz and shocked graphite (with fine size, high density, and mixture with fine amorphous glasses) are reported from the Barringer crater(cf. Miura, 1991). The detailed characterization of shocked materials is required to explain two different shocked materials under dynamic formation processes.

I-1. Samples: Graphite nodule of the Barringer crater used in this study is considered to be one of the evaporated sample collected near at north-east rim. The samples are compared with graphite standard samples from Korea, Kagoshima and Madagascar, and artificial impact graphites.

I-2. Experimental methods: X-ray calculated density has been determined by X-ray diffractometer as following equation: $\Delta\rho(\%)=100\cdot\{(\rho-\rho_0)/\rho_0\}$, where standard density ρ_0 is 2.255 g/cm^3 in Korean graphite. Single sample data are checked from the strongest X-ray peaks by micro X-ray diffractometer and 4-axes X-ray diffractometer. Chemical compositions of shocked materials have been obtained by analytical-electron microscopy (AEM).

I-3: Optical observation: There are four different mineral-aggregates of the Barringer graphite nodule sample. (a) Shocked graphite-1 (with Fe) in the matrix (b) Shocked graphite-2 (with kamacite, cliftonite and hexagonal diamond) in vein metal, (c) shocked quartz-1 (with kamacite) in the rim, and (d) calcite in the rim. These shocked aggregates indicate dynamic accretion process of three different aggregates.

I-4. X-ray diffraction data: X-ray diffraction peaks of shocked graphites reveal that (a) low X-ray intensity (abrupt stopping of reaction), (b) high Bragg-angle shift of X-ray diffraction peak (high X-ray density), and (c) mutiple splitting of X-ray diffraction peaks (aggregates of quenched materials).

I-5. X-ray density data: High density values of shocked graphite are obtained in the Barringer graphite ($\Delta\rho=+1.1\pm0.4\%$ and $+0.6\pm0.1\%$; Table 1). Shocked chaoite of hexagonal diamonds shows high vaule of $\Delta\rho=+0.6\pm0.9\%$ (Table 2).

I-6. Compositions of two shocked graphites: AEM data reveal the four different aggregates of the graphite nodule samples as follows (Fig.1, Table 3):

(a) Shocked graphite-1 in the matrix: Black shocked graphites contain uniformly Fe (from kamacite) and trace of Ca (from Kaibab limestone) which are formed under mixed gas state.

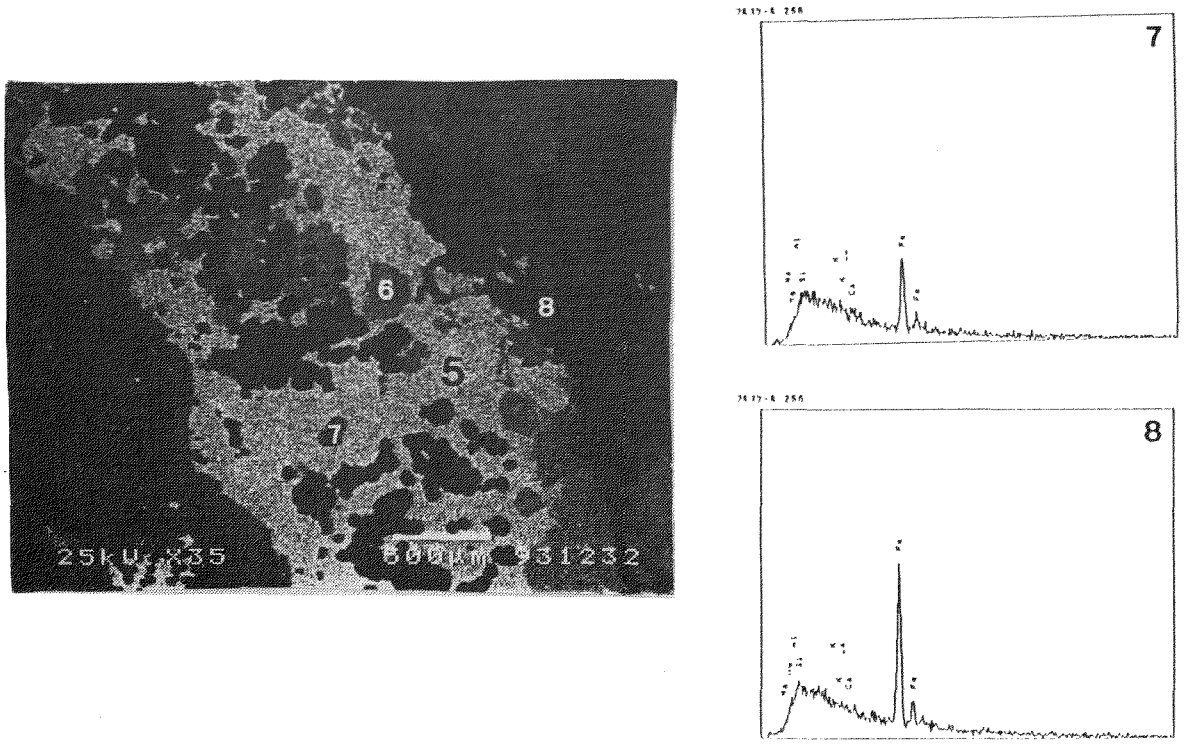

Fig.1. BEI microphotograph and EDX spectra of shocked graphite-1 (No.8) with chaoite (No.7) in kamacite (No.5) vein of the Barringer crater.

Table 1. X-ray data of standard and shocked graphites.

Sample Name	a(Å)	c(Å)	Vol. (Å^3)	ρ (g/cm^3)	$\Delta\rho$ (%)	I (002)
Standard graphite:						
Sri Lanka	2.464(1)	6.725(1)	35.38(1)	2.255(1)	standard	- (ASTM)
Korea	2.466(1)	6.715(2)	35.37(3)	2.255(2)	0.0(1)	33033
Shocked graphite:						
Barringer	2.458(5)	6.688(10)	35.00(16)	2.279(10)	+1.1(4)	430

Table 2. Density data of shocked graphite and hexagonal diamond (chaoite) in the Barringer crater.

Sample Name	a(Å)	c(Å)	Vol. (Å^3)	ρ (g/cm^3)	$\Delta\rho$ (%)
Shocked graphite (single crystal data)					
SG-2	2.459(1)	6.719(4)	35.17(3)	2.268(2)	+0.6(1)
Shocked chaoite (single crystal data)					
SC-2	8.93(4)	14.06(8)	970.6(99)	3.45(3)	+0.6(9)

(b) Shocked graphite-2 in vein metal: Crystallized shocked graphites and shocked hexagonal diamonds (chaoite) are surrounded by kamacite-rich metal under

gas states of various compositions from iron meteorite, sandstones and limestone. Aggregates with chlorine or sulfur are coexisted with the kamacite-vein.

(c) Shocked quartz-1 and kamacite in the rim: Kamacite-rich metal contains elements from Kaibab limestone, and shocked quartz (mainly from Coconino sandstone). Shocked quartz-1 grains with high density contain Fe and Ca.

(d) Limestone in the rim: Calcites from Kaibab limestone are only fixed without melt after hitting to the surface from the original graphite aggregates.

Table 3. AEM data of kamacite and shocked quartz grains of the Barringer crater.

Oxides/ Elements	Kamacite-1 (in original meteorite)	Kamacite-2 (in rim of graphite nodule)	Shocked quartz-2 (in rim of graphite nodule)	Kamacite-5 (in mass vein)	Kamacite-6 (in center of vein)
SiO_2	-	14.15	96.71	5.47	9.45
CaO	-	2.24	0.00	0.00	2.05
FeO	-	-	1.15	-	-
NiO	-	-	0.05	-	-
Fe	92.54	80.24	-	87.74	81.53
Ni	7.46	3.37	-	6.79	6.01
Cl_2	-	-	-	-	0.96
Total	100.00	100.00	100.00	100.00	100.00

II. Shocked graphites formed by impact experiments

Shocked graphites formed by artificial impact experiments (2.9km/s and 1.3g) show fine-grained and high-density ($\Delta\rho$=+0.7%), which are easily checked by high Bragg-angle shift as shown in Table 4 and Fig. 2.

Table 4. X-ray density data of shocked graphites in artificial impact runs.

Target rocks	a(Å)	c(Å)	Vol.(Å^3)	ρ (g/cm^3)	$\Delta\rho$ (%)	I (002)
Run-AG1	2.455(3)	6.722(13)	35.11(10)	2.272(7)	+0.7(3)	1068
Run-G1	2.462(2)	6.697(4)	35.16(6)	2.269(4)	+0.6(1)	3592
Run-G2	2.461(2)	6.693(4)	35.12(6)	2.271(4)	+0.7(1)	4709

III. New shocked quartz aggregates in the Barringer crater

The previous shocked quartz reported by Miura (1991) is mixture of silica glass with composition of SiO_2=100(wt.%) (cf. Table 5). Thus, there are two types of (1) shocked quartz-1 (which composition is 97wt% SiO_2, 3%Fe/Ni, trace Ca, and found in graphite-nodule near at the rim) of mixture from the sandstone, iron meteorite and Kaibab limestone, and (2) shocked quartz-2 (which is pure SiO_2, and found in fine-grained ejecta at the rim) of origin of Coconino sandstone.

IV. Dynamic formation process of shocked graphite and quartz

Shocked graphites and hexagonal diamond (chaoite or lonsdaleite) have been found in this study. The compositions of two type shocked graphites indicate that there are two formation stages of shocked graphites. The first shocked graphite aggregates-1 has been formed from gas-state of C, Fe and Ca under the highest pressure and temperature condition. Fe,Ni,Ca-bearing shocked quartz aggregates-1 was formed at the same formation stage as the shocked graphite-1. The second shocked graphite aggregates-2 has been formed from gas-melt states of C, Fe, Ni, Ca, and Si.

Origin of carbon of shocked graphites is considered to be Kaibab limestone. This is mainly because shocked graphites contain inclusions from the target rocks of Kaibab limestone and Coconino sandstone.

Table 5. AEM data of shocked quartz of the Barringer crater.

Oxides	Shocked quartz-2 (in rim of graphite nodule)	Shocked quartz-1 (in rim of crater; Miura, 1991)
SiO_2	96.71	100.00
CaO	0.00	0.00
FeO	1.15	-
NiO	0.05	-
Total	100.00	100.00

IV. Summary

High density of fine-grained shocked graphite and quartz aggregates formed by natural shock metamorphism has been found in the Barringer meteorite crater, and confirmed by artificial impact craters.

Shocked graphites formed by artificial impact crater experiment show similar high density (density-deviation=+0.7%) to that of natural Barringer meteorite crater.

Shocked hexagonal diamonds formed by impact experiments are determined by microarea X-ray diffraction which is almost difficult to detect shocked diamond due to mix amorphous carbon.

It is considered that shocked graphite, hexagonal diamond (chaoite) and quartz can be formed under dynamic processes of quenching and rapid depression.

References

Foote A.E. (1891): A new locality for meteoritic iron with a preliminary notice of dicovery of diamonds in the iron. American Journal of Science, 42, 413-417.

Hannemann R.E, Strong H.M. and Bundy F.P. (1967) : Hexagonal diamonds in meteorites and their implications. Science, 155, 995-997.

Miura,Y. (1991) : Evidence for shock wave effect of meteoritic impact. Shock Waves (Springer-Verlag), 1, 35-41.

Miura Y. (1992): Shock metamorphic crystals in meteorites. Proc. Shock Waves (Japan), 2, 54-57.

SHOCK FORMATION OF KEROGEN-LIKE ORGANIC MATTER IN CARBONACEOUS CHONDRITES FROM GRAPHITE

Tatsushi Murae
Department of Earth and Planetary Sciences, Faculty of Science, Kyusyu University, Hakozaki, Fukuoka, 812 Japan

Introduction Although existence of several carbon phases in carbonaceous chondrites has been shown[1], kerogen-like organic matter (poorly characterized macromolecular organic compounds) may account for from about 70 percent to essentially all of the meteoritic carbon[1-3]. Despite the importance of the kerogen-like organic matter as a noble-gas carrier[4] and as a product possibly formed at the outside of solar nebula[5], the structure and the formation process of this material are still in controversy. In this paper the author reports shock formation of the kerogen-like organic matter from graphite by collision experiments of graphite using a high-speed rail-gun

Experiments The high-speed rail-gun system at the institute of space and astronautical science was used in this investigation. Commercial powdered graphite (200 mesh, 99%) was used as starting material. The graphite was tightly packed in a steel vessel which was set up as a target of the rail-gun. A polycarbonate projectile (0.97g) was shot toward the target. The speed of the projectile just before collision was 7.27 km/sec. After the shock experiment, the carbonaceous matter in the steel vessel was taken out by careful shaving of the vessel. The IR spectra were obtained using a FT-IR microscope by the same method as mentioned before[6]. The x-ray diffraction patterns were determined using a small sample sticked on an edge of a fine glass needle.

Results and discussions Figure 1 shows the X-ray diffraction of (a) graphite used as starting material, (b) carbonaceous matter recovered after shock experiments, and (c) an acid-resistant carbonaceous residue from ALH-77307(C3). These patterns indicate that the starting graphite is highly ordered, and the structure of shocked sample is almost amorphous like as the meteoritic carbon. Although the shocked graphite contains small amount of poorly ordered graphite, the meteoritic carbon graphite contains spinel and iron oxide instead of graphite.

Figure 2 indicates IR spectra of (a) the graphite before shock experiments (b) the carbonaceous matter recovered after shock experiments (c) the acid-resistant residue from ALH-77307. The IR absorption bands of recovered carbonaceous matter (b) are very different from those of graphite (a) used for the shock experiments. This fact means that the highly ordered graphitic structure was broken by the shock to form many edge defects in the graphitic structure. The increase of the number of edge defects is observed as the enhancement of the intensity of absorption bands due to aromatic functional groups (1600, 1328, and 1280 cm-1). The IR-spectral feature of the shock-formed carbonaceous matter (b) is almost the same with that of the meteoritic carbon (c). This fact proves the author's proposal that the major organic matter in carbonaceous chondrites has the graphite-like condensed polyaromatic structure bearing remarkable number of edge defects[7]. The findings in this investigation afford a new scenario for the formation of carbonaceous matter in carbonaceous chondrites.

References

1. Ming, T., Anders, E., Hoppe, P. & Zinner, E. *Nature* 339, 351-354 (1989).
2. Hayes, J.M. *Geochim. Cosmochim. Acta* 31, 1395-1440 (1967).
3. Han, J., Simoneit, B.R., Burlingame, A.C., & Calvin, M. *Nature* 222, 364-365 (1969).
4. Lewis, R.S., Srinivasan, B., & Anders, E. *Science*, 190, 1251-1262 (1975).
5. Kerridge, J.F., Chang, S., & Shipp, R. *Geochim. Cosmochim. Acta*, 51, 2527-2540 (1987).
6. Murae, T. *Abst. 17th Symp. Antarct. Meteorites*, 63 (1992).
7. Murae, T., Masuda, A, and Takahashi, T. *Mem. Natl. Inst. Polar Res., Spec. Issue*, 46, 196-204 (1987).

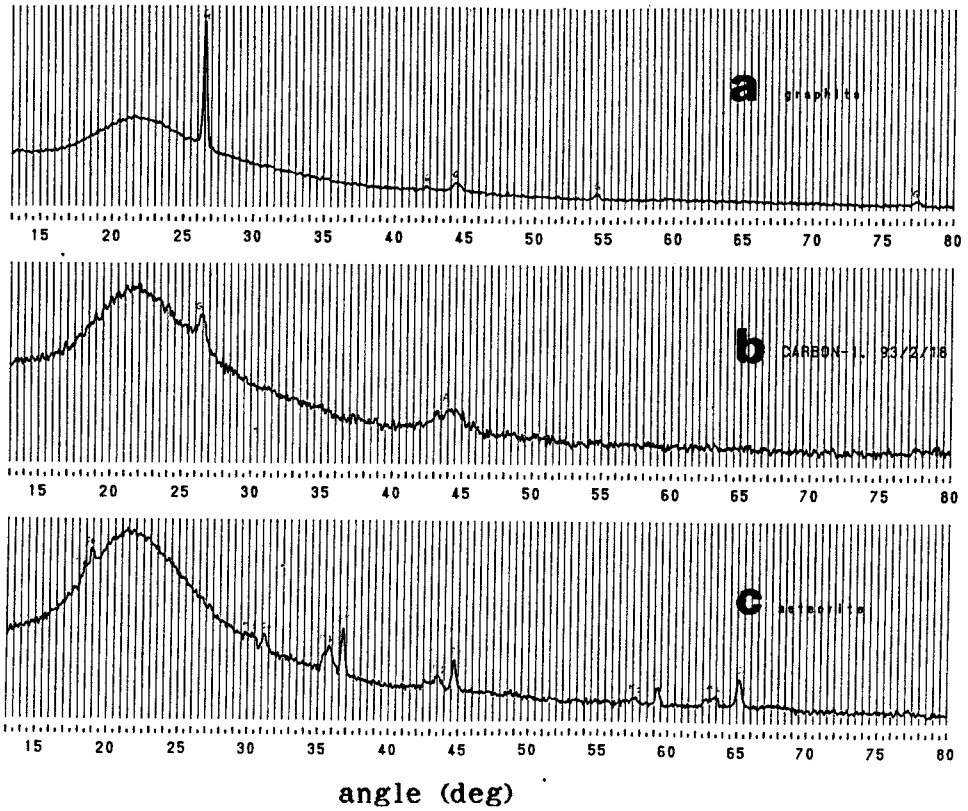

Fig. 1 X-ray diffraction for (a) graphite before the collision, (b) recovered carbonaceous matter after the collision, and (c) acid-resistant residue from carbonaceous chondrites. Camera type: Debye (9cm), Wave: Cu-Kα.

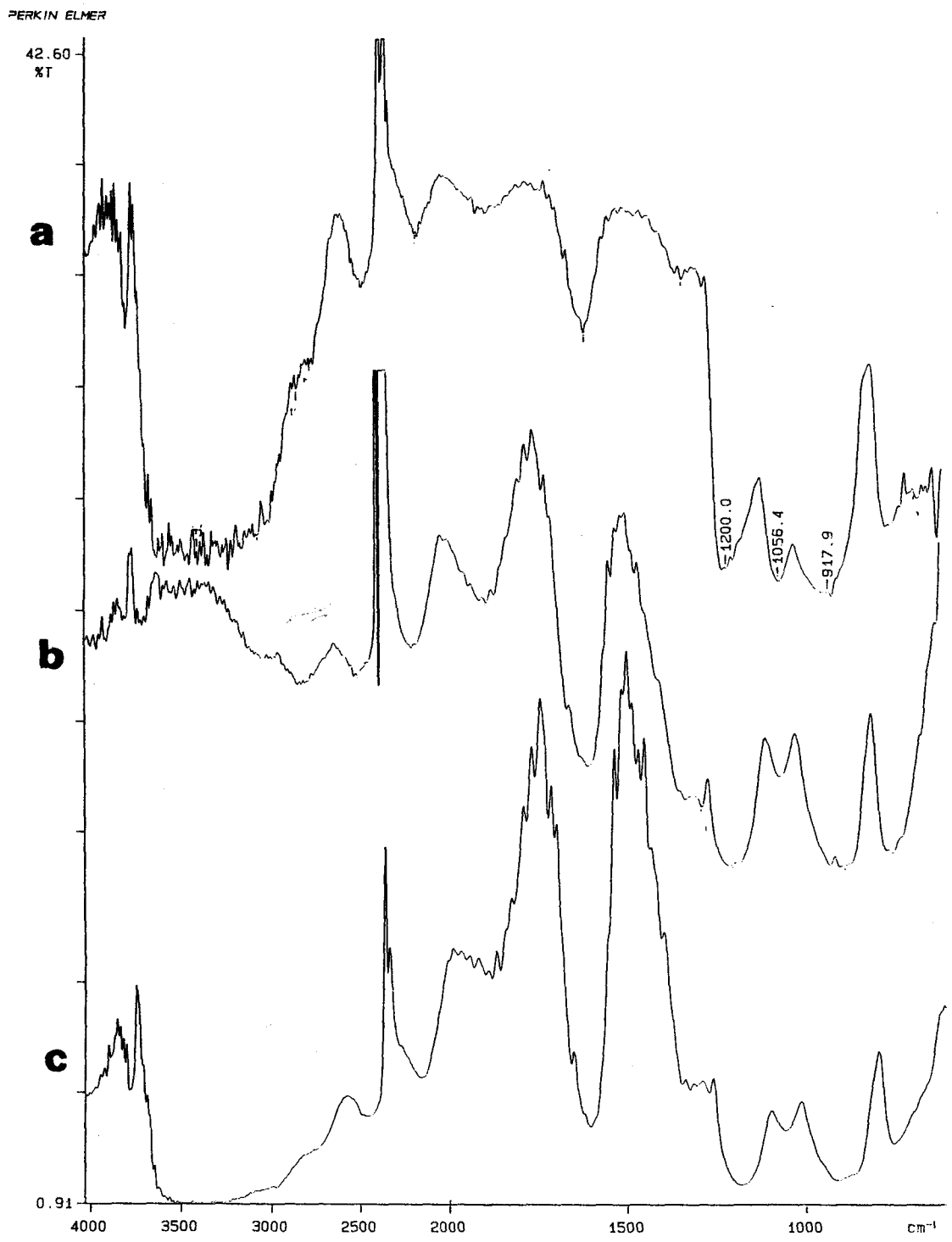

Fig. 2 IR spectra for (a) graphite before the collision, (b) recovered carbonaceous matter after the collision, (c) acid-resistant residues of carbonaceous chondrite. Obtained by Perkin Elmer FT-IR attached with Spectra-Tech microscope. Absorption spectra were obtained by reflection mode.

Special Session

Unique Inclusions in Ordinary Chondrites

GENERAL FEATURES OF SOME UNIQUE INCLUSIONS IN YAMATO ORDINARY CHONDRITES; **Keizo Yanai** and **Hideyasu Kojima**, National Institute of Polar Research (NIPR), 9-10, Kaga 1-chome, Itabashi-ku, Tokyo 173 Japan

Introduction: Several unique inclusions were identified in the ordinary chondrites of NIPR meteorites collections from Antarctica. Three of them are being studied as the international consortium studies for approaching their genesis. Three chondrites; Yamato-75097, Yamato-793241 and Yamato-794046 are provided for this studies, and samples have been chipped from both of the host parts and inclusions of each chondrites in the NIPR.

Yamato-75097: L6 chondrite, 2570 g(Fig. 1a).

Yamato-75097 is a nearly complete, subangular stone with a thin blackish brown to dull black fusion crust. The stone contains several lithic inclusions with shiny-black fusion crust. The fusion crusts of the inclusions are clearly distinguished from those of the host part. The largest of these inclusion was selected for this study. The inclusion is angular shape, 2.5x2.5 cms, with shiny-black fusion crust which similar to those of some achondrites.

Host: Petrographically, Y-75097 contains a chondritic structure, but chondrules and chondrule fragments show extensive integration with the granular groundmass which consists of olivine and pyroxene with minor amounts of plagioclase, merrilite, nickel-iron and troilite. Chondrule types include granular olivine and olivine-pyroxene, barred olivine and weakly radial pyroxence. The stone is traversed by thin black veinlets probably produced by shock. The meteorite appears to be mainly unweathered.

The compositions of the olivine and orthopyroxene are; average Fo75.8(range Fo74.7-77.0, % M.D.=1.5) and En78.1Fs20.1Wo1.7 (range En76.8-79.4Fs19.3-21.5Wo1.3-2.1, % M.D.=2.2) respectively. The composition of clinopyroxene is En48.7Fs8.0Wo43.3.

Inclusion: Megascopically, the inclusion appears light gray and consists of a fine-grained aggregate with a relatively coarse-grained aggregate in the core. Microscopically, the inclusion is a fine-grained aggregate consisting mostly of olivine with minor merrillite and plagioclase; opaques are rare

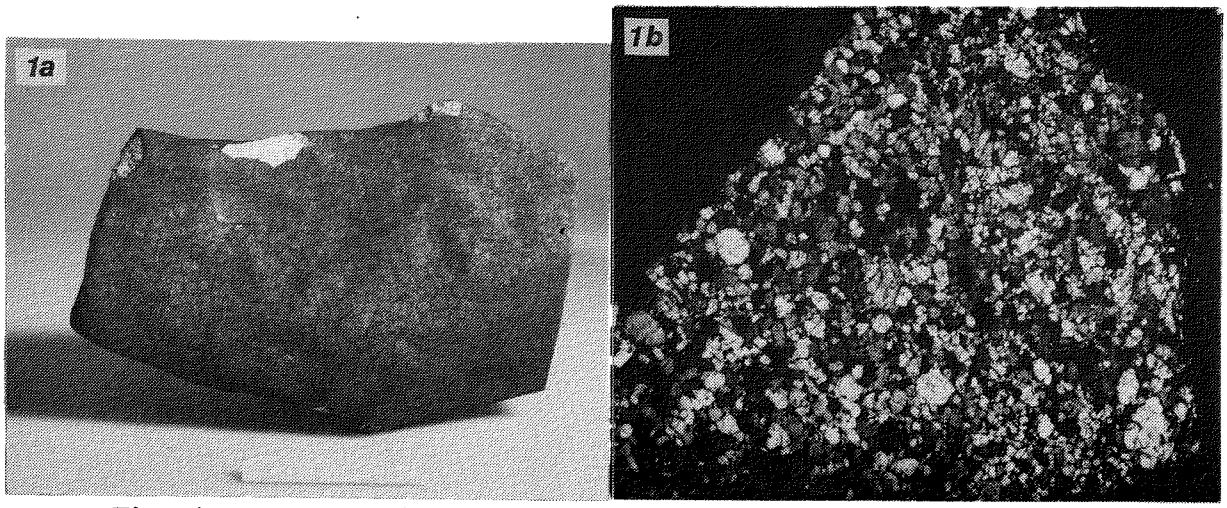

Fig. 1a: Yamato-75097, L6 chondrite and 1b: photomicrograph of the thin section of the inclusion, 6.1 mm wide.

(Fig. 1b). It shows a possible cumulate texture. The mineral assemblage and texture of the inclusion are similar to those of the Brachina meteorite. However, there are some extreme differences in their occurrences, and a little difference chemically and mineralogically. Plagioclase is isotropic and is presumably maskelynite. Pyroxene, nickel-iron and troilite were not identified. The texture is dominated by subhedral to anhedral olivine, but there is some variety in the texture. In the relatively coarse part the texture is dominated by subhedral olivine with interstitial merrillite and plagioclase. However, in the fine-grained part the texture is dominated by granular olivine (relatively coarse) and fine-grained olivine with a trace of merrillite, and plagioclase is found interstitially among them. Largely olivine was elongate and seakly orientated. Some veinlets in the section were recognized.

Olivine is compositionally homogeneous and relatively Mg-rich, Fo75.8, compared with Brachina. The range is Fo75.0-76.5, % M.D.=1.1. The olivine composition is very similar to that of the host chondrite. Plagioclase is anhedral, and appears as interstitial grains between olivine grains. In the core, plagioclase is less abundant than merrillite, but in the mantle part plagioclase is more abundant attaining to about 10%. It occurs between olivine grains, and some plagioclase encloses olivine grains poikiliticaly. Most plagioclase is isotropic and is maskelynite. The plagioclase is albite-rich, An15Ab75Or10. Merrillite is anhedral and occurs as interstitial grains(0.2-0.3 mm) among olivine grains similar to plagioclase; some encloses olivine poikiliticaly. Chromite is a trace mineral in the inclusion and appears as subhedral grains, 0.2-0.3 mm in diameter.

Yamato-793241: L6 chondrite, 938 g.

This ordinary chondrite is almost half of original, about 30% fusion crust (dark brown to dull black) partly fructured and moderatly weathered. The broken interior surface shows hight grey with brown spots, possible metal grains and numerous exposed chondrules up to one millimeter in diameter. Relatively large bolder-like inclusion(clast) reveals itself on the other

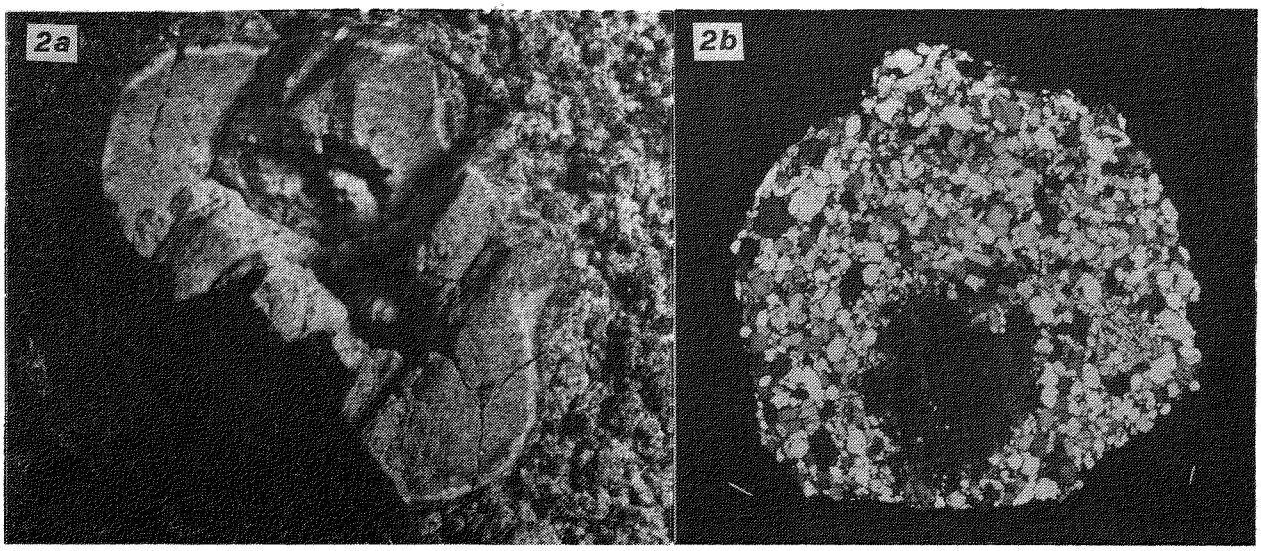

Fig. 2a: Yamato-793241, L6 chondrite and 2b: photomicrograph of the thin section of the chondrule bearing inclusion, 6.9 mm wide.

side of the meteorite(Fig. 2a). The inclusion can be easily distingish from the host for its quite unique lithology that is more light gray in color, very fine-grained with no chondrules, and no or traced opaques(metal and troilite). It is about 3x3 cms, egg-shaped, and consists of three different lithologies as the white core (relatively coarse-grained), light gray mantle (fine-grained) and an almost white rim (about 1 mm thick, very fine-grained).

Host: Petrographically, Y-793241 contains a chondritic texture, but chondrules and chondrule fragments integrated with the granular matrix, which consists of olivine and pyroxene with plagioclase, nickel-iron and troilite. The compositions of the olivine and orthpyroxene are: average Fo75.4 (range Fo74.5-76.5, %M.D.= 1.6 and Fs20.4 (range Fs19.4-21.3, %M.D.= 2.1) respectively. This chondrite is classified as an L6.

Inclusion: Petrographically, the inclusion consists mostly of a fine-grained and a close packed aggragate of subrounded olivine (about 0.1 mm across) and interstitial plagioclase. The inclusion is depleted in metal and troilite in comparison with normal L-group chondrite. The compositions of the olivine and plagioclase are: average Fo75.7 (range Fo74.8-77.0. %M.D.= 1.4), and range An10.7-17.2 in rim, and An15.1-30.6 in core respectively. Plagioclase is more Ca-rich in core them those in rim.

One chondrule has been found from the tiny chip of the inclusion core (Fig. 2b). This show clearly barred olivine chondrule texture, up to 1.3 mm across mantled by the fine granular olivine aggragates. But the chondrule integrated with the mantle. The chondrule consists mostly of olivine with traced plagioclase (complstely maskerynite) and chromite. The composition of olivine of chondrules is almost same as that of the olivine in the mantle. Olivine is Fo75.3 (range Fo74.5-76.0) and plagioclase is An28.5-32.2Or1.9-2.5.

Yamato-794046: H4 chondrite, 206 g.

Y-794046 was recovered as an almost half stone after fall and covered near half of whole specimen with dark brown-dull black fusion crust. The specimen was deeply weathered and distingished an intensive oxidigation by brown stains of the broken interior surface. The fine-grained interior showing light grey in color can be easily distingish from the deeply weathered host portion by the difference of weathering degree(Fig. 3a). The fine-grained part is so-called "inclusion", and it has quite differenteial lithology from the host. The inclusion is 3x4 cms in diameter and shows fresh interior of white to light gray with pale brown stain on the broken interior surface.

Host: Petrographically, Y-794046 shows a chondritic structure, but chondrules and chondrule fragments slightly integrated with the granular matrix. Chondrule types include granular olivine, barred olivine and radial pyroxene. It consists mainly of olivine, pyroxene and metal with troilite and traced merrillite. The compositions of the olivine and pyroxene are: average Fo81.5 (range Fo80.5-82.5, %M.D.= 1.6) and average Fs16.2 (range Fs14.9-18.6). This chondrite is classified as an H4.

Inclusion: Petrographically, the inclusion consists of an aggragate of euhedral-subhedral and equigranular olivine crystals(0.1-0.2 mm), brown pyroxene and twined coarse orthpyroxene laths (up to 2 mm) with glassy groundmass, and traced metal and troilite (Fig. 3b). Some of olivine and

pyroxene grains are included in the large orthopyroxene. No chondrules or relic chondrules are visible. The compositions of olivine and pyroxene are: average Fo80.6 (range Fo79.6-81.8, %M.D.= 2.5), Fs14.7 (range Fs12.7-16.4, %M.D.= 4.9) and clinopyroxene En58.3Fs10.9 Wo30.8.

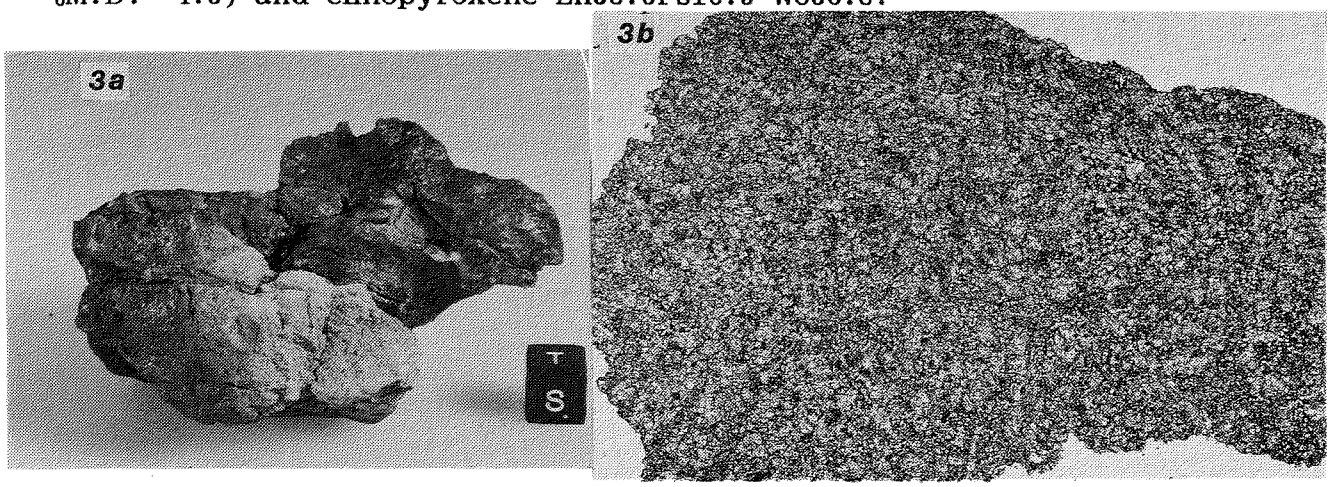

Fig. 3a: Yamato-794046, H4 chondrite and 3b: photomicrograph of the thin section of the inclusion, 10 mm wide.

The major-element composition of the chondrite hosts and inclusions was determained by standard wet chemical analysis by H. Haramura. The results are presented in Table 1.

Table 1 Major-element chemical analyses of chondrite and inclusion in the Yamato ordinary chondrites in weight percent.

	Host		"Inclusion"		
	Y-75097 (L6)	Y-793241 (L6)	Y-75097	Y-793241	Y-794046
SiO_2	39.71	38.63	39.13	38.92	46.14
TiO_2	0.21	0.07	0.09	0.08	0.11
Al_2O_3	2.60	2.44	2.49	2.71	3.01
Fe_2O_3		0	1.26	1.01	-
FeO	15.77	15.04	19.41	19.82	13.71
MnO	0.34	0.33	0.38	0.39	0.38
MgO	26.03	25.66	33.96	34.35	31.83
CaO	1.82	1.86	0.65	0.45	2.02
Na_2O	0.95	0.93	1.00	1.07	1.16
K_2O	0.08	0.11	0.05	0.06	0.15
$H_2O(-)$	0.02	0.0	0.00	0.00	0.10
$H_2O(+)$	0.0	0.2	0.09	0.21	0.38
P_2O_5	0.26	0.21	0.36	0.15	0.06
Cr_2O_3	0.58	0.54	0.97	0.58	0.66
FeS	5.94	6.34			0.25
Fe	4.88	7.05			
Ni	0.73	0.81	236(ppm)	296(ppm)	0.06
Co	0.008	0.053	<30(ppm)	<30(ppm)	< 30(ppm)
NiO	0.59				
Total	100.52	100.27	99.84	99.80	100.02

Analyst: H. Haramura

CONSORTIUM STUDY OF THREE INCLUSIONS IN YAMATO ORDINARY CHONDRITES: a progress report

Noboru Nakamura[1], Robert Hutchison[2], Keizo Yanai[3], Noritoshi Morikawa[1] and Osamu Okano[4]
[1]Department of Earth and Planetary Sciences, Kobe University, Kobe 657, [2]Mineralogy Department, The Natural History Museum, London, [3]Natl. Inst. Polar Res., Tokyo 173, [4]Department of Geosciences, Okayama University, Okayama 700.

Three large igneous-like inclusions were identified in Yamato (Y) ordinary chondrites, Y-75097 (L6), Y-793241 (L6) and Y-794046 (H)[1]. According to preliminary studies [2-4], the inclusions in Y-75097 and Y-793241 have unique chemical and petrographic features. In order to obtain evidence of their origins, a (mini) consortium study on inclusions in Antarctic ordinary chondrites has started. Here presented a progress report of a part of the study.

Brief petrographic descriptions:
Y-75097: A dunitic inclusion lies within an L6 host. The host is heavily shocked. Shock veins of green/dark brown isotropic glass run within the inclusion. The inclusion is composed of euhedral to subhedral olivines with homogeneous composition ($Fa_{24.8}$), plagioclase (An_{12-19}) (now maskelynite), minor chromite and chlorapatite/and merrillite. The olivine Fa composition is indistinguishable from that in the host. Crystals are commonly fractured. Phosphates are unevenly distributed, being completely absent in most of inclusion but comprising ~10Vol% of the coarse area.
Y-793241: A dunitic inclusion lies within an L6 host. Both are unshocked. An acuate, granular textured zone, 200x500μm wide, separates host from inclusion. More than 4 mm from the host, the texture again coarsens as the minimum grain-size of the olivine increases to about 100um. Olivine is $Fa_{24.7}$, within experimental error of that in the host, $Fa_{25.2}$. Anhedral chromites and plagioclase (An_{12-19}) fill the interstices. Metal is extremely rare. Pyroxene and phosphate are completely absent from the inclusion in this section.
Y-794046: A harzburgitic inclusion is associated with an H5 host. The inclusion comprises abundant anhedral olivines 25-150μm in size, commonly in granular clusters. The olivines are enclosed within poikilitic plates of twinned, low-Ca pyroxene with augite rims. A few large low-Ca pyroxenes have cores with abundant polysynthetic twins and numerous fractures. The cores probably were protopyroxene that co-precipitated with olivine before the poikilitic pyroxene crystallised. The interstices are irregular and filled with turbid, grey-green to brown microcrystalline plagioclase (devitrified maskelynite?). A few granular areas (60μm) probably represent recrystallised melt-pockets. Host and inclusion are not in equilibrium. In the host, olivine (Fa_{19}) is less Fe-rich and the pyroxene ($Fs_{17.5}$) more Fe-rich than those in the inclusion ($Fa_{20.5}$ and $Fs_{14-16.5}$). The alkali compositions of plagioclase are variable with An_{3-5},Ab_{81-95},Or_{0-16}. The inclusion probably formed slow crystallization from high temperature, followed by rapid cooling and /or reheating and quenched.

Oxygen isotopic compositions: [ref.5 and R. Clayton, personal communication] **(Host)** Based on oxygen isotopic composition, the host meteorites Y-75097 and Y-793241 are assigned to L-group and Y-794046 to H-group. **(Inclusion)** The oxygen isotopic compositions of inclusions from Y-75097 and Y-794046 lie within the range of H-group chondrites. The inclusion in Y-793241 has a composition close to but somewhat deviates from that typical of H-group.

Age determinations: The K-Ar and/or Ar-Ar ages are 490 Ma for both host and inclusion of **Y-75097** [6,7]. This age may be assigned to the time of the young major impact-melting event at L-chondrite parent body [8]. The Rb-Sr systematics obtained in this work are shown in Fig. 1. Data points of both bulk and mineral separates of host (and inclusion) deviate from the 4.5 Ga reference line and indicate no clear age trend, suggesting that the Rb-Sr system were incompletely reset by the event. For **Y-793241**, the K-Ar age is 4.3-4.4 Ga for host and inclusion [7]. The Rb-Sr model age calculated from Rb-Sr data of host is 4.4 Ga. The concordant K-Ar and Rb-Sr model ages suggest that the petrographic features above observed were established by an early thermal process. The K-Ar age for **Y-794046** is 2.0 and 1.9 Ga for Host and inclusion, respectively [7], indicating a late degassing event. The Rb-Sr systematics also suggest to have been subjected to a young intense impact event [9].

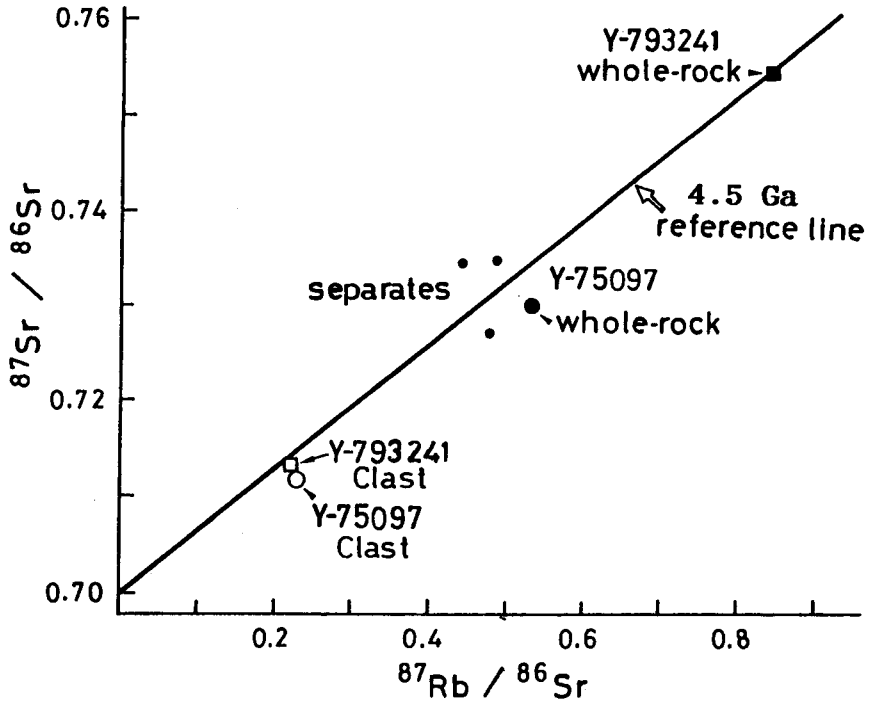

Fig. 1 ^{87}Rb-^{87}Sr evolution diagram for inclusions and hosts of Y-75097 and Y-793241 L6 chondrites.

Lithophile trace-element analyses: Trace element patterns are shown in Figs. 2 and 3. Compared to typical L6 chondrites [10], the host meteo-rites of Y-75097 and Y-793241 indicate somewhat fractionated REE patterns with a negative Eu anomaly. The inclusions in the meteorites show a similar but remarkable REE fractionation with middle REE depletion (V-shaped) and a large positive Eu anomaly. Because distributions of phosphates in the Y-75097 inclusion are quite heterogeneous, it is suspected that the pattern represents the bulk inclusions. The pattern may represent phosphate-poor area of the inclusion. As noted previously[11,12], this may be the largest REE fractionation ever found for this type of REE pattern. The V-shaped REE pattern are occasionally found for chondritic materials with mineral assemblage of olivine + plagioclase, and thus have specific petrogenetic implications [13]. The inclusion from Y-794046 indicates a flat REE pattern but has two times higher alkali abundances relative to ordinary chondrites.

We acknowledge a useful contribution of data and discussion from Dr John Bridges.

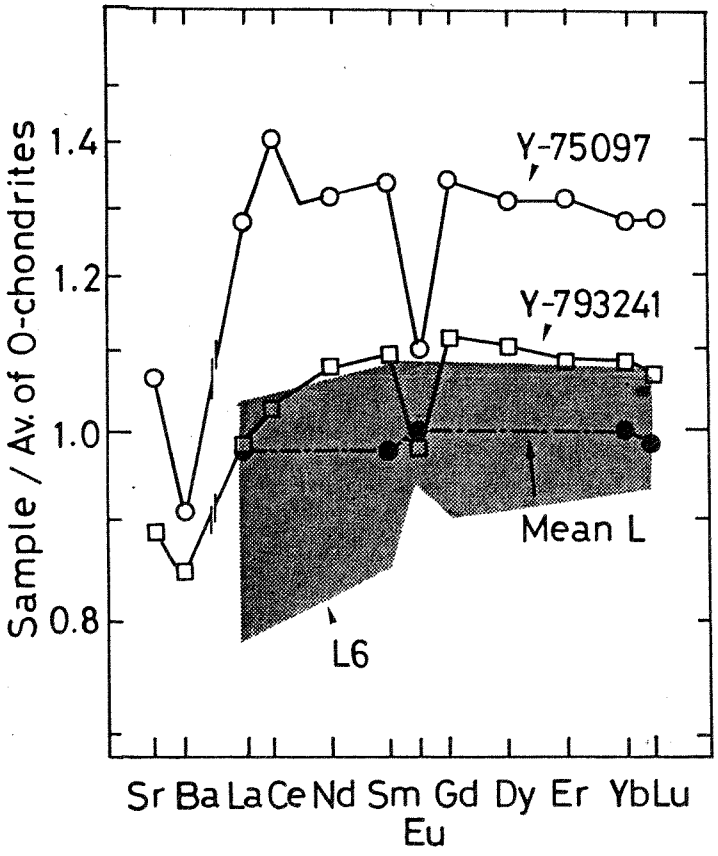

Fig. 2 Trace element abundance patterns for bulk samples of Y-75097 and Y-793241, compared with typical L6 chondrites [10].

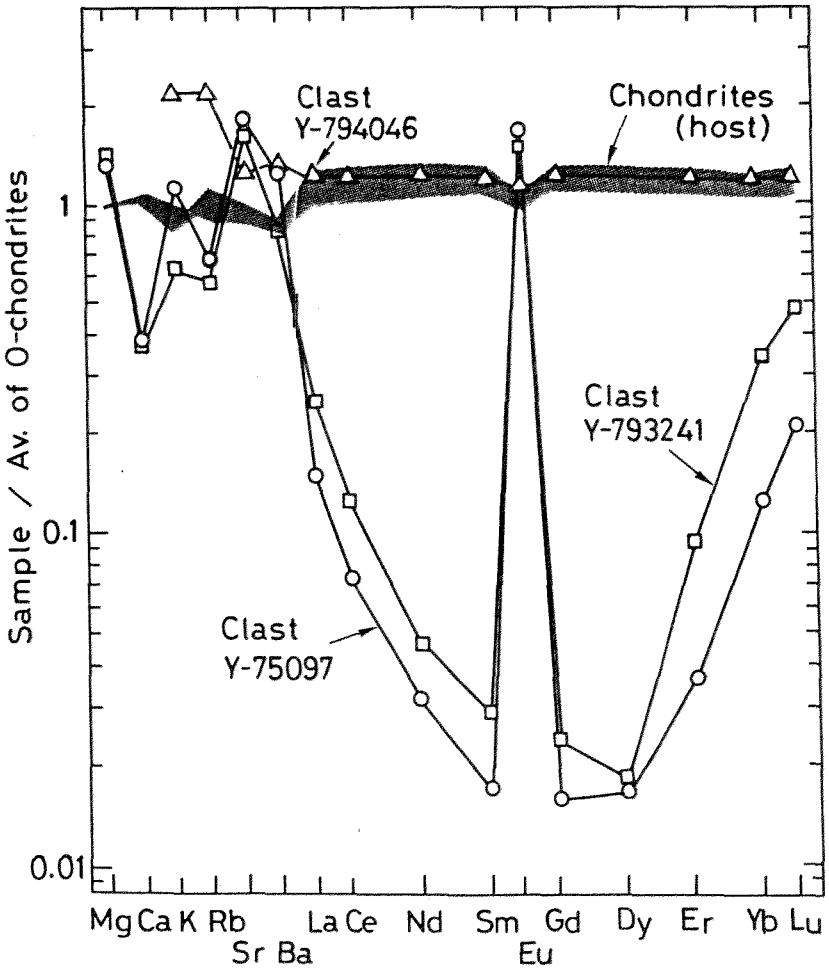

Fig. 3 Trace element abundance patterns for inclusions in Y-75097 (L6), Y-793241 (L6) and Y-794046 (H5).

References; [1] Yanai K. and Iguchi M.(1981); Yanai K. and Kojima (1987) Photographic Catalog of the Selected Antarctic Meteorites. [2] Yanai K. and Kojima H. (1983) Mem. Natl Inst. Polar Res., Spec. Issue, 46, 144-150. [3] Prinz M. et al. Meteoritics 19, 292-293. [4] Yanai K. and Kojima H. Proc. NIPR Symp. Antarc. Meteorites 4, 118-130. [5] Mayeda T.K. et al. (1987) Mem. Natl Inst. Polar Res., Spec. Issue 46, 144-150. [6] Kaneoka I. et al. (1988) Proc. NIPR Symp. Antarct. Meteorites 1, 206-214. [7] Nagao K. (1993) Papers 18th Symp. Antarct. Meteorites (this volume). [8] Nakamura N. et al. (1990) Nature 345, 51-52, [9] Fujimaki H. et al (1993) Papers 18th Symp. Antarct. Meteorites (this volume). [10] Kallemeyn G.W. et al. (1989) Geochim. Cosmochim. Acta 53, 2747-2767. [11] Nakamura N. et al. (1984) Meteoritics 19, 278-279. [12] Warren P.H. and Kallemeyn G.W. (1987) Proc. 19th Lunar Sci. Conf. 475-486. [13] Torigoye N. et al. (1993) Proc. NIPR Symp. Antarct. Meteorites, 6 (in press).

MINERAL CHEMISTRY AND FORMATION OF IGNEOUS INCLUSIONS FROM CONSORTIUM SAMPLES Y 75097, Y 793241, AND Y 794046. Richard O. Sack† and Michael E. Lipschutz*, †Departments of Earth and Atmospheric Sciences, and *Chemistry, Purdue University, W. Lafayette, IN 47907-1393, U.S.A.

Introduction. As part of the consortium formed to study igneous inclusions in three Antarctic ordinary chondrites – Y 75097 and Y 793241 (both L6) and Y 794046 (H) – we studied the mineral chemistries of the inclusions and hosts to establish the genetic history of the samples. In an accompanying paper [1], composition data are reported based upon instrumental and radiochemical neutron activation and electron probe microanalysis – fused bead.

Experimental. The following PTS were used in this study: Y 75097, 86-4 (chondrite host and igneous inclusion); and Y 793241,91-1 (host) and ,94-2 (inclusion); Y 794046,71-5 (host) and ,53-3 (inclusion). All sections were studied using the CAMECA SX-50 electron microprobe in the Department of Earth and Atmospheric Sciences. An accelerating voltage of 15 kV, and beam currents between 10 and 20 nA, and beam sizes between 1 and 10 microns were used in all cases. Standards for SiO_2, TiO_2, Al_2O_3, Cr_2O_3, FeO, MnO, MgO, NiO, CaO, Na_2O, K_2O, and P_2O_5 were enstatite (SiO_2 and MgO), synthetic ulvöspinel, synthetic anorthite (Al_2O_3 and CaO), chromite, synthetic fayalite, rhodonite, synthetic nickel olivine, albite, orthoclase, and apatite, respectively. CAMECA–supplied PAP correction software was employed.

Results. Both the igneous inclusions of Y 75097 and Y 793241 have achondritic textures, and are troctolites (i.e. they are composed predominately of olivine and plagioclase), with minor amounts of chromite, merrillite, and trace secondary ilmenite intimately intergrown with chromite. The igneous inclusion in Y 75097,86-4 is about 70% olivine, 22% plagioclase, 6% merrillite, and 2% chromite, and Y 793241,94-2 is about 82% olivine and 16% plagioclase, with on the order of 2% chromite and merrillite. Compositions of olivines in these inclusions (Table 1) are nearly identical to those in their hosts, while plagioclases in the inclusions, particularly in Y 793241,94-2, are more Ca-rich than in their hosts (Fig. 1). The chromites in Y 793241,94-2 inclusion are distinctly more aluminous than those in the igneous inclusion of Y 75097,86-4 (Table 1). Pyroxenes in the L6 hosts are primarily orthopyroxenes, with minor fine-grained and lamellar high-Ca clinopyroxenes. Ortho- and clinopyroxenes in the L6 hosts have similar Fe/(Fe+Mg) and Ca/(Ca+Fe+Mg) ratios (Figs.2-3), and the Na_2O-, MnO-, Al_2O_3-, Cr_2O_3-, and TiO_2-contents of these pyroxenes average about 0.05, 0.45, 0.2, 0.2, and 0.2 wt. %, respectively (orthopyroxene) and 0.6, 0.25, 0.55, 0.6,and 0.5 wt. %, respectively (clinopyroxene).

Y-794046,53-3 differs from the igneous inclusions of Y 75097 and Y 793241 texturally and in mineral assemblage and chemistry. The major portion (~90 %) of Y-794046,53-3 is about 49 % olivine, 22 % orthopyroxene, 14 % clinopyroxene, 13 % plagioclase, and 1 % chromite, with minor to trace amounts of Fe-metal, troilite, and secondary ilmenite and rutile; the remaining portion of Y-794046,53-3 contains several coarse grains of Fe-metal and troilite, and distinctly less clinopyroxene. In the main portion of Y-794046,53-3 coarse pyroxene laths up to about 1 mm in length are set in a matrix of medium to fine-grained olivine and ophitic to sub-ophitic feldspar. The feldspars of this inclusion are substantially poorer in calcium than its H host and the igneous inclusions and L6 hosts of Y 75097 and Y 793241 (Fig. 1). The olivines of this inclusion are slightly more ferroan than its host (Fig. 2), and its clino- and orthopyroxene pyroxenes are respectively more Ca-poor, and more variable in Ca- and Mg-contents than those in its H host or the L6 hosts of Y 75097 and Y 793241. Its H host is highly brecciated.

Table 1. Representative spinels and olivines in igneous inclusions (wt. % oxides).

	1	2	3	4	5	6
SiO_2	37.63(0.32)	---	37.41(0.34)	0.03(0.03)	0.05	52.56
TiO_2	0.01(0.02)	4.30(0.18)	0.06(0.04)	2.85(0.32)	1.29	0.31
Al_2O_3	0.03(0.03)	6.53(0.17)	0.07(0.01)	10.89(0.14)	11.00	1.18
Cr_2O_3	0.05(0.07)	50.67(0.06)	0.04(0.05)	48.93(0.78)	53.15	1.55
FeO	22.48(0.32)	31.81(0.35)	22.22(0.47)	30.89(0.61)	26.10	7.40
MnO	0.46(0.05)	0.76(0.06)	0.49(0.04)	0.64(0.04)	0.70	0.37
MgO	37.64(0.24)	2.31(0.07)	37.80(0.42)	2.60(0.13)	4.46	19.51
CaO	0.03(0.02)	0.01(0.02)	0.03(0.02)	---	0.08	14.17
Total	98.33	96.39	98.12	96.83	96.83	97.52

1. Average of 18 olivine analyses from Y 75097,86-4 (inclusion and host).
2. Average of 3 chromite analyses from the igneous inclusion in Y 75097,86-4.
3. Average of analyses of 5 olivines coexisting with chromites in Y 793241.
4. Average of analyses of 5 chromites in Y 793241.
5. Magnesian chromite in Y 794046,53-3.
6. Clinopyroxene coexisting with 5. (Na_2O = 0.35 and others= 0.12 wt. %).

Discussion. It is clear from the data displayed in Table 1 and Fig. 1 that the igneous inclusions differ in their spinel and feldspar compositions, providing convincing evidence that Y 75097 and Y 793241, in particular, are not paired with each other. It appears, however, that the inclusions from these two L6 chondrites originated by a similar genetic process involving magma formation elsewhere in the parent body. The magma formed by melting of L-type parent, together with some alkali-rich material. The resultant magma was olivine- and feldspar-rich and crystallized under equilibrium conditions. Equilibration temperatures calculated for olivine-spinel pairs in the igneous inclusions of Y 75097 and Y 793241 from a calibration for the Fe-Mg exchange reaction between these phases [2], 711 ± 12 and 702 ± 14°C, are in accord with corresponding temperatures obtained for olivine-orthopyroxene pairs in their hosts (Fig. 2).

The resemblance of the igneous inclusion from Y 75097 to Brachina has been noted by Yanai et al. [5] and our data confirm this similarity. It should be noted that our PTS for sample Y 75097,86-4, was quite small and exhibited a typical achondritic texture. In this respect, Y 75097,86-4 resembles the coarsely crystalline part of Y 793241: however, the compositions of these regions differ markedly. In particular, feldspars are particularly abundant in Y 75097: this inclusion contains more rare earth elements (REE) and phosphorous than does Y 793241 [1].

The textures and mineralogy of the L6 hosts of Y 75097 and Y 793241 exhibit substantial evidence of heating, a conclusion consistent with the labile trace element data [1]. This heating seems to reflect contact with melts that produced the igneous inclusions.

The assemblage of Y 794046 clearly differs from those of Y 75097 and Y 793241. The mineral chemical data for Y 794046,53-3 indicates that the inclusion crystallized rapidly, under disequilibrium conditions, with various mineral-pair thermometers indicating temperatures of 1160 to 800°C [3-5, Figs. 2-3]. The chondrite host is strongly brecciated, and its mineral compositions are consistent with derivation of the igneous inclusion from its host, given severe heating and the reactions consequent therefrom. These observations suggest that the igneous inclusion Y 794046,53-3 formed in situ from a melt produced by severe shock heating of the host. This melting was accompanied by loss of metal and sulfide, presumably in Fe-FeS eutectic

that has a threshold temperature in the neighborhood of 988°C. Compositional data for siderophiles and chalcophiles [1] accord with this conclusion. Cooling times for the inclusion Y 794046,53-3 can be estimated as days to months, demonstrating that the shock-heated assemblage now represented by Y 794046, was near the surface of a breccia regolith, but was insulated by overburden on the meter-scale.

Conclusions. The data indicate that the three meteorites Y 75097, Y 793241, and Y 794046 have brought to Earth samples of three parent regions. The inclusions in the L6 hosts sample at least two parts of the same magma pool or two pools, each of which was on the path to producing achondrites. These meteorites, like the LL7 chondrite Y 74160 [6], contain important clues to parent body processes that converted chondrite-like parent material to achondrites.

Acknowledgments. Various aspects of this research were supported by NASA grant NAGW3-393 and NSF grant EAR-92-19083. We are grateful to Prof. N. Nakamura and Dr. K Yanai for inviting us to join this consortium.

References. [1] Wang, M.S., Michlovich, E., Vogt, S., Lindstrom, D.W., Mittlefehldt, D.W., and Lipschutz, M.E. (1993) (this volume). [2] Sack, R.O., and Ghiorso, M.S. (1991) Am. Mineral. 76, 827–847. [3] Sack, R.O., and Ghiorso, M.S. (1989) Contrib. Mineral. Petrol. 102, 41-68. [4] Sack, R.O., and Ghiorso, M.S. (1993) Contrib. Mineral. Petrol. (in press). [5] Yanai, K., Matsumoto, Y., and Kojima, H. (1983) Proc. 8th Symp. Antarctic Meteorites 30, 29-35. [6] Takeda, H., Huston, T.J., and Lipschutz, M.E. (1984) Earth Planet. Sci. Letters 71, 329-339.

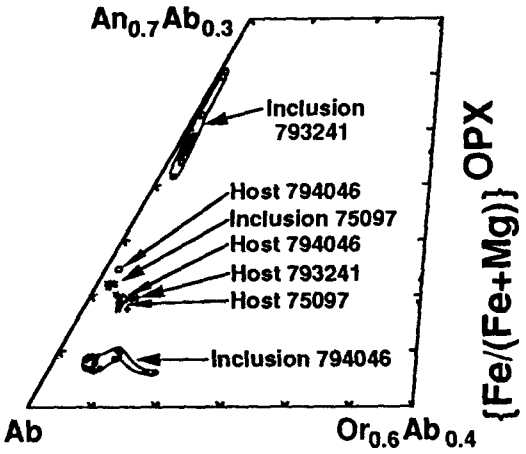

Fig. 1. Molar Ca/Na and Ca/K ratios of feldspars in Y-75097, Y-793241, and Y-794046 compared with a portion of the comp--osition triangle defined by $NaAlSi_3O_8$ (Ab), $CaAl_2Si_2O_8$ (An), and $KAlSi_3O_8$ (Or) components.

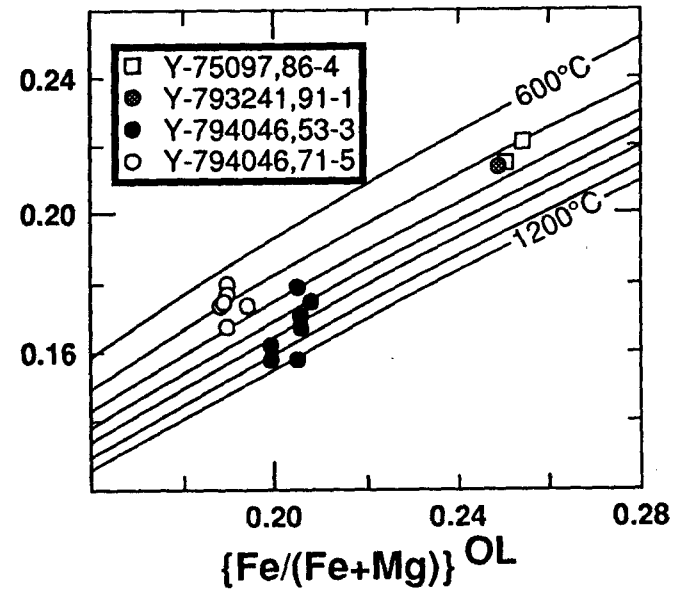

Fig. 2. Molar Fe/(Fe+Mg) ratios of olivines and low-Ca pyroxenes in Y-75097, Y-793241, and Y-794046 compared with the calibration for the Fe-Mg exchange reaction between orthopyroxenes with Ca/(Ca+Fe+Mg) = 0.016 and Fe-Mg olivines given by Sack and Ghiorso [2,3].

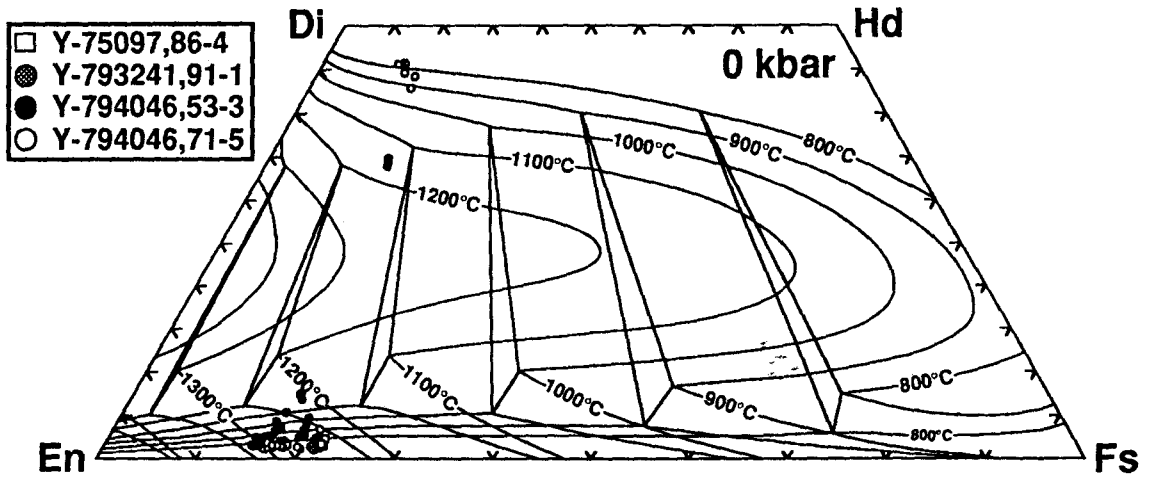

Fig. 3. Molar Ca/Fe and Ca/Mg ratios of Y-75097, Y-793241, and Y-79046 pyroxenes compared with the 1 atm. calibration for stable and metastable phase relations between Pbca and C2/c pyroxenes in the $Mg_2Si_2O_6$ (En) - $CaMgSi_2O_6$ (Di) - $CaFeSi_2O_6$ (Hd) - $Fe_2Si_2O_6$ (Fs) system of Sack and Ghiorso [4].

CONTENTS OF TRACE ELEMENTS AND COSMOGENIC RADIONUCLIDES IN CONSORTIUM SAMPLES Y 75097, Y 793241 AND Y 794046. Ming-Sheng Wang*, Edward Michlovich†, Stephan Vogt*, Marilyn M. Lindstrom‡, David W. Mittlefehldt§, Michael E. Lipschutz*. Departments of Chemistry* and Physics†, Purdue University, W. Lafayette, IN 47907. Mail Code SN2, NASA Johnson Space Center‡ and Lockheed Engineering and Science Co.§, Houston, TX 77058, USA

Introduction. As part of the consortium formed to study igneous inclusions in three Antarctic ordinary chondrites – Y 75097 and Y 793241 (both L6) and Y 794046 (H) – we determined contents of trace elements by INAA and RNAA (instrumental and radiochemical neutron activation analysis, respectively) and EPMA (electron probe microanalysis) – fused bead, and cosmogenic radionuclides by AMS (accelerator mass spectrometry). Samples both of chondritic hosts and igneous inclusions were studied using INAA and/or RNAA while only the hosts were examined using AMS. In an accompanying abstract, Sack and Lipschutz [1] report mineral chemical data obtained by EPMA of both hosts and inclusions in the three consortium samples.

Our purposes in analyzing these samples in this fashion are to study the genetic histories of the igneous inclusion (EPMA and INAA), the thermal histories of hosts and inclusions (RNAA), and the cosmic ray irradiation histories of the three meteorites and their terrestrial ages (AMS). We also wished to evaluate whether Y 75097 and Y 793241 are paired, or represent different parent regions.

Experimental. The samples received for study included: host – Y 75097,107 (1.683 g), Y 793241,62 (1.955 g) and Y 794046,62 (1.894 g); inclusions – Y 75097,52 A through F (each 0.057-0.167 g) which represent a column of material taken through the inclusion (A→F) from near the fusion crust into the chondritic host (F), Y 793241,62 (0.195 g) and Y 794046,97 (0.291 g).

We removed about 200-260 mg from each of the three host samples for RNAA and reserved much of the remainder for AMS. Two inclusions – Y 793241,62 and Y 794046,97 – were homogenized at NASA-JSC: about half of each sample were taken for INAA and EPMA-fused bead, the remainder being sent to Purdue for RNAA. The 6 subsamples, A→F, of Y 75097,52 were studied individually by INAA and were then forwarded to Purdue for RNAA.

The INAA, RNAA, EPMA-fused bead and AMS techniques used in this study were similar to those used for consortia studies of e.g. lunar meteorites Y 793274, Y 82192 and Y 86032 [2] and the Noblesville regolith breccia [3]. Species quantified by INAA, RNAA and EPMA-fused bead include the major, mineral-forming elements (expressed as oxides, SiO_2, TiO_2, Al_2O_3, FeO, MgO, CaO, Na_2O, K_2O) and 33 trace and ultratrace elements, ranging from highly refractory rare earths (REE) to highly labile ones, like Bi, Tl and In. Cosmogenic radionuclides measurable by AMS include ^{10}Be (1.6 My), ^{26}Al (730 ky) and ^{36}Cl (301 ky).

Results and Discussion. At the preparation time of this abstract, compositional data are incomplete but all should be available by the date of the 18th Antarctic Symposium. At present, data (obtained by the technique(s) listed) indicate the following:

1. Fragments A through E of inclusion Y 75097,52 demonstrate strong compositional variation by INAA and RNAA.

2. Inclusion Y 794046,97 seems to have formed by a different genetic path than that followed by the other two meteorite inclusions (INAA).

3. Tentatively, inclusion Y 794046,97 seems to have originated from molten host, which had lost ~75% of the metal and sulfides, presumably in a brief but severe heating accompanied by gravitational fractionation and loss of Fe-FeS eutectic at temperature > 988°C (INAA). Mineral-chemical data indicate peak temperatures ≥ 1100°C and cooling times of days to months for the inclusion [1].

4. Small compositional differences between otherwise-similar hosts of Y 75097 and Y 793241 and between inclusions in them, hint that the two meteorites may not be paired: however, both hosts suffered severe heating (INAA, RNAA, AMS). The mineral-chemical data [1] demonstrate that the meteorites are unpaired.

When all data are available we expect to be able to answer the following questions:

1. How are the inclusions related to their hosts and, in the case of Y 75097 and Y 793241, to each other?

2. By what genetic processes did the inclusions form?

3. When did the meteorites fall on Earth?

Acknowledgements. Various aspects of this research were supported by NASA grants NAGW3-396 and NAG3-460 (to MEL) and RTOP 152-13-40-21 (to M.M.L.). Additional aid was provided by DOE grant DE-FG07-80ER1 072SJ (to M.E.L.).

References. 1. Sack R. and Lipschutz M. E. (1993) Abstracts Eighteenth Symp. Antarctic Meteorites, this volume. 2. Lindstrom M. M., Mittlefehldt D. W., Martinez R. R., Lipschutz M. E. and Wang M.-S. (1991) Proc. 15th Symp. Antarct. Meteor. 1990, 12-32. 3. Lipschutz, M. E., Wolf S. F., Vogt S., Michlovich E., Lindstrom M. M., Zolensky M. E., Mittlefehldt D. W., Satterwhite C., Schultz L., Loeken T., Scherer, P., Dodd R. T., Sears D. W. G., Benoit P. H., Wacker J. F., Burns R. G. and Fisher D. S. (1993) Meteoritics, submitted.

CHEMISTRY OF THE LITHIC INCLUSIONS IN YAMATO-793241 AND -794046 METEORITES

Fukuoka, T.

Department of Chemistry, Gakushuin University, Mejiro, Tokyo 171.

Yamato-75097 (L6), -793241 (L6) and -794046 (H) chondritic meteorites have igneous-like inclusions (1). Yanai et al. (2) indicated the lithic inclusion of Y-75097 has unique mineral and chemical compositions, by their preliminaly examination. Clayton et al. (3) assigned the lithic inclusions in Y-75097, -73241 and -794046 meteorites are H group by the oxygen isotopic compositions. Chemical studies of these inclusions and host meteorites provide possible informations of the early solar system.

We have analyzed more than 27 major, minor and trace elements in lithic inclusion and host samples of Y-793241 and -794046 meteorites by conventional instrumental neutron activation analysis (INAA). Two aliquots of host samples of these meteorites have been analyzed, respectively. Preliminary analytical results are shown in Table 1 together with the results of control samples, JB-1 and Allende bulk powder.

The analytical values of total iron contents confirm the hosts of Y-793241 and -794046 meteorites belong to the L and H groups, respectively. The REE patterns of hosts of Y-793241 and -794046 both meteorites are basically chondritic, although small sample heterogeneity can be seen in Fig. 1. The abundances of siderophile elements in both inclusions of Y-793241 and -794046 are highly depleted, compared with their hosts (Fig. 2). This implies the inclusions suffered igneous process such as partial melting. They lost the most metal phases under the igneous process. This is consistent with the petrographical observations in (1).

The REE pattern of inclusion of Y-793241 is highly fractionated and has a large positive Eu anomaly (Fig. 1). The REE and Sc abundances in inclusion except Eu are deplete factor 0.5 ~ 0.2, compared with those of hosts. This pattern implies the inclusion consists of cumulate of plagioclase and olivine. The REE pattern of inclusion of Y-794046 is flat and parallel to the patterns of host (Fig. 1). The abundances of REE and Sc in this inclusion are enriched factor 1.5 compared with the host. This suggests the inclusion is a melt phase of igneous process.

The chemical data in this study suggest the parent bodies of Y-793241 and -794046 sufferd some igneous process on the evolution of early solar system.

REFERENCES:

(1) "Photographic catalog of the Antarctic meteorites" p.49, 135, 158, (1987).
(2) Yanai *et al.* (1983) Mem. Natl Inst. Polar Res., Spec. Issue, **30**, 29.
(3) Clayton *et al.* (1991) Geochim. Cosmochim. Acta, **55**, 2317.

Table 1. Preliminary results of chemical abundances by INAA

		Y-793241				Y-794046				Controls		Error*
		Host A 89, 1	Host B 89, 2	Wtd.mean host	Inclusion 64	Host A 65, 1	Host B 65, 2	Wtd.mean host	Inclusion 101	JB-1	Allende	(%)
Wt	mg	122	107		121	119	119		143	118	123	
Ti	%	0.04	0.08	0.06	0.07	0.11	0.04	0.08	0.06	0.80	-	35-60[2]
Al	%	0.99	1.06	1.02	1.61	1.01	0.84	0.93	1.33	7.09	-	4-9
Fe[1]	%	24.0	22.2	23.2	15.2	25.0	25.5	25.3	11.4	=6.30	23.2	0.5
Mg	%	14.6	15.6	15.1	19.5	14.2	14.0	14.1	18.5	4.51	-	2-4
Ca	%	1.19	1.41	1.29	0.74	1.21	1.14	1.18	1.55	6.85	-	6-11[3]
Na	%	0.749	0.740	0.745	0.852	0.591	0.639	0.615	0.920	=2.07	0.366	0.5
K	%	0.076	0.099	0.087	0.049	0.032	0.045	0.040	0.176	1.12	0.046	10-18[4]
Mn	%	0.259	0.276	0.267	0.312	0.239	0.226	0.233	0.304	0.119		0.5
Cr	%	0.242	0.319	0.278	0.303	0.263	0.275	0.269	0.366	=0.0414	0.247	0.5
V	ppm	65	71	68	79	82	59	71	87	214		6-9[5]
Sc	ppm	9.58	7.62	8.66	2.54	7.46	8.31	7.89	10.9	=28.9	12.1	0.5-1
La	ppm	0.30	0.41	0.35	0.18	0.28	0.35	0.32	0.48	=38.8	0.54	4-7[6]
Ce	ppm	0.65	1.10	0.86	0.43	0.51	0.72	0.63	0.99	=63	1.14	9-23[7]
Sm	ppm	0.195	0.220	0.207	0.045	0.165	0.182	0.174	0.250	=5.02	0.320	1-2
Eu	ppm	0.097	0.080	0.089	0.120	0.070	0.081	0.076	0.103	=1.59	0.156	8-15
Dy	ppm	0.32	0.32	0.32	0.16	0.35	0.26	0.31	0.47	4.00		50-70[8]
Ho	ppm	0.070	0.082	0.076	n.d.	0.086	0.092	0.089	0.058	=0.70	n.d.	15-20
Yb	ppm	0.26	0.27	0.26	0.073	0.20	0.27	0.24	0.31	=2.4	0.28	10-15[9]
Lu	ppm	0.038	0.041	0.039	0.014	0.035	0.033	0.034	0.051	=0.37	0.066	8-21
Hf	ppm	0.19	0.09	0.14	0.16	0.12	0.14	0.13	0.18	3.28	0.29	7-19[10]
As	ppm	1.83	1.45	1.65	n.d.	2.26	2.34	2.30	0.078	2.61	1.76	5-6[11]
Se	ppm	15.7	15.9	15.8	0.37	12.1	11.8	12.0	2.3	n.d.	=11	4-9[12]
Co	ppm	728	563	651	47.5	775	786	781	33.0	=39.1	655	0.5
Ni	%	1.69	1.58	1.64	0.0718	1.78	1.84	1.81	0.0550	0.0160	=1.55	0.5-3[13]
Os	ppb	320	334	327	46	377	506	442	n.d.	n.d.	=674	8-11[14]
Ir	ppb	410	392	402	70.9	491	574	533	17.0	n.d.	=853	0.5-3
Au	ppb	186	156	172	2.52	205	210	208	2.13	n.d.	=157	1-2[15]

* Errors for INAA are due to counting statistics.

1) Total iron as Fe. 2) Except for JB-1(3%). 3) Except for JB-1(2%). 4) Except for Y-794046,101(6%) and JB-1(4%). 5) Except for JB-1(2%). 6) Except for Y-793241,64(11%). 7) Except for Y-794046,65,1(35%). 8) Except for JB-1(6%). 9) Except for Y-793241,64(27%). 10) Except for JB-1(1%). 11) Except for Y-794046,101(44%). 12) Except for Y-793241,64(40%). 13) Except for JB-1(10%). 14) Except for Y-793241,64(36%). 15) Except for Y-793241,64(18%) and Y-794046,101(18%).

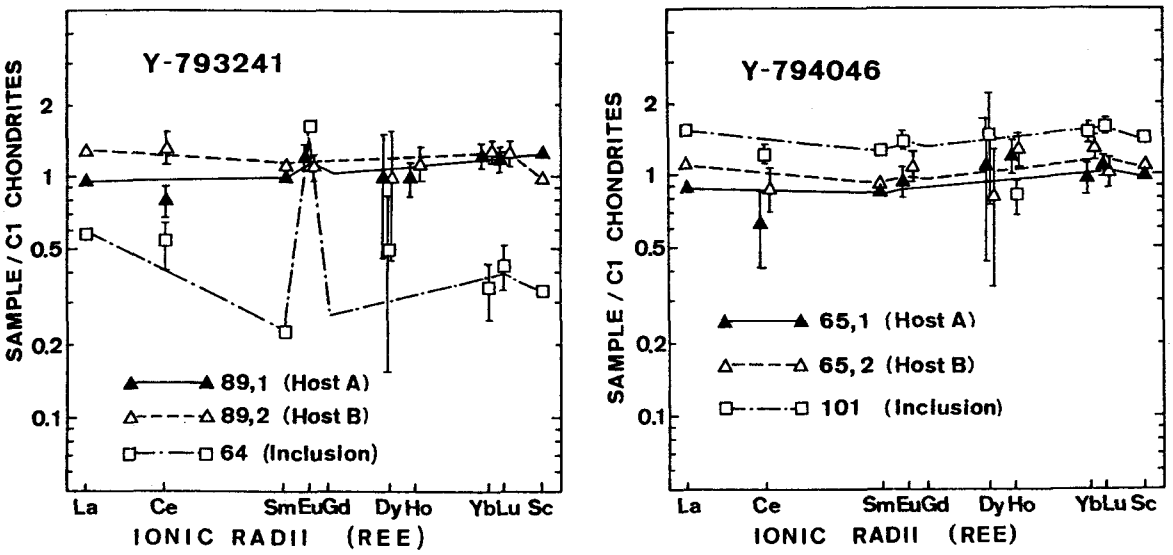

Fig.1. C1 chondrite (non-volatile) normalized abundance patterns of rare earth elements (REE) and Sc.

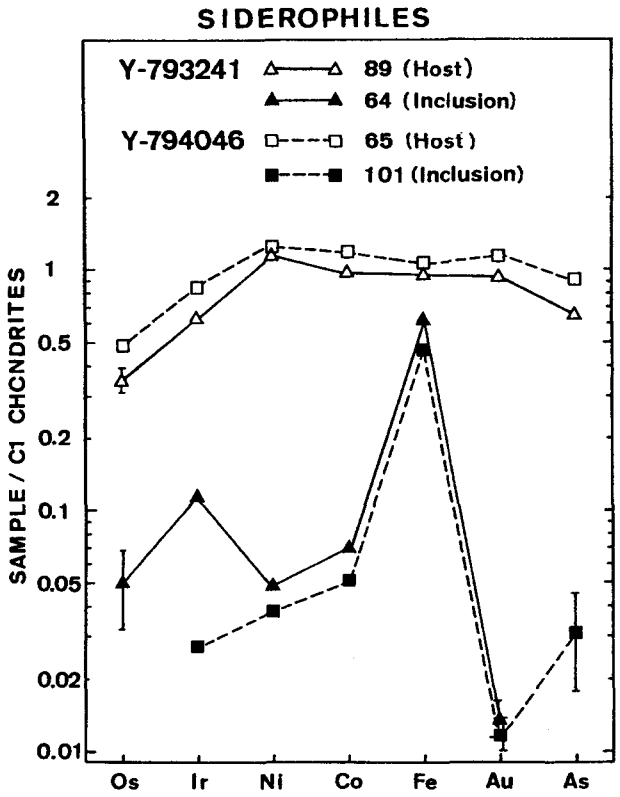

Fig.2. Siderophile elements abundance ratios relative to C1 chondrite (non-volatile) for Y-793241 and -794046 meteorites.

Rb-Sr isotopic study of Yamato-794046 and its inclusion

Hirokazu Fujimaki, Ken-ichi Ishikawa, and Ken-ichiro Aoki
Institute of Mineralogy, Petrology and Economic Geology
Tohoku University, Aoba, Sendai, Miyagi 980, Japan

Yamato-794046 chondrite records melting event induced probably by impact(s) and includes exotic lithic inclusion. The inclusion belongs to H-type chondrite (NIPR catalog, 1987), while its host seems altered and the type of the host chondrite was not identified. Recent oxygen isotopic study clarified both the host meteorite and its inclusion have oxygen isotopic affinity with H-type chondrite (Clayton, personal communication through N. Nakamura, 1993). Therefore, Yamato-794046 can be recognized as an H-type chondrite with fragmental inclusions of the same type chondrite. We participated in a part of Rb-Sr study of the consortium study of inclusions to characterize the chronological and isotopic relationships between the host chondrite and its inclusion. The importance of this kind of investigation has been emphasized (Nakamura et al., 1984; Kaneoka et al., 1988).

Our samples are Yamato-794046,61 (0.605g, host) and 794046,94 (0.474g, clast). Although Yamato-794046,94 seems only partly altered, Yamato-794046,61 is severely altered and porous, and it is reddish brown. Both have once partly melted by impact(s).

The experimental procedures are essentially the same as that of Fujimaki et al. (1992) with some trivial modifications. The inclusion was washed in ultrapure hot water in an ultrasonic cleaner for approximately three hours, and the host chondrite was repeatedly rinsed in the same way till the water became clean. The amount of the leached and stripped-off substance from the host chondrite was considerable. After dried up, each sample was crushed under 100-mesh size and separated into five fractions according to their magnetic susceptibility. Metallic iron was extracted before the separation for the inclusion, but not for the host chondrite. Each fraction was decomposed and dissolved in HCl, then the solution was split. Rb-Sr composite spike was added to one of the aliquot for isotope dilution analysis, and the other was used for analysis of Sr isotopic composition.

All the fractions of the host chondrite are very depleted in Rb and rather poor in Sr. The maximum concentration of Rb is as small as 0.7 ppm and Rb abundances are mostly less than 0.5 ppm. Sr concentrations never exceed 9 ppm. The bulk Rb and Sr concentrations are ca. 0.34 and 4 ppm, respectively. Al-

though such depletion may be attributed to the thorough rinsing that could leach the elements to some extent from the altered sample, we regard this is intrinsic chemical features of the host chondrite. In contrast, all the fractions of the inclusion are more enriched in Rb and Sr than the host chondrite; Rb is more than 4 ppm and Sr is more than 16 ppm. The Rb/Sr abundance ratios largely differ between the host and inclusion. The contrast might have been caused by different severeness of impact. The $^{87}Sr/^{86}Sr$ ratios of the fractions of the host chondrite are much lower than those of the inclusion. The low $^{87}Sr/^{86}Sr$ ratios of the host fractions are in accord with the low Rb/Sr abundance ratios. Without two failed analyses, the results were plotted in the isochron diagram. The results apparently seem good, but the associated errors are quite large and MSWDs are also large as well. Either complicated thermal history on or in the parent body, terrestrial alteration, the experimental procedure, or all of them may be responsible for this uncertainty. Therefore, the calculated ages should be treated with great care.

The age of the host is ca. 3.6 Ga and that of the inclusion ca 3.8 Ga. The difference between the inclination of the isochron lines is small but clear. They

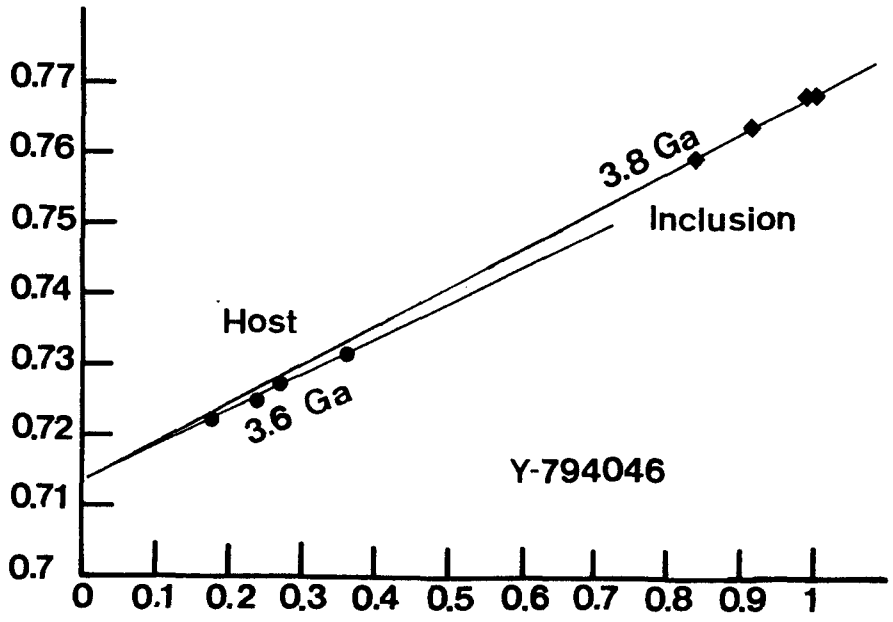

Figure Isochron plot of Yamato-794046 host and inclusion. Two analytical results are not shown.

have similar initial $^{87}Sr/^{86}Sr$ ratios (host, 0.7128; inclusion, 0.7123 with large uncertainty). Although an isochron can be drawn using all the points and the age is also ca. 3.8 Ga with large uncertainty, the host and the inclusion should be treated independently.

Presumed scenario is as follows. Yamato-794046,94 clast passed a melting or near-melting event ca. 3.8 Ga. The melting event was not so intense. After Yamato-794046,61 host included the clast, the host chondrite experienced a severe melting event 3.6 Ga. Meteoritic impacts should have been violent during 3.8 - 3.6 Ga period. The Rb-Sr chronometer of the inclusion might have been partly reset.

Fujimaki, H., Ishikawa, K., and Aoki, K., 1992, Prc. NIPR,
Kaneoka, I. Takaoka, N. and Yanai 1988, Proc. NIPR,
Nakamura. N., Yanai, K. and Matsumoto, Y. 1984, Meteoritics,
NIPR catalog, 1987

BULK COMPOSITION AND CLASSIFICATION OF THE TAHARA CHONDRITE

Yasunori MIURA[1], Hiroshi HARAMURA[2], Keizo YANAI[2], Makoto OKAMOTO[3] and O.G. IANCU[1]
[1]Faculty of Science, Yamaguchi University, Yoshida, Yamaguchi 753, Japan.
[2]Department of Antarctic Meteorites, National Institute of Polar Research, Kaga, Itabashi-ku, Tokyo, 173, Japan.
[3]Faculty of Science, Okayama University, Tsushimanaka, Okayama 700, Japan.

The largest piece with partial fusion-crust of new chondritic meteorite in Japan (No.1 in Table 1) was "found" at Matsue-shi, Shimane, Japan on December 28, 1992, after new fall of Mihonoseki chondrite near Matsue-shi on December 10, 1992 [1]. The Tahara meteorite hitted the deck of car-transport ship with quasi impact impact crater of about 40cm in diameter during anchor at Tahara, Aichi-ken, Japan on March 26, 1991. Eleven broken pieces of the Tahara meteorite are at least found from eight crew-members, though the main mass was thrown into the sea with other small pieces. Among the remained pieces, the smallest piece of the Tahara-2D was used in this study, as shown in Table 1.

Table 1. Main pieces of the Tahara meteorites.

Fragments	Collector	Size	Others
Tahara-1	Hidenobu Minao	422.5g (9.0x6.0x4.0 cm)	Natl Museum
Tahara-2A	Tetsuyoshi Ayabe	217 g (8.2x4.3x4.2 cm)	
2B		145 g (6.9x4.8x2.3 cm)	
2C		80 g (5.4x3.9x2.9 cm)	Natl Museum
2D		39 g (4.5x3.5x2.8 cm)	In this study (51,52)
Tahara-3	Minoru Hamaguchi	75 g (5.0x3.5x3.5 cm)	
Tahara-4	Hidetoshi Suzaki	5 g (2.7x1.1x1.1 cm)	
Tahara-5	Terutoshi Shimada	Lost	(Takasago, Hyogo)
Tahara-6	Mr.X	Lost	(Tokushima-ken)
Tahara-7	Mr.Y	Lost	(Kagoshima-ken)
Tahara-8	Mr.Z (Main mass)	Lost (more than ca.5kg)	(Into the sea?)

1. Sample

The sample used in this study is Tahara-2D (39g) by courtesy of Mr. Ayabe (Fig.1). Fragments of Tahara-2D,51 (1.134 g) and 52 (2.069 g) were used for polished thin section and bulk chemical analysis, respectively. The first descriptive data of Tahara-2D meteorite were obtained with electron probe microscopy (JXA-8900; JSM-5400) and bulk chemical analysis.

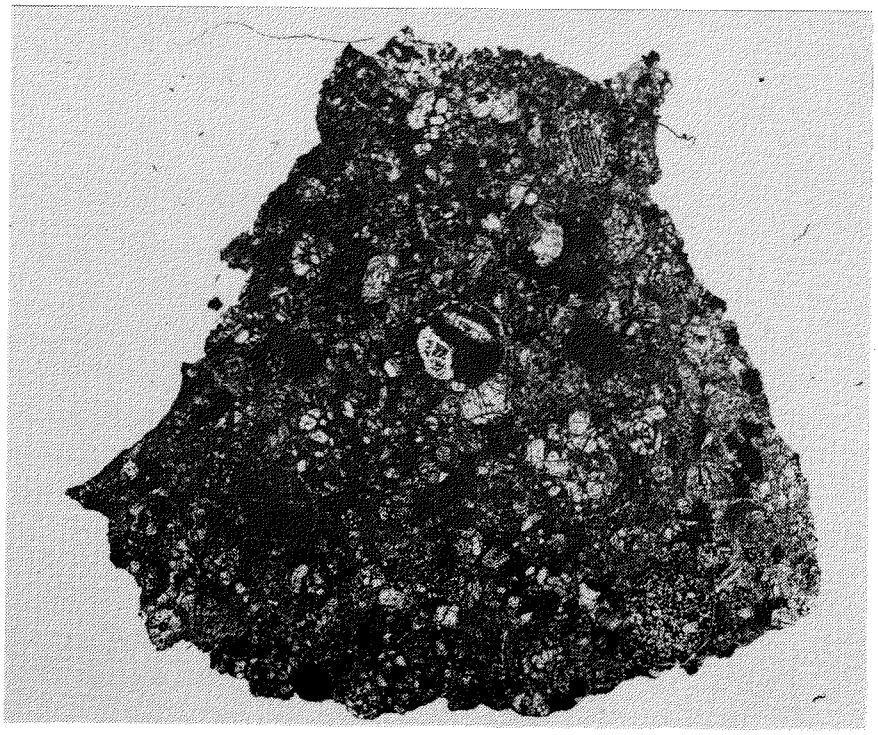

Fig.1. Photomicrograph of the Tahara-2D,51 chondrite. Field view is 10mm.

2. Bulk chemical composition

Bulk chemical composition of the Tahara-2D meteorite has been obtained as listed in Table 2. Chemical data of iron oxide (wt.%) and Fe in metal and FeS (wt.%) in Table 2 indicate that chemical group of the Tahara-2D,52 is classified as H chondrite.

Table 2. Bulk composition of the Tahara-2D,52 chondrite (H group) in Japan[1].

Oxides/ Elements	Tahara-2D,52	Oxides/ Elements	Tahara-2D,52
SiO_2	36.77	$H_2O(-)$	0.00
TiO_2	0.07	$H_2O(+)$	0.00
Al_2O_3	1.63	P_2O_5	0.22
Fe_2O_3	0.29	Cr_2O_3	0.33
FeO	10.62	FeS	6.34
MnO	0.31	Fe	15.18
MgO	24.67	Ni	1.41
CaO	1.68	Co	0.081
Na_2O	0.77		
K_2O	0.08	Total	100.45

[1] Analyzed by H. Haramura.

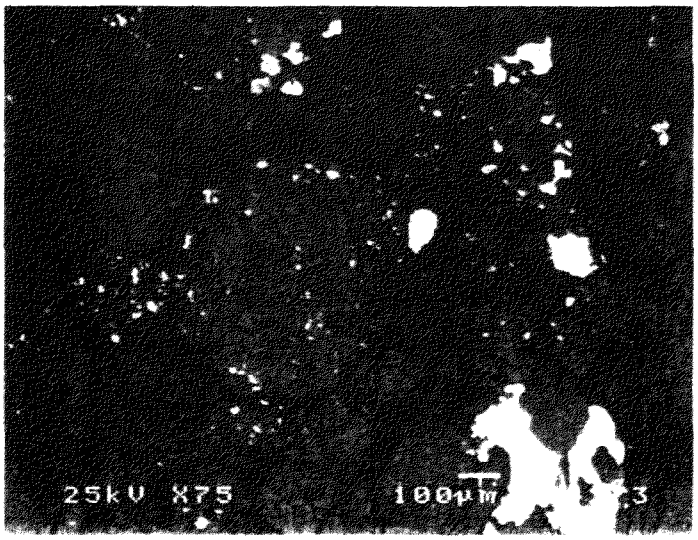

Fig.2. Olivine chondrule (center of Figure) with plagioclase-like grains in the Tahara-2D,52 chondrite (BEI).

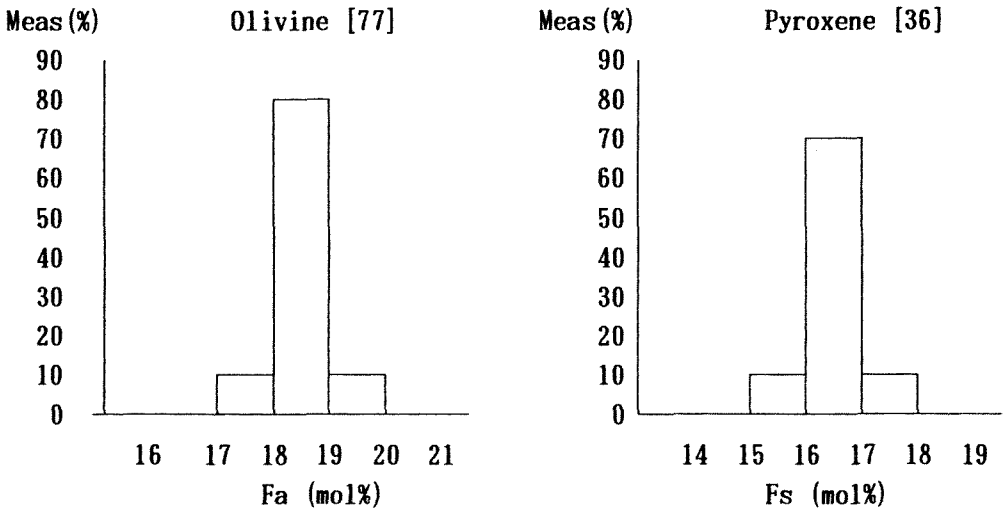

Fig.3. Histogram of iron-contents of olivines and orthopyroxenes in the Tahara-2D,51 chondrite.

3. Petrological type of the Tahara chondrite

Thin section with cross-nicols revels that olivine or pyroxene chondrules show readily delineated texture of chondrule with crystalline or turbid glassy veins, and microcrystalline or recrystallized texture of matrix (cf. Fig.1). Troilite and Fe-Ni metals are found with silicate fragments. Plagioclase-like dark microcrystalline grains (10～50μm) are observed in olivine chondrule (ca. 17 to 22 An mol.%) and in pyroxene chondrule (Fig.2).

Olivine grains of 77 analytical points are Fa:17.5-19.6 (av.18.6) with 1.5 %.M.D [2] (cf. Fig.3). Pyroxene grains show Fs:15.6-17.0 (av.16.3) with 1.8 % M.D. of in 36 analytical points (cf. Fig.3).

Petrologic type of the Tahara-2D,51 from textural characteristics indicates that it is classified as 4～5 (or 4.6 in average).

4. Evaluation of the Tahara meteorite

The Tahara meteorite is classfied as H5-4 chondrite in this study. In order to investigate whether the Tahara meteorite is heterogeneous or nor, the other pieces should be analyzed in the next study.

The two chondritic meteorites of the Tahara and the Mihonoseki are found at the same month (December, 1992) and locality (Shimane-ken), but classfication data in this study are completely different mass and fall. In fact, homogeneous observed feature of whitish inside with very thin black fusion-crust in the Tahara chondrite reveals completely different with heterogenous Mihonoseki chondrite [1] which gray or partially whitish inside with partially remained black fusion-crust.

The Tahara chondrite is 42nd remained meteorite of Japanese non-Antarctic meteorites, 33rd chondrite in Japan, and 15th chondrite of remained total weight. The Tahara meteorite are the first chondrite which is fallen on the deck of ship (maybe as meteoritic shower), and found at distant landed place from the fallen site (ca. 500 km) which are storred by the crew-members.

References:

[1] Miura Y. and Noma Y. (1993): Lunar and Planetary Science, 24, 997-998.
[2] Dodd R. T. (1981): In Meteoritics (Cambridge Univ. Press), p.24,

Existence of divalent chromium in YAMATO-691 determined by Micro X-ray Absorption Near Edge Structure analysis

Nakai, I. and Tsuchiyama, A.*
Department of Chemistry, University of Tsukuba, Tennodai, Tsukuba 305, Japan
*College of General Education, Osaka University, Toyonaka, Osaka 560, Japan

Introduction Chemical state analysis of transition elements in a meteorite provide useful information for the study of the formation condition and history of the sample. However, it has been difficult to examine chemical state of an element in micro-region by conventional analytical techniques such as Mossbauer spectroscopy and ESR. A combination of the XANES technique with X-ray fluorescence detection using a Si(Li) detector and Synchrotron Radiation X-ray microbeam source makes it possible to determine chemical state of trace elements in a small sample area nondestructively[1,2].

We have examined chemical states of chromium, titanium and iron in some important meteorites. Though existence of Cr(II) in a silicate phase of meteorite has been theoretically estimated, none of experimental study has provided clear direct evidence of the existence of Cr(II) in them [3]. Haggerty et al (1970) assumed presence of Cr(II) in olivine from Mare Tranquillittis based on optical absorption measurements [4]. We report the first experimental evidence of Cr(II) in meteorites.

Experimental Samples used are as follows: Yamato-691, Allende, Murchison, Krymka and Semarkona. SR-XRF measurements were made using monochromatized radiation with Si(111) double crystals from the bending magnet beam-line (BL-4A) at the Photon Factory, KEK, Tsukuba. Samples were placed on a XZ stage in a vacuum chamber. Fine parallel beam of desirable size (50-200 μm) was obtained by a simple set of vertical and horizontal slits, and if necessary, by pin hole with focusing mirror optics.

Cr, Ti and Fe K-XANES spectra of the samples were measured by X-ray fluorescence detection using a Si(Li) detector. XANES spectrum was obtained by normalizing the intensity of the fluorescent X-ray with the incident X-ray intensity and by plotting the data against the X-ray energy. Roughly polished specimens of the meteorites were used in the measurements.

Results and Discussion Ti K-edge XANES spectra of some reference samples are given in Fig. 1, which shows shift of the absorption edges depending on the oxidation states of Ti. It is clearly seen that not only the chemical shift but also the shapes of the spectra are characteristic to each compound. For X-ray photon energies near the core-level binding energy, transitions occur to bound states of the metal atom, giving rise to characteristic spectral feature in the vicinity of the absorption edge. For example, the XANES spectrum of TiO_2 (rutile) has a triplet pre-edge absorption (Fig. 1). Since the initial 1s state is a gerade state, the 1s $\rightarrow$ 3d transition is strictly dipole forbidden. However, the pre-edge absorption becomes dipole allowed due to a combination of stronger 3d-4p mixing and overlaps of the metal 3d orbitals with the 2p orbitals of the ligand [5,6]. It is found that this information can be used to characterize the Ti atom in a sample. Figure 2 shows Ti-K XANES spectrum of chondrule in the Semarkona meteorite. The concentration of Ti may be less than 1%. It is remarkable that such a trace amount of Ti gave a clear XANES spectrum. The spectrum closely resembles that of sphene with characteristic single pre-edge peak. From this information, it is found that Ti in the chondrule exists in the Ti(IV) state as a component of a silicate but not in the form of simple titanium oxides.

Cr K-edge XANES spectra of some reference samples were given in Fig. 3. It is also found that the chemical shift and the shapes of the spectra are characteristic to the chemical states of Cr in the samples. Figure 3 shows that the XANES spectrum of $K_2Cr_2O_7$ has an intense pre-edge absorption. This intense absorption is characteristic to Cr(VI) and can be used to characterize the oxidation sate of Cr in a sample. Figure 4 shows two examples of

the Cr-K XANES spectra of chondrules in the meteorites with reference to the spectrum of metallic Cr. It is found that Cr in the chondrule of Allende meteorite exists in the Cr(III) state. On the other hand, the spectrum of YAMATO-691 shows a doublet peaks at the absorption edge indicating that both Cr(II) and Cr(III) exist in the chondrule as a component of a silicate. Evidence of Cr(II) in a silicate phase has never been unequivocally identified until this study. Our XANES spectra of Ti and Fe-K edge also showed the existence of Ti(III) and metallic Fe in the YAMATO 691 sample indicating its highly reducing formation condition.

The authors are grateful to Dr. S. Hayakawa for his kind help in the focusing experiment and to Dr. T. Noguchi and Dr. M. Kitamura for loan of the samples, Semarkona and Krymka (T.N.) and Yamato-691 (M.K.).

REFERENCES 1)S.Hayakawa, Y.Gohshi, A.Iida, S.Aoki, and K.Sato. Rev. Sci. Instrum. 62(1991)2545. 2)I.Nakai and A.Iida. Adv. in X-ray Analysis, 35(1992)1307. 3)H.D. Schreiber and L.A.Haskin, Proc. Lunar Sci. Conf. 7th(1976)1221. 4)S.E.Haggerty, F.R.Boyd, P.M. Bell, L.W.Finger and W.B.Bryan. Proc. Appolo 11 Lunar Sci. Conf. 1(1970)513. 5)J.Wong, F.W.Lytle, R.P.Messmer, and D.H.Maylotte, Phys. Rev. B30(1984)5596. 6)R.B.Greegor, F.W.Lytle, D.R.Sandstrom, J.Wong, and P.Schultz, J. Non. Cryst. Solids 55(1983)27.

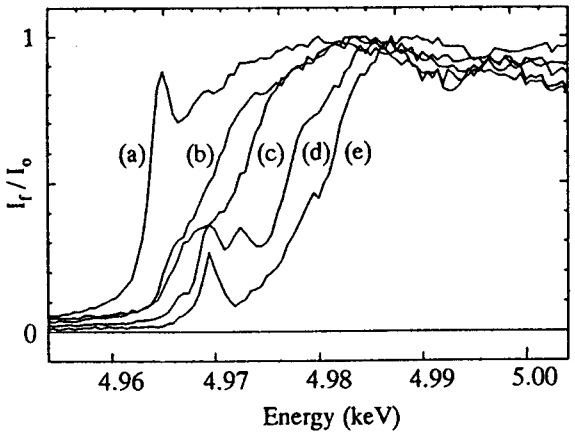

Fig. 1. Ti K-edge XANES spectra of standard samples:(a) metallic titanium, (b) TiO, (c) Ti_2O_3, (d) TiO_2 (rutile), (e) $CaTiSiO_5$ (sphene).

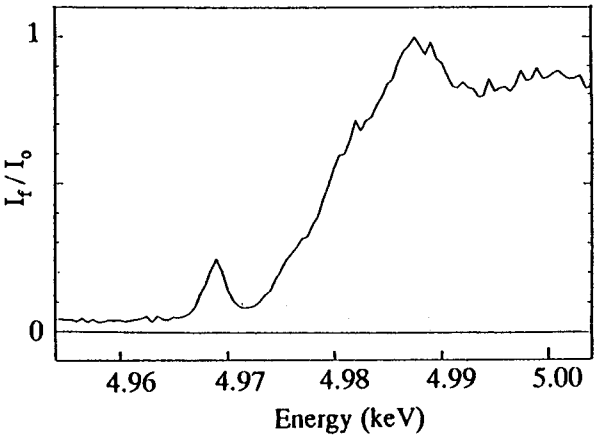

Fig. 2. Ti K-edge XANES spectra of a chondrule in the Semarkona meteorite.

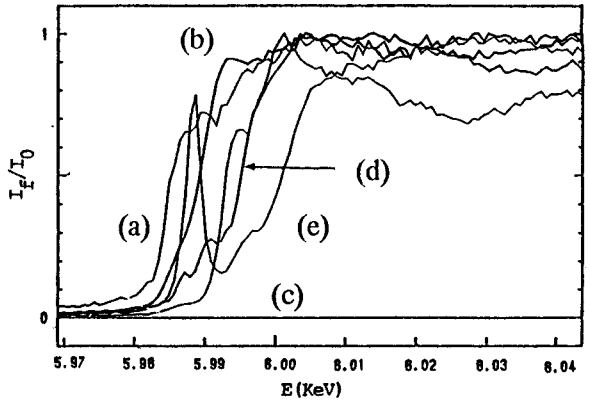

Fig. 3. Cr K-edge XANES spectra of standard samples: (a)Cr, (b)Cr_7S_8, (c)$CrSO_45H_2O$, (d)Cr_2O_3, (e)$K_2Cr_2O_7$.

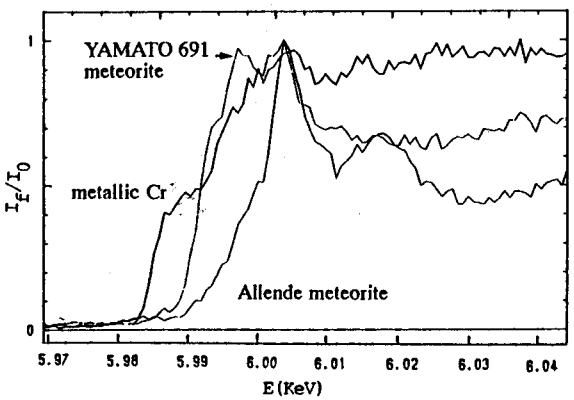

Fig. 4. Cr K-XANES spectra of metallic Cr, YAMATO-691 meteorite and Allende meteorite.

PRELIMINARY COMPARISON BETWEEN QINGZHEN(EH3) AND MAC88136(EL3)

LIN Y.T.[1], EL GORESY A.[2], WANG D.[1] AND OUYAN Z.[3]
[1]Institute of Geochemistry, Chinese Academy of Sciences, Guangzhou, PRC. [2]Max-Planck-Institut für Kernphysik, Heidelberg, FRG. [3]Institute of Geochemistry, Chinese Academy of Sciences, Guangzhou, PRC.

Introduction EH and EL chondrites are the most reduced chondrites found in the solar system up to date. The extremely reducing formation condition made these two clans exhibit many unique features in petrography, mineral chemistry and evolutionary history. Fall of the Qingzhen meteorite, the freshest EH3 chondrite, and classification of MAC88136 as the first EL3 chondrite[1] make comparison between parent bodies of EH and EL chondrites now available, since they are the most primordial samples and experienced rather weak thermometamorphism in their parent bodies.

Petrography Both of the Qingzhen meteorite and MAC88136 were predominantly composed of FeO-free enstatite higher than 70 vol%. The other silicates counted as minor phases in both of the two meteorites were diopside, FeO-rich pyroxene clast, Ca-rich plagioclase, silica, forsterite, and a few grains of pure Mg-spinel. However, roedderite was found only in the Qingzhen meteorite. The most distinct difference between their model composition was unique occurrence of niningerite in the Qingzhen meteorite, while alabandite in MAC88136. In addition, taenite and pentlandite were found only in MAC88136, but mineral A and B (two aqueous alkali Cr-sulfides[2]), and a new $FeCr_2S_4 \cdot H_2O$ [3] were limited in the Qingzhen meteorite. Although a few grains of djerfisherite were discovered in MAC88136 too, its abundance was much less than that in the Qingzhen meteorite, in which the alkali sulphide commonly displayed a discomposed structure referred as to "Qingzhen Reaction"[4]. Oldhamite and perryite were also significantly less in MAC88136 than the Qingzhen meteorite. The other opaque phases counted in the both meteorites were kamacite, troilite, sphalerite, daubreelite, schreibersite and graphite.

There was noticeable difference in occurrences of schreibersite and perryite between the Qingzhen meteorite and MAC88136. In the Qingzhen meteorite, part of schreibersites in shape of round and coarse grains were included in kamacite, and the others occurred as fine-grained spherules (<10μm) in all kinds of sulfides (from the high-temperature oldhamite to troilite and a variety of Cr-sulfides). Most of perryite were confined as thin rim between kamacite and sulfides and/or among sulfides. Contrarily, no schreibersite in MAC88136 was enclosed in sulfides, but, in stead of perryite, occurred as thin rim between kamacite and sulfides and/or among sulfides in metal-sulfide assemblages.

Mineral chemistry Although kamacite was the most abundant phase of the opaque minerals in the both chondrites, electron microprobe quantitative analysis revealed a significantly different Si-content. Kamacite contains much higher Si-content in the Qingzhen meteorite (2.13-3.05 wt%) than MAC88136 (0.12-1.09 wt%) which was at low limit of EL6 chondrites (1.0-2.1 wt%)[5]. In addition, kamacite in the Qingzhen meteorite contains no detectable P, different from that in MAC88136 (P≤0.27 wt%). Taenite was found only in MAC88136, which contained somewhat higher Si-content (0.26-1.59 wt%) than kamacite. Beside Fe(48.2-79.2 wt%) and Ni(18.5-48.8 wt%), taenite also contained minor Co(0.06-0.33 wt%) and Cu(≤0.25 wt%). Schreibersite is much

more Ni-rich and heterogeneous from grain to grain in MAC88136(18.9-49.0 wt%, average 35.5) than the Qingzhen meteorite(12.6-19.7). Different composition of perryite between MAC88136 and the Qingzhen meteorite was demonstrated by Si- and P-contents, the former containing lower Si- but higher P-contents (Si 10.4-11.2 wt%, P 4.76-5.73 wt%) than the later (Si 12.1-13.5 wt%, P 2.44-3.66 wt%). In MAC88136, alabandite was dominantly composed of MnS 48.8-56.8 wt%, FeS 6.0-18.1 wt% and MgS 0.32-2.20 wt%. Its minor Ca-content(0.04-0.18 wt%) was lower than that of niningerite in the Qingzhen meteorite(Ca 0.25-0.99 wt%), which mainly consisted of MgS 23.4-26.2 wt%, FeS 12.3-17.8 wt% and MnS 8.07-13.2 wt%. Both of alabandite and niningerite showed composition zoning, with two normal types and a reverse type discovered in niningerites in the Qingzhen meteorite[6,7] and a normal type in alabandite in MAC88136(FeS-content decreasing from 18.8-20.3 mol% at core to 10.2-9.3 mol% toward coexisting troilite) . This study revealed that Zn-depletion of daubreelite reported in EL6(<0.55 wt%)[5] was not an unique feature of EL clan. Up to 5.70 wt% of Zn-content was analyzed in daubreelite in MAC88136. However, Higher Mn-content of daubreelite in MAC88136(0.84-2.62 wt%) than the Qingzhen meteorite(0.28-0.50 wt%) suggested that Mn-enrichment of daubreelite in EL6 chondrites[5] was a heritage of its parent body. Although sphalerite was common in both of the Qingzhen meteorite and MAC88136, their chemical compositions were clearly different from each other. First, grains in the Qingzhen meteorite contains less MnS-content (3.2-5.1 mol%) than MAC88136 (17-22 mol%)[1]. Second, sphalerite in the Qingzhen meteorite was Ga-bearing, especially, grains included in kamacite contained rather high Ga-content (1.32-4.26 wt). However, all grains in the later was Ga-free. Troilite shows different Cr-content, with higher value in the Qingzhen meteorite (average 1.06 wt%) in comparison with MAC88136 (average 0.37 wt%). Despite of only a few grains found in MAC88136, quantitative analysis revealed its higher Cu-content(5.17 wt%) than that in the Qingzhen meteorite (average 3.23 wt%).

Parent bodies of EH and EL chondrites Before recognizance of MAC88136 as the first EL3 chondrite[1], all EL chondrites were heavily modified by thermometamorphism in parent body and classified into EL6 type, hence it was difficult to determine what differences between EH and EL chondrites really reflected a result of chemical fractionation in the solar nebula. The low Si-content of kamacite in MAC88136 suggested that the former analysis of kamacite with low Si-content in EL6 chondrites was not a result of thermometamorphism in the parent body, but revealed variation on oxygen fugacity between formation location of EH and EL chondrites. Since Si is a typical lithophile element, the higher Si-content of kamacite in EH chondrites indicated a more reduced condition. Furthermore, the different redox probably in turn determined most of the other variation on petrography and mineral chemistry between the parent bodies of EH and EL chondrites. Chemical analysis indicated that EH and EL chondrites contained comparable abundance of Mn. Even, the average ratio of Mn/Mg was higher in EH chondrites(0.02) than EL chondrites(0.012)[8], hence the systematically higher Mn-contents of sulfides (e.g. daubreelite and sphalerite) in EH chondrites than EL chondrites and unique occurrence of niningerite in EH while alabandite in EL chondrites could not be due to variation of bulk composition. However, it was ready to be understood in term of oxygen fugacity. At formation location of EH chondrite, the highly reduced condition made a significant proportion of Mg distribute in form of

MgS(gas), hence condensed MgS-rich niningerite (abundance of Mg was two orders higher than Mn). When oxygen fugacity increased, Mg became more lithophile and almost all of it condensed as silicates. This should dramatically increased MnS(gas)/MgS(gas) ratio and cause MnS-rich alabandite to condense, because Mn is much more chalcophile than Mg. MnS-content of the other sulfides could be buffered by niningerite in EH chondrites or alabandite in EL chondrites, because petrographic feature suggested that they formed later than niningerite or alabandite. In addition, significantly low abundance of oldhamite, djerfisherite and absence of mineral A and B (two aqueous alkali Cr-sulfides), Ga-bearing sphalerite in EL chondrites probably due to its higher oxygen fugacity, because Ca, K, Na, and Ga are typical lithophile elements.

In the Qingzhen meteorite, occurrence of schreibersite as round and coarse-grained inclusion in kamacite and/or find-grained spherules in various sulfides suggested that it formed before kamacite. The condensation of schreibersite should absorb nearly all of P, hence no more of it was left to condense with kamacite. In contrast, schreibersite in MAC88136 formed after and/or together with kamacite, so that higher fugacity of P in the nebula cause it partly to be solved in the metal phase. In addition, we considered that Si-content of kamacite played a key role on sulfurization of kamacite. In case of the Qingzhen meteorite, as kamacite reacted with gaseous H_2S to form sulfides, Si-, Ni-contents of kamacite became oversaturated and began to form perryite. However, in case of MAC88136, phosphorus combined with Ni to form schreibersite due to lack of Si.

Conclusion (1). EH and EL chondrites have different parent bodies, the parent body of EH chondrites formed under a more reduced condition in comparison with that of EL chondrites. (2). Oxygen fugacity, fo_2, probably was the most important cause for main deviations on petrography and mineral chemistry found between EH and EL chondrites. (3). Comparison with equilibrated EH and EL chondrites, it revealed that FeS-content of niningerite or alabandite increased with thermometamorphism. Descent of Zn-content in higher petrographic type suggests the parent bodies of EH and EL chondrites were probably an open system for volatile components.

Supported by Chinese National Foundation of Natural Sciences.

References: 1. Lin Y.T., Nagel H.J., Lundberg L.L., and El Goresy A. (1991) LPS XXII. 2. Ramdohr P. (1973) **The Opaque Minerals in Stony Meteorites**. London, Elsevier. 3. Lin Y.T., Kimura M. and El Goresy A. (1990) **Meteoritics 25**, 379. 4. El Goresy A. (1985) **Meteoritics 20**, 639. 5. Keil K. (1968) **J. Geophys. Res. 73**, 6945-6975. 6. Ehlers K. and El Goresy A. (1988) **GCA 52**, 877-887. 7. Lin Y.T., El Goresy A., Ouyang Z. and Wang D. (1989) **Meteoritics 24**, 293. 8. Kallemeyn G.W. and Wasson J.T. (1986) **GCA 50**, 2153-2164.

Tuesday, June 1, 1993

09:00 - 16:30 Symposium, Auditorium

16:30 - 17:30 Special Lecture (I)

Prof. Gero Kurat (Invited Speaker)

Naturhistoriches Museum, Vienna, Austria

PETROLOGY AND MINERALOGY OF AN ANOMALOUS NINGQIANG CARBONACEOUS CHONDRITE (CV3).

KIMURA M.*, NOGUCHI T.* and WANG D.** * Department of Earth Sciences, Ibaraki University, Mito 310. ** Institute of Geochemistry, Academia Sinica, Guangzhou, China.

An anomalous carbonaceous chondrite, Ningqiang, was petrologically and mineralogically studied, using SEM, TEM and AEM. This meteorite is depleted in refractory lithophile and siderophile elements, in comparison with the other CVs, and the Ningqiang was classified into an anomalous CV chondrite [1]. Later Kallemeyn et al. [2] reclassified it into an anomalous CK chondrite, based on its bulk chemical composition. However, the Ningqiang has characteristic features typical of CV chondrite, such as abundant matrix, large chondrule diameter (1.0 mm in average), and common occurrence of Ni-rich metal.

The Ningqiang consists of various constituent components: chondrule, lithic clast, AOI, CAI, isolated mineral, opaque aggregate and matrix. Five fine-grained CAIs were encountered in a PTS. All of them have melilite and high-Ca pyroxene (fassaite to diopside) with or without anorthite, olivine, spinel and perovskite. Nine AOIs were found. They do not have spinel, but often have tiny inclusions of low-Ca pyroxene. The most striking feature of chondrules in the Ningqiang is that the abundances of mesostasis are fairly low. Such unusual chondrules also occur in Y-86751 CV3 chondrite abundantly [3]. Many chondrules have spherical magnetite - FeNi metal - sulfide aggregates. A few chondrules have barred magnetites among phenocrysts, which were also observed in the Y-86751 [3]. The matrix is interstitial material consisting of fine-grained materials below 1 μm in size. Isolated minerals consist of mineral grains, larger than 2-3 μm, in the matrix.

Olivine phenocrysts in chondrules usually show distinct chemical zoning ($Fo_{45\text{-}99}$). Peripheral parts of clinoenstatite phenocrysts are usually replaced by ferroan olivine ($Fo_{45\text{-}65}$). Isolated olivine grains in the matrix have wide compositional variety ($Fo_{35\text{-}95}$). However, ferroan olivines ($Fo_{40\text{-}50}$) are predominant in them. Two chondrules have magnesian kirschsteinite ($Ca_{0.97}Mg_{0.48}Fe_{0.54}Si_{0.99}O_4$) in their groundmasses. Fe-Ni metals occur in all components. In spite of their various occurrences, they are almost homogeneous in composition (Ni 66.4% and Co 2.1% in average). Co-rich metal (Ni 0.6-1.3% and Co 34-39%) occurs in an opaque aggregate, and it has Ni and Co contents similar to those of phase Y in a LL chondrite, respectively [5].

The matrix is divided into two groups, bright and dark matrix under BSE image. The bright matrix has high abundances of Fe, Ni and S, and is characterized by abundant fine-grained opaque phases, usually below 1 μm in size. The contents of Ni and S are derived from fine-grained Ni-rich metal and pyrrhotite, respectively. However, high Fe content in the matrix may be mainly explained by magnetite. Besides magnetite, sulfide and metal, the bright matrix consists of normative olivine and spinel with high-Ca pyroxene. The dark matrix consists of olivine and nepheline with high-Ca pyroxene, sodalite and spinel in normative composition. The dark matrix is fairly homogeneous in Mg/Mg+Fe atomic ratio, 0.40-0.47 (0.43 in average). TEM observation shows that the dark matrix mainly consists of euhedral olivines, 400-600nm in size (Fig. 1), suggesting that the Ningqiang hardly suffered thermal and shock metamorphism in the parent body. Minor amounts of high-Ca pyroxene and spinel were also observed in the dark matrix by TEM.

From AEM analysis, the euhedral olivines in the matrix are ferroan (Fo_{35-49}), overlapping with compositional range of isolated olivine grains.

Rubin et al. [1] suggested that fractionation of CAIs resulted in the low bulk abundance of Al in the Ningqiang. Especially, chondrules in the Ningqiang are depleted in Al_2O_3 (usually 1.2%> in the bulk compositions). On the other hand, the bright matrix is enriched in spinel component. Unusual low contents of Al in the Ningqiang chondrules may be explained by the occurrence of spinel in the dark matrix, along with the fractionation of CAIs.

Nepheline and/or sodalite commonly occur in the interstices among olivines, pyroxenes and melilites in chondrules, CAIs and AOIs. Especially, 20 of 21 chondrules have nepheline and/or sodalite components that usually occur in peripheral parts of chondrules. Nepheline and/or sodalite replace primary mesostasis with plagioclase component. Such an occurrence is typically observed in Allende chondrules [4]. Kimura and Ikeda [4] concluded that almost all Allende chondrule suffered secondary alteration by the introduction of Na and Cl into chondrules. Most of components in the Ningqiang also experienced such a reaction after the formation of chondrules, CAIs and AOIs and the matrix.

References: [1] Rubin A.E., Wang D., Kallemeyn G.W. and Wasson J.T. (1988) Meteoritics 23, 13-23. [2] Kallemeyn G.W., Rubin A.E. and Wasson J.T. (1991) GCA 55, 881-892. [3] Murakami T. and Ikeda Y. (1993) Meteoritics (in press). [4] Kimura M. and Ikeda Y. (1992) Abs. 17th. NIPR Symp. 31-33. [5] Afiattalab F. and Wasson J.T. (1980) GCA 44, 431-446.

Fig. 1. TEM image of the dark matrix in the Ningqiang chondrite. Fine-grained euhedral olivine crystals are shown.

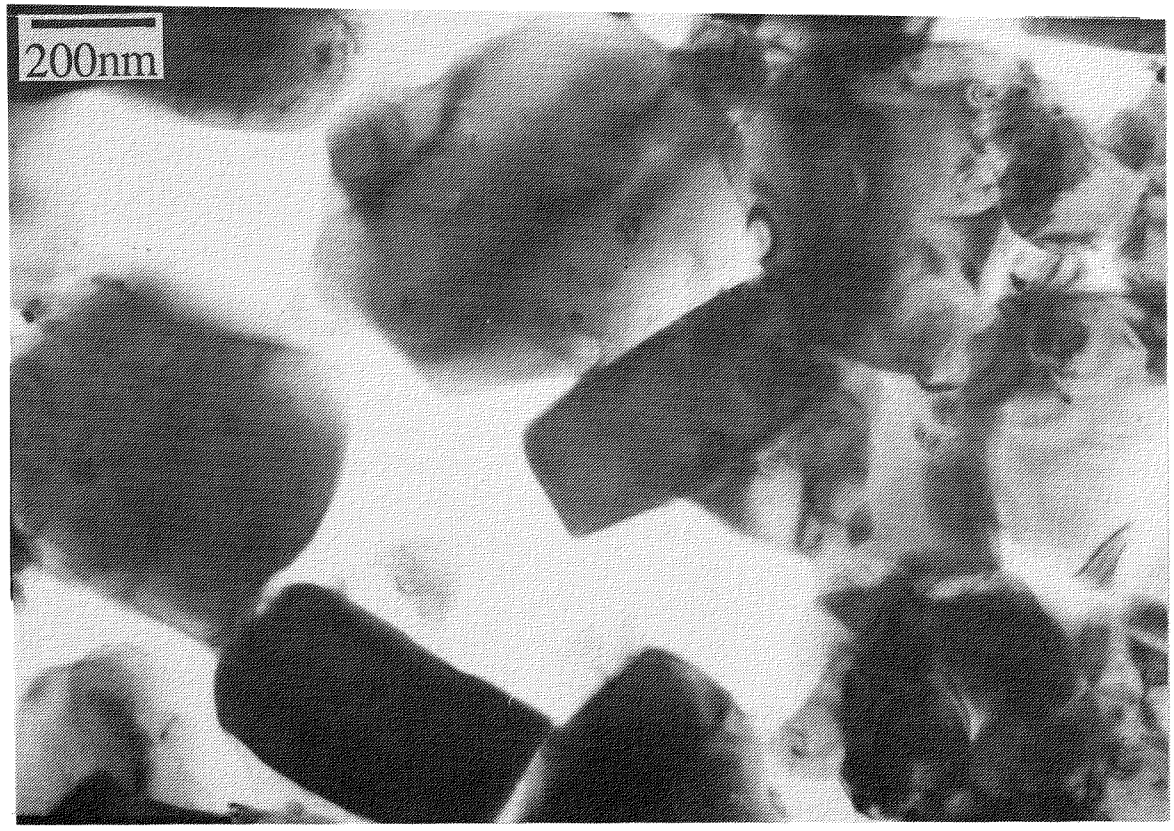

PETROLOGY AND MINERALOGY OF THE COOLIDGE METEORITE (C4) AND ITS COMPARISON TO THE CV AND CK CHONDRITES

Takaaki NOGUCHI
Department of Earth Sciences, Ibaraki University, Mito 310, Japan

Introduction The Coolidge meteorite has been known as one of the equilibrated carbonaceous chondrites (e. g. Van Schmus and Wood, 1967; McSween, 1977; Scott and Taylor, 1985). Most of the other equilibrated carbonaceous chondrites belong to the CK group, which include abundant magnetite without Fe-Ni metal. However, the Coolidge meteorite includes Fe-Ni metals and are tentatively classified as CV4 (Kallemeyn, 1987). In order to access this classification from the standpoint of petrology and mineralogy, I investigated this meteorite by a secondary electron microscope (SEM) and an electron probe microanalyzer (EPMA).

Petrography Coolidge is composed of chondrules, AOIs, CAIs, isolated minerals, metal and sulfide grains, and matrix. Most abundant type of chondrules observed in this meteorite is porphyritic olivine pyroxene (POP) chondrules. Some barred olivine (BO) and radial pyroxene (RP) chondrules were also observed. Many chondrules contain acicular to prismatic plagioclases. The sizes of such plagioclases often reach 10~20 μm x 50~150 μm. Some chondrules are composed mainly of such plagioclase crystals with pyroxenes and/or olivines. Together with chondrules which contains coarse plagioclases, chondrules including weakly devitrified brown glass were found. Low-Ca pyroxenes display polysynthetic twinning. SEM observation reveals that these pyroxenes have the characteristic Fe-Mg zoning which is shown in some of the ordinary, Carlisle-Lakes type, and CK chondrites (Tsuchiyama et al., 1988; Weisberg et al., 1991; Noguchi, 1993). AOIs are relatively small (< a few hundreds μm across). CAIs are various in size, 100~500 μm across. All the CAIs investigated here contain euhedral~subheral spinel crystals. Plagioclases often occur as a mixture with fine-grained (<1~2 μm) minerals. Ca-rich pyroxenes were observed in the rims of CAIs and rare within them. In addition to these minerals, calcite and Ca-phosphate were often found. Isolated olivines which have fragmental shapes were observed in matrix. Metal and troilite grains occur as spherules in chondrules. Most of the metal grains are kamacite with small amounts of taenite. In matrix, there are irregular-shaped inclusions which are composed of aggregates of laths of limonite. Matrix of this meteorite is composed of fine-grained (sub-μm) materials and fragmental olivines (> a few μm in size).

Mineralogy Olivines are homogeneous in this meteorite. Average Fo content is 86 ± 0.6 (1σ), which is consistent with the previous data (van Schmus, 1969; Scott and Taylor, 1985; Geiger and Bischoff, 1989). Pyroxenes in chondrules are relatively heterogeneous. Most of low-Ca pyroxenes are from ~En_{97} to ~En_{85}. Average En content is 88.9 ± 3.7 (1σ). Low-Ca pyroxenes with >En_{96} and <En_{80} were not observed. Mg values of Ca-pyroxenes are relatively homogeneous. Ca-pyroxenes were observed in chondrules and CAIs. Al_2O_3 and TiO_2 contents of Ca-pyroxenes in chondrules are higher than those in CAIs. Plagioclase compositions in chondrules and CAIs are heterogeneous. They vary from ~An_{95} to ~An_{45} in chondrules. However, most of them are > An_{60}. Although most of plagioclases in CAIs have > An_{95}, sodic plagioclases up to ~An_{27} were also observed. Spinels in CAIs display compositional zonings. Mg-Al spinel component decreases from their cores to rims, and chromite component vice versa.

Discussion Existence of acicular to prismatic plagioclases in chondrules is characteristic of Coolidge. Morphology of plagioclase indicates that they were crystallized from chondrule melts. Glass-bearing chondrules coexist with the plagioclase-bearing chondrules in this meteorite. The glass compositions are similar to plagioclase ones. These data exclude the possibility that the persistence of glass in some chondrules results from the difference in composition, rather suggest that the cooling rates after crystallization of olivine and pyroxene were various among chondrules. The existence of glass in chondrules and homogeneous olivines may be explained, if homogenization of olivines (and low-Ca pyroxenes) could happen below the temperatures at which devitrification hardly proceeds. Mg/(Mg+Fe) ratios are different between chondrule olivines (0.86, average) and matrix materials (~0.8). EPMA analyses of matrix suggest that most of matrix materials are represented by a mixture of olivine and a Fe-bearing phase (limonite?, which was perhaps originally Fe-Ni metal). It may be difficult to preserve the difference in Mg/(Mg+Fe) ratios and sub-μm grains which form matrix, even if the homogenization of olivines in chondrules occurred under relatively low-temperatures. These data might suggest homogenization of chondrules occurred before final agglomeration of Coolidge meteorite.

Plagioclases in Coolidge are heterogeneous like those in CK chondrites (e. g. Scott and Taylor, 1985; Geiger and Bischoff, 1991; Noguchi, in press). Although plagioclases often occur in matrices in CK chondrites, the occurrences of plagioclase in Coolidge are restricted to chondrules and CAIs. Similarity of compositions of chondrule glass and plagioclases suggests that plagioclase compositions were probably controlled by bulk compositions of chondrules. On the contrary, plagioclase compositions vary even within a CAI. Because sodic plagioclases exist with calcite and Ca-phosphate in CAIs, they are thought to be secondary minerals.

Kallemeyn (1987) suggested that depletions of Na and K abundances relative to average CV3 values were the result of weathering. However, the depletions can be explained by the abundant calcic plagioclases in chondrules and low Na_2O and K_2O contents in matrix. Regarding with morphology of plagioclases suggesting crystallization from melt and with sluggishness of Ca-Na-K interdiffusion in plagioclase, the depletions of Na and K in Coolidge were perhaps established before accretion of the meteorite.

References Geiger, T. and Bischoff, A. (1989) Meteoritics, 24, 269-270. Kallemeyn, G. W. (1987) Mem. Natl. Inst. Polar Res., Spec. Issue, 46, 151-161. McSween, H. Y. (1977) Geochim. Cosmochim. Acta, 44, 1777-1790. Noguchi, T. (1993) Proc. NIPR Symp. Antarct. Meteor., 6. Scott, E. R. D. and Taylor, G. J. (1985) Proc. Lunar Planet. Sci. Conf., 15th, Pt. 1, C699-C709 (J. Geophys. Res., 90 suppl.). Tsuchiyama, A., Fujita, T., and Morimoto, N. (1988) Proc. NIPR Symp. Antarct. Meteor., 1, 173-184. Van Schmus (1969) In: Meteorite Research. (ed. by Millman, P. M.) pp. 480-491. Van Schmus and Wood, (1967) Geochim. Cosmochim. Acta, 31, 737-765. Weisberg, M. K., Prinz, M., Kojima, H., Yanai, K., Clayton, R. N., and Mayeda, T. K. (1991) Geochim. Cosmochim. Acta, 55, 2657-2669.

A CARBONACEOUS CHONDRITE GROUPLET FROM MACALPINE HILLS, ANTARCTICA. Gregory W. Kallemeyn, Institute of Geophysics and Planetary Physics, University of California, Los Angeles, CA 90024 USA.

Mason (1988,1989) previously described three carbonaceous chondrites from the MacAlpine Hills region of Antarctica (MAC87300, MAC87301 and MAC88107) as type 2 carbonceous chondrites having abundant, small chondrules. He suggested that MAC87300 and MAC87301 were likely paired due to petrographic similarities and the close proximity where they were collected. Other researchers (Browning et al., 1991; Zolensky, 1991) noted abundant phyllosilicates in MAC87300 and MAC88107, similar to CM2 chondrites. Unlike normal CM2 chondrites which have no detectable natural or induced thermoluminescence (TL), these chondrites have both (Sears et al., 1990). the MAC87300 and MAC87301 chondrites have nearly identical natural TL values (17±6 and17±2, respectively), thus reinforcing the notion that both are paired. Sears et al. (1990) also suggested that MAC88107 is paired with the other two chondrites because its natural TL value (14±1) is similar. All three chondrites have induced TL glow curves which are similar to three other interesting carbonaceous chondrites: Allan Hills A77307, Colony and Lewis Cliffs 85332. Unlike the MacAlpine carbonaceous chondrites, though, ALHA77307, Colony and LEW85332 do not have abundant phyllosilicates in their matricies.

Replicate samples of MAC87300, MAC87301 and MAC88107 were analyzed by instrumental neutron activation analysis (INAA) for some 28 elements. MAC87300 and MAC87301 have very similar compositions. Their Mg-normalized abundances for lithophile and siderophile elements are nearly identical. These two chondrites are undoubtedly paired, and henceforth, will be discussed together as MAC87300.

The Mg-normalized lithophile abundances for MAC88107 are very similar to those of MAC87300. A small difference in K abundance is the notable exception. Siderophile and chalcophile element abundances in MAC88107 are generally similar to those in MAC87300, but some elements (Ni, Co, Ir, Os and Br) differ by up to 20%. The four deviant siderophile elements (Ni, Co, Ir and Os) are likely affected by loss of metal in the chondrite due to weathering. The Br abundance is can also easily be affected the redistribution of that element due to weathering or by contamination from wind-transported aerosols. The somewhat different natural TL value, along with the apparent differences in weathering history, suggest that MAC88107 may not be paired with MAC87300.

As noted earlier, MAC87300 and MAC88107 have petrographic similarities to the CM chondrite group. There are also some compositional similarities to CM. Refractory lithophile abundances in MAC87300 and MAC88107 are similar to CM-CO clan levels. Refractory and common siderophile element abundances are also similar to CM-CO levels. The Au abundances in these two chondrites are not depleted relative to the common siderophiles (Ni, Fe), and both have 'positive anomalies' in their

Br abundances. These are also characteristic of CM chondrites, although the high Br values could be from contamination or weathering as noted earlier. On the other hand, there are apparent differences among the more volatile elements. Moderately volatile lithophile element abundances are distinctly lower than those in CM chondrites, closer to CO chondrite levels. Volatile siderophile and chalcophile element abundances tend to be intermediate to CM and CO levels. The established carbonaceous chondrite groups are easily delineated by their Zn/Mn and Zn/Al abundance ratios. The MAC87300 and MAC88107 chondrites have ratios very close to one another. They fall in the hiatus between the CM and CO chondrite group ratios.

Sears et al. (1990) suggested that MAC87300 and MAC88107 are related to Colony, ALHA77307 and LEW85332 based on their TL data. All three of these chondrites were previously analyzed by INAA. Element abundance data for ALHA77307 are similar to those for MAC87300 and MAC88107, whereas LEW85332 is clearly different compositionally. The Colony chondrite is so badly weathered it is difficult to make a meaningful compositional comparison. Colony and ALHA77307, however, are quite different petrographically from MAC87300 and MAC88107. Both look very similar to CO3 chondrites. Colony and ALHA77307 are possibly related by a metamorphic sequence.

Although MAC87300 and MAC88107 are petrographically similar to CM2 chondrites, their compositional data seem to rule out inclusion in the CM group. Both chondrites have TL and compositional data similar to Colony and ALHA77307, but are petrographically distinct from those two chondrites. MAC87300 and MAC88107 likely form an independent grouplet, with their nearest relatives being Colony and ALHA77307.

REFERENCES:

Browning L., Zolensky M. and Barret R. (1991) *Lunar Planet. Sci. Conf.* **22**, 145-146.
Mason B. (1988) *Ant. Met. Newsl.* **11**(2), 34.
Mason B. (1988) *Ant. Met. Newsl.* **12**(3), 20.
Sears D.W.G., Sears H. and Myers B.M. (1990) *Lunar Planet. Sci. Conf.* **21**, 1121-1122.
Zolensky M. (1991) *Meteoritics* **26**, 414.

SIMILARITY OF REFLECTANCE SPECTRA BETWEEN C, G, B, F ASTEROIDS AND THERMALLY METAMORPHOSED CARBONACEOUS CHONDRITES.

Takahiro Hiroi[1], Carlé M. Pieters[2], Michael E. Zolensky[3], and Michael E. Lipschutz[4]. [1]SN3, NASA Johnson Space Center, Houston, TX 77058, USA, [2]Dept. of Geological Sciences, Brown University, Providence, RI 02912, USA, [3]SN2, NASA Johnson Space Center, Houston, TX 77058, USA, [4]Dept. of Chemistry, Purdue University, West Lafayette, IN 47907, USA.

Introduction A large number of dark asteroids whose reflectance spectra (0.3-1.1 μm) are relatively flat — previously classified as the C asteroids — have spectral property similar to carbonaceous chondrites [1]. The C asteroids were later subdivided into four classes: C, G, B, F [2]. Evidence of aqueous alteration similar to those in CM2 chondrites have been detected on some of those asteroids [3,4], and the possible thermal metamorphism on the G, B, F asteroids have been pointed out [2,5]. In spite of the above similarities between the C, G, B, F asteroids and carbonaceous chondrites, not many studies have been done to compare those reflectance spectra in the wide wavelength range (0.3-2.6 μm) that contains significant mineralogical information [6]. In this paper, the wide-range reflectance spectra of 23 C, G, B, F asteroids are compared with those of carbonaceous chondrites including thermally metamorphosed ones: B7904, Y86720, Y82162, and heated Murchison [7].

Experimental Carbonaceous chondrites Orgueil and Ivuna (CI1), ALH83100, Nogoya, and Bells (CM2), Renazzo (CR2), Vigarano and Allende (CV3), and B7904, Y86720, and Y82162 (Unique) were ground with a mortar and a pestle into powders of <100 or <125 μm in grain size. Bulk powder samples of Murchison (CM2) were heated in low-pressure (initially 10^{-5} atm) hydrogen atmosphere for 1 week at 400, 500, 600, 700, 800, 900, and 1000°C [7]. Each Murchison powder was sieved into grain size <63 μm. Laboratory bidirectional reflectance spectra (0.3-2.6 μm) of the above samples were measured at the viewing geometry of 30° incidence and 0° emergence angles. Telescopic reflectance spectra of 23 C, G, B, F asteroids [8,9,10] were combined to cover the wide wavelength range 0.3-2.6 μm. Classifications are based on Tholen [2].

Mineralogy Detailed mineralogical and compositional descriptions of meteorite samples discussed here are reported by Zolensky *et al.* [11]. CM2 meteorites consist, dominantly, of serpentine minerals (including cronstedtite), tochilinite, olivine (mean Fo = 95), Fe-Ni sulfides, Mg-rich pyroxenes (mean En = 98), and Fe-Ni metal, with the majority of the anhydrous minerals residing within matrix-supported chondrules and aggregates. Profound changes occurred to all of these minerals during the heating experiments on Murchison. By 600°C the serpentines have begun to dehydrate, and recrystallize to olivine and orthopyroxene, which are iron rich (see Fig. 1), and tochilinite has largely been converted to troilite. At 800°C Fe-Ni metal has increased in abundance, at the expense of Fe-Ni sulfides, and coarsen in grain size. At 1000°C chondrules have begun to recrystallize, and the meteorite now consists dominantly of olivine (mean Fo = 80) and pyroxenes (mean En = 90) with abundant scattered metal, and lesser sulfides. Similar mineralogical changes have occurred to the three unique chondrites Y82162, Y86720 and B7904, although to a varied and diminished extent [11,12,13,14].

Spectral fittings Reflectance spectra of 23 C, G, B, F asteroids were fit with two sets of end-member reflectance spectra by the isograin model [15,16] for opaque minerals. One set is 11 carbonaceous chondrites including three thermally metamorphosed ones, and another set is Murchison (CM2) and 7 heated ones. Reflectance spectra of those two sets of end members and the spectral fits of the 10 best-fit asteroids are shown in Figs. 2 and 4. The calculated volume abundances of component meteorites are plotted in Figs. 3 and 5. In both sets of fittings, thermally metamorphosed meteorites are abundant on all the best-fit asteroids. Y82162 is the most abundant and especially similar to B and F asteroids because of its weak UV absorption. Y86720 is G-like and B7904 is C-like in terms of their reflectance spectra. The CP asteroids (P-like C asteroids) have the smallest amount of 1000°C Murchison component, and the B asteroids have the largest amount of high-temperature (900 and 1000°C) Murchison components.

Discussion It has been known that reflectance spectra of carbonaceous chondrites can greatly change if the finest grains (<63 μm for example) are removed [1]. It is because the absorption bands at 0.7, 0.9, and 1.1 μm and red overall spectral profile are due to phyllosilicates that preferentially exist as submicron grains [11]. Such fine grains tend to exist on the surfaces of larger grains by some kind of force much stronger than gravity in laboratory environment. If that mechanism works on asteroids as well, fine grains are believed to exist and dominate the reflectance spectra. There are some terrestrial weathering in meteorite samples, especially Antarctic ones. However, weathering usually causes stronger UV absorption, which is not this case where unique

carbonaceous chondrites have weaker UV absorption. If the spectral comparisons in this work are correct, the most common carbonaceous chondrites (CI, CM, etc.) don't exist on the observed C, G, B, F asteroids. One possible reason for that discrepancy is that the parent bodies of carbonaceous chondrites were thermally zoned, with relatively unheated materials outside and heated materials inside. The outer unheated portions could have been easily removed by impact processes as smaller pieces (carbonaceous chondrites), and the current larger observable C, G, B, F asteroids may have been the inner heated portions of their parent bodies. However, such outer portions of the parent bodies must have been heated moderately (>0°C) to produce the aqueous alterations found in carbonaceous chondrites. The internal heating by radioactive isotopes can form a thermal zoning [17].

Conclusions

1. Thermally metamorphosed carbonaceous chondrites B7904, Y86720, and Y82162 are likely to be the actual fragments of the C, G, B, F asteroids.
2. If the parent bodies of the C, G, B, F asteroids were made of Murchison-like material, they must have been heated at various temperatures around 600-1000°C.
3. Most of carbonaceous chondrites that fell to the Earth may have been the outer, relatively unheated portion of their parent bodies.

Acknowledgments We thank Dr. Jeffrey F. Bell for the 52-color asteroid reflectance spectra. We also thank Drs. M. Miyamoto, H. Y. McSween, Jr., and F. Vilas for helpful suggestions. Antarctic meteorite samples were loaned from the National Institute of Polar Research and the Meteorite Working Group. Reflectance spectra of meteorite powders were measured at RELAB in Brown University. We thank S. Pratt for assistance with the measurements. RELAB is a multiuser facility operated under NASA grant NAGW-748. This research was supported in part by NASA grant NAG 9-48 to M. L. and the NASA Origins of Solar Systems Program to M. Z. This work was done while T. H. held a National Research Council-NASA/JSC Research Associateship.

References [1] Johnson T. V. and Fanale F. P. (1973) *JGR* **78**, 8507-8518. [2] Tholen D. J. (1984) thesis, Univ. of Arizona. [3] Vilas F. and Gaffey M. J. (1989) *Science* **246**, 790-792. [4] Vilas F. and McFadden L. A. (1992) *Icarus* **100**, 85-94. [5] Bell J. F. *et al.* (1989) in Asteroids II, pp. 921-945. [6] Gaffey M. J. (1976) *JGR* **81**, 905-920. [7] Matza S. D. and Lipschutz M. E. (1977) *Proc. Lunar Sci. Conf.* **8**, 161-176. [8] Chapman C. R. and Gaffey M. J. (1979) in Asteroids, pp. 1064-1089. [9] Zellner B. *et al.* (1985) *Icarus* **61**, 355-416. [10] Bell J. F. *et al.* (1988) Lunar Planet. Sci. **XIX**, 57-58. [11] Zolensky M. E. *et al.* (1993) *GCA* **57** (in press). [12] Ikeda Y. (1992) *Proc. NIPR Symp. Antarct. Meteorites* **5**, 49-73. [13] Akai J. (1990) *ibid.*, 55-68. [14] Paul R. L. and Lipschutz M. E. (1990) *ibid.*, 80-95. [15] Hiroi T. and Takeda H. (1990) *Icarus* **88**, 205-227. [16] Hiroi T. and Pieters C. M. (1992) *Proc. Lunar Planet. Sci.* **22**, 313-325. [17] Miyamoto M. (1991) *Meteoritics* **26**, 111-115.

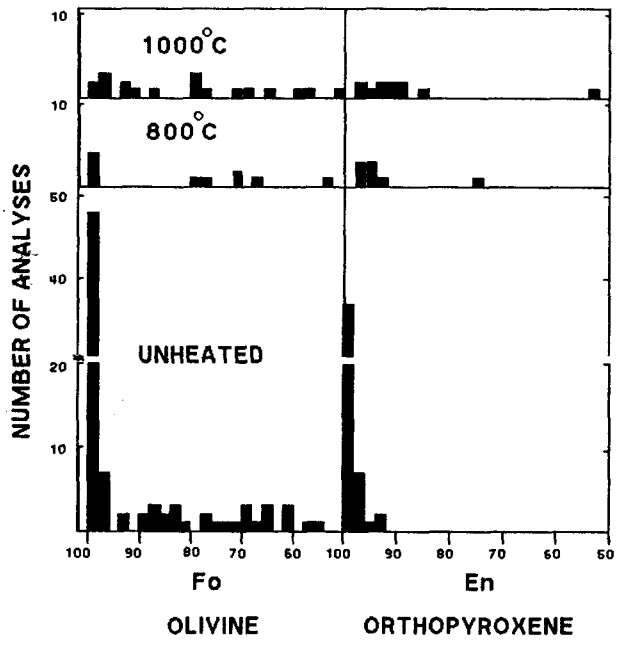

Fig. 1. A histogram of the abundances vs. Fe contents of olivine and orthopyroxene grains in Murchison matrix and chondrules analyzed by an electron microprobe.

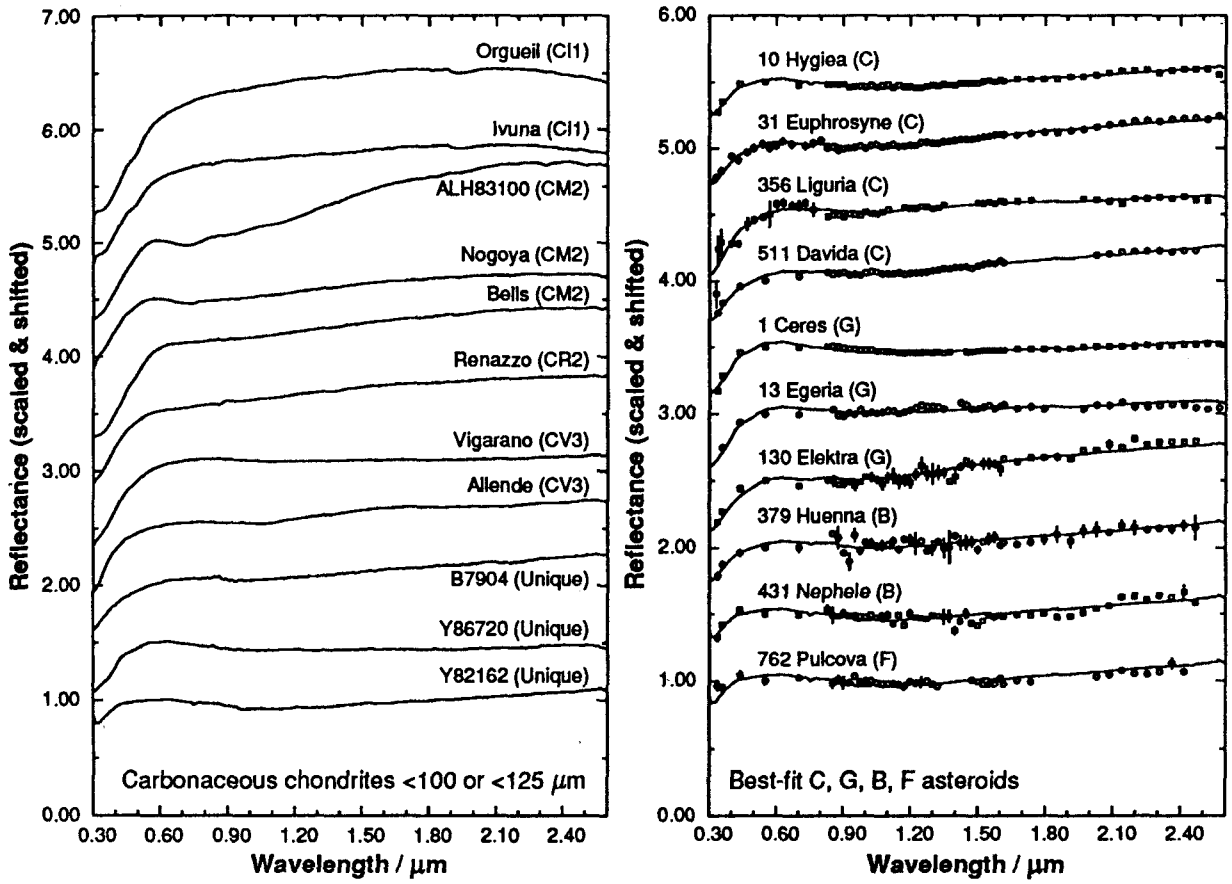

Fig. 2. Laboratory bidirectional reflectance spectra (30° incidence and 0° emergence angles) of carbonaceous chondrites and telescopic reflectance spectra of the C, G, B, F asteroids [8,9,10] best fit with those of carbonaceous chondrites by the isograin model [15,16]. Reflectances are scaled to 1 at 0.55 μm and shifted by 0.5 each.

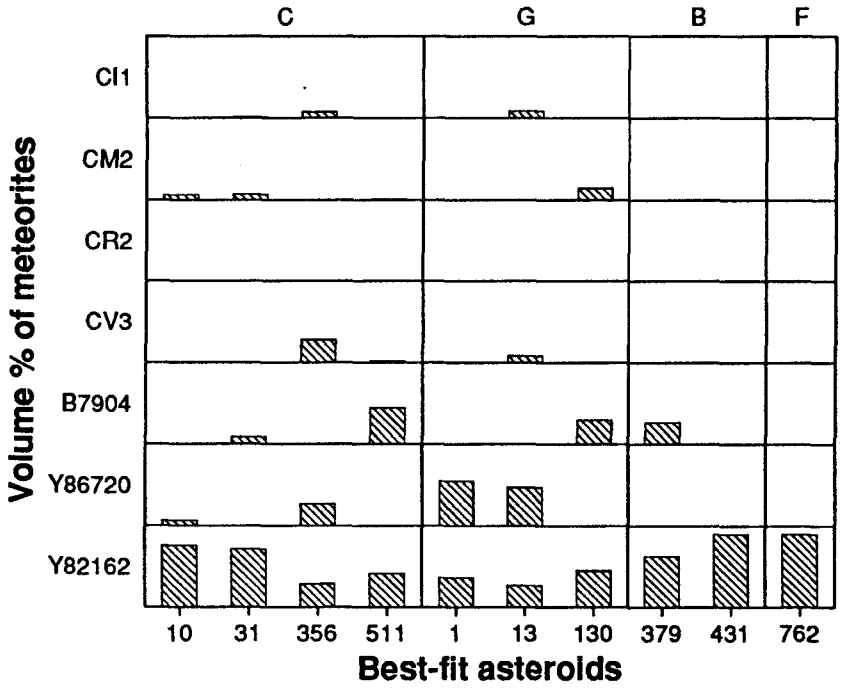

Fig. 3. Volume abundances of carbonaceous chondrites on the best-fit C, G, B, F asteroids calculated from the spectral fits shown in Fig. 2. Asteroid numbers are grouped according to their spectral types indicated at the top of the figure.

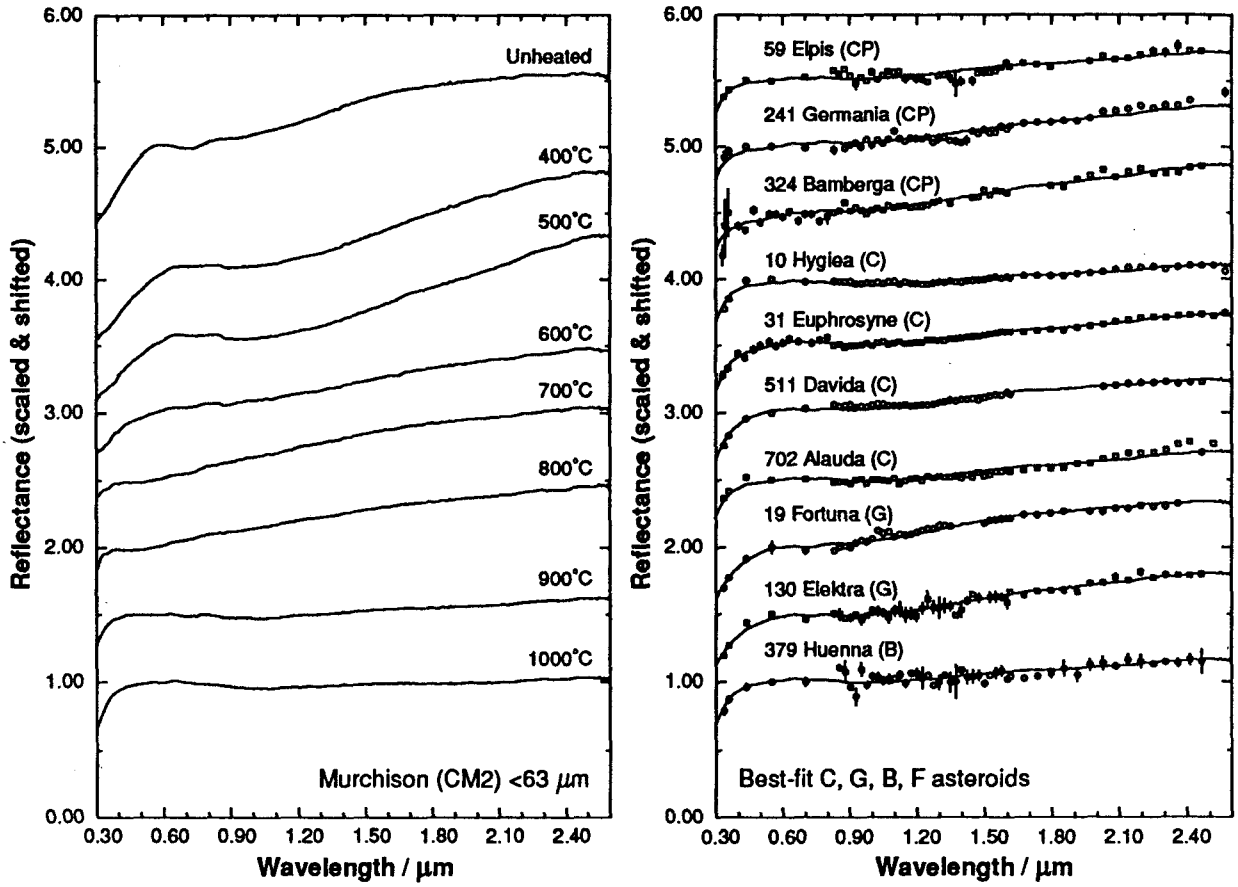

Fig. 4. Laboratory bidirectional reflectance spectra (30° incidence and 0° emergence angles) of Murchison heated at various temperatures and telescopic reflectance spectra of the C, G, B, F asteroids [8,9,10] best fit with those of Murchison by the isograin model [15,16]. Reflectances are scaled to 1 at 0.55 μm and shifted by 0.5 each.

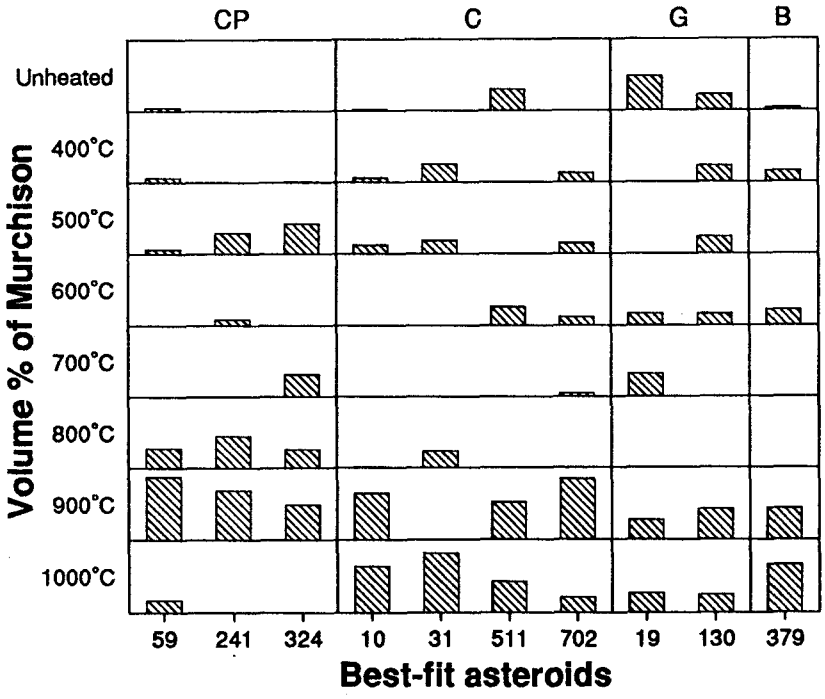

Fig. 5. Volume abundances of heated Murchison on the best-fit C, G, B, F asteroids calculated from the spectral fits shown in Fig. 4. Asteroid numbers are grouped according to their spectral types indicated at the top of the figure.

PRIMITIVE FE-NI METAL AND PHOSPHATE MINERALS IN YAMATO-82094 CARBONACEOUS CHONDRITE

Yasuhiro SHIBATA and Hiroharu MATSUEDA

Department of Geology and Mineralogy, Hokkaido University, Sapporo 060, Japan.

Introduction

The Yamato-82094 carbonaceous chondrite had been classified as Ornans type (Yanai and Kojima, 1987), but recently it was classified as a unique type 3 carbonaceous chondrite (Scott et al., 1992). This study is aimed at making clear existence of possibly primitive material with special emphasis of the Fe-Ni metal and phosphate minerals in Y-82094. Yamato-791717, Yamato-790992 and Yamato-81020 CO3 chondrites were also investigated in this study with microscopic observation and EPMA chemical analyses.

Occurrence and chemical composition of Fe-Ni metal

Major Fe-Ni metal is kamacite in Y-82094, but occasionally tiny taenite grains (<20 micron in diameter) occur in kamacite grains. Ni contents of kamacite within chondrules are about 6-7 atom.%, while those in matrix are about 5-7 atom.%. Co contents of kamacite are about 0.4-0.7 atom.% irrespective of occurrence. Ni and Co contents of metal grains tend to show negative correlation, but only kamacite grains show positive correlation. Cu contents are very low (max: 0.11 atom.%) in kamacite, while higher in taenite (max: 0.46 atom.%). Ni and Cu contents of metal grains show positive correlation.

Based on the partition of Co between coexisting taenite and kamacite (Afiattalab and Wasson, 1980), obtained equilibrium temperature are as follows; about 800-550 ℃ for Y-82094, about 700-500 ℃ for Y-791717, about 550-500 ℃ for Y-790992, about 550-420 ℃ for Y-81020, respectively. Compositional ranges of taenite in the three carbonaceous chondrites except Y-82094 are relatively narrow, while Ni content of taenite in Y-82094 shows wide range (15-45 atom.%) (Fig. 1). The interface between troilite and Fe-Ni metal in Y-82094 consists of micron-sized intergrowths of the both phases.

Na-rich phosphate minerals in Fe-Ni metal

Fe-Ni metal grains in the four carbonaceous chondrites include olivine, pyroxene, magnetite, chromite and phosphate minerals. The phosphate inclusions are mainly composed of fine-grained whitlockite (typically <10 micron in diameter). However, Fe-Ni metal in Y-82094 also include coarse-grained whitlockite (max:20 micron in diameter) and especially Na-rich phosphate minerals (brianite and

panethite). Whitlockite with round-shaped usually exist in marginal part of Fe-Ni metal grain. Brianite and panethite with fragmental shape exist as isolated grains, not adjacent to Na, Ca and Mg bearing minerals.

Discussion

It is considered that carbonaceous chondrites of petrographic type 3 have not been affected by severe thermal metamorphism in the evolutional process of parent body. Assuming that Fe-Ni metal had appeared to predate chondrule formation and variation of chemical composition and texture for Fe-Ni metal depend mainly on heating and cooling process in the chondrule formation, we discuss the property of primitive material for Fe-Ni metal in Y-82094 based on the above results.

Variety of the estimated temperature on the basis of Co partition are considered to reflect the different cooling rate of Fe-Ni metal. In case of faster cooling rate of Fe-Ni metal, partition of Co could be stopped at the higher temperatures. Cooling rate of Fe-Ni metal in Y-82094 is the fastest in the four carbonaceous chondrites. The micron-sized intergrowths of troilite and Fe-Ni metal in Y-82094 also appear to result from fast cooling.

Na-rich phosphates might have existed within Fe-Ni metal before heating event of chondrule formation. Because it does not seem that they had been formed as reaction products between phosphorus in Fe-Ni metal or phosphide, and gas phase or Na, Ca and Mg bearing mineral based on their mode of occurrence. They could be remained within Fe-Ni metal due to insufficient heating and fast cooling.

It seems that the wide Ni range of taenite grains in Y-82094 might be also resulted from insufficient heating and fast cooling. Based on the partition of Co, low Ni taenite grains show higher temperature (about 800-700 ℃), while high Ni taenite grains dotted within kamacite show lower ones (about 600-550 ℃). It is considered that composition of the metal grains before heating process influence on taenite grains with high Ni content. Because the composition of taenite and kamacite grain could not be homogenized owing to insufficient heating and fast cooling.

As a concluding remark, it is inferred that Fe-Ni metal in Y-82094 is the most primitive one in the four carbonaceous chondrites investigated in this study.

References

Afiattalab F. and Wasson J.T. (1980) *Geochim. Cosmochim. Acta* 44, 431-446.

Scott E.R.D., Keil K., and Stoffler D. (1992) *Geochim. Cosmochim. Acta* 56, 4281-4293.

Yanai K. and Kojima H. (1987) *Photographic Catalog of the Antarctic Meteorites*. NIPR, Tokyo.

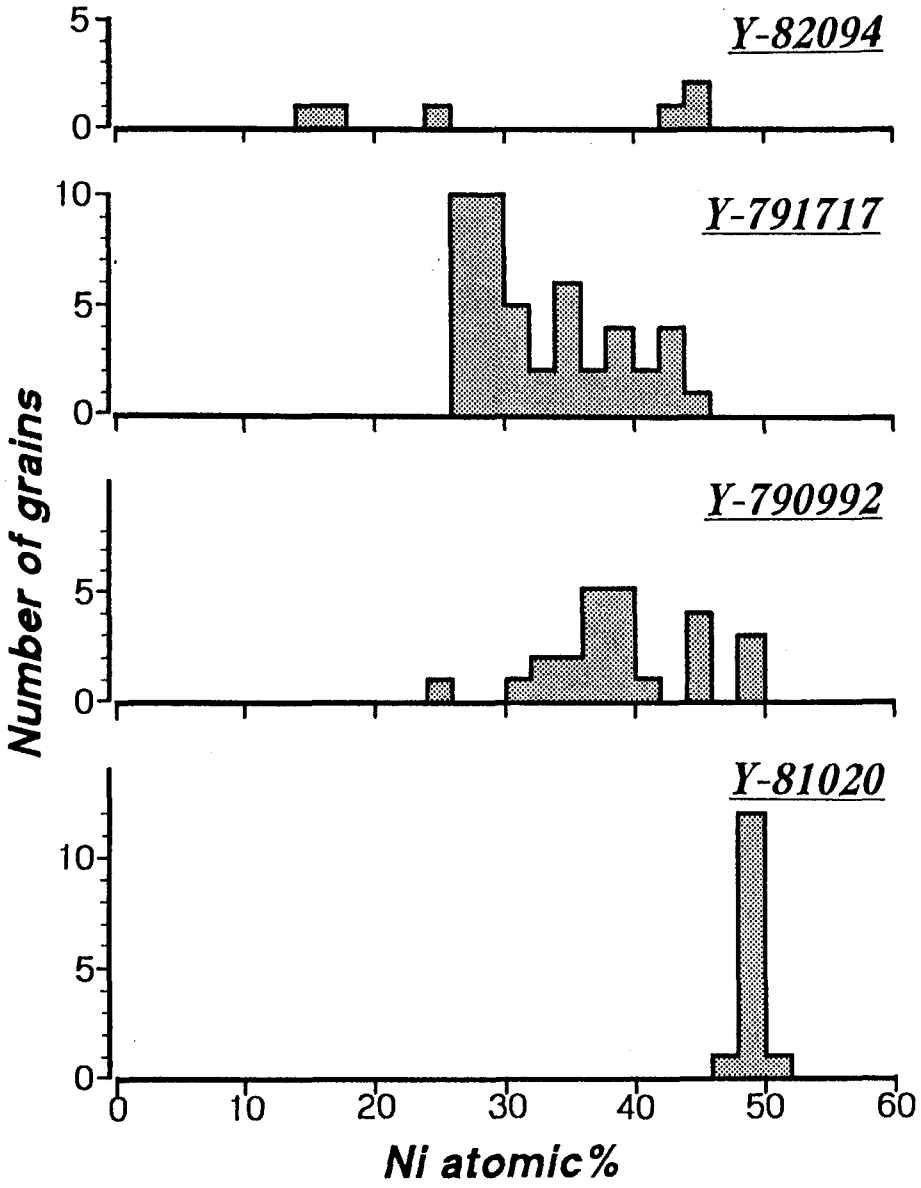

Fig. 1. Histograms of Ni contents in taenite grains in Y-82094, Y-791717, Y-790992, and Y-81020.

PHYLLOSILICATES IN CHONDRULES AND MATRIX IN THE MURCHISON CM2 CHONDRITE

Takaaki NOGUCHI[1], Kiyoshi FUJINO[2], Hitoshi MOMOI[3].

1) Department of Earth Sciences, Ibaraki University, Mito 310. 2) Department of Geology and Mineralogy, Hokkaido University, Sapporo 060. 3) Department of Earth Sciences, Ehime University, Matsuyama 790.

The CM chondrites experienced aqueous alteration (e. g. Bunch and Chang, 1980; Tomeoka and Buseck, 1985). There is a controversy whether the aqueous alteration of the CM chondrites occurred before or after accretion to their parent body. Recently, some clues to the aqueous alteration before accretion were suggested by some researchers (e. g. Nakamura et al., 1991; Metzler et al., 1992). On the contrary, Kojima and Yanai (1993) reported some veins which were formed by the aqueous activity after accretion in a highly altered CM chondrite. It seems to be required to distinguish which minerals were formed by aqueous alteration before or after accretion. To clarify these processes, it is important to characterize the alteration products by a transmission electron microscope (TEM) in chondrules and inclusions as well as those in matrix.

In this study, we investigated the Murchison CM chondrite. A demountable polished thin section of Murchison was prepared and investigated by a secondary electron microscope (SEM) and an electron probe microanalyzer (EPMA). Based on these data, three chondrules were selected for TEM and analytical electron microscope (AEM) study.

In Murchison, many chondrules including magnesian olivine and low-Ca pyroxene phenocrysts showing no significant Fe-Mg zonings. Such chondrules include so-called "spinach" (Fuchs et al., 1973), the green, fibrous phyllosilicate material. However, it is not clear that what kinds of phyllosilicates consist of "spinach" (Zolensky and McSween, 1988). Back-scattered electron image (BEI) photographs in these chondrules show that "spinach" consist of coarse tabular crystals (< several μm across) and interstitial materials among the coarse crystals.

EPMA analyses of these alteration products show that FeO^* contents in coarse phyllosilicates in some chondrules of this kind are higher than those in phyllosilicates in matrix. Such phyllosilicates have compositions near pure cronstedtite. EPMA analyses show that Al_2O_3 contents in phyllosilicates in chondrules tend to be higher than those in matrix. However, it is difficult to identify mineral species and chemical compositions of coarse phyllosilicates and interstitial materials only by EPMA analyses.

Two magnesian porphyritic olivine pyroxene (m-POP) chondrules were selected for TEM and AEM study. One includes phyllosilicates with near cronstedtite compositions. The other includes phyllosilicates with more magnesian phyllosilicates than those in the former. In this study, the former is called m-POP1 and the latter m-POP2. In addition to these two chondrules, a ferroan porphyritic olivine (f-PO) chondrule in which alteration products showing colloform texture, was also chosen for TEM and AEM study.

Figure 1 shows the alteration products in m-POP1. This photomicrograph shows that coarse phyllosilicates set in fibrous phyllosilicates. High resolution photomicrographs of the coarse phyllosilicates show ~7 Å lattice fringes. High resolution photomicrographs of the fibrous phyllosilicates reveal that the phyllosilicates contain volumes of minute crystals (< a few tens nm across) with ~7 Å lattice fringes, although electron diffraction photographs of

the fibrous phyllosilicates give only halo patterns. Phyllosilicates in m-POP2 display similar texture to those in m-POP1. In m-POP2, both coarse and fibrous phyllosilicates display ~7 Å lattice fringes as is the case of m-POP1. These data suggest that most of phyllosilicates in chondrules are serpentine group minerals.

Fig. 2 displays Si-Mg-Fe and [Mg+Fe]-Al-Si diagrams of phyllosilicates in m-POPs and f-PO. These data were taken by an AEM. Area analyses (50 nm x 50 nm) were performed in order to prevent compositional change during analysis. Structural and compositional data of the coarse phyllosilicates in m-POPs suggest that they are cronstedtite. As inferred from EPMA data, coarse phyllosilicates in m-POP1 have near cronstedtite compositions. Fibrous phyllosilicates in m-POPs are Al-Fe-rich serpentines (berthierine). Al_2O_3 contents in these fibrous phyllosilicates range from 10 to 18 wt. % when the total wt. % is normalized to 100. The coarse phyllosilicates contain more FeO^* than the fibrous phyllosilicates. The coarse phyllosilicates are fairly homogeneous in comparison to the fibrous phyllosilicates. Although compositional features of coarse and fibrous phyllosilicates are similar between m-POP1 and 2, there are also differences in chemical compositions of phyllosilicates between them. There is a compositional gap in $Mg/(Mg+Fe^*)$ ratio between the coarse and fibrous phyllosilicates in m-POP1, but not exist in m-POP2.

There are fibrous phyllosilicate materials with compositions between berthierine and talc (Fig. 2a and d). They were observed in a specific area of the altered mesostases. The appearance of these materials may have depended on local differences in materials which participated in alteration reactions. Under high magnifications, fine-grained phyllosilicates (< a few ten nm across) with ~7 Å lattice fringes were observed but those with ~10 Å lattice fringes were not. At present it is not clear whether materials with talc compositions are crystalline or not.

In f-PO, fibrous phyllosilicates could not been observed under low magnifications. However, electron diffraction gives powder pattern and phyllosilicates with lattice fringes of ~7 Å are observed under high magnifications. Figure 2c and f shows that phyllosilicates in f-PO are FeO-rich serpentine. Their compositions are different from phyllosilicates in m-POPs. In f-PO, phyllosilicates are more magnesian than those in m-POPs though Fo contents of olivine in f-PO (Fo_{84}~Fo_{56}) are much higher than those in m-POPs.

Structural and compositional data of phyllosilicates in m-POPs indicate that "spinach" is not a single phyllosilicate but a mixture of cronstedtite and berthierine (and talc?). Mineral species of phyllosilicates are different among magnesian and ferroan chondrules.

Alteration products in matrices of the CM chondrites are represented by a mixture of ferroan serpentine, magnesian cronstedtite, and tochilinite (e. g. Tomeoka et al., 1989). On the contrary, secondary phases in chondrules are not represented by these phases. Probably this difference resulted from materials which participated in alteration reactions in chondrules were different from those in matrix. Along with mineral assemblages of secondary phases, chemical compositions of cronstedtite are different between in chondrules and matrix. In m-POP1, cronstedtites include less than a few wt. % MgO (100 % normalized value). If PCPs, mixtures of magnesian cronstedtite and tochilinite, were formed firstly during the aqueous alteration of the CM chondrites, cronstedites in chondrules could not include more FeO^* than magnesian cronstedtites in PCPs.

References Bunch, T. E. and Chang, S. (1980) Geochim. Cosmochim. Acta, 44, 1543-1577. Fuchs, L. H., Olsen, E., and Jensen, K. J. (1973) Smithsonian Contrib. Earth Sci., 10. Kojima, H. and Yanai, K. (1993) Abstract for the 100th Annual Meeting of the Geol. Soc. of Japan, 645 (in Japanese). Metzler, K., Bischoff, A., and Stöffler, D. Geochim. Cosmochim. Acta, 56, 2873-2897. Tomeoka, K. and Buseck, P. R. (1985) Geochim. Cosmochim. Acta, 49, 2149-2163. Tomeoka, K., McSween, H. Y., and Buseck, P. R. (1989) Proc. NIPR Symp. Antarct. Meteorites, 2, 221-234. Nakamura, T., Tomeoka, K., and Takeda, H. (1991) Papers presented to the 16th Symp. on Antarct. Meteor., 40-41. Zolensky, M. and McSween, H. Y. (1988) In: Meteorites and the early solar system, pp. 114-143.

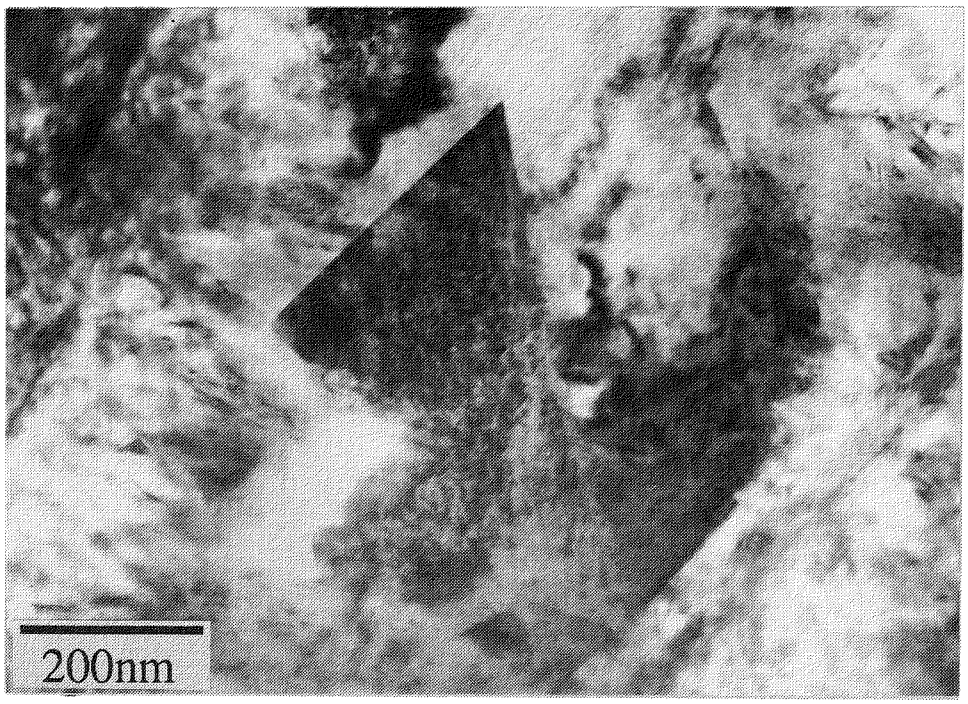

Fig. 1 TEM image of phyllosilicates in m-POP1. Coarse phyllosilicates (cronstedtite) set in fibrous phyllosilicates (berthierine).

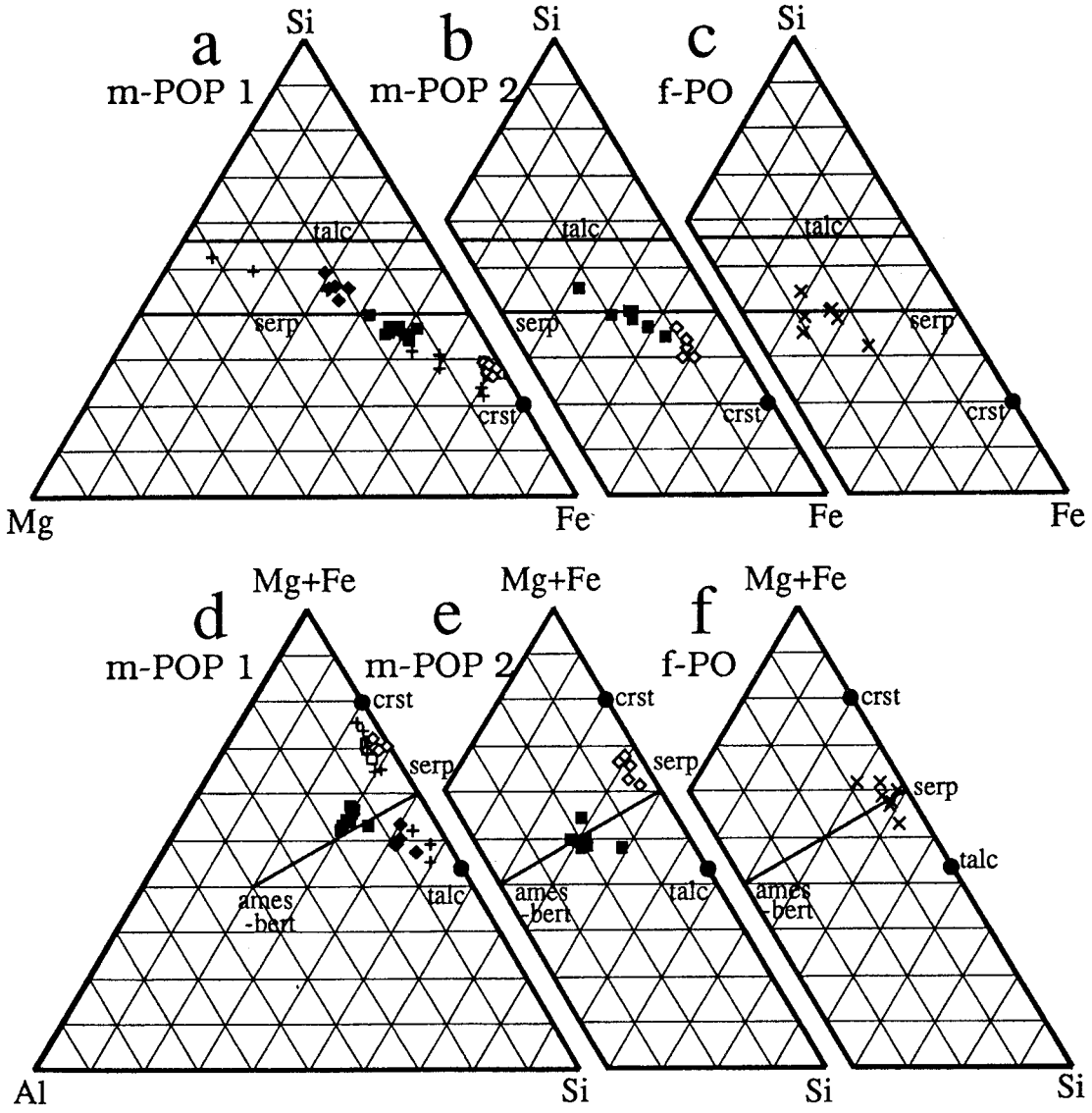

Fig. 2 Si-Mg-Fe and [Mg+Fe]-Al-Si diagrams of phyllosilicates in chondrules (AEM analyses). open symbols: coarse tabular phyllosilicates, solid symbols: fibrous phyllosilicates, plus: phyllosilicates in chondrule rim, cross: phyllosilicates in f-PO.

34

Where has the CM chondrite been altered?

Hideyasu Kojima and Keizo Yanai; National Institute of Polar Research, 9-10, Kaga 1-chome, Itabashi-ku, Tokyo 173, Japan

The aqueous alteration is the typical features of CI and CM carbonaceous chondrites. It is doubtless that CI chondrite has been altered on the parent body, because of the existance of carbonate and sulfate veins(Richardson, 1978) and surpentine veins (Tomeoka, 1990) in it. on the other hand, CM chondrite does not have clear evidence that shows where it has been altered such as the CI chondrite. Previous investigators proporsed two candidates of the place for the alteration. One is the solar nebular and the other is the parent body. We discus s where CM chondrite has been altered based on the petrographical features of the Antarctic CM chondrites.

EET83334 and ALH88045 were classified into CM chondrite. They are completely altered stones. No high temperature components such as the olivine and the pyroxene are not observed. They have been completely altered to phyllosilicate minerals. We found small carbonate vein in ALH88045 and vein-like texture in EET 833334. Existance of the veins are the evidence which shows that the aqueous alteration, at least the heavy aqueous alteration have occured in the parent body.

We observed glass which directly contacted with phyllosilicate matrix in Y-75293. This fact indicate that the alteration has not proceeded after the contact of two components. Y-75293 has suffered the brecciation by regolith-gardening. Textural feature indicate that two components, glass and phyllo-silicate matrix have contacted by the brecciation. Thus it is clear that the alteration has not proceeded by cause of the regolith-gardening.

Y-793321 include fragments that have suffered different degree of the alteration. This indicate that the parent body of the CM chondrite consists of lithology with different degree of the alteration. They have been mixed by the regolith-gardening.

Formation of PCP in PCP-rich layer outside of the rim is pre-accretion to the parent body(Kojima and Yanai, 1989)

These evidences lead authors to following conclusions. The alteration of the CM chondrite has proceeded inside of the parent body except the formation of PCP in PCP-rich layer. However it is not clear that the weak alteration of matrix-consisting components began already in the solar nebular or not.

References

Richardson(1978) Meteoritics, Vol 13, 141-160. Tomeoka K.(1990): Nature, 345, 138-140. Kojima H. and Yanai K.(1989): Meteoritics, Vol. 24, 288.

SILICA-FAYALITE-BEARING CHONDRULES IN ORDINARY CHONDRITES: EVIDENCE OF OXIDATION IN THE SOLAR NEBULA. Alexander N. Krot and John T. Wasson. Institute of Geophysics and Planetary Physics, University of California, Los Angeles, CA 90025, USA.

Introduction Most ordinary chondrite (OC) chondrules have compositions that are similar to those of bulk OC in terms of lithophile element abundances (e.g., Grossman and Wasson, 1983). There are only a few rare chondrule classes that deviate significantly from OC-like compositions; these include Al-rich chondrules (Bischoff and Keil, 1984), chromitic and chromite-bearing silicate chondrules (Krot et al., 1993; Krot and Rubin, 1993) and silica-rich chondrules (Brigham et al., 1986). Based on their mineralogy and chemistry, silica-bearing objects in OC can be divided into four categories: (1) silica-pyroxene chondrules (Olsen et al., 1981; Planner, 1983; Fredriksson and Wlotzka, 1985; Brigham et al. 1986; Matsunami et al., 1992; Ivanova et al., 1993), (2) silica-fayalite clasts (Brigham et al., 1986), (3) silica-plagioclase-pyroxene fragments (Ruzicka and Boynton, 1992; Bischoff, 1993), and (4) silica-rich spherules within chondrule rims and opaque matrix (Matsunami et al., 1990). We report here the discovery and investigation of additional silica- and silica-fayalite-bearing chondrules in type-3 OC and discuss their possible origin.

Results We studied 41 thin sections of unequilibrated OC and found 82 silica-bearing chondrules which can be divided into two major categories (corresponding to categories 1 and 2 mentioned above): silica-pyroxene chondrules and silica-fayalite-pyroxene chondrules. These chondrules are more common in H (>3/cm^2) than in L and LL chondrites (<1/cm^2). They differ in mineralogy and chemistry from the silica-bearing pyroxene-plagioclase fragments of possibly magmatic origin (impact melting?) (Ruzicka and Boynton, 1992; Bischoff, 1993). In all cases silica is pure; it contains only small amounts of FeO (<0.8 wt.%).

Silica-pyroxene chondrules consist of low-Ca pyroxene, silica and accessory high-Ca pyroxene, plagioclase mesostasis, metallic Fe,Ni and troilite. These chondrules have radial and porphyritic textures.

Silica-bearing radial pyroxene (RP) chondrules contain 5-10 vol.% silica which forms skeletal, elongated and ellipsoidal grains randomly oriented with respect to the radiating pyroxene crystals. Petrographic observations suggest that these chondrules were completely molten and cooled rapidly. Low-Ca pyroxene is typically uniform in composition in the individual chondrules but varies significantly from one chondrule to another ($Fs_{10.2}$ $Wo_{0.9}$ - $Fs_{31.5}$ $Wo_{1.9}$). Two silica-bearing chondrules in H regolith breccia Weston and H3.8 Dhajala have low-Ca pyroxene grains that are compositionally zoned: ferrosilite contents decrease from the rim to the center (centers: $Fs_{21.6\text{-}24.5}$ $Wo_{2.5\text{-}2.2}$ and $Fs_{29.8}$ $Wo_{2.8}$, rims: $Fs_{19.6}$ $Wo_{1.6}$ and $Fs_{18.1}$ $Wo_{1.8}$). The zoning probably results from diffusional exchange with matrix material during parent body metamorphism.

Silica-bearing porphyritic pyroxene (PP) chondrules contain 15-40 vol.% silica occurring as compact, irregularly shaped areas (relict grains) in the center parts of the chondrules or as compact rims around the pyroxene cores. Petrographic observations suggest that some of these PP chondrules were not completely molten; they appear to have cooled more slowly than the silica-bearing RP chondrules. Low-Ca pyroxene varies in composition within individual PP chondrules and it is more MgO-rich on average than low-Ca pyroxene in the silica-bearing RP chondrules ($Fs_{5.0}$ $Wo_{0.7}$ - $Fs_{21.1}$ $Wo_{0.2}$).

Silica-fayalite-pyroxene chondrules consist of silica, fayalite ($Fa_{18.6\text{-}100}$) and low-Ca pyroxene; accessory high-Ca pyroxene, plagioclase mesostasis, troilite and metallic Fe,Ni are also

present. Based on texture and the modal abundances of pyroxene and silica these chondrules can be divided into two types: radial or porphyritic silica-fayalite-pyroxene chondrules containing 5-40 vol.% silica and granular silica-fayalite-pyroxene chondrules consisting almost entirely (90-95 vol.%) of silica.

Silica-fayalite-bearing pyroxene chondrules are texturally and compositionally similar to the silica-bearing pyroxene chondrules described above. The only difference between these chondrule categories is the presence of fayalite forming veins within or rims around the silica grains. There is a continuum between these chondrule categories suggesting that they are genetically related: we infer that the fayalite veins and rims formed by alteration of the silica grains. The fayalite in H3.4 Sharps varies in composition from one chondrule to another ($Fa_{51.7-99.6}$) and has a high content of MnO (0.57-1.1 wt.%). The fayalite content originally present within the silica-bearing chondrules in H regolith breccia Culbertson and Tysnes Island was reduced by exchange with matrix olivine of the chondrite hosts during metamorphism.

Granular silica-fayalite-bearing chondrules consist almost entirely of silica. Low-Ca pyroxene forms euhedral inclusions in the silica or rims around silica cores. Fayalite forms veins along the silica grain boundaries; the thickness of these veins varies within a single chondrule reflecting different degrees of alteration. Fragments of granular silica chondrules as relict clasts have been found within two pyroxene chondrules in Sharps. These fragments experienced were altered after chondrule solidification.

Discussion Based on our petrographic observations we conclude that: (1) Silica-bearing chondrules have similar textures to common mafic silicate chondrules and were formed by melting of silica-rich precursor material (which itself may have been produced by fractional condensation; Nagahara and Kushiro, 1987). (2) The higher abundance of silica-bearing chondrules in H than in L and LL chondrites may be connected with the higher modal abundances of olivine in L and LL than in H chondrites; the additional olivine in L and LL chondrites could have reacted more completely with silica during chondrule melting. Alternatively, there may have been less effective fractional condensation of silica in the L and LL formation regions. (3) Silica-fayalite-bearing chondrules formed by alteration of silica-bearing chondrules. The common occurrence of both categories in the same chondrite suggests that the silica-pyroxene chondrules experienced a different pre-agglomeration oxidation history than silica-fayalite-bearing chondrules. This may be connected with (a) formation at a different time or in different regions of the solar nebula or (b) more effective isolation from oxidized solar gas.

References 1. Grossman J.N. and Wasson J.T. (1983) GCA 47, 759-771. 2. Bischoff A. and Keil K. (1984) GCA 48, 693-709. 3. Krot A.N., Ivanova M.A. and Wasson J.T (1993) EPSL (submitted). 4 Krot A.N. and Rubin A.E. (1993) GCA (submitted). 5. Brigham C.A., Yabuki H., Ouyang Z., Murrell M.T., El Goresy A. and Burnett D.S. (1986) GCA 50, 1655-1656. 6. Olsen E.J., Mayaeda T.K. and Clayton R.N. (1981) EPSL 56, 82-88. 7. Planner H.N. (1983) In Chondrules and Their Origins (ed. E.A. King), 235-242. 8. Fredriksson K. and Wlotzka F. (1985) Meteoritics 30, 467-478. 9. Matsunami S., Nishimura H. and Takeshi H. (1990) Proc. 3rd Symp. Antarct. Meteor., 147-180. 10. Ivanova M.A., Kononkova N.N. and Petaev M.I. (1993) LPS 24, . 11. Ruzicka A. and Boynton W.V. (1992) Meteoritics 27, 283. 12. Bischoff A. (1993) LPS 24, 113-114. 13. Matsunami S., Ninagawa K., Kubo H., Fujimura S., Yamamoto I., Wada T. and Nishimura H. (1992) Proc. 5th Symp. Antarct. Meteor., 270-280. 14. Nagahara H. and Kushiro I. (1987) EPSL 85, 537-547.

GLASSY CHONDRULES IN ORDINARY CHONDRITES: EVIDENCE OF FINE-GRAINED PRECURSOR MATERIALS RICH IN REFRACTORY (Ca, Al, Ti) AND MODERATELY VOLATILE (Na, K) ELEMENTS. Krot A.N., Rubin A.E. and Wasson J.T. Institute of Geophysics and Planetary Physics, University of California, CA 90025, USA

Introduction. Chondrules, the most abundant constituent of ordinary chondrites (OC), display a wide variety of textures, sizes and compositions. Common mafic silicate chondrules contain 5-40 vol.% glassy to microcrystalline mesostases. Several schemes have been devised to classify chondrules by (1) texture and mineralogy (e.g., Gooding and Keil, 1981), (2) texture, mineralogy and chemistry (e.g., McSween, 1977; Scott and Taylor, 1983; Jones and Scott, 1989; Jones, 1990), and (3) cathodoluminescence characteristics, and olivine and mesostasis compositions (Sears et al., 1992). However, several categories of rare OC chondrules are excluded by these schemes, including chromitic chondrules (Ramdohr, 1967; Krot et al., 1993), chromite-bearing silicate chondrules (Krot and Rubin, 1993), silica-bearing chondrules (Brigham et al., 1986; Krot and Wasson, 1993) and Al-rich chondrules (Bischoff and Keil, 1984). Glassy chondrules are a subset of Al-rich chondrules containing >50 vol.% glass (or devitrified glassy mesostasis); in this paper we report the results of detailed petrologic study of 14 glassy chondrules from ten type-3 OC and two OC regolith breccias.

Results. Glassy chondrules range from 250 to 1300 μm in apparent diameter. Some contain >95 vol.% glass; in addition to >50 vol.% isotropic or devitrified glass, the other chondrules contain skeletal phenocrysts of olivine, low-Ca pyroxene and/or high-Ca pyroxene; these chondrules have porphyritic olivine (PO), porphyritic olivine-pyroxene (POP) and porphyritic pyroxene (PP) textures. A few chondrules contain accessory spinel, troilite and metallic Fe-Ni. Four chondrules contain relict forsterite grains ($Fa_{0.6-0.7}$) which have a blue cathodoluminescence and high contents of Al_2O_3 (0.14-0.17 wt.%), TiO_2 (0.10-0.14 wt.%) and CaO (0.27-0.59 wt.%); one of these chondrules also contains a 100x200 μm-size fragment of a BO chondrule and a cluster of relict (100-250 μm) euhedral spinels. The relict forsterite grains are similar in composition and cathodoluminescence to relict forsterite grains in unequilibrated OC and carbonaceous chondrites described by Steele (1986) and to porphyritic forsterite grains in chondrules of type IA (Jones and Scott, 1989). Low-Ca pyroxene and pigeonite grains ($Fs_{0.6-16.6}$ $Wo_{0.5-11.1}$) in the glassy chondrules have high contents of Al_2O_3 (2.3-8.8 wt.%). Augite and high-Ca pyroxene ($Fs_{0.3-4.4}$ $Wo_{11.2-52.5}$) have high contents of TiO_2 (1.6-3.0 wt.) and Al_2O_3 (5.6-20.3 wt.%). The glass itself is Na-, Al- and Si-rich and has a corundum-quartz-albite normative composition; in those glassy chondrules where the mesostasis is devitrified, it is Ca- and Al-rich and contains dendritic crystals of fassaite. Two glassy chondrules have compositionally zoned mesostases. In one of them the mesostasis near the rim is Na-poor whereas that near the center is Na-rich; this chondrule probably experienced some volatilization from the surface during a flash heating event. In contrast, another

chondrule has mesostasis with higher contents of Na in its outer zone than in its center; this probably resulted from Ca-Na diffusional exchange with matrix material during parent body metamorphism (Bischoff, 1988).

Discussion. Although the glassy chondrules contain the same phases (i.e., olivine, low-Ca pyroxene, high-Ca pyroxene and glass or devitrified glassy mesostasis) as do common types of mafic silicate chondrules, they do not fit easily into any of the existing chondrule classification schemes (which are based on chondrule mineralogy and texture). The glassy chondrules have some unusual features: (a) glass is a predominant phase, (b) olivine and pyroxene grains typically have skeletal morphologies, and (c) low-Ca and high-Ca pyroxenes have high concentrations of Al_2O_3 and TiO_2. Common mafic silicate chondrules contain glassy to mostly microcrystalline mesostases (5-40 vol.%), euhedral and subhedral olivine and low-Ca pyroxene grains with low contents of Al_2O_3 and TiO_2; furthermore, high-Ca pyroxene is rare and it typically rims low-Ca pyroxene grains or forms dendritic, quench crystals in the mesostasis (Scott and Taylor, 1983; Jones, 1990). Glassy chondrules are similar in mineralogy and bulk composition to previously studied Al-rich chondrules (Bischoff and Keil, 1984).

Bischoff and Keil (1984) suggested that Al-rich chondrules were formed by melting of unusual precursor materials rich in refractory (Ca, Al, Ti) and moderately volatile elements (Na, K). However, Bischoff and Palme (1988) and Bischoff et al. (1989) found that three Al-rich chondrules in H4 Ybbsitz had bulk fractionated rare earth element (REE) patterns and an overall similarity to the mesostases of common mafic silicate chondrules; they concluded that Al-rich chondrules were formed from mesostases lost from normal mafic silicate chondrules during collisions. They suggested that the existence of compound chondrules provided evidence for abundant collisions among partially or completely molten chondrules. However, there are several arguments against this model: (1) Ybbsitz is an equilibrated chondrite and the REE patterns of its chondrules were probably significantly modified during metamorphism. By contrast, three Al-rich chondrules in the less equilibrated H3.8 Dhajala have nearly flat (4-8xCI) REE patterns (Boynton et al., 1983). (2) The model predicts that the compositions of mesostases in type-3 OC chondrules are similar in compositions to those of bulk Al-rich chondrules (Bischoff and Keil, 1984). However, Na-Al-rich mesostases similar in composition to the bulk compositions of glassy chondrules are extremely rare. (3) Most compound chondrules were not formed by collisions between partially molten chondrules resulting in the loss of their mesostases (Wasson, 1993); many seem to have been formed by remelting fine-grained material adhering to the chondrule surface and by low-velocity collisons without significant mesostasis. (4) The sizes of glassy chondrules are similar to those of common mafic silicate chondrules in OC. We thus reject the model of chondrule collisonal disruption as the mechanism for forming glassy chondrules in OC.

Our petrographic observations and chemical data on the glassy chondrules support the model of Bischoff and Keil (1984). The high glass contents and the skeletal morphologies of olivine and pyroxene crystals suggest virtually complete melting of the presursor materials followed by rapid cooling. These features could have resulted from melting unusual precursor materials rich in refractory (Ca, Al, Ti) and moderately volatile (Na, K) elements; these materials may have had low melting temperatures and/or small grain sizes (Hewins, 1988; Connolly and Hewins, 1991). Such precursors may have formed by alkali condensation on fine-grained refractory-rich particles. The occurrence of relict forsterite grains and chondrule fragments in some glassy chondrules suggests that these glassy chondrules formed by remelting fine-grained moderately-volatile-rich precursor materials that had admixed with coarse-grained forsterite grains.

References: 1. Gooding J.L. and Keil K. (1981) Meteoritics 16, 17-43. 2. McSween H.Y. (1977) GCA 41, 1843-1860. 3. Scott E.R.D. and Taylor G.J. (1983) Pros. LPSC 14, B275-B286. 4. Jones R.H. and Scott (1989) Proc. LPSC 19, 523-526. 5. Jones R.H. (1990) GCA 54, 1785-1802. 6. Sears D.W.G., Lu J., Benoit P.H., DeHart J.M. and Lofgren G.E. (1992) Nature 357, 207-210. 7. Ramdohr P. (1967) GCA 31, 1961-1967. 8. Krot A.N., Ivanova M.A. and Wasson J.T. (1993) EPSL (submitted). 9. Krot A.N. and Rubin A.E. (1993) GCA (submitted). 10. Krot A.N. and Wasson J.T. (1993) 18th Symp. Antarct. Meteor. 11. Brigham C., Yabuki H., Quyang Z., Murrell M.T., El Goresy A. and Burnett D. (1986) GCA 50, 1655-1666. 12. Bischoff A. and Keil K. (1984) GCA 48, 693-709. 13. Steele I.M. (1986) GCA 50, 1379-1395. 14. Bischoff A. and Palme H. (1988) LPS 19, 86-87. 15. Bischoff A., Palme H. and Spettel B. (1989) EPSL 93, 170-180. 16. Boynton W.V., Hill D.H., Wark D.A. and Bischoff A. (1983) Meteoritics 18, 270-271. 17. Wasson J.T. (1993) Meteoritics 28 (in press). 18. Hewins R. (1988) In Meteorites and the Early Solar System (eds. J.F. Kerridge and M.S. Matthews), 660-679. 19. Connolly H.C. and Hewins R.H. (1991) GCA 55, 2943-2950.

Fe-Mg zoning in olivines of Allende chondrules

S. Maruyama, H. Yurimoto, S. Sueno, and K. Kurita
(Institute of Geoscience, The University of Tsukuba)

Introduction

Many people have hypothesized the formative process of chondrules. In these days, it is thought that chondrules were formed by rapid solidification of molten silicate dust (e.g. GROSSMAN et al, 1988). Dust separated from the solar nebula became matrix of chondrules. Part of dust accreted onto chondrules and formed dust mantles before the formation of parent bodies (KRING, 1991).

In this report, we analyze the Fe-Mg zoning profile in chondrules of Allende meteorite. Most chondrules in Allende meteorite are classified to three textual categories, which are porphyritic olivine (PO), porphyritic olivine-pyroxene (POP), and barred-olivine (BO) chondrules (GOODING and KEIL, 1981).

Many chondrules include olivine grains, and the Fe-Mg zoning is commonly observed at the rim in these olivine grains. Since the Fe-Mg zoning was formed as a result of the Fe-Mg interdiffusion after chondrule solidification, it is a record of the effect of the environment surrounding chondrules (JONES and RUBIE, 1991).

There are two possible periods when the Fe-Mg interdiffusion between chondrules and the outside could occur in the formative process of the chondrite. One possibility is a period when chondrules drifted in the solar nebula. In this case, the diffusion occurred between the solar nebular gas and chondrules. The other is a period after chondrules accreted in the parent body. In this case, the diffusion occurred between matrix and chondrules.

Penetration depth on the diffusion phenomena depends on temperature and time. If the Fe-Mg interdiffusion achieved by metamorphism in the parent body, the diffusion profiles are same among chondrules because temperature-time condition was same in a meteorite specimen sample.

On the other hand, if the interdiffusion occurred in the solar nebula, the zoning profiles depend on the uniformity of the environment of the solar nebula. If the solar nebula was widely uniform, zoning profiles of olivine grains among chondrules would be same because the diffusion in each chondrule occurred on the same condition. If the environment of solar nebula was not uniform, the Fe-Mg diffusion would progress at different rates in each places of the solar nebula. As a result, zoning profiles of olivine grains would be different from each chondrule.

In this report, we analyze the Fe-Mg zoning profile in chondrules of Allende meteorite. We analyzed 8 PO, 2 POP, and 1 BO chondrules. We attempted to understand the formative process of the zoning in chondrule olivines in Allende meteorite.

Results

Fig.1 shows Fe X-ray concentration image of the typical Fe-Mg zoning of PO chondrule. Characteristic Fe-Mg zoning was only observed in olivine grains at the chondrule rim. However, there are no such zoning observed clearly in interior olivine grains. The feature indicates that Fe penetrated from the outside of chondrule after solidification.

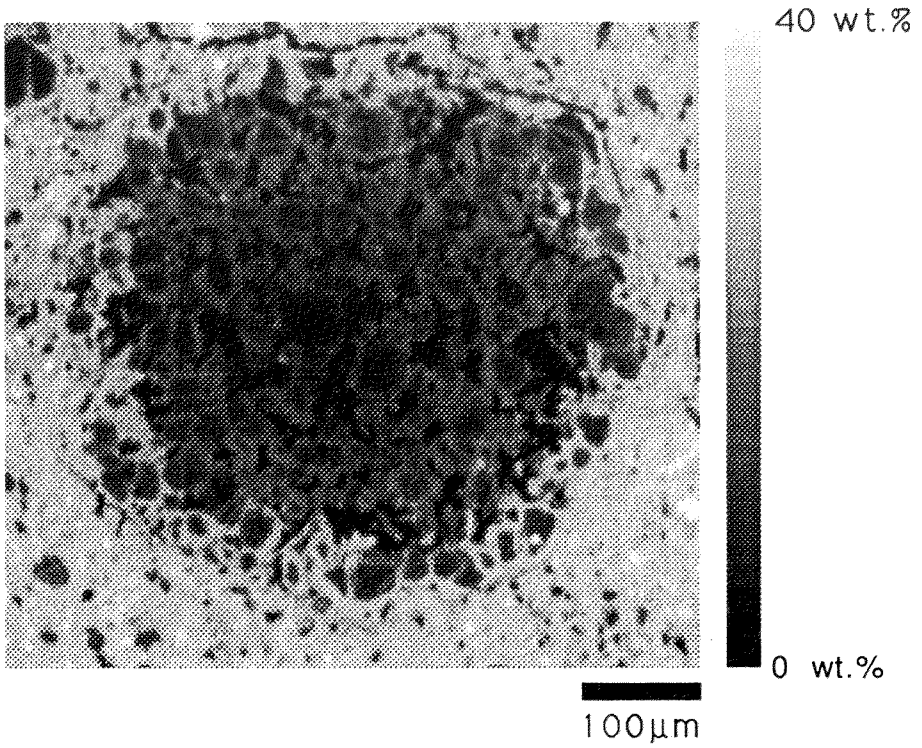

Fig.1. The Fe X-ray concentration image of the typical Fe-Mg zoning of PO chondrule.

Zoning profiles of olivine grains at each chondrule rims are obtained from the Fe concentration maps of the chondrules. Fig.2 shows the relationship between the Fe-penetration depth and the fayalite content at the olivine-matrix boundary. The penetration depth was defined by the distance from the boundary at the 10% concentration of the surface concentration. Olivine grains in a chondrule are displayed by the same symbol. The scatter of the penetration depth of the same symbol is due to the surface of the thin section cut the individual olivine grain by different degree. The scatter of the fayalite content is due to the ununiformity of the matrix. The Fe-penetration depth of most chondrules ranges from 5 μm to 12 μm. However, the penetration depth of one POC (A5-3-19) is several times deeper than the other chondrules. And one POC (A5-3-15) is not observed the Fe penetration from the outside. These two exceptions suggest that Fe-Mg interdiffusion did not occur in the parent body of Allende meteorite.

The chondrule types were classified by the Fa content at the matrix-chondrule boundary, that is, the Fa contents of POPC chondrules are the smallest, whereas those of BOC are the largest, and those of POC is medium. The difference may be result of oxygen fugacity difference of surrounding environments which chondrules formed.

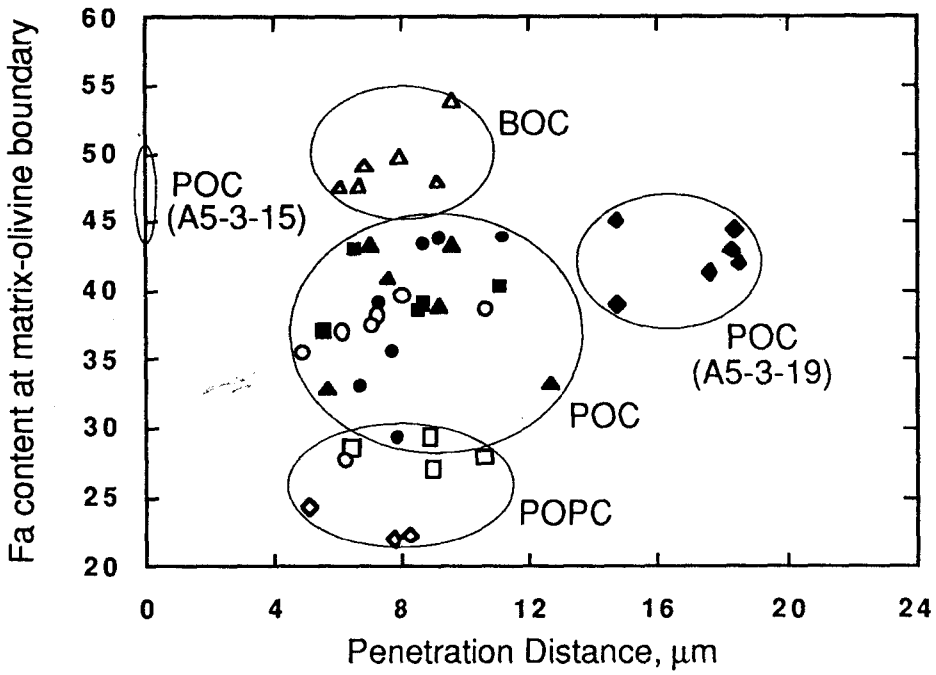

Fig.2. The relationship between the Fe-penetration depth and the fayalite content at matrix-olivine grain boundary. Same symbols indicate different olivine grains in a chondrule.

Discussion

The above results conduct to a scenario for the formation of the Fe-Mg zoning of chondrules as follows; each type of the chondrules formed at different environments in the solar nebula. Fe component in the solar nebular gas penetrated toward the chondrules after solidification. The chondrules mantled by the accretionary dust mantles assembled and then Allende parent body formed. On this scenario, chondrules observed long Fe-penetration depth, such as A5-3-19, were drifted in the hotter solar nebula or Fe-penetration continued in longer period than the other chondrules. Chondrules observed short penetration, A5-3-15, was maintained in cold environment after the formation or it was fixed in the

parent body just after the formation.

These results support the hypothesis that the solar nebula at the time when chondrites formed was ununiform and dynamic environment (METZLER et al., 1992).

Reference

GOODING J.L. and KEIL K. (1981) : Relative abundances of chondrule primary textual types in ordinary chondrites and their bearing on conditions of chondrule formation. *Meteoritics.* **16**, pp.17-43.

GROSSMAN J.N., RUBIN A.E., NAGAHARA H., and KING E.A. (1988) : Properties of chondrules. *METEORITES AND THE EARLY SOLAR SYSTEM.* pp.619-659.

JONES R.H. and RUBIE D.C. (1991) : Thermal histories of CO3 chondrites : application of olivine diffusion modelling to parent body metamorphism. *Earth Planet. Sci. Lett.* **106**, pp.73-86.

KRING D.A. (1991) : High temperature rims around chondrules in primitive chondrites : evidence for fluctuating conditions in the solar nebula. *Earth Planet. Sci. Lett.* **105**, pp.65-80.

METZLER K., BISCHOFF A., and STOFFLER D. (1992) : Accretionary dust mantles in CM chondrites : Evidence for solar nebula processes. *Geochim. Cosmochim. Acta.* **56**, pp.2873-2897.

A RELICT SPINEL GRAIN IN AN ALLENDE FERROMAGNESIAN CHONDRULE

Keiji Misawa[1], Takashi Fujita[2], Masao Kitamura[2], Noboru Nakamura[3], and Hisayoshi Yurimoto[4], [1]Dept. of Antarctic Meteorites, NIPR, 9-10, Kaga 1-chome, Itabashi-ku, Tokyo 173, [2]Dept. of Petrology & Mineralogy, Kyoto Univ., Sakyo-ku, Kyoto 606, [3]Dept. Earth & Planet. Sci., Kobe Univ. Nada-ku, Kobe 657, [4]Inst. of Geosci., Univ. of Tsukuba, Tsukuba, Ibaraki 305, Japan.

It is generally accepted that one of the refractory lithophile precursors in CV-CO chondrules was a high-temperature condensate from the nebular gas and related to Ca, Al-rich inclusions (CAIs) [1,2]. On the basis of Mg isotopic compositions of relict spinel grains in plagioclase-olivine inclusions (POIs) from CV chondrites, Sheng and coworkers [3] also suggested that the major fractionation processes were common to CAIs and chondrules. Rubin and Wasson [4] suggested that at high temperatures, refractory siderophiles (*e.g.*, Os and Ir) were present as fine metal grains. As the nebula cooled, a large fraction of the common siderophiles (Fe, Ni, and Co) nucleated on some of these pre-existing grains. However, little is known about refractory siderophile precursors in chondrules [5]. We report a unique barred olivine chondrule from Allende and discuss the genetic implications of refractory chondrule precursor materials.

Allende R-11 mainly consists of olivine (Fa_{7-18}), pyroxene ($En_{93}Fs_1Wo_6$, $En_{66}Fs_1Wo_{33}$), plagioclase (An_{80}), Fe-poor spinel, and alkali-rich glass with minor amounts of Fe-sulfides, and shows barred olivine texture. Thus, the chondrule can be assigned to a ferromagnesian type. The CI-chondrite normalized REE abundance pattern of the chondrule, excluding a spinel grain, are fractionated, HREE-depleted (4.6–7.8 x CI-chondrite) with a large positive Yb anomaly. The REE abundances are hump-shaped functions of elemental volatility, moderately refractory REE-enriched (Fig. 1), suggesting that the refractory lithophile precursor component of R-11 could be a condensate from the nebular gas and related to Group II CAIs [1,2].

An interior portion of spinel is almost Fe-free but in an outer zone, about 20-40 μm width, FeO contents increase rapidly. TiO_2, Cr_2O_3, and V_2O_3 contents in core spinel are less than 0.5%, which is different from V-rich nature of spinel in fluffy Type A CAIs [6]. The Fe-Mg zoning of spinel may have been generated by diffusional emplacement of Mg and Fe during chondrule-forming event. The spinel contains silicate inclusions and tiny metallic grains. The largest silicate inclusion is composed of Al, Ti-rich pyroxene and an Al, Si, Ca-rich phase. Because of the difficulty of contamination-free analyses from this phase, we use a molar Si-Al-Ca plotting. Assuming fassaite is a contaminant, this phase seems to be Åk~40 melilite. On an Al_2O_3 *vs*. TiO_2 diagram, R-11 fassaite is plotted at the high Al_2O_3/TiO_2 region.

One of the submicron-sized grains was analyzed by SEM-EDS and found that it is composed of refractory Pt-group metals with minor amounts of Fe and Ni. This is the first occurrence of refractory Pt-group metal nuggets in a ferromagnesian chondrule from the Allende (CV3) meteorite. The CI-chondrite normalized elemental abundances for one of the nuggets are compared with those for a nugget in Type A CAI (Fig. 2). W, Os, Ir, Mo, and Ru are enriched, 2-6 x 10^5 relative to CI-chondrite, and abundances of Pt and Rh decrease, 2-10 x 10^4, with increasing volatility. In addition, abundances of Fe and Ni in the nugget are equal to or less than CI-chondrite level. A depletion of Mo relative to other refractory metals may have resulted from high-temperature oxidation [7]. Chondrule R-11 exhibits both similarities (spinel and plagioclase chemistry; Group II REE pattern) and differences (fassaite chemistry; existence of RPM nuggets and melilite) with respect to POIs [3] carrying isotopically fractionated Mg.

It is generally accepted that refractory Pt-group metal nuggets in CAIs were produced during high temperature events at least 1,300°C and before total condensation of Fe in the early solar nebula [8-11]. By analogy of the formation history with CAIs, we suggest that one of the refractory siderophile precursor components of Allende chondrules is a high-temperature condensate from the nebular gas and associated with refractory oxide and silicates. Because the nuggets in chondrule R-11 were surrounded by Mg-spinel, they may have been separated from the common siderophiles (Fe, Ni, and Co) during early stage of condensation and have not been affected by low-temperature alteration [12]. Because diffusion rate of oxygen in spinel is sufficiently slower than diffusional Fe-Mg emplacement rate during chondrule melting condition, Fe-poor relict spinel grains may have preserved primary oxygen isotopic compositions.

REFERENCES: [1] Misawa, K. and Nakamura, N. (1988) *GCA*, **52**, 1669. [2] Misawa, K. and Nakamura, N. (1988) *Nature*, **334**, 47. [3] Sheng, Y. J. et al. (1991) *GCA*, **55**, 581. [4] Rubin, A. E. and Wasson, J. T. (1987) *GCA*, **51**, 425. [5] Grossman, J. N. et al. (1988) in *Meteorites and the early solar system* (eds. Kerridge, J. F. and Matthews, M. S.), pp. 619, The Univ. of Arizona Press, Tucson, AZ. [6] MacPherson, G.J. & Grossman, L. *GCA*, **48**, 29 (1984). [7] Fegley, B. Jr., and Palme, H. (1985) *EPSL*, **72**, 311. [8] Wark, D. A. and Lovering, J. F. (1976) *Lunar Sci.*, **VII**, 912. [9] Palme, H. and Wlotzka, F. (1976) *EPSL*, **33**, 45. [10] El Goresy, A. et al. (1978) *PLPSC*, **9th**, 1279. [11] Blander, M. and Fuchs, L. H. (1980) *PLPSC*, **11th**, 929. [12] Blum, J. D. et al. (1988) *Nature*, **331**, 405. [13] Wark, D. A. (1979) *Astrophys. Space Sci.*, **65**, 275.

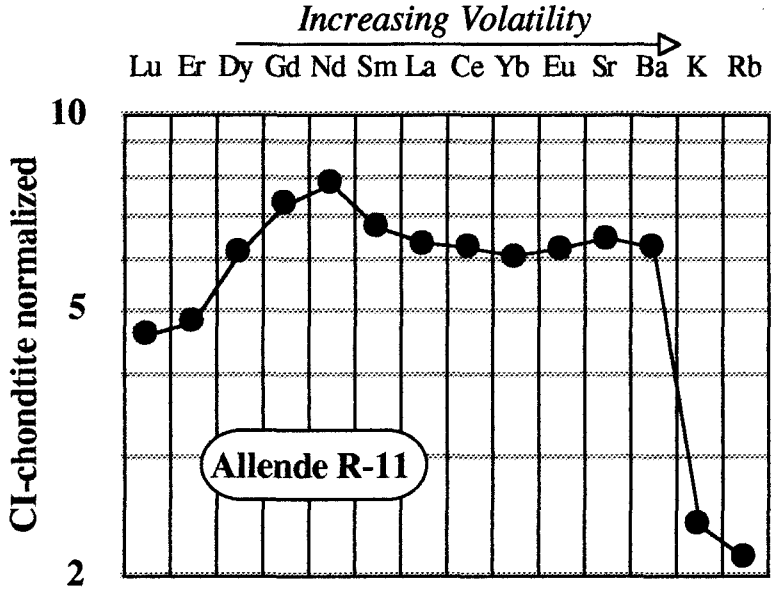

Fig. 1
CI-chondrite normalized lithophile trace element abundances of Allende chondrule R-11 (excluding the spinel grain). Elements are plotted according to volatility from left to right.

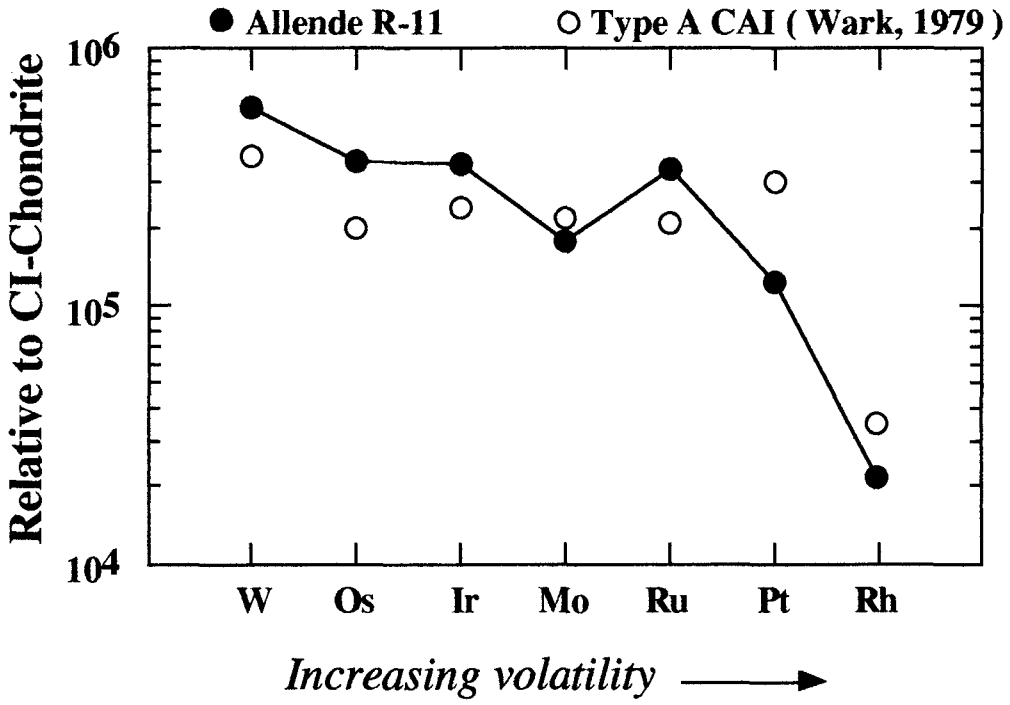

Fig. 2
The CI-chondrite normalized refractory platinum-group metal nuggets in R-11 and in Type A CAI [13] from the Allende (CV3) meteorite. Elements are plotted according to volatility from left to right. Analyzed by SEM-EDS. High pure metals were used as standards. Normalized to 100% after ignoring Mg, Al, and Fe contributions to the analyses from contamination of the spinel.

A CAI FROM EFREMOVKA WITH SUPERREFRACTORY REE PATTERNS AND ENORMOUS ENRICHMENTS IN Sc, Zr, AND Y IN FASSAITE AND PEROVSKITE. *A. El Goresy, S. Matsunami, Max-Planck-Institut für Kernphysik, D-6900 Heidelberg, Germany; E. Zinner, Washington University, St.Louis, Mo 63130, USA; H. Palme, Max-Planck-Institut für Chemie, D-6500 Mainz, Germany; Y. Lin, Institute of Geochemistry, Guangzhou, P.R. China; and M. Nazarov, Vernadsky Institute, Moscow, Russia*

Efremovka 101.1 is a complex object with more than 90% melilite (Ak_1-Ak_{41}). Minor phases are Sc- and Zr-rich fassaite, Y-bearing perovskite, FeNi, and a FeRu phase. The CAI is surrounded with a uniform 5-layer rim sequence consisting of spinel-diopside + Sc-poor fassaite (up to 0.7 wt.% Sc_2O_3) - forsteritic olivine (Fo_{97}-Fo_{100}) - diopside - forsteritic olivine. The melilite-rich core contains two complete but small captured CAIs with their rim sequences consisting of diopside and anorthite. Fassaites are characterized by enormous enrichment in Sc (up to 12.9 wt.% Sc_2O_3) and Zr (up to 5.4 wt.% ZrO_2). They occur as individual grains enclosed in melilite or, as rims around perovskite or rims around FeNi metal grains. Fassaite rims around the metal are enriched in V (up to 5.4 wt.% V_2O_3) and display zoning in their Sc-, Zr-, and V-contents. At direct contact to FeNi they display high V-concentrations decreasing towards their outer rims. Sc- and Zr-contents increase from the metal-fassaite contact to the fassaite-melilite interface. Perovskite is enriched in Y (up to 1.5 wt.% Y_2O_3) with a maximum ZrO_2-content of 1.2 wt.%. The CAI also contains several sinuous fragments with the same layering as in the two captured CAIs, thus suggesting that they are fragments of other captured CAIs.

The REE concentrations in various minerals reveal a distinct superrefractory pattern with depletions in Tm and Yb. CI normalized Zr, Y, and Sc abundances are indicative of crystal-liquid fractional crystallization effects: Fassaite is relatively depleted in Y and enriched in Zr and Sc. The individual mineral layers in the captured CAI rims, the sinuous inclusions, and the rim sequence of the whole CAI display a similar superrefractory REE pattern but do not show fractionations between Sc, Y, and Zr. This indicates that the rim sequences did not form from the same liquid the CAI crystallized from, but condensed from the same gas reservoir with their distinct superrefractory REE signature. Melilite contains excess ^{26}Mg evident for live ^{26}Al with an inferred initial $^{26}Al/^{27}Al$ ratio of (4.4×10^{-5}). The Mg-Al system in the anorthites in the captured sinuous inclusions and small CAIs is disturbed.

IN-SITU OXYGEN ISOTOPE ANALYSIS IN ALLENDE CAI

Hisayoshi Yurimoto [1], Hiroshi Nagasawa [2] and Yoshiharu Mori [3]

[1] Institute of Geoscience, The University of Tsukuba, Tsukuba, Ibaraki 305, Japan, [2] Department of Chemistry, Gakushuin University, Mejiro, Tokyo 171, Japan, [3] National Laboratory for High Energy Physics (KEK), Tsukuba, Ibaraki 305, Japan.

Calcium, aluminium-rich inclusions (CAIs) from carbonaceous chondrite are believed to be among the first solids to have formed in the early solar system and thus to preserve a record of conditions and processes that prevailed early in the solar nebula. We have measured inter- and intra- crystalline oxygen isotope distribution in Type B1 CAI of Allende meteorite. Secondary ion mass spectrometry (SIMS) using negative Au^- primary ion was applied to *in situ* oxygen isotope ratio analysis on an polished thin section of the CAI.

Samples and Experimental Methods: The sample used in this study was a polished thin section (HN3-1c) from Allende HN3-1 Type B1 CAI. Petrological characteristics of the inclusion is described by NAGAHARA et al.[1]. Oxygen isotope data for individual minerals in the inclusion were reported by Mayeda et al. [2]. The polished thin section was coated with ~30 nm of gold film for SIMS analysis. Oxygen isotope ratios were measured by the Tsukuba University CAMECA IMS-3F ion microprobe equipped with BLAKE-V ion source [3]. All O isotopic measurements were made with a focused negative primary ion beam of gold. Primary beam currents were adjusted for each run to obtain a $^{16}O^-$ count rate of ~3 x 10^5 counts s^{-1}. The beam size was 10~20 μm in diameter. A mass resolution power was set to ~2,000 (1% valley), which was sufficient to resolve all significant interferences. Measurements were made by cycling through the mass sequences 16 and 18 in a magnetic peak jumping mode. After the magnetic peak jumping, a precise peak centering of each mass was made by electrostatic peak switching scan. Principle of the electrostatic peak switching equipment was described by SLODZIAN et al. [4]. Secondary ion signals were detected with electron multiplier operated in a pulse counting mode. Signals measured in the electron multiplier were corrected for the counting system dead time. The isotopic composition measured by the SIMS differs from true isotopic composition of the sample by the matrix dependent instrumental mass fractionation. In order to correct the instrumental mass fractionation, a terrestrial crystals was prepared as an internal standard. A measurement run consisted of 100 cycles was divided into "blocks" of 10 cycles each for purpose of time interpolation and peak centering.

Results and Discussion: Intra and inter-crystalline distribution of $\delta^{18}O$ values among crystals in HN3-1 CAI are shown in Fig. 1. The delta values were represented the deviation from the terrestrial standards of corresponding minerals. Distribution of rare earth elements (REE) pattern are also shown in Fig. 1. The REE content in the fassaite is abruptly increased at the rim part, although the pattern is unchanged. The distribution of REE content may be

corresponding to growth of the crystal. In order to detect intra-crystalline variation along the crystal growth, we analyzed $\delta^{18}O$ at four different spots. Locations of the SIMS analysis and the values are shown in Fig. 1. The results indicate that there are no clear evidence for heterogeneous $\delta^{18}O$ distribution in the fassaite single crystal. The $\delta^{18}O$ value is about -30 ‰ relative to Taka-shima augite. Those of anorthite and alteration products and of spinel adjacent to the fassaite are about 0‰ and -40‰ relative to terrestrial standards, respectively. All values are consistent to conventional results of Mayeda et al. [2]. In conclusion, present data indicate that O isotope composition is homogeneous inside of minerals as well as among minerals in the HN3-1 CAI. Since any oxygen isotope heterogeneity in a crystal were not observed, we conclude the heterogeneous oxygen isotope distribution is preserved on initial state at crystallization.

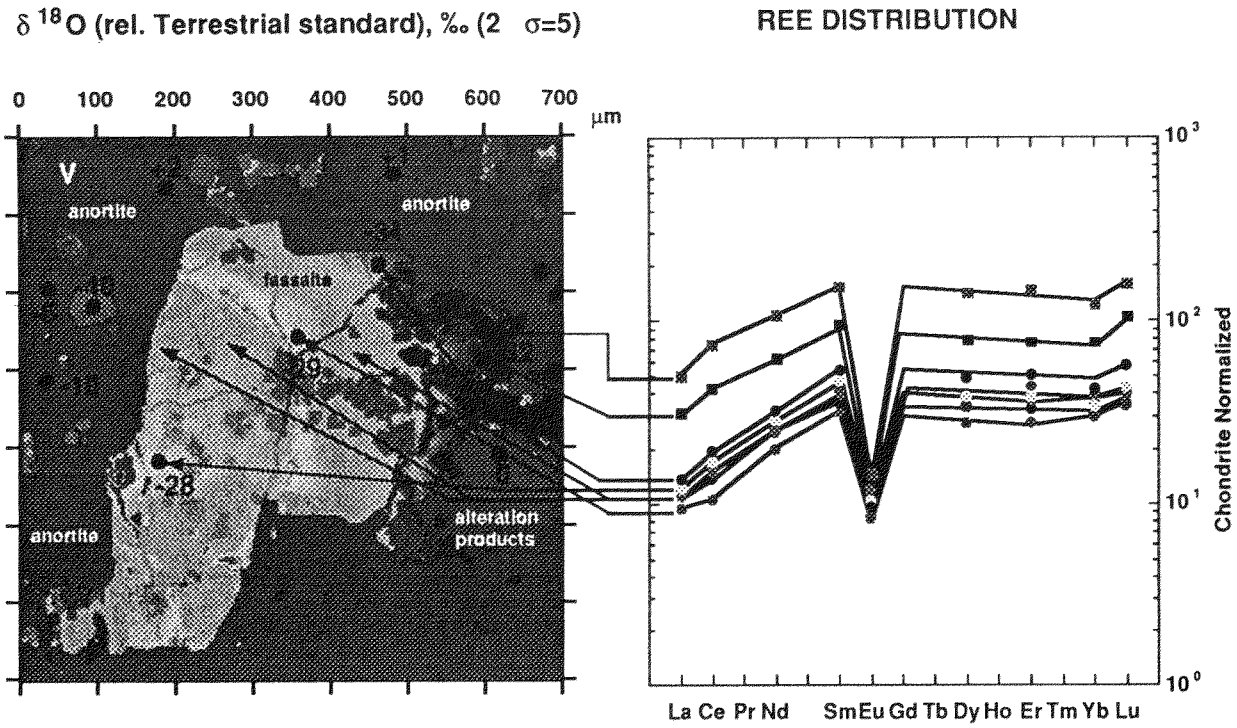

Fig. 1 Oxygen isotope distribution in a large fassaite single crystal and the adjacent phases in HN3-1 CAI. The crystal coexists with anorthite and alteration products. Many small grains in the figure correspond to spinel crystals. REE distribution is also shown in the right figure.

References: [1] Nagahara, H., Nagasawa, H., Nakamura, N., and Matsui, T. (1987) *Lunar Planet. Sci.* **XVIII**, 694-695. [2] Mayeda, T. K., Clayton, R. N., and Nagasawa, H. (1986) *Lunar Planet. Sci.* **XVII**, 562-563. [3] Yurimoto, H., Mori, Y. and Yamamoto, H. (1993) *Rev. Sci. Instrum.* (in press). [4] Slodzian, G., Lorin, J. C., Dennebouy, R., and Havette, A. (1984) *Secondary Ion Mass Spectrometry SIMS IV*, ed. by Benninghoven, A., Okano, J., Shimizu, R., and Werner, H. W. Springer-Verlag Berlin, 153-157.

EVAPORATION RATE AND OXYGEN-ISOTOPIC FRACTIONATION OF SiO_2 IN EQUILIBRIUM, IN VACUUM, AND IN HYDROGEN GAS.

Hiroko NAGAHARA[1], Edward D. YOUNG[2], AND TOM C. HOERING[2], (1)Geol. Inst., Univ. Tokyo, Hongo, Tokyo 113, Japan, (2) Geophysical Laboratory, Carnegie Institution of Washington, 5251 Broad Branch Road, N. W., Washington, D. C. 20015, U. S. A.

Oxygen isotopic composition is one of the most powerful tools for the genetic relationships of meteorites, which gives important clues for the structure and evolution of the solar nebula. Difference in oxygen isotopic compositions among meteorite groups are believed to have been due to mixing of gas and dust from different oxygen reservoirs [1] and effect of isotopic fractionation is thought to be negligible small for most meteorites except for some CAIs [2]. However, the possibility of mass-independent fractionation has been also pointed out [3]. In this study, evaporation rate and oxygen isotopic fractionation during evaporation of SiO_2 (originally quartz, and high cristobalite at experimental conditions) in equilibrium, in constant evacuation (free evaporation), and in hydrogen gas were investigated. The starting material is a single crystal of natural quartz. The details of experiments are described elsewhere [4]. Experimental temperature was 1600°C and 1700°C.

Figure 1 is the summary of the experiments. In equilibrium and in vacuum, weight loss is a linear function of time regardless of temperature and fO_2 (both in a Mo or C capsule). Evaporation rate in a reducing condition (in a C-capsule) is about 3.5 times more rapid than that in equilibrium (in Mo-capsule). In vacuum, evaporation rate is smaller than that in equilibrium by a factor of about 0.02, which coincides with literature data (0.011-0.015 at 1560-1685°C) [5]. This lowering of evaporation rate in vacuum compared to that in equilibrium may be due to formation of metastable gas species [5] or surface kinetics in solid such as crystallographic plane, purity, surface roughness, and porosity.

In hydrogen gas, the evaporated fraction is not a linear function of time, which is smaller than that in equilibrium, and the difference from equilibrium value becomes larger with time. At hydrogen pressure of 10^{-7} bar, the evaporation rate is nearly the same as that in vacuum, but it is about 3-4 times of magnitude larger at 10^{-5} bar of hydrogen pressure. Contrary to higher total pressure, vaporization is more effective in hydrogen gas, which suggests that the mode of evaporation in hydrogen gas (and also in the solar nebula) is different from that in equilibrium and that in vacuum.

In order to investigate vaporization rate and fundamental process controlling evaporation, the relationships are shown in logarithmic scale. Equilibrium evaporation rate and free evaporation rate have slope of 1 in the figure, showing that evaporation rate is limited by decomposition of SiO_2 at the surface of the crystal. On the contrary, evaporation rates in hydrogen gas have slope of 1/2. Slope of 1/2 represents that the process is controlled by diffusion.

Possible diffusion processes are (1) formation of $SiO+H_2O$ layer above the crystal surface, (2) reaction of hydrogen with SiO_2 to form amorphous layer. The possibility (1) is implausible, because the mean free paths in the experimental conditions is about 3m at 10^{-5} bar and 300m at 10^{-7} bar, which are far beyond the size of the experimental chamber. The generated $SiO+H_2O$ layer should be evacuated away in a second and it can not be a rate limiting factor. The possibility (2) may be plausible, although the presence of amorphous material has not yet been probed with the X-ray technique. Hydrogen diffusion in SiO_2 is more rapid than oxygen by 3 to 8 orders of magnitude in the temperature range of [6]. If the data of [6] is extended to the present experimental temperatures, hydrogen diffusion distance is in the order of grain size of the present work, and it can not be a rate limiting factor.

Oxygen isotopic compositions ($^{18}O/^{16}O$) were measured with the CO_2-laser heating fluorination technique. A part of the results are shown in Fig. 2, where the degree of isotopic fractionation as a function of the evaporated fraction is compared between vacuum and in the hydrogen gas conditions. Oxygen isotopic fractionation is remarkable in vacuum, but is negligible in hydrogen gas of 10^{-5} bar total pressure. In summary, the evaporation rate is large but the degree of isotopic fractionation is small in hydrogen gas, and the evaporation rate is small but the isotopic fractionation is effective in vacuum. These results gives a possibility that we can estimate the nebular gas pressure during formation of high temperature objects combining with isotopic fractionation of other elements such as Si for SiO_2 and Si and Mg for forsterite and enstatite.

REFERENCES: [1] Clayton, R. et al. (1977) *EPSL* **34** 209-224, [2] Clayton, R. N. and Mayeda, T. K. (1977) *GRL* **4** 295-298, [3] Thiemens, M. H. and Heindrich, J. E. (1983) *Science* **219** 1073-1075, [4] Nagahara, H. *et al.* (submitted), [5] Hashimoto, A. (1990) *Nature* **347** 53-55, [6] Dennis, P.F. (1984) *JGR* **89** 4047-4058; Kronenberg, A. K. *et al.* (1986) *JGR.* **91** 12723-12744.

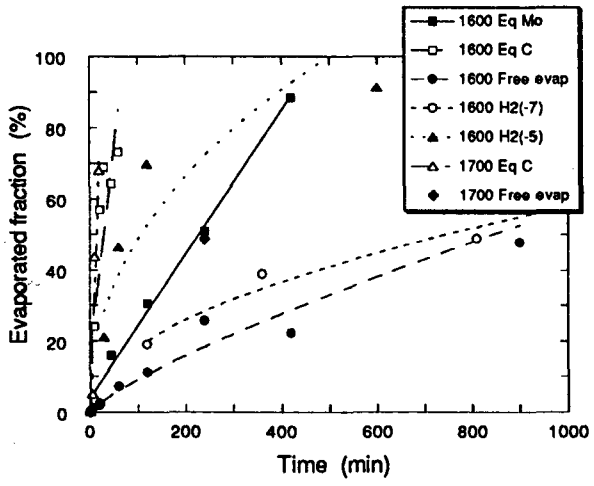

Fig. 1 Degree of evaporation of SiO2 in different conditions.

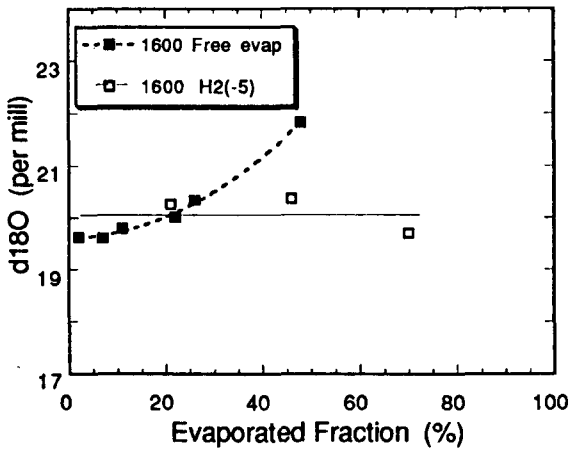

Fig. 2 Oxygen isotopic fractionation during free evaporation and in H2 gas.

AN EXPERIMENTAL STUDY OF EVAPORATION KINETICS OF FeS, AND ITS COSMOCHEMICAL SIGNIFICANCE.

Akira Tsuchiyama, Chiaki Uyeda and Yumi Makoshi.
Institute of Earth and Planetary Sciences, College of General Education, Osaka University, Toyonaka 506, JAPAN

Introduction. Major elements consisting the terrestrial planets are Mg, Si, Fe, S, O, and H. According to the thermochemical calculations in the H-rich solar nebula (*e.g.*, [1]), the systems Mg-Si-O-H and Fe-S-H can be regarded as independent reaction systems at high temperatures, and the two systems are in cotectic relation. Thus, the kinetics of the reactions during evaporation and condensation in the two systems are important to understand chemical evolution in the primordial solar nebula. In the system Mg-Si-O-H, Imae *et al.* [2] carried out reaction experiments of forsterite with Si-rich gas and determined the mode and rates of enstatite formation by this reaction. Incongruent evaporation rates of enstatite have been determined in the field of ceramics [3]. In the Fe-S-H system, the kinetics of $Fe_{1-\delta}S$ formation by the reaction of iron with H_2S gas has been determined precisely in the field of metallurgy [4]. However, kinetics of incongruent evaporation of FeS has not been known. In the present study, mode and rates of the FeS evaporation under H-rich conditions were determined by evaporation experiments. The results were applied to evaporation rate of FeS in the primordial solar nebula.

Experiments. It is important to use a single crystal as a starting material in this kind of experiments. However, it is difficult to obtain a large single crystal of troilite (FeS), which is common in meteorites as an iron sulfide. Thus, a single crystal of natural pyrrhotite from Chihuahua, Mexico, ($Fe_{0.886}S$) was used as a starting material. The crystal is chemically homogeneous and free from inclusions under an SEM. It was cut into parallelepipeds (2.5 x 3.5 x 4.5 mm^3), and their surfaces were polished. This parallelepiped was put into an alumina crucible, and heated in a one-atmosphere, H_2-CO_2 gas mixing furnace at temperatures ranging from 500 to 1300°C at oxygen fugacities one log unit below the iron-wustite buffer curve. After heating for different durations from 0.5 to 90 hrs, samples were pulled from the hot spot of the furnace and cooled in a cold part of the furnace in the H_2-CO_2 gas stream to avoid oxidation during cooling.

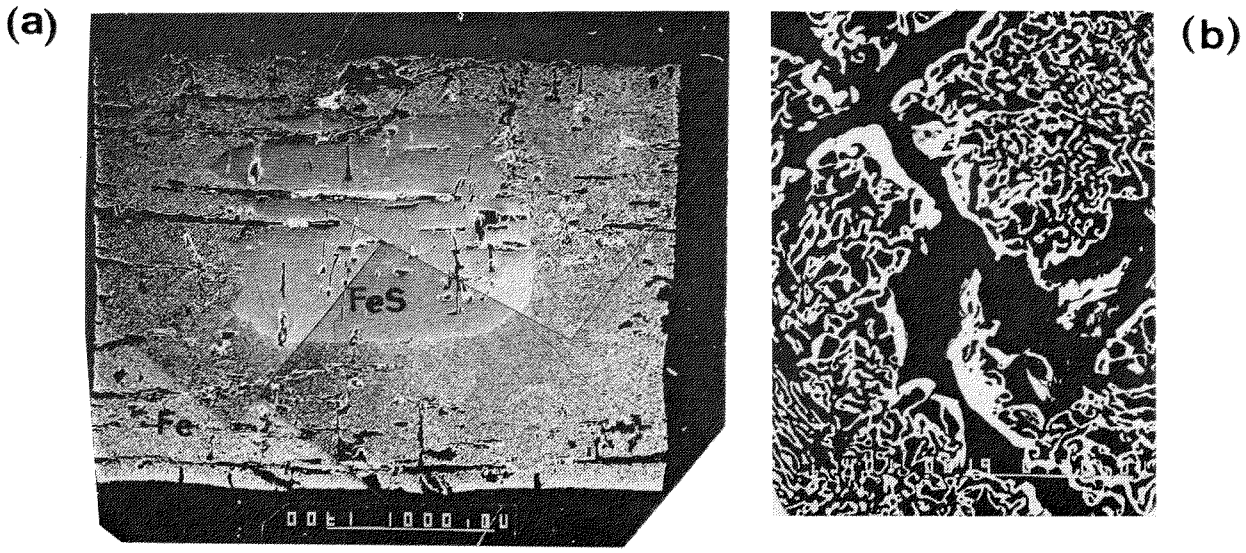

Figure 1. A run product of the evaporation experiment (900°C, 12hr). (a) An iron layer is covered on the $Fe_{1-\delta}S$ crystal (scal bar is 1 mm). (b) Spongy texture of the iron layer (scale bar is 100 μm).

Results. At temperatures below the eutectic point of Fe-FeS (988°C), the pyrrhotite crystal evaporated incongruently, and an iron layer was formed on the pyrrhotite crystal as an evaporation residue (Fig.1a). The iron layer is very porous (Fig.1b), and the size of the sample was not changed after heating. At the temperatures between the eutectic point and the FeS melting point (1195°C), an Fe-S melt surrounded by the pyrrhotite crystal was formed due to the Fe-FeS eutectic melting. At the temperatures above the melting point, the melt became rich in Fe by incongruent evaporation. In some runs especially at high temperatures, pyrrhotite became stoichiometric (troilite) probably by S diffusion in the $Fe_{1-\delta}S$ crystal.

The width of the spongy iron layer, X(Fe), advances linearly with time (Fig.2), or the evaporation reaction obeys the "linear rate law";

$$X(Fe) = kt, \qquad (1)$$

where k is the linear rate constant, and t the time. In the case of incongruent evaporation it is generally expected that the width of evaporation residue layer is proportional to the square root of time ("parabolic rate law") because the evaporation rate is controlled by diffusion of elements in the evaporation residue layer [3]. In the present experiments, on the other hand, the reaction obeys the linear rate law because the evaporated gas species can move through the pores in the spongy iron layer, and the rate is controlled by reaction at the sulfide surface. The linear rate constant, k, shows the Arrhenius relation (Fig.3) with the pre-exponent term, $k_0 = 2.37$ cm^2/sec, and the activation energy, E = 28.0 kcal/mol.

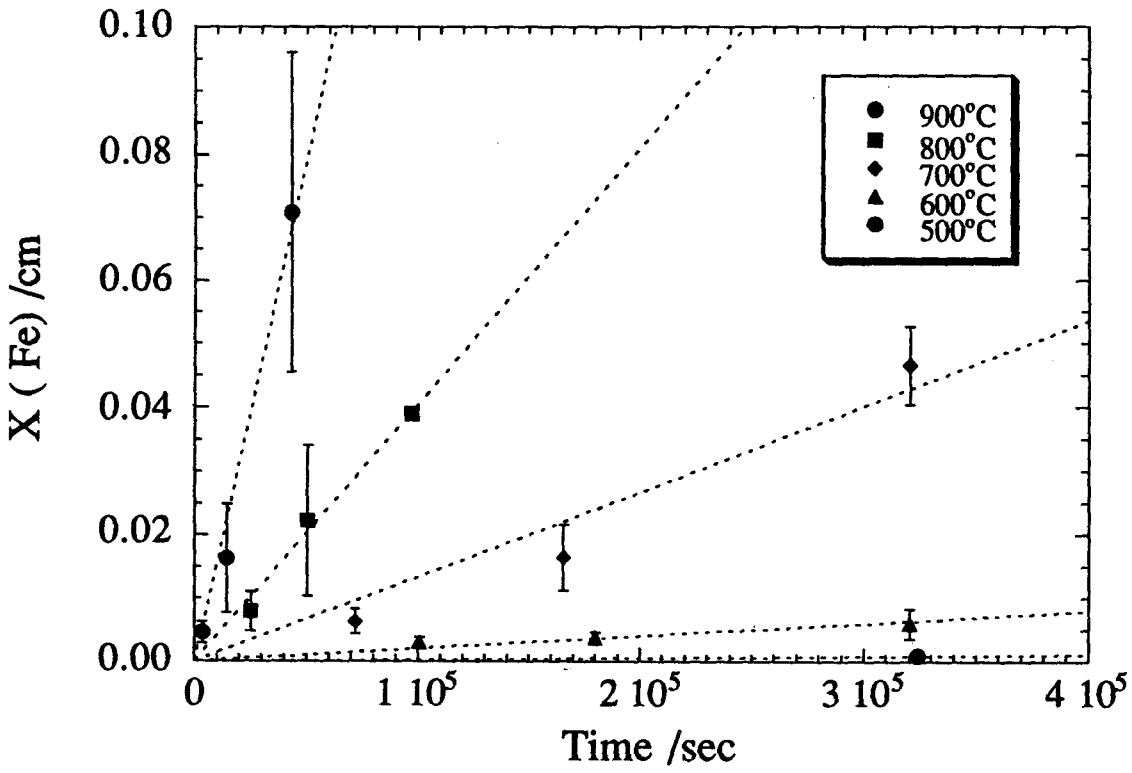

Figure 2. The width of Fe layer formed by the incongruent evaporation of $Fe_{1-\delta}S$, X(Fe), plotted against time.

Discussion. If the evaporation is controlled by the following reaction at the sulfide surface;

$$FeS(s) + H_2(g) \rightarrow Fe(s) + H_2S(g), \quad (2)$$

it is expected that the linear rate constant, k, is proportional to the equilibrium partial pressure of $H_2S(g)$, $p(H_2S)$. Because the reaction constant of (2), K_{FeS}, is follows;

$$K_{FeS} = p(H_2S)/p(H_2), \quad (3)$$

then k is proportional to the partial pressure of H_2 in the atmosphere, $p(H_2)$. In this case, we can estimate the evaporation rate of FeS in the primary solar nebula from the present experimental results. The width of the iron layer, X(Fe), formed by the evaporation of FeS at $p(H_2) = 10^{-4}$ atm. is given as a function of time and temperature in Fig.4.

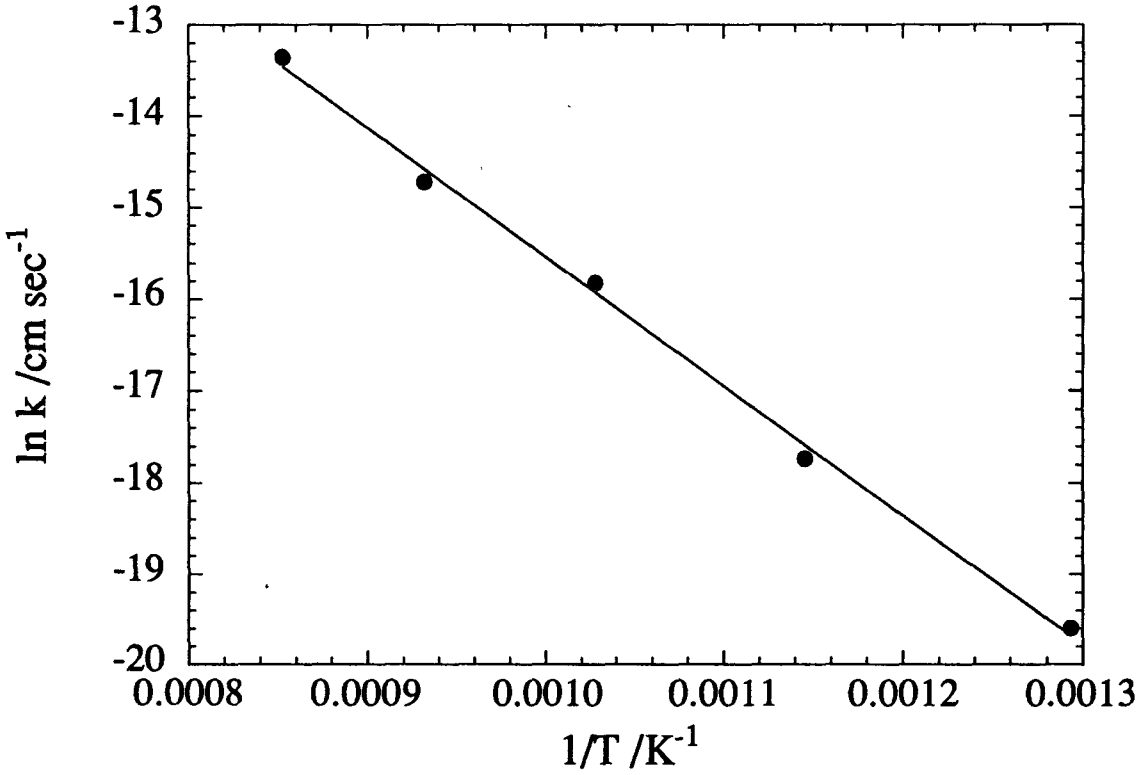

Fig. 3 Arrhenius plot of the linear rate constant, k.

The evaporation rate of iron can be also estimated based on the following evaporation reaction;

$$Fe(s) \rightarrow Fe(g). \quad (4)$$

In this case, the width of the evaporated iron, $X(Fe)_{vap}$, is given by

$$X(Fe)_{vap} = \alpha_v(K_{Fe}/\rho_{Fe})(M_{Fe}/2\pi RT)^{1/2}t, \quad (5)$$

where α_v is the evaporation coefficient, K_{Fe} the reaction constant of (4), ρ_{Fe} the density of iron, M_{Fe} the mass of iron, and R the gas constant. The value of α_v is less than unity [3], but is not determined at present. $X(Fe)_{vap}$ with $\alpha_v = 1$ is also shown in Fig.4.

When we compare the evaporation rate of FeS and Fe in Fig.4, the evaporation of FeS is much faster than that of Fe at low temperatures (<1000K), while the evaporation of FeS and Fe is comparable at high temperatures especially near the eutectic temperature, 1261K. In the later case, FeS might evaporate almost congruently due to kinetic effect. Data for the evaporation rate of FeS under low $p(H_2)$ conditions and evaporation of Fe, especially about α_v in the equation (5), are required for more precise discussion on the FeS evaporation in the solar nebula.

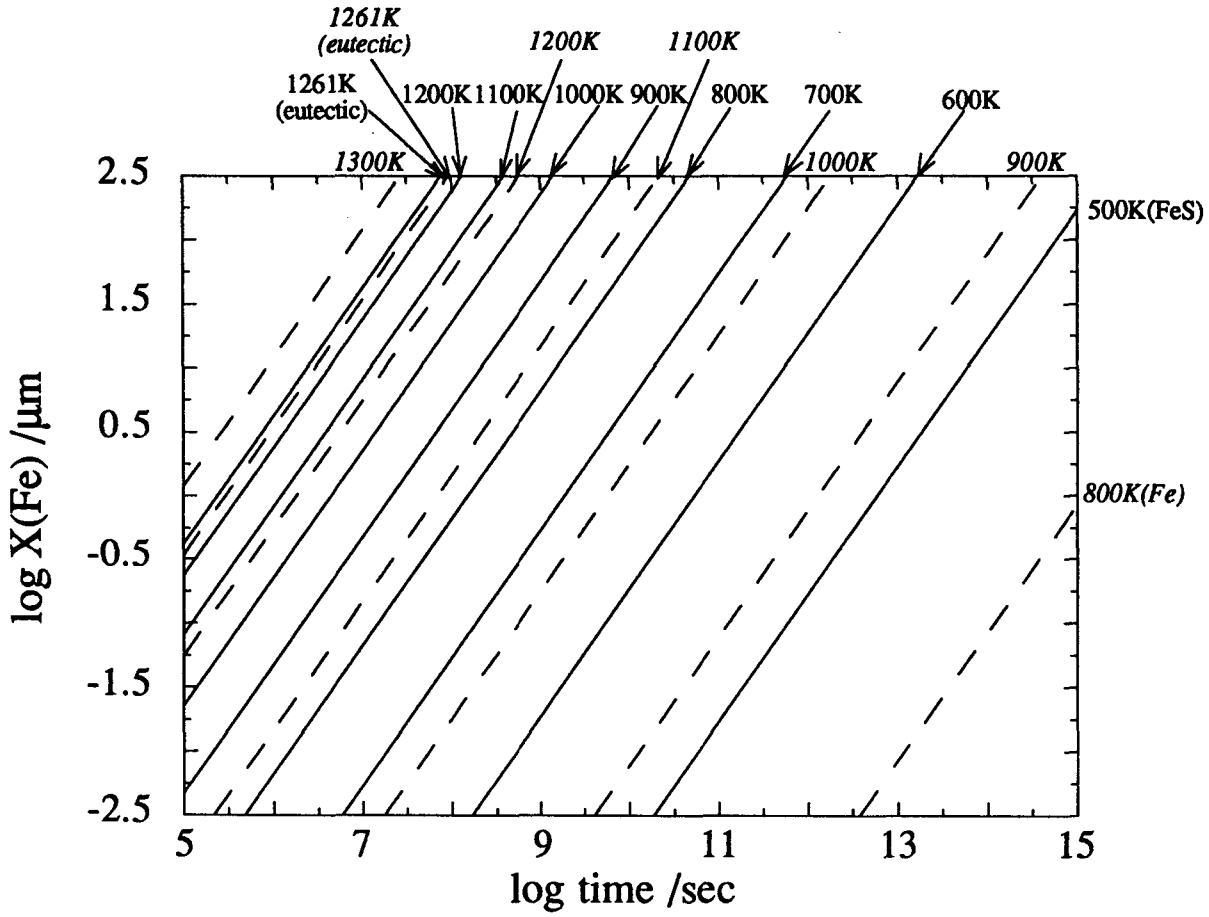

Fig. 4 Evaporation rates of FeS (solid lines) estimated from the present experimetnal results and those of Fe (dotted lines) estimated from the evaporation theory (equation (5) with α_v=1) at different temperatures.

References: [1] Grossman, L. and J. W. Larimer (1974) *Rev. Geophys. Space Phys.*, 12, 71-101. [2] Imae, N., A. Tsuchiyama, M. Kitamura, submitted to *Earth Planet. Sci. Lett.* [3] Sata T., T. Sasamoto, H. L. Lee, and E. Maeda (1978) *Rev. int. Hautes Temp. Refract., Fr.*, 15, 237-248. [4] Fryt, E. M., V. S. Bhide, W. W. Smeltzer, and J. S. Kirkaldy, (1979) *Jour. Electrochem. Soc.*, 126, 683-688.

Isotope Line Analysis on Primitive Meteorites using Ion Microprobe II - Measurement of sulfur-

Chiaki Uyeda & Akira Tsuchiyama
College of general Education,Osaka Univ.Toyonaka Osaka 560, Japan.

Up to now, the measurement of isotopic abundance of major elements in primitive meteorites has been limited mainly on refractory inclusions. As a result, various types of isotopic anomalies were observed from the micron-sized inclusions which derives from the mixing of extra solar components[1-6], as well as from the mass fractionation due to evaporation and condensation processes.

The isotopic fractionation data of major elements among various primitive materials has been considered to provide useful information in estimating the kinetic processes of the elements during the evolution of solar nebula, as well as that of the planet bodies. A comprehensive isotopic data of all the major elements are required for this purpose. However, among the major rock forming elements of primitive materials, the isotopic behavior have not been studied extensively for sulfur and iron.

Sulfur holds an unique position because it is both volatile and sidrophile element among the major rock forming elements. Other major element are generally lithophile and refractory. Sulfur should have experienced a large scale of physical and chemical transfer in various stages of planet evolution. For example, the condensation and evaporation of FeS phase in the solar nebula, evaporation from the magma ocean after the formation of the primitive planet as well as the formation of the metal phase may cause a large scale of isotopic mass fractionation.

Sulfur isotope abundances have been measured for various primitive materials such as the C1 chodrites, various types of ordinary chondrites[5], the FeS inclusions of the mantle derived diamonds or the FeS phase of the iron meteorites[6]. The amount of mass fractionation of these materials with respect to the C1 chondrite, representing the initial nebula gas, is less than 2 to 3 permils. If the actual planet formation followed the conventional model mentioned above, a large difference should be observed between

the primitive materials. The following three reasons can be considered for the inconsistency of isotopic data with respect to the conventional model.

① The effective mass fractionation rate of each fractionation process is negligibly small.

② The choice of reference sample is inadequate.

③ The conventional model on planet formation is incomplete.

The isotopic fractionation coefficient of sulfur was studied in connection with the degasing of SO_2 from basalt melt,following the layleigh process[7]. The rate of mass fractionation changed considerably according to the O_2 concentration of the gas phase. In order to estimate the actual mass fractionation in the primitive solar nebula, a similar study is required for sulfur evaporation and condensation in a more reduced condition. For refractory major elements, a number of experimental studies have been performed to understand the mechanism of isotopic behaviors of refractory elements in the evaporation-condensation processes [8-11]. It became clear that not only the residues but also the condensates were fractionated in the heavy isotopes according to the fraction of the residual gas phase[10,11]. The evaluation of isotopic mass fractionation between the condensed phase and the residual gas phase is considered to be essential for the analysis of various isotopic data observed in the meteorites. The evaporation-condensation experiments are extended for sulfur, and a preliminary reslut of such study is reported by Tsuchiyama[12].

Meteorite	$^{34}S/^{32}S$ v.s.CDT
Orgueil (C1)	-1.8 ～ 3.4 ‰
Murray(C2)	-2.0 ～ 2.5 ‰
Mokoia(C3)	-1.2 ～ 1.3 ‰
Abee(E4)	-1.8 ～ 1.6 ‰
Bjurbole(L4)	-1.7 ～ 0.3 ‰
Ehole(H5)	-1.1 ～ 0.2 ‰
Iron meteorites	-0.1 ～ 0.5 ‰
Norton County(achondrite)	-5.7 ～ 1.6 ‰
Mantle deriving sulfide	1.7 ～ 9.5 ‰

Table 1. Sulfur mass fractionation of refactory inclusion observed in the primitive materirals. CDT represents Canon Diabro Troilte.

Considering the choice of reference sample[②], the sulfur isotopes have been measured mostly for bulk samples. The micron-sized sulfur phases consisting the material has not been studied separately, however, previous isotopic studies on primitive materials reveal the necessity of microprobe studies. Therefore, we have newly set up a system for in-situ isotope line analysis for measuring sulfur $^{34}S/^{32}S$ ratio using the ion microprobe.

In the conventional ion microprobe method of measuring isotopic abundance, a single micron-sized grain separated from the bulk sample was mounted on a metal foil. In situ profile measurements of the bulk section has not been carried out intensively due to various instrumental difficulties. A new method for Mg isotopes, which realizes the in situ line analysis for non-conductive samples, was developed by improving the conductivity of the sample surface. It was seen that line analysis of Mg isotopes can be performed for non-conductive samples over a range of 5mm on the sample surface with the aquracy of 3%[13]. The method of this line analysis is extended to the measurement of sulfur. Figure 2-(a) shows the measured result of the NBS standard(Δ 34=+20.34 ‰ v.s. Canon Diabro Troilite) arranged together with the chip of Canon Diabro Troilite(CDT). It is seen that the measured data clearly reproduces the expected isotopical difference of the samples. It is also seen that the isotopicaly homogeneous profile is observed with the error of less than 3 ‰. The isotopic variation of an unknown sample with respect to the standard sample may be evaluated precisely by placing the unknown sample in the position of the standared $BaSO_4$ in Fig.1 (a), and perform the same line analysis described above. It is also noted that the sample preparation described above is effective to check the amount of instrumental mass fractionation. The amount of instrumental mass fractionation changes considerably with the position of the primary ion at the sample surface, and it is necessary to evaluate this effect in the course of everyday measurements in the case of line analysis.

The result of a preliminary measurement for Allende troilite is also shown in the right portion of the Fig.2. No significant

deviation with respect to the CDT is seen for this particular inclusion. However, it is seen that in-situ isotopic measurement can be performed on the meteorite surface with the spatial resolution of 100 μ m with the acquracy of about 3‰ . Detailed and comprehensive analysis on various sulfur bearing phases in primitive meteorites can be carried out in terms of this method. The origin of the inconsistency of sulfur isotopic data mentioned above can be investigated after the accumulation of microprobe sulfur data on various meteorites are accomplished.

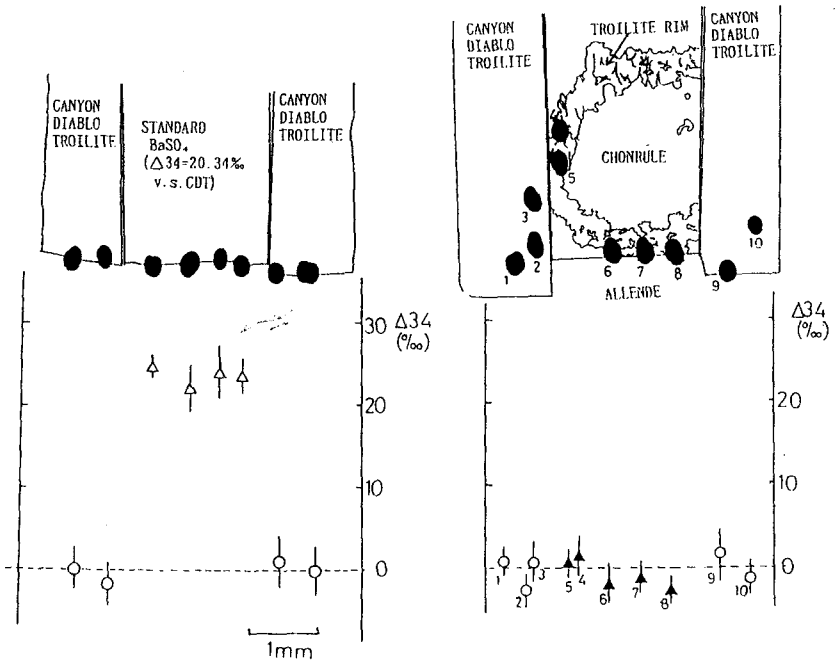

Fig.2 S-isotopic line analysis of sulfur bearing materials.

References

[1]NISHIMURA.H & OKANO.J (1974) J.Appl.Phys.Suppl.2 Pt.1 339. [2]McKEEGAN,J.& ZINNER,E. (1987) GCA 51 1468. [3]LEE,T.,PAPANASTASSIOU,D.A.& WASSERBURG,G.J.(1977)Geophys.R.L3 109.[4]CLAYTON,R.N., et al.(1988)Phil.Trans.R.Soc.Lond.A325,481.[5]KAPLAN,I,R & HULSTON,J,R(1965)GCA 30 479-496 [6]CHAUSSIDON,M et al.(1987) 330 242-243. [7]SAKAI,H et al.(1982) 46 729-738.[8]ESAT,T.M.SPEAR, R.H. & TAYLOR,S.R.(1986)319,576.[9]DAVIS.A.,HASHIMOTO,A.,CLAYTON. R.N. MAYEDA,K.(1990) Nature 347.[10]UYEDA.C, TSUCHIYAMA,A.& OKANO, J.(1989b) EPSL 107 138. [11]TSUCHIYAMA,A(1988)Abst.17th Symp. Antarctic ,123-127. [12]TSUCHIYAMA,A(1993)Abst.18th Symp.Antarctic [13]UYEDA C(1992) Abst.17th Symp.Antarctic. polar 154-157.

FeS formation reaction between metallic iron and H_2S gas in the primordial solar nebula.

Naoya Imae and Masao Kitamura.
Department of Geology and Mineralogy, Kyoto University, Kyoto 606, JAPAN.

The phase diagram of the system of Fe-S-H (Fig. 1) was constructed to understand the condensation processes of metallic iron and iron sulfides from gas at low pressure using the thermochemical data (JANAF). The method is essentially the same as used by Grossman (1972). Although the Fe-S phase relation at one atmosphere in the hydrogen free condition has an eutectic system with no reaction between solid and melt, the Fe-S-H system at low pressure in the condition of $P_{Total} = p(H_2)$ has a peritectic system with reaction between metallic iron and H_2S gas, *i. e.* Fe(s) and FeS(s) are in a reaction relation in the system.

When we consider the cooling of the solar nebula gas with the solar ratios of Fe, S and H, the first condensates are metallic iron, and the condensation temperature is 1280 K (Fig. 1). By further cooling, the metallic iron starts to react with H_2S(g) to form iron sulfide (pyrrhotite-troilite) at 700 K. As can be understood from the phase diagram, the peritectic curve is very close to the H-S tie line. Therefore, iron atoms in the gas phase are almost consumed by the reaction between metallic iron and H_2S gas. As a result, the resultant condensing mineral species and the amount of minerals strongly depend upon whether the process is in equilibrium or fractional crystallization. Thus, the kinetics of FeS formation between metallic iron and the gas may play a very important role on the fractionation of the primordial solar nebula gas.

FeS formation kinetics has been studied experimentally in the field of corrosion science by Fryt (1979). The data were used to estimate the degree of formation of the FeS layer surrounding metallic iron in the cooling primordial solar nebula environment by extrapolating them to very low $p(S_2)$ partial pressure region. The reaction is a diffusion controlled reaction of iron in the FeS layer. The reaction rate, k (parabolic rate constant), in the low $p(S_2)$ pressure region is approximately reformed such as

$$k\ (cm^2/s) = p(S_2)^{1/2}\ (6.7 \times 10^{-2})\ \exp(20.1 - 0.015\ T)\ \exp(-10500/T). \quad (1)$$

$p(S_2)$ is calculated from the equilibrium relations among H_2S, H_2 and S_2 ($2H_2S = 2H_2 + S_2$). The equilibrium constant, K, is written as $p(H_2)^2p(S_2) / p(H_2S)$. In the condition of $P_T = p(H_2) = 10^{-5}$ atm, the relation between $p(S_2)$ and $p(H_2S)$ is expressed as $p(S_2)=p(H_2S)^2 \times 10^{(14.97-9244/T)}$ using JANAF thermochemical data and the value of K. Then using the conservation equation of solar abundance of sulfur between $p(S_2)$ and $p(H_2S)$, the reaction rate, k, is approximately rewritten under the solar nebula conditions as

$$k = 0.26 \exp(-35000/RT). \quad (2)$$

We can discuss the FeS formation in the primordial solar nebula, using eq.(2) of reaction rate of FeS formation between metallic iron and H_2S gas. The cooling of the solar nebula gas is assumed to be expressed as

$$T = T_e \exp(-t/\tau), \tag{3}$$

where T_e is the temperature when the reaction between metallic iron and H_2S gas starts, and τ, the cooling time scale of the nebula. The thickness of FeS layer, x, as the reaction product on the metallic iron condensed from the gas is expressed as

$$x = [k(T_e)\, RT_e\, \tau / 35000]^{1/2}. \tag{4}$$

In this calculation, the H_2S gas consumption from the gas phase due to the FeS formation reaction was not taken into account in the above discussion as a first approximation. The grain size of the metallic iron before the reaction has been determined as functions of the cooling time scale, τ, and the total pressure of the nebula, P_{Total}, according to the time dependent homogeneous nucleation theory by Kozasa and Hasegawa (1987). Therefore we can estimate the degree of the FeS formation reaction as functions of the total pressure and the cooling time scale of the nebula. Fig. 2 shows the degree of the reaction around the iron grains. In Fig. 2, the line of $x^* = 0.36$ r (r: the grain size of metallic iron) shows the limitted line (equilibrium line) of the reaction due to the completion of the reaction. As can be understood from Fig. 2, the reaction degree is fairly large, and the reaction is completed over the wide range of the cooling time scale, especially in the rapid cooling.

[References]

Fryt E. M. *et al.*, *J. Electrochem. Soc.* 126 673-683, 1979.
Fryt E. M. *et al.*, *J. Electrochem. Soc.* 126 683-688, 1979.
Grossman L., *Geochim. Cosmochim. Acta* 36 597-619, 1972.
JANAF thermochemical tables third edition, *J. Phys. Chem. Data* 14 1985.
Kozasa T. *et al.*, *Prog. Theor. Phys.* 77 1402-1410, 1987.

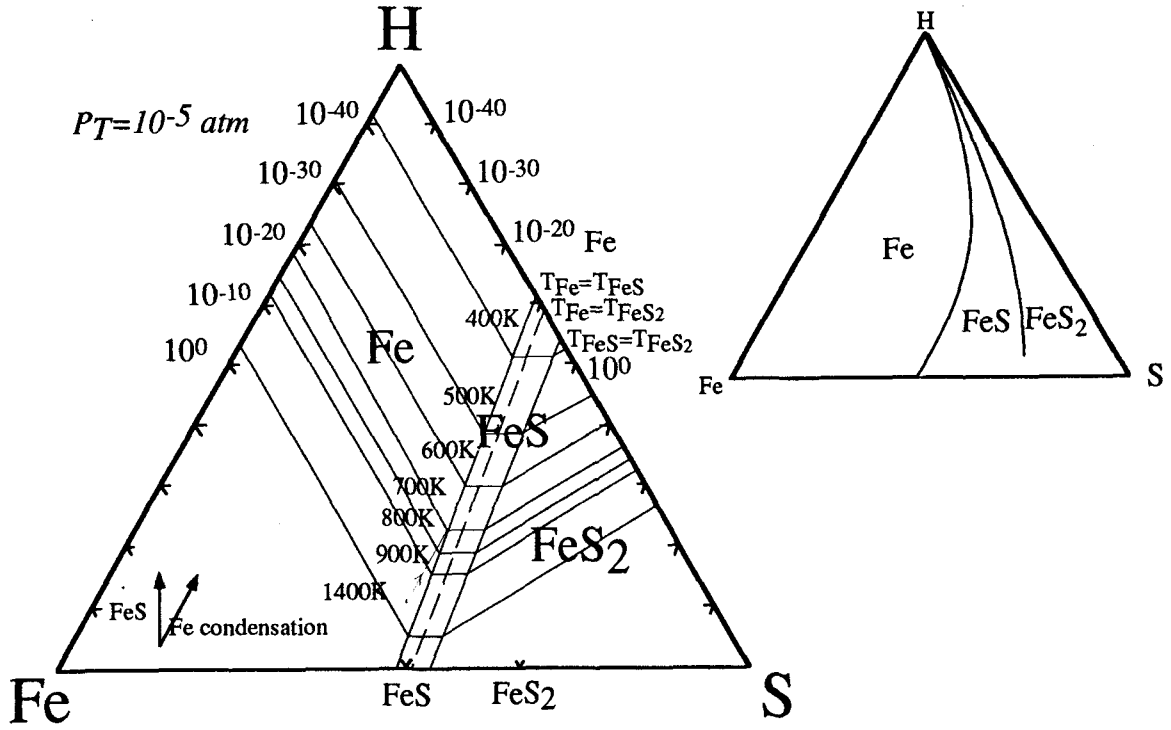

Fig. 1 Calculated phase diagram of Fe-S-H system at $P_T=P_{H_2}=10^{-5}$ atm. The graph is shown as logarithmic plot in order to show the peritectic curve clearly.

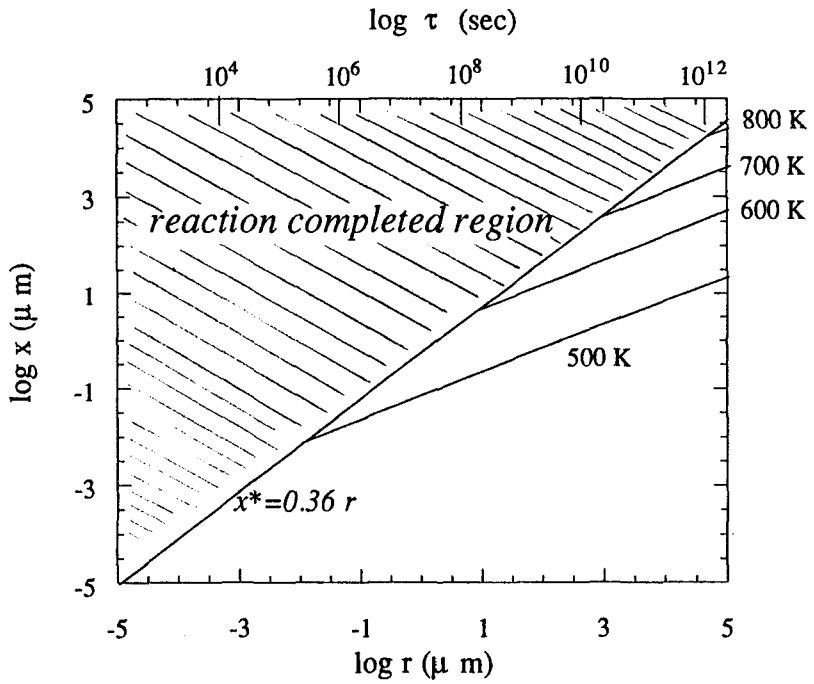

Fig. 2 FeS formation scale (x) around the iron grain (r) in the cooling solar nebula at $P_T=10^{-5}$ atm. τ is the cooling time scale. The lines are defined as less than the line of the reaction completion, $x^*=0.36$ r.

DOWN-SHIFTED RAMAN SPECTRA OBSERVED IN INTERSTELLAR GRAPHITE GRAINS.

Hiroyuki Kagi[1], Ikari Tsuchida[1], Masao Wakatsuki[1], Kazuya Takahashi[2], Nao Kamimura[3] and Hideki Wada[3]. [1]Institute of Materials Science, University of Tsukuba, Ibaraki 305, Japan. [2]Earth Science Laboratory, Institute of Physical and Chemical Research (RIKEN), Saitama 351-01, Japan. [3]Institute of Geosciences, Shizuoka University, Shizuoka 422, Japan.

Introduction

LRM (Laser Raman Microprobe) Spectroscopy has several technical advantages; non-destructive, *in situ* observation and has an excellent spatial resolution, especially, LRM is one of the most useful techniques for the investigation of structural ordering of carbonaceous materials. Recently, several anomalous Raman spectra have been found out for some natural graphite samples; terrestrial graphite contained in metamorphic rocks [1,2,3] and interstellar graphite grains extracted from the Murchison meteorite [4]. They show considerable down-shifts in Raman frequency about 10-15 cm^{-1} compared with typical graphite samples, and Si-doping into graphite lattice was proposed as a possible reason for the down-shift [1,2]. In this study, we investigated the physical mechanism of the spectral down-shift observed in natural graphite samples.

Presence of down-shifted graphite grains

Highly ordered graphite gives a single first-order Raman band derived from in-plane vibrational mode (E_{2g}). Generally, its vibrational energy can be detected at constant value (1582 cm^{-1}) for various kinds of graphitic materials. Wopenka *et al.* reported the Raman spectra of "graphite" flake from a strongly metamorphosed marble in Ontario, and they pointed out that the individual graphite grains show Raman peak positions ranging from 1565 to 1577 cm^{-1} which are displaced to lower wavenumbers than that for well crystallized pure carbon graphite (1582 cm^{-1}) [1,2]. Further, these grains showed presence of Si with energy-dispersive X-ray analysis by SEM and TEM. Generally, it is known that intercalation of exotic element into graphite results in substantial changes in Raman spectra of graphite [4], they suggested that the down-shift is attributable to the silicon-doping into graphite lattice.

Apart from the terrestrial graphitic materials, similar down-shifting was observed for highly crystallized graphite grains extracted from the Murchison meteorite [5]. We do not know whether the down-shifted interstellar grains contain considerable amount of Si or not, so any spectral considerations have not made for the down-shift. Anyway, it is an essential problem to solve the enigma of the down-shifted Raman spectra of graphite.

Experimental

Our attention was directed into the residual strain of graphite crystal. For the purpose of introducing stress into graphite samples, artificial graphite rods were ground in an agate mortar in air at room temperature for a few minutes. Raman spectra of both ground and not ground samples were recorded on a Jobin Yvon micro Raman spectrometer (RAMANOR U-1000). All spectra were obtained using 514.5 nm green line of an argon gas laser with 10 mW power at the sample surface. Laser beam size was about 2 μm in diameter, and grain by grain observation was carried out. Raman spectra were collected in the region ranging from 1200 cm^{-1} to 1700 cm^{-1}, which is of interest for the structural ordering of graphitic materials.

Results

Obtained Raman spectra are shown in Fig. 1. Untreated graphite (Fig. 1(a)) rod exhibits the E_{2g} mode at 1582 cm^{-1} as same as normal graphite samples. On the contrary, the ground graphite samples reveal the substantial down-shifted Raman band at 1567 cm^{-1} as shown in Fig 1(b). We performed the same treatment for several times, then down shifting was well-reproduced for all ground samples and they gave Raman frequency ranging from 1567 to 1576 cm^{-1}. It should be noted that this energy range for the ground graphite samples shows a fair agreement with the Raman spectra of the down-shifted geological graphite samples [1,2,3]. It suggests the close relationship between the down-shift observed in natural graphite samples and some (unidentified) geological processes just like mechanical grinding.

Discussion

It is known that grinding of graphite leads to deviation of *c-plane* (basal plane) followed by transformation from hexagonal form (ABAB stacking sequence) to rhombohedral form (ABCABC stacking sequence), because the basal planes of graphite are weakly bound by Van der Waals interaction and easy to deviate. Therefore, it seems to be the simplest way of thinking to attribute the down-shift observed in our study to the ABCABC stacking sequence, however, this idea is in conflict with some physical properties of layer compounds. For example, BN (boron nitride) has two stacking sequences (ABAB and ABCABC) just same as graphite and they have also Raman-active intralayer E_{2g} mode. The most intriguing point is that these two polymorphisms of BN exhibit the strictly same wavenumber of E_{2g} mode at 1366 cm^{-1}. This means that the vibrational energy of *intralayer* mode is *not* affected by the *interlayer* interaction; the difference of stacking sequences. Same kind of discussion can be applied to graphite.

We conclude that the down-shifted Raman spectra observed in terrestrial, extraterrestrial and artificially ground graphite samples derive from some residual stress in the honeycomb lattice. This physical finding will give a clue to the origin of naturally down-shifted graphite grains.

References

[1] Wopenka B. and Pasteris J.D. (1988), *Microbeam Analysis* (D.E.Newbury ed. San Francisco Press.) 196-200. [2] Wopenka B. *et al.* (1988), *EOS* **69**, 501. [3] Wada *et al.*, *submitted.* [4] Dresselhaus M.S. and Dresselhaus G. (1981), *Advances in Physics* **30**, 139-326. [5] Zinner E. and Wopenka B. (1990), *Lunar and Planetary Science* **XXI**, 1379-1380.

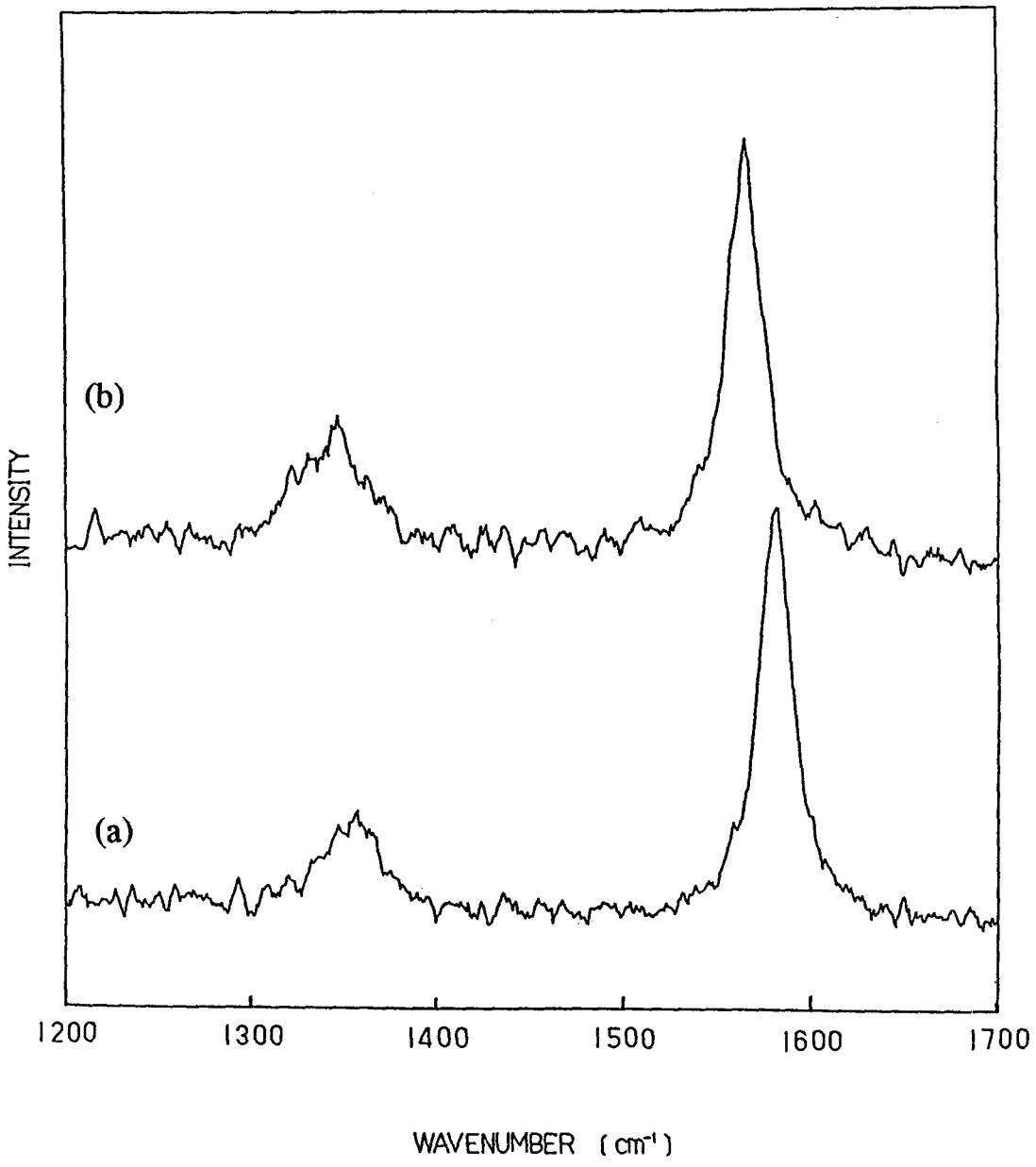

Fig.1. Raman spectra of artificial graphite
(a) untreated graphite rod
(b) ground graphite powder

INTERSTELLAR GRAPHITE FROM THE MURCHISON METEORITE: MORPHOLOGIES CORRELATE WITH CARBON ISOTOPIC RATIOS

Sachiko Amari[1,2], Ernst Zinner[1], and Roy S. Lewis[2] [1]McDonnell Center for the Space Sciences and Physics Department, Washington University, One Brookings Dr., St. Louis MO 63130-4899 [2]Enrico Fermi Institute, The University of Chicago, 5640 S. Ellis Ave., Chicago, IL 60637-1433

INTRODUCTION Graphite has been identified as the carrier of Ne-E(L) [1], which is almost pure ^{22}Ne. So far, studies of graphite grains have been performed on four density graphite fractions from the Murchison meteorite. These previous studies have revealed the existence of several different components as defined by Ne-E(L) thermal release patterns, Kr isotopic ratios, and C isotopic ratios of single graphite grains [2,3,4,5]. The goal of this study is to understand how many different components are present in these fractions and to connect these components to their stellar sources. To do that, we have attempted to characterize the graphite fractions in many different ways and to minimize any bias in the selection of grains. For previous ion probe measurements [3,5], we tended to select large grains to make precise multielement isotopic measurements on single grains.

SAMPLE PREPARATIONS The Murchison meteorite was treated with HF-HCl, H_2O_2, and $Cr_2O_7^{2-}$ to remove silicates, sulfur, and reactive kerogen. After that, four graphite fractions were extracted by density (Table 1) and by size separation with a size cut-off of 1μm [6]. For this work, we measured grains from KFB1 (72 grains) and KFC1 (157 grains). Grains were deposited onto a gold foil from suspension. We chose a certain area and documented all round grains (>0.5μm) for ion probe measurements. After SEM-EDX analyses without C coating, we took SEM pictures to examine morphologies and grain sizes. Unfortunately, the KFB1 mount was contaminated, apparently with some kind of organic matter from the suspension. Therefore, to get reliable C isotopic data, we had to concentrate on larger grains (>1μm) than originally planned. Carbon and N isotopic ratios were measured on all the larger grains and $^{18}O/^{16}O$ on selected ones.

RESULTS AND DISCUSSION Nitrogen is normal in most of the grains we measured. From KFB1, only two grains have heavy N ($^{14}N/^{15}N$=156±6 and 153±19) and from KFC1 six grains have $^{14}N/^{15}N$ ratios smaller than 195. In contrast, the C isotopic ratios display large variations. Figure 1 shows distributions of $^{12}C/^{13}C$ ratios and grain sizes in both fractions, together with the results of previous measurements [3,5]. The distributions of C isotopic ratios do not differ too much between the two studies, except that the population of heavy C grains in KFB1 is more obvious in the previous measurement.

In the two density fractions studied, most of the grains can be classified into two types; grains of the first type (Cauliflower-type) look like dense aggregates of small scales. Those of the second type (Onion-type) have smooth surfaces and often show shell-like structure. Bernatowicz et al. (1990) [7] studied sliced graphite grains in the TEM and found that cauliflower-type grains consist of poorly crystallized graphite, while onion-type grains are well crystallized in their outer regions but have amorphous cores. Cauliflower-type grains sometimes contain TiC subgrains. Thus, external morphologies are closely correlated with internal structures. Differences in morphologies thus indicate differences in formation conditions of the grains. We compiled all the data [3, 5, and this work] on the basis of morphology to check whether there is any relationship with C isotopic ratios and grain sizes (Fig. 2).

The two types of grains have quite different distributions of C isotopic ratios. In KFB1 cauliflower-type grains have mostly isotopically normal C and only a small fraction

has heavy C. Only few grains have light C. In contrast, grains with light C are most abundant among onion-type grains and the abundance of grains with normal C and with light C is moderate. Grains of the cauliflower type are slightly bigger than grains of the onion type. However, due to the contamination problem, we were unable to measure smaller grains, most of which are of the onion type. Therefore, the true grain sizes of onion-type grains are smaller than those of the grains in our selections.

In KFC1, grains of the onion type appear to belong to two populations; one with heavy C and another one with light C, the second one having much larger grain sizes than the first. Only few grains have normal C. Most of the cauliflower-type grains have light C. The KFC1 cauliflower-type grains are much larger than onion-type grains, but the second type dominates in abundance. In previous studies, according to their C isotopic ratios, four groups have been identified in the four graphite fractions [5,8]. If we take morphology into account, each group consists of subgroups.

Another objective of this work was to find out whether there are any grains with ^{18}O excesses in the two heaviest density fractions. Previously, Hoppe et al. [9] have found that the two lightest fractions contain ^{18}O-rich grains. The interesting feature is that ^{18}O excesses are correlated with ^{15}N excesses. We have found one grain with ^{18}O excess ($^{18}O/^{16}O=275\pm47$, solar ratio is 499) in KFC1. However, it does not fall on the trend for grains in the two light fractions, that is, the ^{18}O excess is much less than expected from the ^{15}N excess ($^{14}N/^{15}N=93\pm17$).

References 1. Amari S., Anders E., Virag A., and Zinner E. (1990) Nature **345**, 238-240. 2. Amari S., Lewis R. S., and Anders E. (1990) LPS **XXI**, 19-20. 3. Amari S., Zinner E., and Lewis R. S. (1990) Meteoritics **25**, 348-349. 4. Lewis R. S. and Amari S. (1992) LPS **XIII**, 775-776. 5. Hoppe P., Amari S, Zinner E., and Lewis R.S. (1992) LPS **XXIII**, 553-554. 6. Amari S., Lewis R.S., and Anders E. (1993) GCA submitted. 7. Bernatowicz T. J., Amari S., Zinner E., and Lewis R.S. (1990) Ap. J. **373**, L73-L76. 8. Amari S, Hoppe P., Zinner E., and Lewis R.S. Nature submitted. 9. Hoppe P., Amari S, Zinner E., and Lewis R.S. (1992) Meteoritics **27**, 235.

Table 1. The graphite fractions extracted from Murchison

Fraction	Density (g/cm^3)
KE1	1.6-2.05
KFA1	2.05-2.10
KFB1	2.10-2.15
KFC1	2.15-2.20

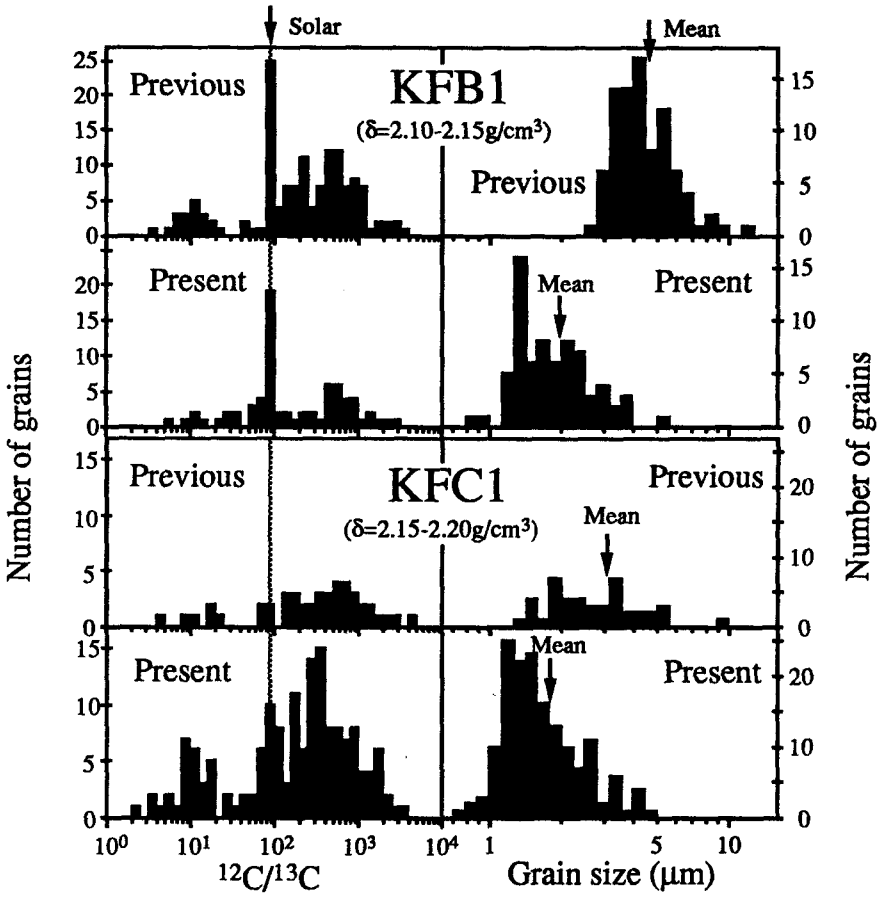
Solar
Mean
Previous
KFB1
(δ=2.10-2.15g/cm³)
Previous
Present
Mean
Present
Previous
KFC1
(δ=2.15-2.20g/cm³)
Previous
Mean
Present
Mean
Present
Number of grains
Number of grains
12C/13C
Grain size (μm)

Fig. 1

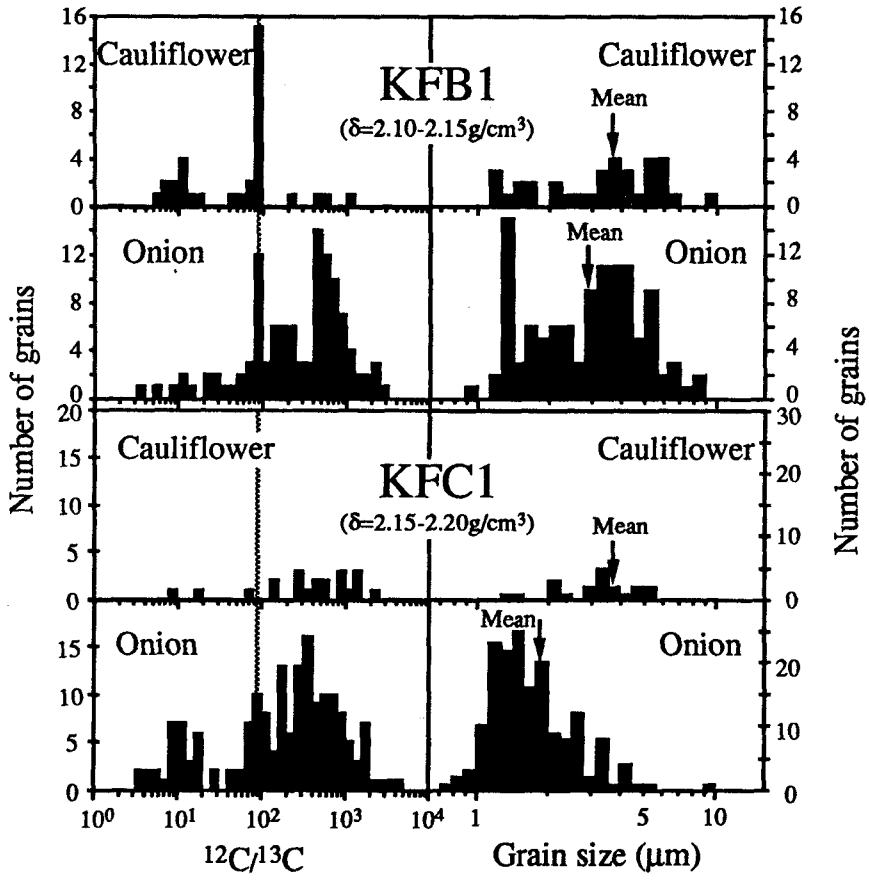
Cauliflower
KFB1
(δ=2.10-2.15g/cm³)
Cauliflower
Mean
Onion
Mean
Onion
Cauliflower
KFC1
(δ=2.15-2.20g/cm³)
Cauliflower
Mean
Onion
Mean
Onion
Number of grains
Number of grains
12C/13C
Grain size (μm)

Fig. 2

ISOTOPICALLY LIGHT NITROGEN IN UOCS WHICH IS NOT DUE TO PRESOLAR DIAMONDS NOR SIC.

Kiyota, K, Sugiura, N. and Hashizume, K.
Department of Earth and Planetary Physics, Faculty of Science, Univ. of Tokyo, Japan.

Introduction

In search for new presolar grains, we have measured nitrogen isotope ratios of many UOCs. We have reported isotopically anomalous nitrogen components which are not due to diamonds nor SiC, in ALH77214 and Yamato74191 [1]. Here, a light nitrogen component found in some UOCs is reported.

Results and discussion

Seven UOCs (ALHA81251, ALH83007, ALH83010, EET83399, LEW86022, Yamato791500 and Yamato82038) have been found to have similar degassing profiles of nitrogen and primordial ^{36}Ar by stepped combustion method (from 200℃ to 1200℃ every 100℃). They degassed isotopically light nitrogen and primordial ^{36}Ar mainly around 1000℃ or 1100℃. Among them ALHA81251 (H3.2/3.4) has the largest amount of light nitrogen and $\delta^{15}N$ goes down to -60 ‰ at 1100℃. To remove terrestrial nitrogen and to estimate the abundance of isotopically anomalous nitrogen, excess^{15}N which is defined as excess^{15}N = [nitrogen abundance] $\times \delta^{15}N \times [^{15}N/^{14}N]_{air}$, is introduced. Excess$^{15}N$ (≥600℃) of bulk sample of ALHA81251 is -6.3 ppb and H_2O_2 treatment removed about 80% of the light nitrogen (Fig.1), while almost all primordial ^{36}Ar remained after H_2O_2 treatment (Fig.2).

If the light nitrogen is due to diamond or due to SiC, assuming that nitrogen concentrations of Cδ diamond and SiC are 6900 ppm [2] and 1% [3], respectively, and the $\delta^{15}N$ are -340 ‰ [4] and -600 ‰ [5], respectively, the light nitrogen in ALHA81251 corresponds to 760 ppm of diamond or 280 ppm of SiC. The abundance of ^{22}Ne-E in ALHA81251 is calculated to be less than 0.1×10^{-8}ccSTP/g [6] which corresponds to only 6 ppm of SiC [7]. Also 80% of light nitrogen is removed by H_2O_2 treatment. Therefore, most of the light nitrogen of ALHA81251 is not that of presolar SiC.

Judging from Ne composition of Allende [6] and its diamond concentration [8], 1 ppm of diamond contains $1\text{-}6\times10^{-10}$ccSTP/g of ^{20}Ne-A.

Diamond degases around 500℃ by stepped combustion and since the abundance of ^{20}Ne-A in ALHA81251 is calculated as less than 1.6×10^{-8}ccSTP/g [6], it has less than 200 ppm of diamond. Therefore, most of light nitrogen of ALH81251 is not that of presolar diamond.

As reported before [1], ALHA77214 has light nitrogen which is not due to diamond nor SiC. It has two degassing temperatures of light nitrogen , and the degassing profile of high temperature is similar to that of ALHA81251, while the δ^{15}N values are different. Whether the carrier of light nitrogen in ALHA81251 is the same as that in ALHA77214 or not is not known yet.

Most of primordial ^{36}Ar in ALHA81251 is not that of the light nitrogen carrier, since the resistance to H_2O_2 treatment is different. However, it is possible that the light nitrogen carrier in ALHA81251 contains primordial ^{36}Ar in the ratio like diamond ($N / ^{36}Ar = 1.8 \times 10^5$) or SiC ($N / ^{36}Ar = 3.2 \times 10^6$).

References

[1] Sugiura N. and Hashizume K. (1992) *Earth Planet. Sci. Lett.*, **111**, 441-454. [2] Russell S. S. and Pillinger C. T. (1990) *Lunar Planet. Sci.*, **XXI**, 1051-1052. [3] Bernatowictz T. et al. (1987) *Nature*, **330**, 730-732. [4] Alexander C. M. O'D. et al. (1990) *Lunar Planet. Sci.*, **XXI**, 9-11. [5] Zinner et al. (1987) *Nature*, **330**, 728-730. [6] Schultz K. and Kruse S. (1989) *Meteoritics*, **24**, 155-172. [7] Huss G. R. (1990) *Nature*, **347**, 159-162.

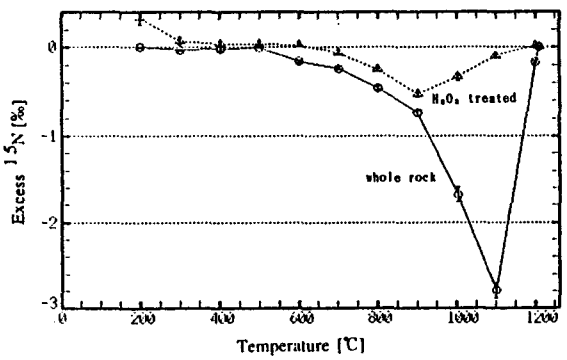

Fig. 1. Excess ^{15}N released by stepped combustion of ALH81251.

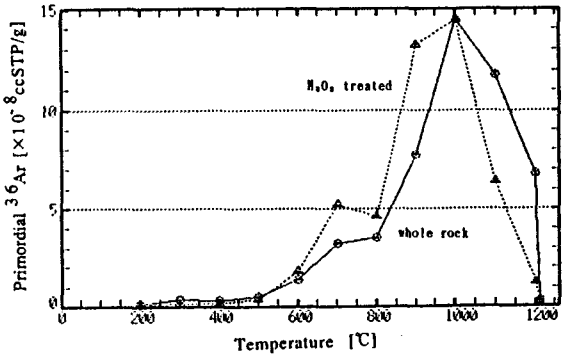

Fig. 2. Primordial ^{36}Ar released by stepped combustion of ALHA81251.

NANO-DIAMONDS IN PRIMITIVE CHONDRITES : (1) THEORY. M.Ozima and Keiko Mochizuki. Department of Earth and Space Science, Faculty of Science, Osaka University, Toyonaka City, 560, Japan.

Micro-diamonds in primitive chondrites are characterized by Xe-HL which was supposed to have formed in Supernova. Several models has been proposed for the origin of the micro-diamonds. These include chemical vapor deposition i.e., CVD (e.g., 1), interstellar shock (2), and UV-annealing of small graphite particles (3). However, all these models have a common difficulty in explaining the unique association of Xe-HL with the micro-diamonds. We suggest that the formation process of a particular terrestrial diamond, Carbonado, may apply to the micro-diamonds in primitive meteorites. The process then would give a reasonable explanation for the unique association of Xe-HL with the micro-diamonds.

Kaminsky (4) first suggested that carbonado, an aggregate of sub micron-size diamonds, was formed by irradiation of coal with high energy particles produced from U, Th-decays. Ozima and Zashu (5) found a large amount of parentless fission Xe and Kr in carbonados. Since the existence of the parentless fission Xe and Kr requires very proximate existence of uranium to the carbonado, they supported the Kaminsky's speculation. The next paper given at this Symposium by Mochizuki et al. (6) reports the formation of nanometer-size diamonds in carbonaceous materials due to radiation.

We assume that carbonaceous materials (amorphous carbon, graphite, hydrocarbon grains) in the outer environment of a supernova was irradiated by energetic particles (including Xe-HL) emitted during supernova explosion. The energetic particles then interact with the carbonaceous matter: most of the energy is dissipated through electronic interaction, and at the end of the journey the particles produce cascade displacement of target atoms. We suggest that the displaced carbon atoms then recrystallized to form micro-diamonds as is inferred from the origin of terrestrial carbonados. We also note that for sufficiently small particle size (less than a few nano-meters) diamond may be more stable than graphite in interstellar environment (e.g. 7). We show that for a target particle of 1 μm, the number of the displaced cascade atoms is about 10^4. If the displaced atoms re crystallized to form a diamond, the size of the diamond would be about 20 nano-meter, which is comparable to the average size of the micro-diamonds in primitive chondrites. It is also easy to see that the process necessarily leads to the association of Xe-HL with thus formed micro-diamonds.

References. 1. Anders,E. (1987) Phil. Trans. R. Soc. London *A323*, 287-304. 2. Tielens, A.G.G.M., Seab,C.G., Hollenbac h,D.J., and McKee,C. (1987) Ast. J. *319*, L109-L113. 3. Nuth III,J.A., and Allen, Jr., J.E. Astrophysics and Space Science *196*, 117-123. 4. Kaminsky,F.

(1987) Dokl. Akad. Nauk SSSR 294 439-440. 5. Ozima, M. and Zashu, S. (1991) Nature *351* 472-474. 6. Mochizuki,K., Ozima, M., Tuchiyama, A., Kitamura, M. and Shimobayashi, N. (1993) This issue. 7. Nuth III, J.A. (1987) Astrphysics and Space Sciences *139* 103-109.

NANO-DIAMONDS IN PRIMITIVE CHONDRITES: RADIATION-INDUCED ORIGIN? ---- (2) EXPERIMENT. K.Mochizuki[1], M.Ozima[1], A.Tuchiyama[2], M.Kitamura[3] and N.Shimobayashi[3]
1)Department of Earth and Space Science, Osaka University, Toyonaka City, 560, Japan, 2) College of General Education, Osaka University, Toyonaka City, 560. 3)Department of Geology & Mineralogy Faculty of Science, Kyoto University Sakyo, Kyoto 606

Introduction Ozima and Mochizuki (1) suggested that micro-diamonds in primitive meteorites were formed by irradiation of carbonaceous matters such as graphite or hydrocarbons with enregetic particles emitted from Supernova. To test this hypothesis, we carried out the following experiments. (1) We examined uranium-enriched natural coal to see whether or not diamonds were formed in radiation-damaged zones in the coal. (2) We irradiated several carbonaceous materials such as graphites, glassy carbon, and natural coals with high energetic particles to see whether the irradiation produced micro-diamonds.

Experimental results (i) We investigated a uranium rich coal (carburanium) from Cluff lake, Canada. Electron Microprob Analysis of this sample showed that there are numerous uranium oxide grains of about 10-20 μm almost uniformly distributed in hydrocarbon matrix. A small amount of PbS was also identified by the EPMA analysis. If the U, Th-induced radiation were to produce diamonds, they are most likely to be found in radiation-damaged regions around the uranium oxide grains. Hence, we very carefully searched for micro-diamonds in the radiation-damaged regions by TEM (transmission electron microscope). We observed many crystalline particles of about 20nm (Fig.1-a), of which concentration in the radiation damaged region is about 500ppm. Electron diffraction analysis on the crystalline particles gave a powder ring pattern (Fig.1-b). Because of the limitted resolution of the TEM, the electron diffraction was taken over an area (about 0.5 μm x 0.5 μm) which contained several grains. The pattern is most reasonably explained by assuming that the grains consist of diamond and galena(PbS) crystals as shown in Table 1. Hence, the experiment seems to confirm the Kaminsky's hypothesis(2), that is, high energy particles produced from U, Th-decays interacted with hydrocarbon (i.e., natural coal) to form micro-diamonds.

(ii) We irradiated 50 mesh graphite powder by argon beam of 50 MeV with a RILAC linear accelerator at Riken, and examined the irradiated sample by TEM. We observed a crystalline particle which showed a diffraction pattern similar to diamond. Though less likely, the diffraction pattern may also be attributed to graphite. Since we could take the diffraction only from one direction, it is difficult to rule out the latter possibility. To resolve the ambiguity, it is essential to make the electron diffraction analyses of the crystalline particle at least from two directions. For the irradiated coal, we did not find diamond. Although the experimental results so far obtained are encouraging, we undoubtedly need more TEM observation on the irradiated sample to

so far obtained are encouraging, we undoubtedly need more TEM observation on the irradiated sample to establish that the energetic particle irradiation of graphite produces diamonds. Currently we are trying to see the irradiation effect on different target materials (amorphous carbon, graphite, and hydrocarbon) with different beams (Kr or Xenon).

Reference

1. M.Ozima, and M.Mochizuki (1993) Nano-diamonds in primitive chondrites: (1) Theory. (this volume). 2. Kaminsky,F.(1987)Dokl. Akad.Nauk SSSR 294 439-440.

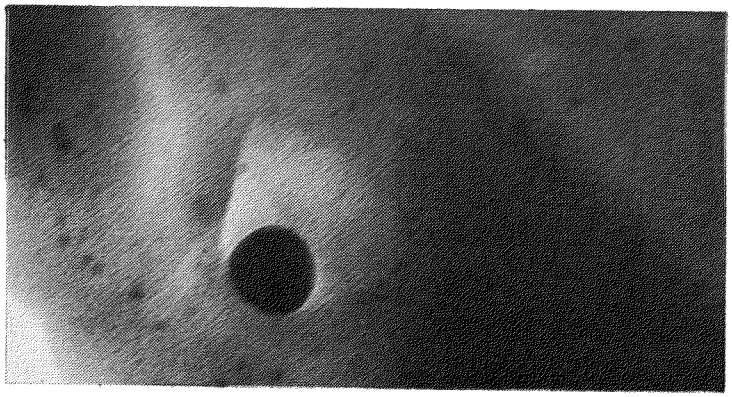

Fig.1-a Diamond-like grain (dark pherical area in the center of the figure) in a carburanium from Cluff lake,Canada.

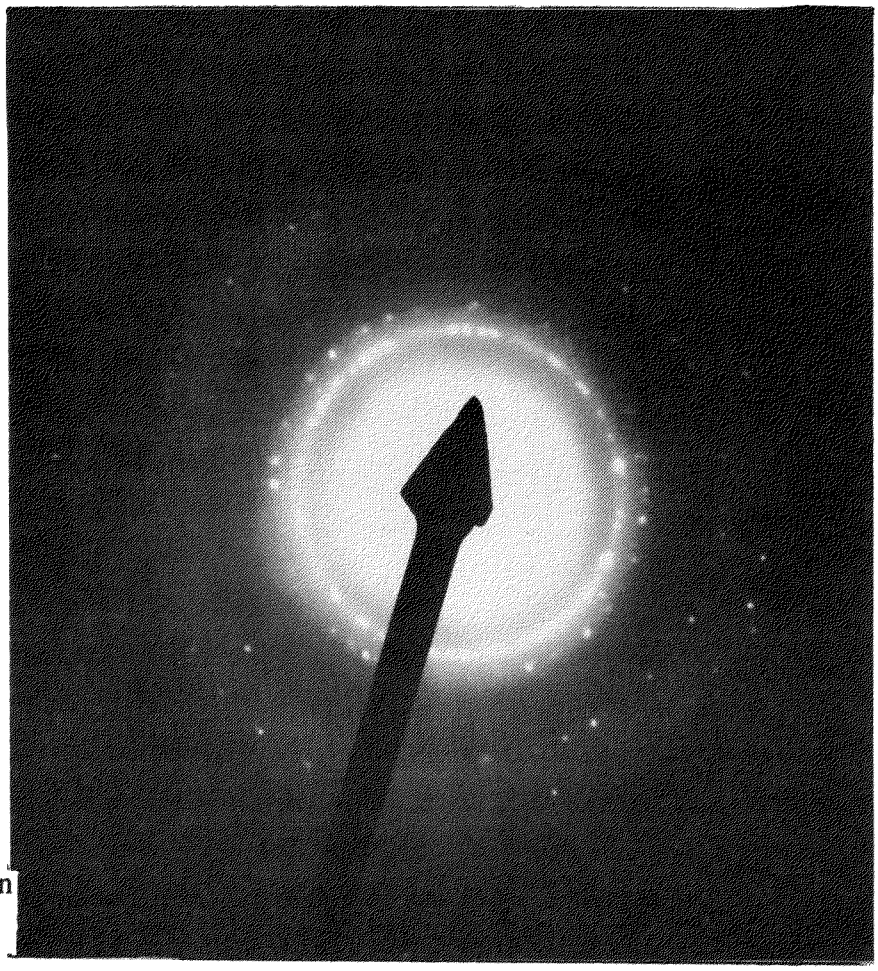

Fig.1-b The diffraction pattern of grains in the carburanium.

D(Å)	d(dia)(Å)	d(graph)(Å)	d(PbS)(Å)	D/d(dia)	D/d(graph)	D/d(PbS)
2.183	2.060	2.030	2.0990	***1.060***	1.075	1.040
2.008						
1.950		1.800			1.083	
1.877		1.678	1.7900		1.118	***1.048***
1.599		1.544	1.4840		1.035	1.077
1.334	1.2610	1.232	1.2120	***1.058***	1.083	1.101
1.128	1.0754	1.054	1.0489	***1.049***	1.070	1.075
1.074		0.994	1.0034		1.080	1.070
0.9401	0.8916		0.8952	1.054		1.050
0.8633	0.8182			1.055		
0.8426						

Table 1. Capital D is the d-spacings determined from our observation of the crystals in a carburanium from Cluff lake, and d is the theoretical d-spacings for diamond, graphite, and PbS, respectively. The observed D-sacings are normalized to the theoretical values; we show D/d ratios in the table. If the ratios D/d of a crystal calculated for all diffrcation spacings give the same value, we can conclude that thus chosen theoretical d-spacings truly represents the crystal. As seen in the table, the choice of diamond for the theoretical d-spacings gives almost the same ratios for the 3 strong peaks (shown by bold letters in the fifth column in the table), indicating that the crystal is best represented by a diamond structure. A strong peak at D = 1.877, however, cannot be attributed to diamond, and this can be attributed to PbS.

NEUTRON INDUCED PROMPT GAMMA-RAY ANALYSIS OF CHONDRITES IN CONJUNCTION WITH ISOTOPIC ANALYSIS OF IRON.

Akira Nakamura[1)], Mitsuru Ebihara[2)], Kanako Kobayashi[2)], Yasuo Ito[3)], Chushiro Yonezawa[4)] and Michio Hoshi[4)]

1) Deptartment of Chemistry, Akita University, 2) Department of Chemistry, Tokyo Metropolitan University, 3) Research Center for Nuclear Science and Technology, The University of Tokyo, 4) Department of Chemistry, Japan Atomic Energy Research Institute.

Introduction

The Subcommittee on Assessment of Isotopic Composition of the Element of IUPAC reported the ranges of isotopic abundance of iron as ^{54}Fe(5.77-6.04), ^{56}Fe(91.52-91.79), ^{57}Fe(2.11-2.25) and ^{58}Fe(0.28-0.34) in atom percent unit. At the same time, the committee had mentioned that most of these rages should be regarded as unresolved experimental discrepancies and not as natural variability of iron stable isotopes[1]. The possibility of isotopic enrichment and/or stripping, however, can be proposed from an applicable concept of isotope effects in chemical reaction, e.g., the ordinary mass isotope effects and the magnetic isotope effect[2, 3]. Our main interest on this study is focused on two points; determination of non-destructive isotopic analysis by the prompt gamma-ray spectroscopic assembly recently introduced at JRR-3 atomic reactor of Japan Nuclear Research Institute[4, 5] and the comparison of isotopic ratio of stable isotopes of iron in mineral resources with those of meteorites. Iron ore, for example, can be understood as a mineral resource which is believed to be produced by a thermal metamorphic process effected on the biological metabolic iron-rich substances at an early stage of evolution of life. If the early lives can enrich some iron isotopes in some way, the isotopic ratios in meteorites could be a standard index for this purpose.

Activation analyses are not usually recognized as a reliable method with high accuracy. The most recent determination of abundance of ^{58}Fe, however, was carried out by an instrumental neutron activation analytical technique[6]. Monitoring the prompt gamma-ray emitted from an activated isotope produced by the (n, γ) nuclear reaction, every stable isotope abundance of any element can be determined in principle. At the same time, as this emission of gamma-ray is to be measured simultaneously with irradiation of neutron, the discrepancy derived by cooling period accompanied by the ordinal instrumental neutron activation technique can also be excluded.

We report the determination of isotopic analysis by prompt gamma-ray analysis with using cold neutron guide beam as well as the analytical results of isotopic ratio of several iron ores and chondrite meteorites.

Experiments and Results

The detailed description of the equipment employed in this experiment was reported in the literatures[4, 5]. The standard samples for the calibration were prepared by mixing enriched

$^{54}Fe_2O_3$ and $^{57}Fe_2O_3$ into high-purity Fe_2O_3 in several molar ratios. In Figure 1, a spectrum of whole energy region was shown as an example. For the actual determination of isotope of ^{57}Fe and ^{56}Fe, energy peaks at 811keV and 692keV were selected to monitor, respectively. On the other hand, peaks at 9296keV and 7632keV were chosen, respectively when the ratio of ^{54}Fe and ^{56}Fe was determined (Figure 2). The peak area was carefully calculated by a Gaussian curve fitting with 1% error value for the monitoring peak. The calibration curve to determine the ratio of ^{57}Fe and ^{56}Fe thus obtained had a satisfactory linearity as shown in Figure 3.

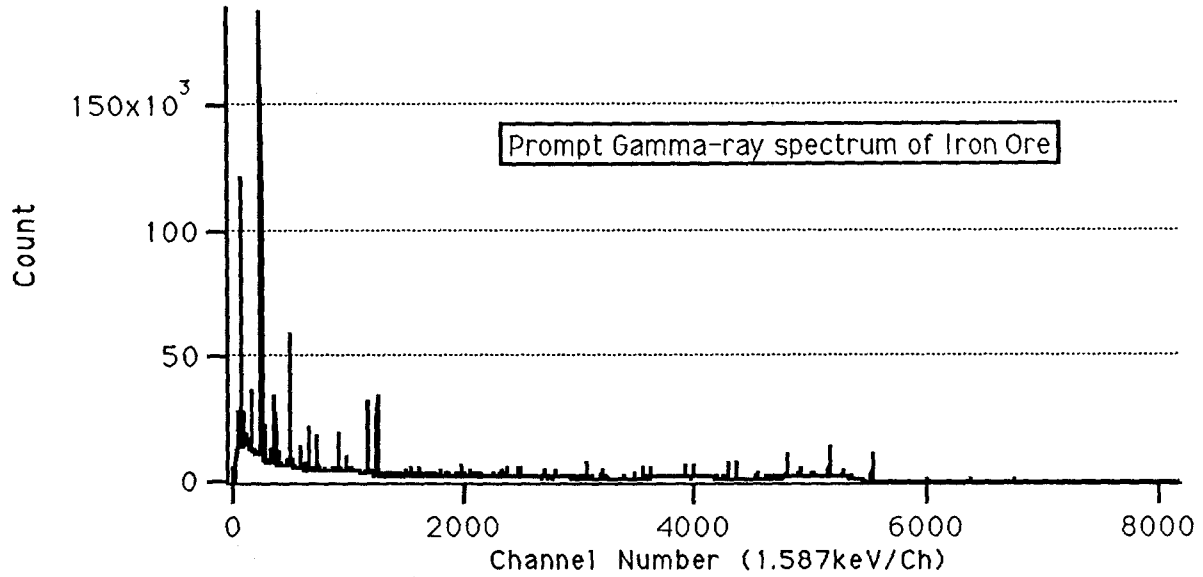

Figure 1. An Example of Whole Energy Spectrum of Iron Ore (Hamerslay).

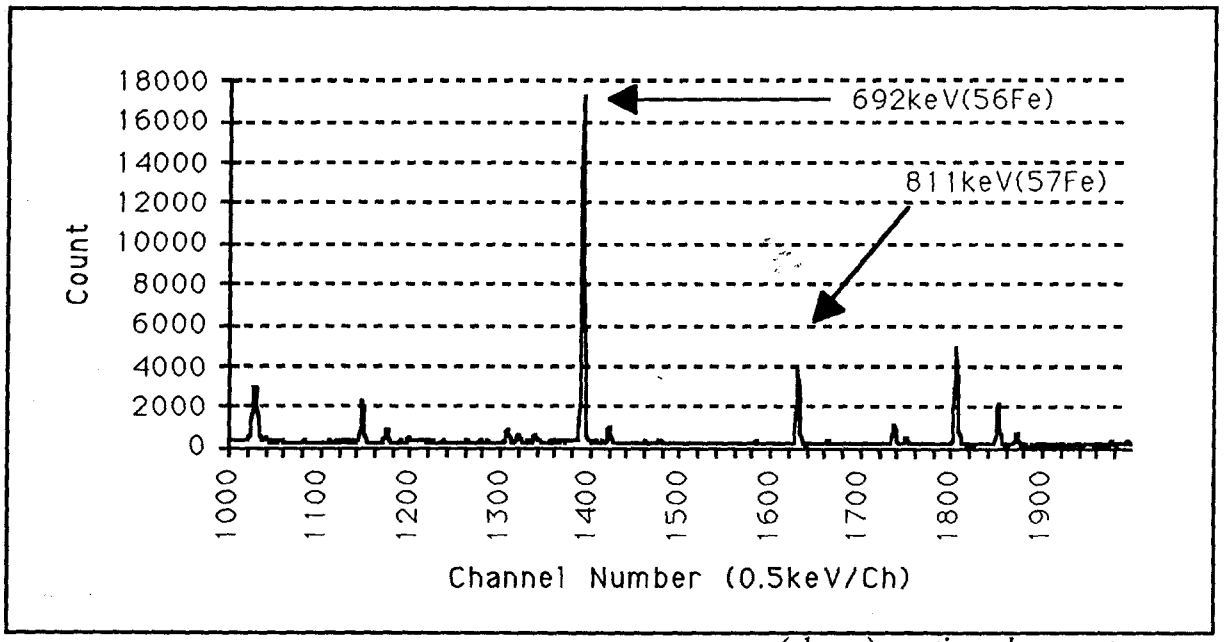

(above) *continued on next page*

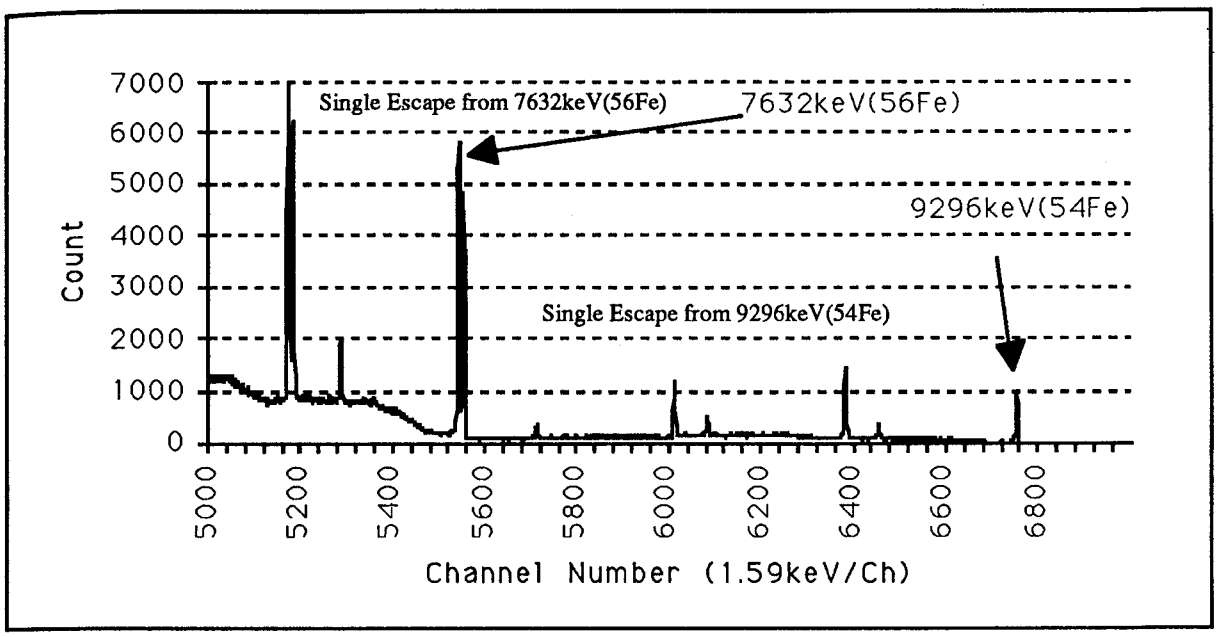

Figure 2. The Prompt Gamma-ray Spectra of Low Energy (above) and High Energy (below) Region of Interest (ROI's).

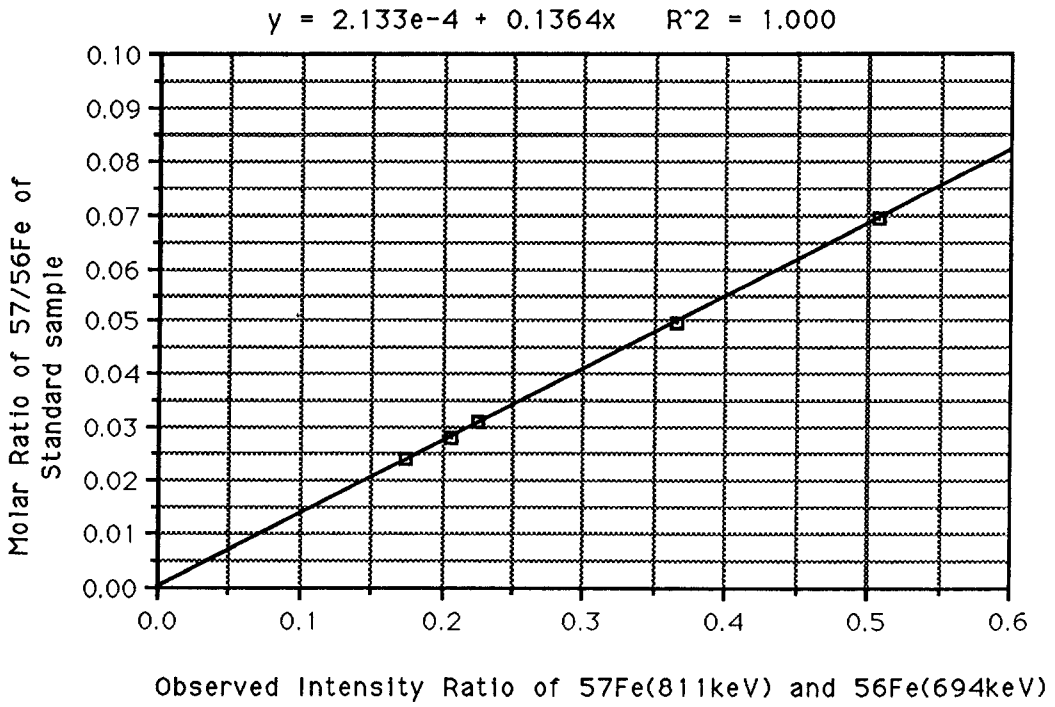

Figure 3. Calibration Curve of Standard Samples to Determine the Molar Ratio of ^{57}Fe and ^{56}Fe.

Table 1. Isotopic Ratios of ^{57}Fe vs. ^{56}Fe of Iron Ores and Chondrite Meteorites.

Sample	Source	Peak Area 811keV(57Fe)	Error (Gaussian)	Peak Area 692keV(57Fe)	Error (Gaussian)	Ratio of Area 57Fe/56Fe	Molar Ratio of 57Fe/56Fe
Iron Ore	Iskor	18220.3	226.47	106234.0	915.73	0.1715	0.0236
Iron Ore	Carajas	22336.2	253.96	127719.0	799.96	0.1749	0.0239
Iron Ore	Hamerslay	35687.4	229.48	202169.0	2105.19	0.1765	0.0243
Iron Ore	Rio d'Ose	21231.1	248.42	122570.8	572.27	0.1732	0.0238
Iron Ore	Lobe	18864.6	162.46	106003.2	382.37	0.1780	0.0245
Chondrite	Y79-1717	10799.1	133.57	63991.5	319.87	0.1688	0.0232
Chondrite	Y79-2769	8032.6	164.78	47951.5	210.9	0.1675	0.0231
Chondrite	Y74-014	10873.3	128.09	63239.2	290.9	0.1719	0.0237

The samples, e.g., some iron ores from different sites and several chondrite meteorites were analyzed, and the results are summalized in Table 1.

In addition to the above results, a series of Chondrite Meteorites of the class of CV3, CI and CM2 were also analyzed to determine the isotopic ratio by the same technique.

References

1. Commission on Atomic Weights and Isotopic Abundances, (1984) Pure & Appl. Chem., **56**(#6), 695.
2. "The Biological Fractionation of Isotopes." Eric M. Galimov, Academic Press (1985).
3. "Spin Polarization and Magnetic Effects in Radical Reactions." Ed. by Yu. N. Molin, Elsevier (1984).
4. C. Yonezawa, A. K. Haji Wood, M. Hoshi, Y. Ito and E. Tachikawa, Nucl. Instrm. Method. A , in press.
5. C. Yonezawa, A. K. Haji Wood, M. Hoshi, Y. Ito and E. Tachikawa, Proc. 4th Intern. Symp. on Adv. Nucl. Energ. Res. , in press.
6. W. D. James and J. J. Carni, (1980) J. Radioanal. Chem. **57**, 223.

The measurement of ^{26}Al in meteorites by using ultra-low background γ-ray detector

H. Tazaki, H. Ejiri, and H. Ohsumi

Department of Physics Osaka University, Toyonaka, Osaka 560, Japan.

This work addresses the precise measurement of ^{26}Al radionuclide in meteorites as an application of the ultra low background γ-ray detector ELEGANTS (electron gamma neutrino spectrometer) IIIs[1]. This detector was originally developed for the study of double beta decay of ^{76}Ge, and now it is using for the measurement of low-level radio activities in developing new detector materials, which is used for the study of nuclear rare decays.

The data of long-lived cosmogenic radionuclide in meteorites provide important information about the cosmic ray exposure age, terrestrial age, and complex irradiation history of the meteorites. Accelerator mass spectrometry (AMS) is now widely used for the measurement of long-lived cosmogenic radioactive nuclei such as ^{10}Be, ^{14}C, ^{26}Al and ^{36}Cl. Besides AMS method, γ-ray counting is very useful method to measure ^{26}Al, because relatively high energy γ-ray (1.809 MeV) is emitted with large branching ratio of 82% in the beta decay of ^{26}Al. The advantage of γ-ray counting is that the concentration of ^{26}Al can be directly measured non-destructively.

Concentrations of ^{26}Al activities in some meteorites need to be measured in an order of dpm/kg. We need an ultra low background detector for the γ-ray measurement of ^{26}Al in it. Our ELEGANT IIIs detector satisfies such a low background condition. Details of the ELEGANTS IIIs are shown in fig. 1. The Ge detector is made of coaxial-type 171cm^3 pure Ge. Materials used for the detector are such light element as Ti, OFHC-Cu, Mg, etc. Radioactivities in all detector materials were checked to be less than $(1-2)\cdot10^{-15}$ Ci/g. Experimental shields consists of 10cm thick OFHC (oxygen free high conductive copper) and 10cm thick lead. OFHC is known to be quite free from radioactive contamination. The whole assembly is kept airtight and nitrogen gas evaporated from liquid nitrogen is introduced around the detector to purge out air containing natural radioactive radon gas. Typical sensitivities (detectable limits) obtained for U-chain, Th-chain and ^{40}K are $\sim$1 pCi/kg, $\sim$1 pCi/kg, and $\sim$10 pCi/kg, respectively.

The typical γ-ray spectrum of natural background without and with shielding is shown in Fig. 2. This measurement was done in the overground laboratory, and if we measure in the Kamioka underground laboratory, the background rate is reduced in one order of magnitude.

For an accurate measurement, the absolute efficiency for γ-ray photopeak is calculated by Monte Carlo method and it was checked by the measurement of standard γ-ray sources with known intensities. The self absorption of γ-ray in the sample is calculated in the Monte Carlo method. The shape of the sample is roughly simulated by numerical values, and the tabulated concentrations of known elements in the sample material is used in the calculation to evaluate the self absorption of γ-ray.

As an example, we measured the ^{26}Al radionuclide in ALH-767 meteorites. The sample is roughly rectangular shape with the size of 8.5×2.7cm×0.48cm. The weight of the sample is 32g and the live time of the measurement is 50 hour. The measured ^{26}Al concentration is 58.6±7.3 dpm/kg.

Our minimum ^{26}Al concentration to be measured is about $3/\sqrt{t}$ dpm/kg with t days measurement by using ELEGANT IIIs in overground laboratory. If we measure in the Kamioka underground laboratory, the minimum concentration to be measured is one oreder of magnitude smaller than in overground laboratory.

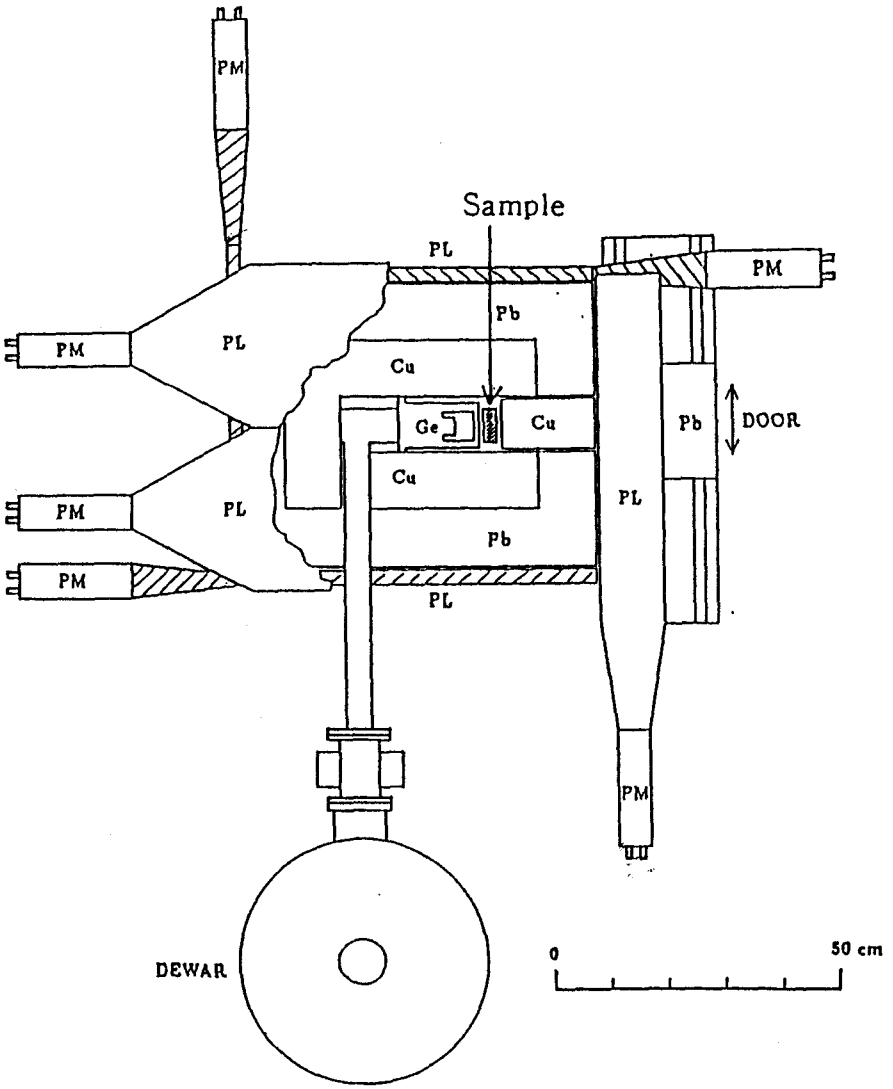

Fig. 1. TOP view of ELEGANTS IIIs
Ge, PL, PM, Cu and Pb are the Ge-detector, plastic scintillators, photomultipliers, copper shield bricks (OFHC), and lead shield bricks, respectively.

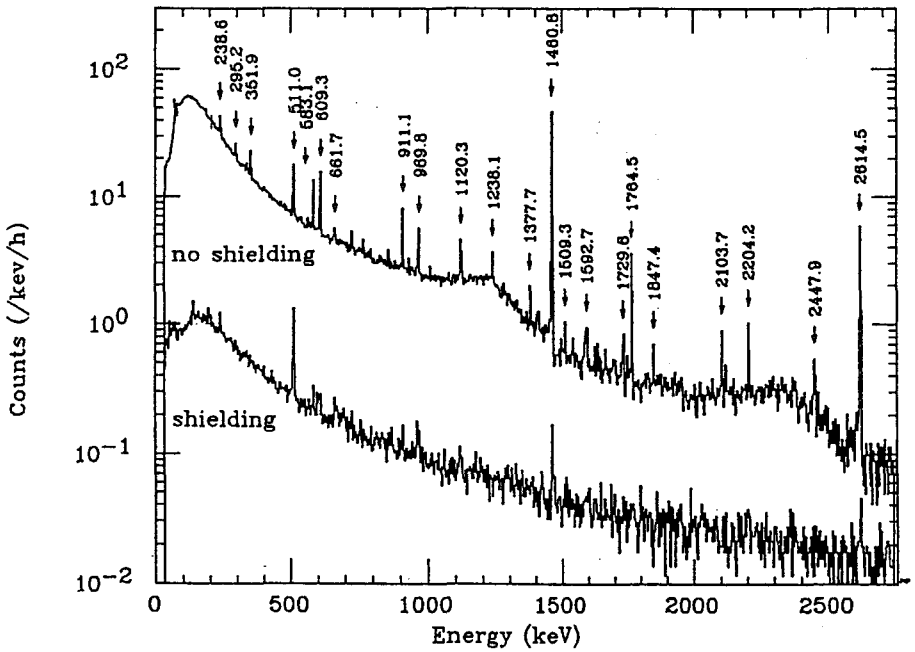

Fig. 2. Typical γ-ray background spectrum of ELEGANTS IIIs

The Authors thank National Institute of Polar Research for the ALH-767 meteorite.

1) H. Ejiri et al., Nucl. Phys. A448 (1986) 271. N. Kamikubota et al., Nucl. Instr. Meth. A245 (1986) 379.

^{26}Al IN YAMATO-86009 AND -86770 AND ASUKA-8603 METEORITES —Determination of ^{26}Al in small samples using extremely low background γ-ray counting system—

Fukuoka, T.[1], Yamakoshi, K.[2] and Nishio, F.[3]

[1]Department of Chemistry, Gakushuin University, Mejiro, Tokyo 171.
[2]Institute for Cosmic Ray Research, University of Tokyo, Tanashi, Tokyo 188.
[3]Hokkaido University of Education, Kushiro, Hokkaido 085.

Determination of terrestrial ages of Antarctic meteorites supplys useful informations for the frequency of meteorite fall, the mechanism of accumulation of meteorites and the age of ice and tephra (volcanic ash) layer (1). ^{26}Al ($T_{1/2}$ = 7.02 x 10^5y) is a useful tool for the dating of terrestrial age of meteorite.

In this study, ^{26}Al contents in Yamato-86009 and -86770 and Asuka-8603 meteorites have been determined non-destructively by extremely low background γ-ray counting system of Nokogiriyama station for measurements of extremely low level radioactivities, Institute for Cosmic Ray Research, University of Tokyo. The counting system consists of a well type of large volume high pure Ge detector (relative efficiency ~28% at 1.33 MeV) coupled with anti-coincedence counters and a 4096 channel analyzer. Absolute counting efficiency of the detector was 1.65% at 1809keV γ-ray of ^{26}Al. 1.45 to 2.52g of crushed samples were packed in plastic vials prior to put into the well of detector.

The determination results are shown in Table 1 with the sample weight for determination and the count length. The results are generally consistent with those of previous work (2 and 3), although the determination errors are relatively large. Usually, determinations of ^{26}Al contents for more than 100g of samples are performed by γ-ray count non-destructively . However, those for small samples such as less than 20g are very difficult. Recently, accelerator mass spectrometry (AMS) analysis has been applied to determination of ^{26}Al in meteorites. Although the sample amount of AMS analysis is small, this analysis is destructive. For small size of meteorites like Y-86009 and -86770 which original weights are 60.69 and 94.89g, respectively, non-destructive determination of ^{26}Al content using extremely low background γ-ray counting system has a great advantage, because we can get other informations such as chemical, petrological and mineralogical informations from the same sample after ^{26}Al determination.

REFERENCES:

(1) Fukuoka *et al.* (1987) Bull. Volcano. Soc. Japan, Ser. 2, **32**, 103.
(2) Fuse and Anders (1969) Geochim. Cosmochim. Acta **33**, 653.
(3) Komura *et al.* (1982) Mem. Natl. Inst. Polar Res., Spec. Issue, **25**, 178.

Table 1. ^{26}Al in Antarctic meteorites

Sample	Weight (g)	Count length (min)	Net count	^{26}Al contet (dpm/kg)
Y-86009,52 (CV3)	1.450	372,135	657 ± 100	73.9 ± 11.4
Y-86770,60 (C1)	1.813	347,444	393 ± 108	37.9 ± 10.4
Asuka-8603,21 (H4)	2.52	228,002	579 ± 77	61.2 ± 8.2

Special Lecture (I)

Prof. Gero Kurat

Naturhistoriches Museum, Vienna, Austria

MICROMETEORITES FROM THE ANTARCTIC BLUE ICE. Gero Kurat (1), Christian Koeberl (2), Thomas Presper (1), Franz Brandstätter (1) and Michel Maurette (3). (1) Naturhistoriches Museum, Postfach 417, A-1014 Vienna, Austria; (2) Institut für Geochemie, Universität Wien, Dr.Karl Lueger-Ring 1, A-1010 Vienna, Austria; (3) Centre de Spectrométrie Nucléaire et de Spectrométrie de Masse, Bat.108, F-991405 Orsay-Campus, France.

Introduction The recent accretionary flux of extraterrestrial matter onto the Earth is dominated by meteoroides in the size-range 50-500μm [1]. Theory predicts [2,3] that almost all of these meteoroids should in entering the Earth's atmosphere, be frictionally heated to such an extend that total melting will take place and thus the original mineralogy be destroyed and the chemical composition be severely altered. Fortunately, this seems not be the case because the Antarctic blue ice contains large amounts of unmelted extraterrestrial matter of just the particle size mentioned above [4-6]. This offers us the oportunity to study in detail the extraterrestrial matter which accounts for 99% of the daily infall on Earth. We are well aware of the chemical, physical, and mineralogical features of the rare large pieces of extraterrestrial matter we call meteorites. We are also fairly well informed about the features of objects which have been dubbed Interplanetary Dust Particles (IDPs) [7] and which cover the size-range <50μm. The most common matter of the size-range 50-500μm is the least known one. Earlier studies of these micrometeorites (MMs) gave as a result that they are similar to CM chondrites in mineralogy and chemical composition [5,8-14]. However, the match is not perfect and we need to study much more MMs in order to be able to answer the many questions arising from this differences. The most important question to be answered is wether the differences between MMs and CM chondrites are primary ones or of secondary origin [e.g., 11-18]. Here we make an attempt to give some answers by studying the major and trace element contents and the mineralogy of a selection of MMs.

Results Extraterrestrial matter from the Antarctic ice in the size-range 50-500μm consists of a variety of objects which represent all stages of possible alterations due to frictional heating during atmospheric entry. A surprisingly large porportion consists of unmelted micrometeorites which comprises phyllosilicate-dominated MMs or anhydrous coarse-grained silicates or mixtures of phyllosilicates with anhydrous silicates. The phyllosilicates are dominated by smectites and the anhydrous silicates by Fe-poor olivine and low-Ca pyroxene. Phyllosilicate-dominated MMs grade with increasing thermal exposure from slightly recrystallized to partial and total foamy melts. We call such particles scoriaceous MMs. The ultimate products of atmospheric heating are the degassed and droplet-shaped cosmic spherules. Among all objects there is present a considerable proportion which contains solar energetic particles Ne [5] proving that they existed as small objects, true micrometeoroids, in space.

Chemical bulk analyses of unmelted phyllosilicate-rich MMs obtained by electron micropobe (EMP) (Table) and instrumental neutron activation analysis [10,12,14,15,19] are compared to CI chondrites in Figures 1-3. Relative to CI chondrites MMs are depleted in Ca, Na, Ni, Co, S, and occasionally also in Mg and Mn and are enriched in K, Au, As, and occasionally in Br and Fe. The refractory and volatile lithophile elements have abundances very similar to that of CM chondrites (Fig.2).

Discussion. The mineralogical composition of unmelted MMs is quite similar to that of CM chondrites but differs from the latter in the small olivine/pyroxene ratio, the predominance of smectites over serpentine, and the lack of refractory very low-Fe olivines [5, 8, 9, 12, 13, 19]. The bulk major and

trace element contents of MMs also match the CM chondrite composition with the exception of some elemental depletions (Ca, Ni, Co, S, Mg, Mn) and enrichments (K, Au, As, Br, Fe). The mineral chemical differences between MMs and CM chondrites appear to be primary and set the MMs apart from all known meteorite classes. Also, the abundances of olivine and low-Ca pyroxene are unusual for CM chondrites but comparable to that of the unique Kaidun carbonceous chondrite [22]. However, the total lack of carbonates and sulfates in MMs is very probably due to terrestrial leaching processes and is very likely the cause of most of the elemental depletions observed in the MMs. Carbonates and sulfates are very common in CM chondrites [23] and are major sinks for Ca, Mg, Mn, Ni, Co, and S [14, 24 - 25]. Leaching of these phases from the MMs must result in measurable depletions in the elements mentioned and this is exactly what we observe. Similar depletions in IDPs [26 - 28] seem to be the result of the very same processes.

Enrichments of some volatile elements (K, Br, As, Au, Fe) in MMs very probably have also terrestrial causes. It has been shown by [29] for the Br enrichment of IDPs to be the result of terrestrial atmospheric contamination. A similar process - recondensation of meteoritic vapors in the atmospheric E-layer - is probably responsible for all the enrichments observed. The condensation of Fe has a visible effect: many MMs are enveloped by magnetite covers of variable thickness.

Conclusion. The most common extraterrestrial matter accreting onto the Earth today appears to be related to a rather rare class of meteorites, the CM chondrites. The match between MMs and CM chondrites is not perfect and warrants the establishment of a distinct class of MM carbonaceous matter. However, a variety of mineralogical and chemical pecularities of MMs appear to be due to terrestrial alteration process.

There is evidence for condensation processes in the high atmosphere (the base of the ionosphere) and of leaching processes in the lower atmosphere, the ice, and the melt ice water.

Beside the common CM-like MMs described in this contribution there is a variety of other rocks present in the Antarctic dust collection. Certainly at least a few of the mineralogically and chemically fractionated objects present are of extraterrestrial origin and possibly even of a planetary origin. Also some intestellar matter could be present. Much more work needs to be done to extract the wealth of information hidden in this dust sample which - for strange reasons - was so efficiently protected that is only very recently became available for study. Let's take up the challenge.

Acknowledgement. This work was financially supported by FWF, Vienna, Austria (P8125-GEO), by IN2P3 in France and the European Economic Community SCIENCE (Twinning and Operations) Program (Contract No. SCI*-CT91-0618, SMM).

References: [1] Hughes D.W.(1978) In: McDonnell J.A.M.(ed) Cosmic Dust, J.Wiley, 123-1185. [2] Kornblum J.J.(1969) JGR, 74, 1893-1907. [3] Love S.G. and Brownlee D.E.(1991) Icarus, 89, 26-43. [4] Maurette M., Brownlee D.F. and Schramm L.S. (1989) LPSC, 20, 636-637. [5] Maurette M., Olinger C., Christophe-Michel-Levy M., Kurat G., Pourchet M., Brandstätter F. and Bourot-Denise M. (1991) Nature, 351, 44-47. [6] Maurette M., Immel G., Perreau M., Vincent C. and Kurat G.(1992) LPSC, 23, 859-860. [7] Brownlee D.E. (1985) Ann.Rev.Earth Planet Sci. 13, 147-173. [8] Christophe-Michel-Levy M. and Bourot-Denise M.(1992) Meteoritics, 27, 73-80. [9] Klöck W., Beckerling W., Spettel B., Flynn G. and Sutton S.(1992) LPSC, 23, 697-698. [10] Koeberl C., Kurat G., Presper T., Brandstätter F. and

Maurette M. (1992) LPSC, 23, 709-710. [11] Kurat G., Koeberl C., Presper T., Brandstätter F. and Maurette M. (1992) Meteoritics, 27, 246. [12] Presper T., Kurat G. and Maurette M.(1992) Meteoritics, 26, 278. [13] Steele I.M. (1992) GCA, 56, 2923-2929. [14] Presper T., Kurat G., Koeberl C., Palme H. and Maurette M. (1993) LPSC, 24, 1177-1178. [15] Kurat G., Presper T., Brandstätter F., Maurette M. and Koeberl C. (1992) LPSC, 23, 747-748. [16] Maurette M., Kurat G., Presper T., Brandstätter F. and Perreau M. (1992) LPSC, 23, 861-862. [17] Perreau M., Engrand C., Maurette M., Kurat G. and Presper T. (1993) LPSC, 24, 1125-1126. [18] Engrand C., Maurette M., Kurat G., Brandstätter F. and Perreau M.(1993) LPSC, 24, 441-442. [19] Kurat G., Brandstätter F., Presper T., Koeberl C. and Maurette M. (1993) Geol.Geofiz., in press. [20] Palme H., Suess H.E. and Zeh H.D. (1981) In: Landoldt-Boernstein, Scheifers K. and Voigt H.H. (eds). Springer, vol.2, 257-273. [21] Wasson J.T. and Kallemeyn G.W. (1988) Phil.Trans.R. Soc.Lond., A 325, 535-544. [22] Ivanov A.V. (1989) Geochem.Internat. 26, 84-91. [23] Bostroem K. and Fredriksson K. (1966) Smithson.Misc.Coll.,151/3, 1-39. [24] Fredriksson K., Jarosewich E., Beauchamp R. and Kerridge J.(1980) Meteoritics, 15, 291-292. [25] Brandstätter F., Kurat G. and Graham A.L. (1987) Meteoritics,22 336-337. [26] Flynn G.J. and Sutton S.R. (1987) LPSC, 18, 296-297. [27] Flynn G.J. and Sutton S.R. (1991) Meteoritics 26, 334. [28] Flynn G.J. and Sutton S.R. (1992) Proc.LPSC, 22, 171-184. [29] Jessberger E.K., Bohsung J., Chakaveh S. and Traxel K. (1992) EPSL, 112, 91-99.

Table: EMP bulk analyses of selected phyllosilicate-rich MMs.

	91/2-024	91/2-073	91/3-022	91/3-031	91/3-038	91/3-108
SiO2	28,20	30,10	37,90	33,80	32,90	24,40
TiO2	0,08	0,07	0,13	0,07	0,07	0,10
Al2O3	1,71	1,35	2,05	1,92	1,70	2,04
Cr2O3	0,32	0,28	0,53	0,35	0,50	0,60
FeO	45,80	30,40	25,00	33,80	30,90	31,40
MnO	0,06	0,55	0,06	0,15	0,20	0,18
NiO	0,04	0,17	0,11	0,18	0,44	0,64
MgO	2,98	16,40	17,30	13,70	18,30	9,64
CaO	0,12	0,66	0,34	0,12	0,17	0,24
Na2O	0,23	0,21	0,26	0,17	0,28	0,26
K2O	0,91	0,21	0,42	0,17	0,19	0,78
SO3	1,29	0,94	6,81	2,02	2,97	7,04
sum	81,30	81,40	90,91	86,34	88,59	76,44

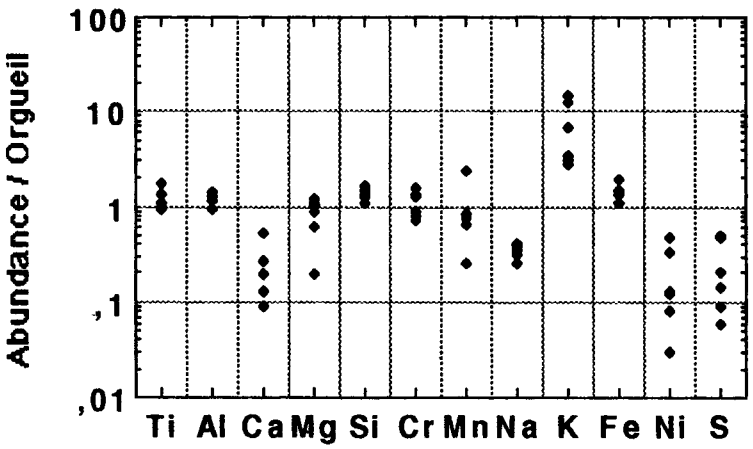

Figure 1: Bulk major and minor element contents of phyllosilicate-rich MMs as determined by EMP normalized to CI chondrites [20].

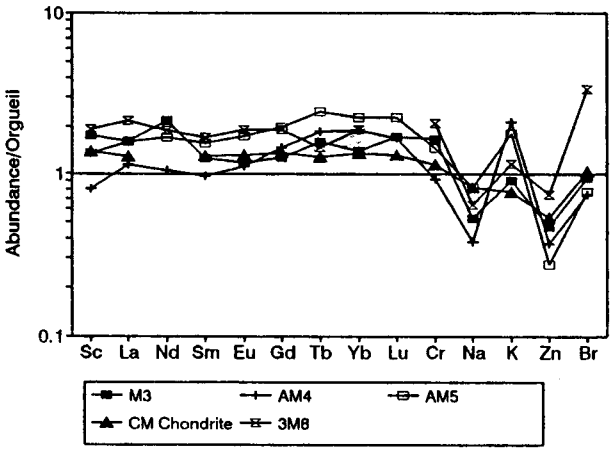

Figure 2: Bulk lithophile trace element contents of phyllosilicate-rich MMs as determined by INAA normalized to CI chondrites [20]. Elemental abundances fo CM chondrites [21] are shown for comparison.

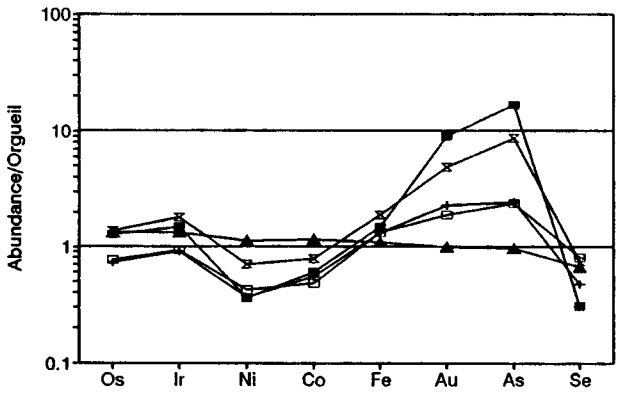

Figure 3: Bulk siderophile trace element contents of phyllosilicate-rich MMs as determined by INAA and of CM chondrites [21] normalized to CI chondrites [20].

Wednesday, June 2, 1993

09:00 - 14:15 Symposium, Auditorium

14:30 - 15:30 Special Lecture (II)

Prof. Stuart Ross Taylor

The Australian National University, Canberra, Australia

A SEARCH FOR SOLAR NITROGEN IN GAS-RICH CHONDRITES. Naoji Sugiura and Kaoru Kiyota, Department of Earth and Planetary Physics, Faculty of Science, Univ. of Tokyo, Tokyo, Japan.

Introduction. Nitrogen isotopic composition is a useful tracer of various processes in the early solar system. The average nitrogen isotopic composition of the solar system (solar nitrogen) is, however, not known at present, which is a serious drawback. Usually the average isotopic composition of volatile elements is determined from the solar wind isotopic composition. But in the case of nitrogen, the isotopic composition in lunar soils, which is presumably solar nitrogen, varies from -200 permil upto 300 permil relative to the terrestrial air nitrogen. Therefore, as an alternative source of solar nitrogen, we examined gas-rich chondrites. Previously [1] we reported results on ALHA77216 which has isotopically heavy nitrogen. Based on fair similarity of the N/Ne/Ar ratios in ALHA77216 and lunar soils, we tentatively concluded that the heavy nitrogen is of solar wind origin. It was, however, noticed that the heavy nitrogen seems to be removed by H_2O_2 treatment while Ne and Ar were not removed by the same treatment. Also, the abundances of heavy nitrogen and solar rare gases did not correlate very well. Thus, alternative interpretations, such as heavy nitrogen as organic materials, and as indigenous nitrogen in metallic grains need to be examined. Here, we report new experimental results on ALHA77216 together with new results on other gas-rich chondrites.

Results.
1) HF/HCL residue of ALHA77216 contains some solar rare gases and slightly heavy nitrogen. But the abundance of the heavy nitrogen is too small to account for the heavy nitrogen in the bulk sample. Therefore, the heavy nitrogen in the bulk sample is not due to organic materials similar to that found in CR chondrites.
2) A large metallic grain (38mg) with some silicate grains sticking on it, which had been treated with H_2O_2, was examined if indigenous nitrogen in metallic grains is isotopically anomalous. It was found that this sample contains both isotipically light (-40 permil) and heavy nitrogen (63 permil). The heavy nitrogen is probably in the metal itself and the light one is either in the silicates or due to presolar grains. At present it is not clear if this heavy nitrogen can account for the heavy nitrogen of the bulk sample, since both the concentration and the delta ^{15}N values in this sample is smaller than those of the bulk sample.
3) Isotopically heavy nitrogen has been found in Weston, ALH77278 and LEW86018. The former two chondrites are well known gas-rich chondrites, while there is no literature data on the third chondrite. The Ne abundance in LEW86018 was close to the detection limit of our Ne measurement system and we are not sure if this is really a gas-rich chondrite. Nitrogen and rare gases abundances in these chondrites, together with new data on ALHA77216 are summarized in the table.

Discussion. Generally speaking, the relative abundances of N/Ne/Ar and release temperatures of the heavy nitrogen are similar for these chondrites. However, their responses to H_2O_2

treatment are rather different; e.g. in the case of ALH77278, all gases (N, Ne and Ar) are reduced by nearly 50 % while in the case of ALHA77216 only nitrogen seems to be affected by the treatment. Thus, although gas-rich chondrites tend to have isotopically heavy nitrogen, we are not yet sure if the heavy nitrogen is of solar wind origin or not.

References. [1] Sugiura,N. Kiyota,K. and Hashizume,K. in Papers presented to the Sixteenth Symposium on Antarctic Meteorites, 1991,126.

Table

Sample	ALHA77216	Weston	ALH77278	LEW86018
Delta^{15}N,max (permil)	157	57	94	62
Nitrogen abundance (T>=600C, ppm)	3.9	3.4	11	26
Excess ^{15}N (T>=700C, ppb)	1.02	0.44	2.46	2.21
Solar ^{22}Ne (E-8 ccstp/g)	46.7	46.1	4.07	1.88
Cosmog. ^{21}Ne (E-8 ccstp/g)	12.0	12.9	7.6	8.1
Non-Cosmog. ^{36}Ar (E-8 ccstp/g)	40.1	27.6	23.9	26.1
Cosmog. ^{38}Ar (E-8 ccstp/g)	1.59	1.83	1.18	0.92

A nitrogen concentrated phase in IA iron meteorite Canyon Diablo.

Ko Hashizume and Naoji Sugiura. Department of Earth and Planetary Physics, University of Tokyo, Tokyo 113, JAPAN.

INTRODUCTION

Iron meteorites are considered to have experienced a complex history, which is indicated by the variations in trace element chemistry (*e.g.* Scott and Wasson, 1975). These variations are considered to have been caused by multiple processes such as oxidation, melting, segregation and fractional crystallization (Kelly and Larimer, 1977). Iron meteorites can be separated into two types, *magmatic* iron meteorites and *non-magmatic* ones. Magmatic iron meteorite groups are the ones which show chemical trends (correlations), for example in iridium contents versus nickel contents, expected to be established during fractional crystallization in a molten body, while the trends observed among non-magmatic groups, such as IAB, IIE and IIICD, cannot be explained by such a process. This implies that these non-magmatic iron meteorites have passed through different formation paths compared to others.

Nitrogen isotopes can be a useful tool to understand origins and formation processes of iron meteorites. Prombo and Clayton (1983) and Franchi et al. (1988) measured nitrogen isotopes in a number of iron meteorites. Nitrogen amounts varied by two orders of magnitude among them. Their $\delta^{15}N$ values ranged from -96 to +153 permil. Iron meteorites seem to be resolved into four distinct families based on their $\delta^{15}N$ values.

Trapping sites of nitrogen in iron meteorites are not all clear. This is an important issue because nitrogen, a typical mobile element, may well reflect thermal structures of their parent bodies (*c.f.*, Hashizume, 1993). Generally, major portion of nitrogen in iron meteorites are expected to be in solid solution in Fe-Ni, especially in f.c.c. Fe-Ni (taenite). Carlsbergite (CrN) and Roaldite ($(Fe,Ni,Co)_4N$) are reported (Buchwald and Scott, 1971, and Nielsen and Buchwald, 1981, respectively), although their occurences are rather rare. Other sites are not well known. Franchi et al. (1988) report that at least 25 to 35% of nitrogen in magmatic iron meteorites is in acid insoluble phases, however, not in those of non-magmatic meteorites. This result contradicts with the result of Murty et al. (1983) who report that a significant portion of nitrogen seems to be trapped in acid residues not only of magmatic meteorites but also of non-magmatic meteorites. The result of Murty et al. (1983) raise an important issue, because nitrogen amounts there are observed to be up to 5500 ppm, almost as much as those in interstellar

micro-diamonds. Unfortunately, they couldn't measure nitrogen isotopic ratios, which can provide information on origin and/or formation processes of these nitrogen concentrated phases.

To resolve the contradiction described above, and to identified the trapping site, if it exists, we started measuring nitrogen isotopes in acid residues of iron meteorites. We report here preliminary results on acid residues of Canyon Diablo (IA).

PROCEDURES

Acid residues were prepared by Dr. J.-I. Matsuda and his colleagues. Different blocks of Canyon Diablo, "Can-1" and "Can-2" were treated by 14M HCl, 10M-HF+1M-HCl, 1M-HCl, and by aqua regia, which destroyed Fe-Ni, sulfides, silicates and shreibersite. Acid residues of these two blocks, "Can-1bn" and "Can-2b", yielded 0.102wt% and 0.299wt% of their original masses, respectively. These residues seem to consist mostly of graphite. No diamond was detected by powder X-ray analysis (Ogata et al., 1990).

Nitrogen is extracted and converted to N_2 gas using a stepwise combustion method (100°C step). Nitrogen isotopes are measured using a static type quadrupole mass-spectrometer. (Refer to Hashizume and Sugiura, 1990.)

PRELIMINARY RESULTS

A predominant portion of nitrogen is released at 500°C and 600°C temperature fractions. Total nitrogen amounts and average $\delta^{15}N$ values of the two acid residues are described here.

Sample	Nitrogen (ppm)	$\delta^{15}N$ (permil)
Can-1bn	12000	$+8.6 \pm 1.3$
Can-2b	3700	-15.8 ± 1.2
Can-2b (duplicate)	2800	-17.2 ± 1.2

DISCUSSION

Sample "Can-1bn" is 3-4 times concentrated in nitrogen than "Can-2b", although its $\delta^{15}N$ value is within terrestrial range ($0 < \delta^{15}N < +20$). Presently, we cannot deny the possibility that nitrogen in "Can-1bn" is dominated by terrestrial nitrogen which may have been acquired during the acid treatment. Nevertheless, nitrogen isotope data of "Can-2b" suggest that indigenous nitrogen is indeed concentrated in the acid residue of Canyon Diablo. Bulk nitrogen isotope data of Canyon Diablo is reported to be $\delta^{15}N=$

-61.8 ± 10.4 (permil) N= 38.0 ± 15.5 (ppm) by Prombo and Clayton (1983). Therefore, $\delta^{15}N$ values of "Can-2b" can be resulted by a mixing of indigenous nitrogen and contaminating nitrogen. However, distinct $\delta^{15}N$ values of these two samples may indicate, in turn, that nitrogen isotopes in inclusions of Canyon Diablo are truly heterogeneous, because carbon isotopes of graphite inclusions in IA iron meteorites seem to be heterogeneous (Deines and Wickman, 1973).

SUMMARY

Nitrogen seems to be concentrated in acid residues of iron meteorite Canyon Diablo (IA). Their total nitrogen amounts are observed to be 2800 - 12000 ppm. Their average $\delta^{15}N$ values ranged from -17.2 to +8.6 permil. The discrepancy in the observed $\delta^{15}N$ values may be due to addition of terrestrial nitrogen, or else, may indicate that nitrogen isotopes in inclusions of Canyon Diablo are heterogenous.

ACKNOWLEDGEMENTS

We thank Dr. J.-I. Matsuda of Osaka Univ. for providing us samples, and also for providing us information on these samples. We thank Dr. T. Hirata of Geological Survey of Japan for discussion on this issue and also for providing us chemical information on acid residues of Canyon Diablo.

REFERENCES

Buchwald V. F. and Scott E. R. D. (1971) *Nat. Phys. Sci.* 233, 113-114.
Deines P. and Wickman F. E. (1973) *Geochim. Cosmochim. Acta* 37, 1295-1319.
Franchi I. A., Wright I. P. and Pillinger C. T. (1988) *Meteoritics* 22, 379-380.
Hashizume K. (1993) *Doctor Thesis.*
Kelly W. R. and Larimer J. W. (1977) *Geochim. Cosmochim. Acta.* 41, 93-111.
Murty S. V. S., Goel P. S., Minh D. V. and Shukolyukov Y. A. (1983) *Geochim. Cosmochim. Acta* 47, 1061-1068.
Nielsen H. P. and Buchwald V. F. (1981) *Proc. Lunar. Planet. Sci.* 12B, 1343-1348.
Ogata Y., Matsuda J. and Miyamoto M. (1990) In *Abstract of the 1990 Annual Meeting of the Geochemical Society of Japan.*, pp. 57.
Prombo C. A. and Clayton R. N. (1983) *Meteoritics* 18, 377-379.
Scott E. R. D. and Wasson J. T. (1975) *Rev. Geophys. Space Sci.* 13, 527-546.

NOBLE GASES IN ACUNA IRON METEORITE

Jun-ichi Matsuda[1], Keisuke Nagao[2], Gero Kurat[3]
1) Deartment of Earth and Space Science, Faculty of Science, Osaka University, Toyonaka, Osaka 560, Japan.
2)Institute for Study of the Earth's Interior, Okayama University, Misasa, Tottori 682-01, Japan.
3) Naturhistorisches Museum, Postfach 417, A-1014 Vienna, Austria.

The formation of iron meteorite is generally considered to have been derived from molten cores of small planets. However, some author insisted that there are several difficulties in this model (1). The Acuna iron meteorite found near Sonora, Coahuila, Mexico in 1981 (2) was classified as IVA, but was reclassified as IIIAB by Wasson et al. (3). Acuna include large schreibersite crystals and troilite nodules. Kurat et al. (4) reported inhomogeneous distribution of Ir in Acuna inspite of its fairly homogeneous distribution in other irons. The apparent schreibersite-metal distribution coefficients of some trace elements were very low, which seems to be difficult to explain the formation of schreibersites by exsolution from the metal (4).

The noble gas studies in minerals and inclusions in iron meteorite may be very useful in understanding the origin of iron meteorite. Especially, the primordial component of noble gases is of great importance in such a study. Therefore, we mecanically separated the metal and the schreibersite in Acuna meteorite, and measured elemental abundances and isotopic ratios of all noble gases in two phases at 700 and 1700°C.

Unfortunately, all noble gases were largely covered by spallation components. The amounts of noble gases at 1700°C were much higher than those in 700°C fraction except for Kr and Xe. The isotopic ratios of He, Ne and Ar at 1700°C fraction were all spallogenic components both in two phases. The spallogenic ^{3}He and ^{38}Ar contents were identical in two phases, but ^{21}Ne content in shreibersite were higher than that in metal phase by a factor of about 6. This is probably due to the spallation effect of target nuclei P of low mass number which does not give effect on ^{38}Ar. The coinsidence of nearly equal ^{3}He amounts in both phases are fortuitous, and it is conceivable that some of ^{3}He in shreibersite were lost. We observed spallation components even in Kr and Xe isotopes, which are not produced from Fe, Ni, and P, and are probably due to the spallation product from the impurity of trace elements with large mass number.

References

1. Bloch M.R. and Müller O. (1971) *Earth Planet. Sci. Lett.* 12, 134-136.
2. Graham A. (1987) *Meteoritics* 22, 157.
3. Wasson J.T. , Ouyang X., Wang J. and Jerde E. (1989) *Geochim. Cosmochim. Acta* 53, 735-744.
4. Kurat G., Palme H. and Spettel B. (1991) Lunar Planet. Sci. 22, 767-768.

NOBLE GAS COMPOSITIONS IN MUONG NONG-TYPE TEKTITES.

Kayo MATSUBARA[1], Jun-ichi MATSUDA[1] and Christian KOEBERL[2]
1. Department of Earth and Space Science, Faculty of Science, Osaka University, Toyonaka, Osaka 560, Japan.
2. Institute of Geochemistry, University of Vienna, Dr.-Karl-Lueger-Ring, A-1010 Vienna, Australia.

Tektites are natural silica-rich glasses and are thought to be produced during meteorite collisions with the Earth, similar to impact glasses. They occur in four geographically restricted areas and can be divided in three subgroups; normal or splash form tektites, aerodynamically shaped tektites and Muong Nong-type tektites [1]. Splash form and aerodynamically shaped tektites are several g in weight and are generally homogeneous in chemistry. On the other hand, Muong Nong-type tektites are up to several kg in weight, are irregular in shape, and show layered structure. They are inhomogeneous in chemistry and are enriched in volatile elements, such as halogens, boron, zinc, etc., compared to splash form tektites [1]. Muong Nong-type tektites have larger vesicles than splash form and aerodynamically shaped tektites. This shows that Muong Nong-type tektites are different from splash form and aerodynamically shaped tektites in several aspects. We measured noble gas compositions in splash form tektites [2] and impact glasses [3,4]. Although Ne concentrations in tektites and impact glasses were similar to each other, heavy noble gas (Ar, Kr and Xe) concentrations in tektites were about two orders of magnitude lower than those in impact glasses. In this study, we studied noble gas compositions in some Muong Nong-type tektites in order to compare them with splash form tektites.

Muong Nong-type tektite samples used in this study originated from Ubon Ratchatani in East Thailand, near the border to Laos. Geochemical studies of the samples were made by Koeberl [5]. We measured noble gas concentrations and Ne and Ar isotopic compositions in four Muong Nong-type tektites using mass spectrometry. Noble gases were extracted by three methods; laser probe, crushing and stepwise heating methods. Chipped samples of two Muong Nong-type tektites were used in laser probe analysis. We used 160-380mg of samples for noble gas analysis by crushing and stepwise heating methods.

Noble gas concentrations in tektites, impact glasses and Muong Nong-type tektites were compiled in the figure. Tektites shown are splash-form type ones collected from three strewn fields [2,6]. Impact glasses shown are Aouelloul, Zhamanshin, Libyan Desert glasses [4] and Darwin glass [3]. Heavy noble gas concentrations in Muong Nong type-tektites are higher than those in splash form tektites and are similar to those in impact glasses. From the results of laser probe and crushing analysis of noble gases in Muong Nong-type tektites, it seems that vesicles are unevenly distributed in these samples and that large amounts of noble gases exist in theses vesicles. Neon isotopic compositions in vesicles in Muong Nong-type tektites agree well with terrestrial atmosphere. $^{40}Ar/^{36}Ar$ ratios in vesicles are higher than that in air, suggesting that radiogenic ^{40}Ar exists in vesicles and/or that radiogenic ^{40}Ar in glass may degas by crushing.

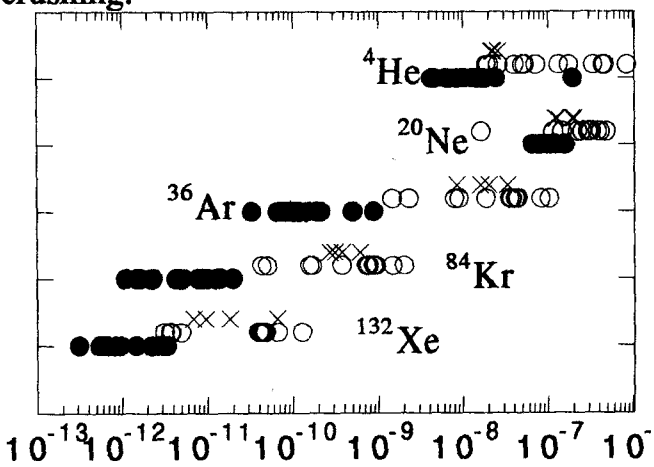

Figure Noble gas concentrations in splash form tektites (filled circles), impact glasses (open circles) and Muong Nong-type tektites (X).

References

1. Koeberl C. (1988) *Proc. NIPR Symp. Antarct. Meteorites* **1**, 261-290.
2. Matsubara K. and Matsuda J. (1991) *Meteoritics* **26**, 217-220.
3. Matsuda J., Matsubara K., Yajima H. and Yamamoto K. (1989) *Geochim. Cosmochim. Acta* **53**, 3025-3033.
4. Matsubara K., Matsuda J. and Koeberl C. (1991) *Geochim. Cosmochim. Acta* **55**, 2951-2955.
5. Koeberl C. (1992) *Geochim. Cosmochim. Acta* **56**, 1033-1064.
6. Hennecke E.W., Mannuel O.K. and Sabu D.D. (1975) *J. Geophys. Res.* **80**, 2931-2934.

NOBLE GAS ELEMENTAL ABUNDANCE SYSTEMATICS IN TERRESTRIAL PLANETS

Naoko WADA and Minoru OZIMA
Department of Earth and Space Science, Faculty of Science, Osaka University, Toyonaka, Osaka 560, JAPAN

Origin of planetary atmospheres is one of the most challenging problems in recent planetary science. Elemental and isotopic abundances of noble gas have been very successfully employed in attacking this problem. Lately, a large amount of high quality noble gas elemental and isotopic data for terrestrial samples such as MORB and hot spot volcanic rocks has become available. In addition to the terrestrial data, noble gas data for Martian atmosphere and its solid interior have been obtained from the analysis of the Martian atmosphere and from SNC meteorites which are supposed to come from Mars.

Owen et al.(1992), plotting noble gas elemental data for Earth and Mars and for amorphous ice in a $^{36}Ar/^{132}Xe$ - $^{84}Kr/^{132}Xe$ diagram in logarithmic scale, found that all the data make a linear array in this plot. Therefore, they suggested that the atmospheres of Earth and Mars have resulted from mixing of two components, one derived from comets and another from an internal component in a planet.

However, a linear array in a logarithmic plot cannot be attributed to mixing of two components except for a very special case, i.e., a case for slope of unity. Hence, Fig. 1 clearly indicates that the terrestrial noble gas cannot be related to the Martian noble gas by the simple two component mixing model proposed by Owen et al. In the same diagram, we plotted newly obtained high quality data for MORB and Loihi volcanic rocks, which also lie on the same linear array (Fig.1). Since all the terrestrial samples have identical noble gas isotopic ratios (except for radiogenic ones), we propose that the linear array for the terrestrial samples is due to various elemental fractionation processes involving absorption, adsorption, partial melting, and bubbling (Ozima and Wada, 1993).

Below, we will discuss fractionation processes which may be responsible for the observed linear array for the terrestrial noble gas data. First, adsorption may be safely ruled out, because the amount of noble gas which would be adsorbed on rocks equilibrated with Earth atmosphere must be very small. Even if there were a substantial amount of adsorbed gases, they would be very easily desorbed.

In equilibrium solubility, partial melting or bubbling, changes of Ar/Xe and Kr/Xe ratios are described by a relation,

$$\frac{\log(Ar/Xe) - \log(Ar/Xe)_0}{\log(Kr/Xe) - \log(Kr/Xe)_0} = k$$

where subscript 0 represents the original values and k is a constant (e.g. Ozima and Alexander, 1976). This formula expresses a linear relation on an Ar/Xe - Kr/Xe diagram in logarithmic scale, where k corresponds to the slope. The slope is further expressed in terms of Henry's law constants of the three noble gases Ar, Kr, Xe in the cases of equilibrium solubility and bubbling. In the case of partial melting, the slope is related to the distribution coefficients of Ar, Kr, Xe.

Because of the relative magnitude of the equilibrium solubility coefficients between air and water among Ar, Kr, Xe, that is, $H_{Xe} > H_{Kr} > H_{Ar}$ (H: Henry's law constant), it is easy to show that the values of Ar/Xe and Kr/Xe ratios in water become smaller than those in air, and we can explain the part of the linear array of the data points, but not all of them. To explain all the data on the basis of the partial melting and bubbling, we should assume that a magma source had smaller values of Ar/Xe and Kr/Xe than the samples, because those values in silicate melt always become larger in both processes. The above assumption can be justified within the frame work of a mantle evolution model on which we are currently working.

In contrary to the terrestrial noble gas, we cannot attribute the noble gas characteristics in SNC meteorites and Martian atmosphere to the above mentioned fractionation processes because of the difference in their isotopic composition. As pointed out by Ott (1988), the data for Shergotty, Chassigny and EETA 79001 glass plotted in a $^{129}Xe/^{132}Xe$ - $^{84}Kr/^{132}Xe$ diagram (Fig.2a) show excellent linearity, which suggests that noble gases in these meteorites were derived from the mixing of two components. Also, the SNC data in Figure 1, replotted in a linear scale (Fig.2b), show a very clear linear correlation, supporting the above suggestion by Ott. For the end members of the mixing, Ott suggested noble gases in Martian atmosphere and those in the solid Mars. However, as Ott pointed out, it is difficult to see why the solid Mars component has less radiogenic ^{129}Xe than the atmospheric component. As one of the possible solutions for this problem, we may suggest a noble gas component derived from the impactor in place of the solid Mars component. It is also interesting to note that Zagami and LEW 88516 data lie distinctly off the linear trends in Figures 2a and 2b. This might indicate that noble gases in Zagami and LEW 88516 may have different origin from those in Shergotty, Chassigny and EETA 79001.

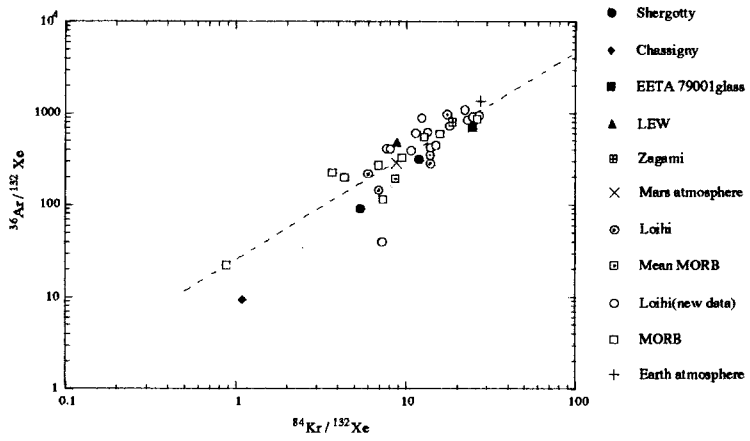

Fig. 1

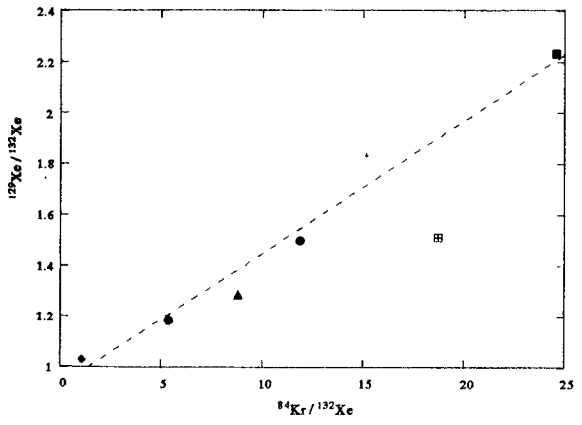

Fig. 2a

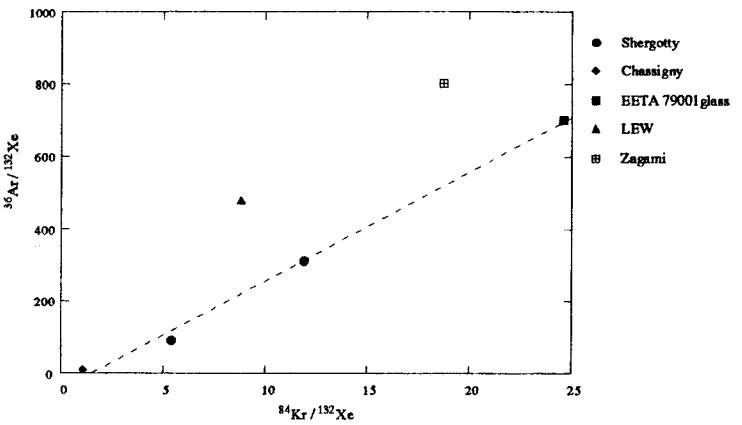

Fig. 2b

Reference
OTT U. (1988) Noble gases in SNC meteorites: Shergotty, Nakhla, Chassigny. *Geochim. Cosmochim. Acta*, **52**, 1937-1948.
OWEN T., BAR-NUN A., and KLEINFELD I. (1992) Possible cometary origin of heavy noble gases in the atmospheres of Venus, Earth and Mars. *Nature*, **358**, 43-46.
OZIMA M., and ALEXANDER, Jr E. C. (1976) Rare gas fractionation patterns in terrestrial samples and the Earth-atmosphere evolution model. *Rev. Geophys. Space Phys.* **14**, 385-390.
OZIMA M., and WADA N. (1993) Noble gases in atmospheres. *Nature*, **361**, 693.

^{40}Ar-^{39}Ar ANALYSES OF EQUILIBRATED LL CHONDRITES FROM ANTARCTICA

Kaneoka, I.[1], Nagao, K.[2] and Pellas, P.[3]
1 Earthquake Research Institute, University of Tokyo, Bunkyo-ku, Tokyo 113
2 Institute for Study of the Earth's Interior, Okayama University, Misasa, Tottori-Ken 682-01
3 National Museum of Natural History, Rue Buffon, 75005 Paris

Among some kinds of chondritic meteorites, there seems to exist a relationship between the degree of equilibrium state and ^{40}Ar-^{39}Ar age (1). Especially, LL chondrites show a tendency that equilibrated chondrites indicate younger ^{40}Ar-^{39}Ar ages compared with unequilibrated ones(2). In order to examine the case in more detail, two extremely equilibrated LL chondrites were examined by the ^{40}Ar-^{39}Ar method.

Y-79160 is a LL7 chondrite, showing a brecciated texture with extensively recrystallized clast. It is composed of olivine, low-Ca pyroxene, augite and albite with smaller amounts of other minerals(3). Y-791067 is also an equilibrated LL7(6.5) chondrite, which shows a breccia texture and consists of coarse-grained olivine and pyroxene with minor amounts of troilite and chromite. A number of large fragments and crystals are seen within a fine-grained matrix(3).

Samples were wrapped in Al-foil and stacked together with the standard sample(MMhb-I, hornblende, K-Ar age;519.5±2.5Ma)under a vacuum in a quartz vial with Cd shielding. The vial was irradiated with fast neutrons in the JMTR of Tohoku University with the total fast neutron flux of about $1x10^{18}$ nvt/cm^2. Ar gas was extracted and purified at the Isotope Center, University of Tokyo, and Ar isotopes were analysed on a VG-5400 mass spectrometer at ISEI, Okyama University. Blanks and the K- and Ca-derived interfering Ar isotopes were corrected. 15 temperature steps were applied for each sample.

The sample Y-74160 indicates a plateau age of 4300Ma for the temperatures of 875-1125°C(5steps) with 48% of the integrated ^{39}Ar. The lower temperature fractions show ^{40}Ar-^{39}Ar ages of 4000-4250Ma with about 50% of the integrated ^{39}Ar. Higher temperature fractions show apparently older ^{40}Ar-^{39}Ar ages, but exceed 4600Ma, indicating no significant meaning. This probably reflects partly insufficient blank correctionc for these temperature fractions.

On the other hand, Y-791067 indicates a more scattered ^{40}Ar-^{39}Ar age spectrum with no plateau age. The temperature fractions of less than 1200°C

show ^{40}Ar-^{39}Ar ages of less than 4260Ma with about 80% of the integrated ^{39}Ar. Higher temperature fractions indicate older ^{40}Ar-^{39}Ar ages, which exceed 4600Ma,indicating no significant meaning.

Thus, both LL7 chondrites show definitely younger ^{40}Ar-^{39}Ar ages compared with LL3 chondrites which show ^{40}Ar-^{39}Ar ages of almost 4500Ma. Since the sample Y-791067 has no plateau age, it is not clear whether the apparent young age has some significant meaning or not. However, Y-74160 indicates a relatively good plateau age of 4300Ma. This meteorite shows a crystallized texture and the age would correspond the time of such a crystallization. Hence, the apparent age gap between the nonequilibrated and the equilibrated chondrites would be real at least for the LL chondrite group.

References

(1) e.g., Kaneoka, I., Mem. Natl Inst. Polar Res., Spec. Issue 17, 177-188, (1980).
(2) Pellas, P., Fieni, C., Trieloff, M. and Jessberger, E. K., Meteoritics, 25, 397, (1990).
(3) Yanai, K. and Kojima, H. (comp.), Photographic Catalog of the Antarctic Meteorites. Natl Inst. Polar Res., Tokyo, 298pp, (1987).

ISOTOPIC, CHEMICAL AND TEXTURAL PROPERTIES OF ACID RESIDUES FROM VARIOUS METEORITES

N. Kano, K. Yamakoshi and H. Matsuzaki
Institute for Cosmic Ray research, University of Tokyo, Tanashi, Tokyo 188, Japan

To study the pre-history and evolution of the solar system based on possible direct evidences for processes of nucleosynthesis in the pre-solar stage and detection of extinct radioactive nuclide, we are planning to carry out systematic isotopic investigations on Ru, Mg, Cr, Ba and so on in primordial samples. We presented the results of chemical compositions of acid residues obtained from three types of meteorites [1) Canyon Diablo (IA) 587.5g, 2) Allende (CV3) 62.4g, 3) Nuevo Mercurio (H5) 45.1g] and the preliminary results of Ru isotopic compositions last time[1]. The acid treatments at that time, however, had been relatively moderate and/or incomplete; so we proceeded with acid treatments still more. The fractions of the acid residues we obtained this time are all 0.5~1 wt.% of the bulk meteorites. We recovered acid residues from meteorites what we had described before[1]. In addition, we are now dissolving Murchison(CM2) [7.56g], La Criolla(L6) [67.9g] and another Allende(CV3) [162.3g] with HCl/HF.

Elemental analyses were carried out by combustion method, INAA and AAS. The light elements concentrations determined by combustion method are shown in Table 1. Besides, Cl and F were detected as a result of acid treatments. The acid residue of Canyon Diablo are composed of these light elements for the most part, and probably contains graphite or something. The principal results of elemental analyses by INAA and AAS are shown in Fig. 1. Refractory elements are generally enriched in acid residue of Allende; and also in case of Nuevo Mercurio, refractory lithophiles are enriched. It is noteworthy that Cr and Au contents in acid residues are much higher than CI and/or bulk of each meteorite. And the considerable diverse chemical compositions of acid residues between these meteorites deserves our attention. It may arise from the diference of generative environmental conditions of these meteorites in space.

The samples were decomposed in sealed teflon vessels by a microwave dissolution method. Ru was extracted by distillation[2]; Mg was separated by cation exchange method[3], and Cr was separated by anion exchange method[4]. In mass spectrometric techniques of Ru, Mg and Cr, the zone-refined (99.995%) outgassed V-shaped Re single filament with silica gel and phosphoic acid was employed. Isotopic analyses were performed by a VG 354 thermal ionization mass spectrometer.

Isotopic analyses of Ru and its preliminary results has previously been described[1], and this time isotopic analyses of Mg was carried out on the basis of recent Mg measurements by this VG 354[5]. Besides, we are preparing to measure Cr isotopic compositions in acid residues.

Mg isotopic compositions of reagent MgO, acid soluble components from Allende and Nuevo Mercurio are shown in Fig. 2. It shows that the instrumental mass fractionation is within 2 per mil per amu. Mg isotopic compositions of acid residues from Allende and Nuevo Mercurio we analyzed until now are shown in Table 2 and Fig. 3. As shown in Fig. 3, mass fractionation effects of Mg for these acid residues of Allende and Nuevo Mercurio are within a ± 2 per mil per amu instrumental resolution band; and nuclear effects ($^{26}Al \rightarrow ^{26}Mg$) for them are within a ± 0.5 per mil resolution band.

That suggests as follows; 1) The vaporization-condensation processes, if ever occurred, were not so significant for these acid residues of Allende and Nuevo Mercurio as to cause isotopic fractionation of Mg. 2) We could not detect the components that evidently originated from interstellar medium in these acid residues of Allende and Nuevo Mercurio so far.

However, it can be expected that acid residues have some kinds of phases judging from analytical results by Energy Despasive X-ray Spectrometer(EDS). We are, therefore, going ahead with identification of minerals in acid residues by transmission electron microscopy (TEM), and preparing to carry out mineral separation by centrifugation in heavy liquids.

Typical EDS spectra of the aliquants of these acid residues are shown in Fig. 4. These

results are not inconsistent with quantitative analyses by INAA and ASS.

In future, much more precise and reliable isotopic data will be obtained, then more detailed discussions on the prehistory of the solar system, the origins and formation processes of acid residues could be done, too.

Aknowledgements-- We would like to thank K. Tomura and staff for neutron irradiations of the samples and use of the counter facilities at the Inst. for Atom. Energy Res. in Rikkyo University; Y. Suzuki of Yamagata University for analyses of samples by TEM-EDS; K. Nogami of Dokkyo University School of Medicine for his help in neutron activation analyses of samples; T. Seki of Tokyo University for determinig C,N,H and S contents in samples by combustion method; H. Naganuma and A. Yanagita of Matsushita Technoreseach, Inc. for determinig O contents.

References

[1] Kano, N. et al. (1993): Proc. NIPR Symp. Antarct. Meteorites, **6**, in press.
[2] Terada, K. et al. (1975): Bull. Chem. Soc. Jpn., **48**, 2567-2571.
[3] Schramm, D. N. et al. (1970): Earth. Planet. Sci. Lett., **10**, 44-59.
[4] Lee, T. and Tera, F. (1986): Geochim. Cosmochim. Acta, **50**, 199-206.
[5] Misawa, K. et al. (1991): Geochem. J., **26**, 29-36.

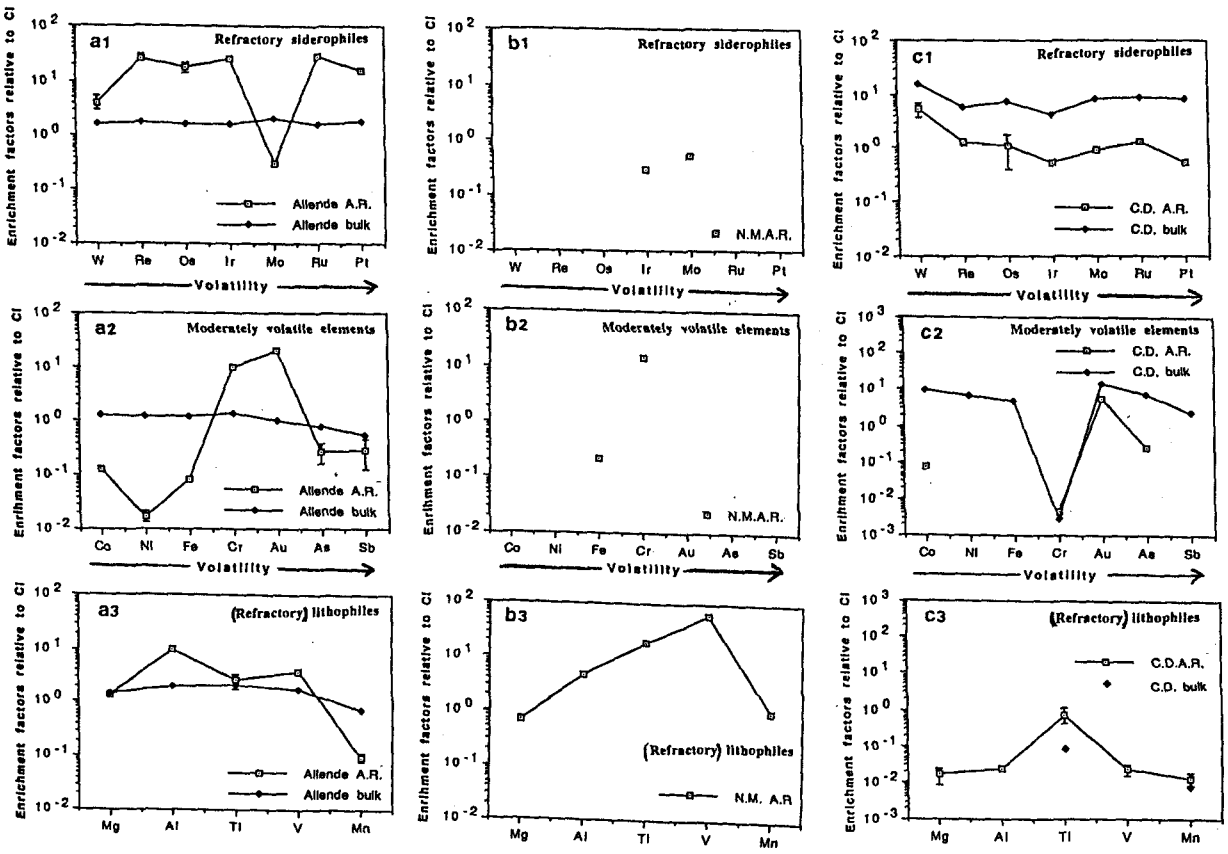

Fig. 1 Enrichment factors in acid residues relative to CI ((a): Allende, (b): Nuevo Mercurio, (c): Canyon Diablo). 1 σ error bars are shown when they are larger than the symbols.

Table 1 Element concentrations in acid residues(%) (combustion method)
—— stands for "not detected".

	C	H	O	N	S
Canyon Diablo	43.50	3.22	40	2.45	——
Allende	15.09	1.83	17	——	0.20
Nuevo Mercurio	——	0.29	33	——	2.22

Table 2 Mg isotopic compositions of acid residues from Allende and Nuevo Mercurio

	measured raw ratios $^{25}Mg/^{24}Mg$ ±2σ	measured raw ratios $^{26}Mg/^{24}Mg$ ±2σ	frac.corrected* $^{26}Mg/^{24}Mg$ ±2σmean
Av. of Normals (weighed mean)	0.124686 ± 70	0.135277 ± 121	0.139604 ± 44
Allende (acid residue)	0.124952 ± 294	0.135767 ± 648	0.139598 ± 78
	0.124521 ± 164	0.134895 ± 482	0.139584 ± 142
	0.124408 ± 380	0.134803 ± 576	0.139608 ± 76
Nuevo Mercurio (acid residue)	0.124418 ± 128	0.134689 ± 324	0.139625 ± 94
	0.124506 ± 192	0.134765 ± 248	0.139588 ± 92

*) All frac. corrected $^{26}Mg/^{24}Mg$ ratios are normalized to $^{25}Mg/^{24}Mg$=0.12663 by power law (Catanzaro et al. 1966).

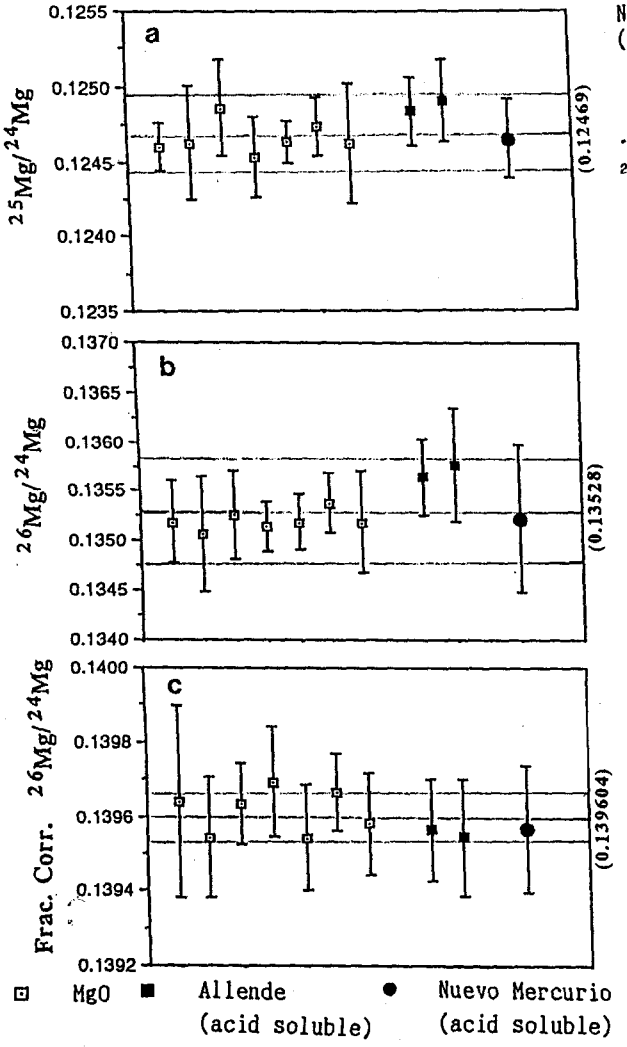

Fig. 2 Mg isotopic compositions of reagent MgO, acid soluble components from Allende and Nuevo Mercurio. The areas between the solid lines for (a), (b),(c) are ±2 per mil, ±4 per mil, and ±0.5 per mil error bands respectively.
(a): Uncorrected $^{25}Mg/^{24}Mg$ ratios. The grand mean value of uncorrected $^{25}Mg/^{24}Mg$ is 0.12469.
(b): Uncorrected $^{26}Mg/^{24}Mg$ ratios. The grand mean value of uncorrected $^{26}Mg/^{24}Mg$ is 0.13528.
(c): Fractionation corrected $^{26}Mg/^{24}Mg$ ratios. The grand mean value of fractionation corrected $^{26}Mg/^{24}Mg$ is 0.139604.
All ratios are normalized to $^{25}Mg/^{24}Mg$ = 0.12663 by power law (Catanzaro et al. 1966).

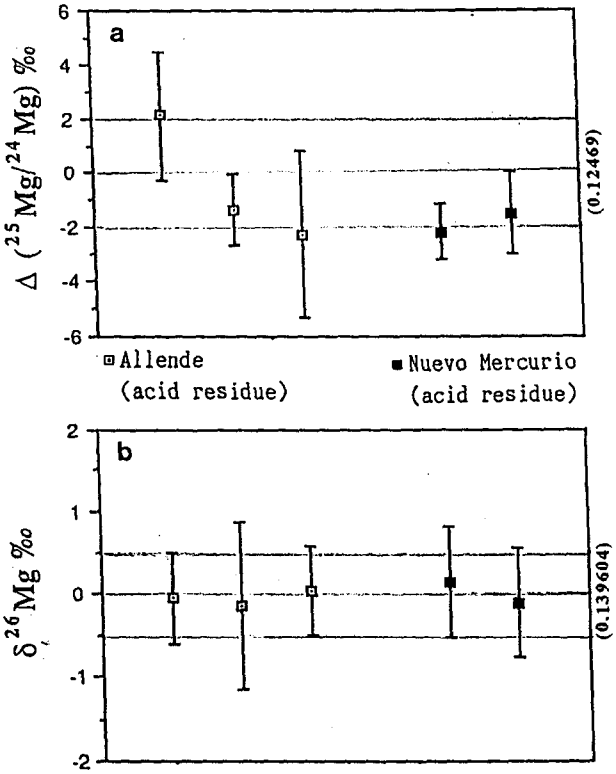

Fig. 3 Mg isotopic compositions of acid residues from Allende and Nuevo Mercurio. The areas between the solid lines for (a) and (b) are ±2 per mil per amu instrumental resolution band and ±0.5 per mil resolution band, respectively.
(a): $\Delta(^{25}Mg/^{24}Mg) = [(^{25}Mg/^{24}Mg)_m / 0.12469 - 1] \times 1000$
(b): $\delta^{26}Mg = [(^{25}Mg/^{24}Mg)_m / 0.139604 - 1] \times 1000$

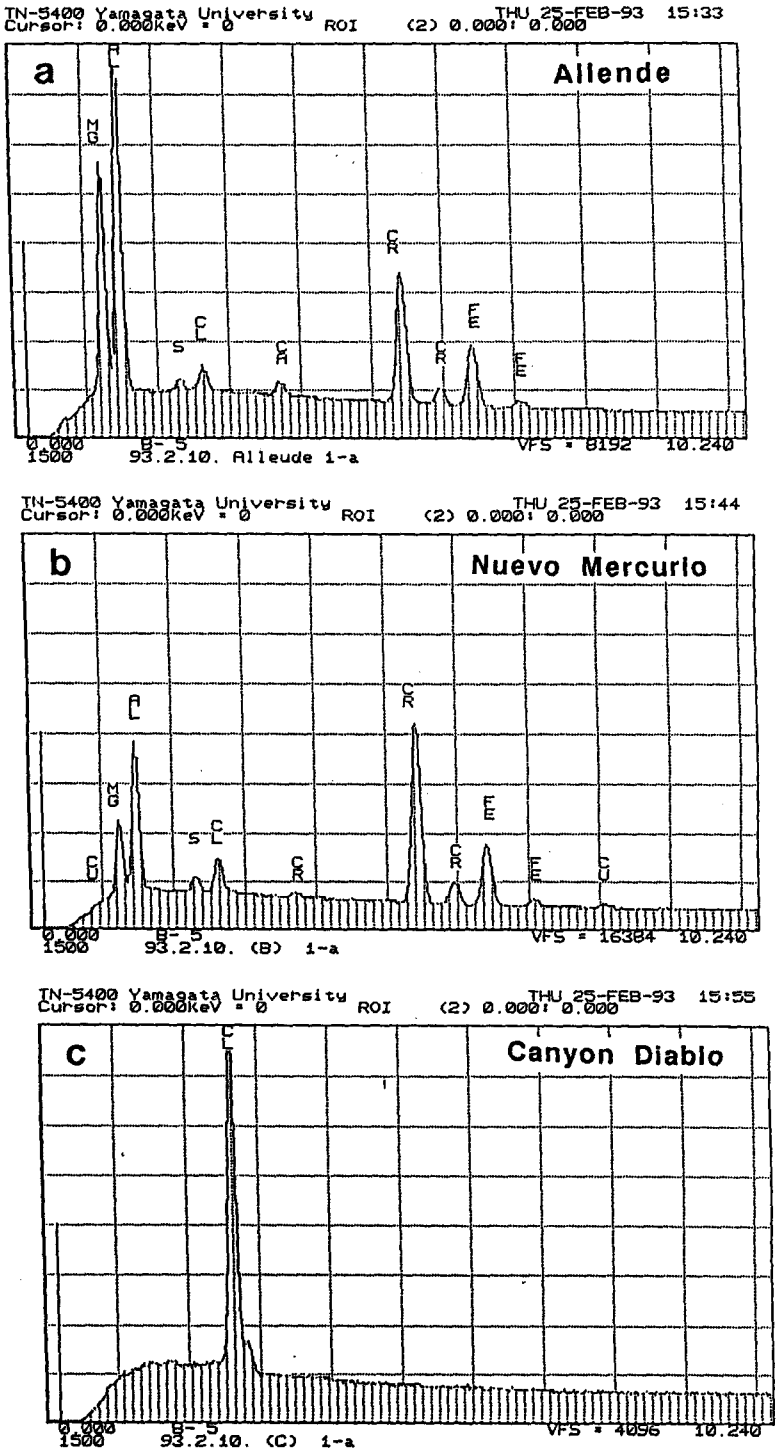

Fig. 4 Typical EDS spectra of the aliquants of these acid residues.
((a): Allende, (b): Nuevo Mercurio, (c): Canyon Diablo).

Comparison between carbonaceous chondrite and microspherule in Paleozoic-Mesozoic bedded chert II

Shigeyoshi Miono

Osaka City University, Sumiyoshi-ku, Sugimoto, Osaka, Japan.

〈abstract〉

The author suggested that interstellar dust particles may have penetrated into Solar System based on PIXE analysis of microspherules collected from Paleozoic-Mesozoic bedded chert in southwest Japan.[1] Recently we investigated the microspherules from Pacific Ocean deep sea sediment as shown in Fig.1 and detected the recent microspherules are clearly different from the ancient microspherule.

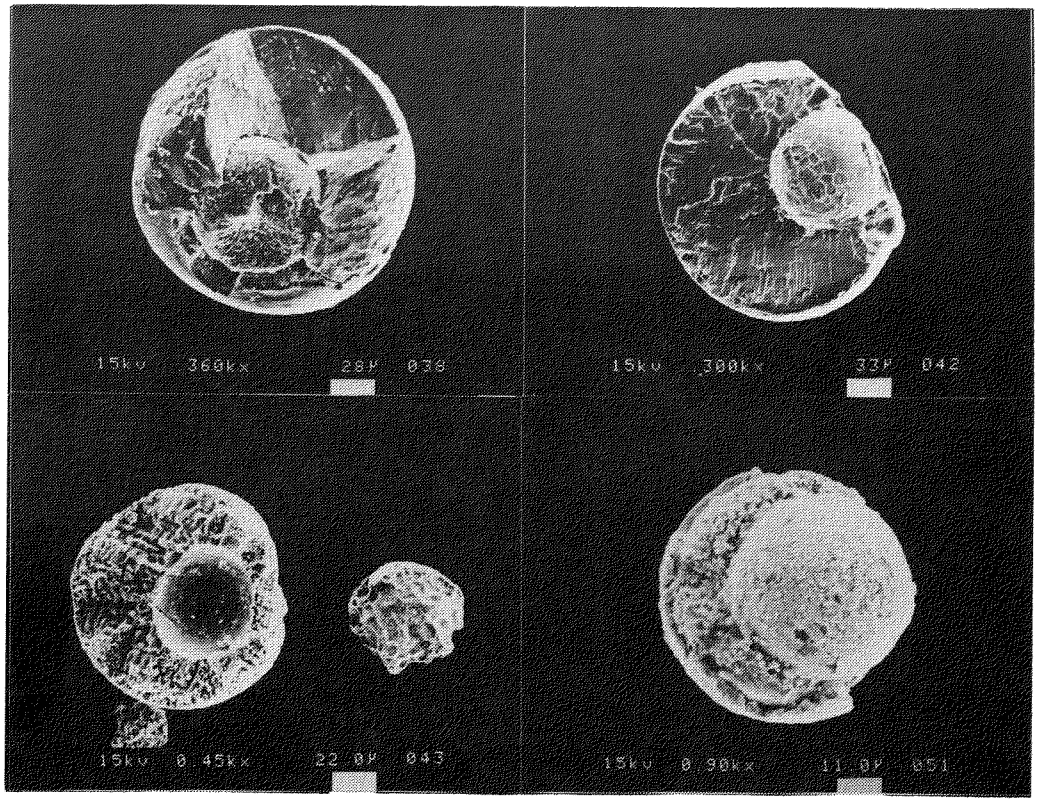

Fig.1 The microspherules with metallic nucleus collected from recent Pacific Ocean deep sea sediment.

We also found respectable "soccer ball shape microspherules" in bedded chert as shown in Fig.2, which are ascertained the perovskite structure. This could be estimate from the heating experiment of Allende meteorite by Prof. Onuma.[2] *i.e.*,"soccer ball shape microspherule" is one of the possible evidences origenated from carbonaceous interstellar dust.

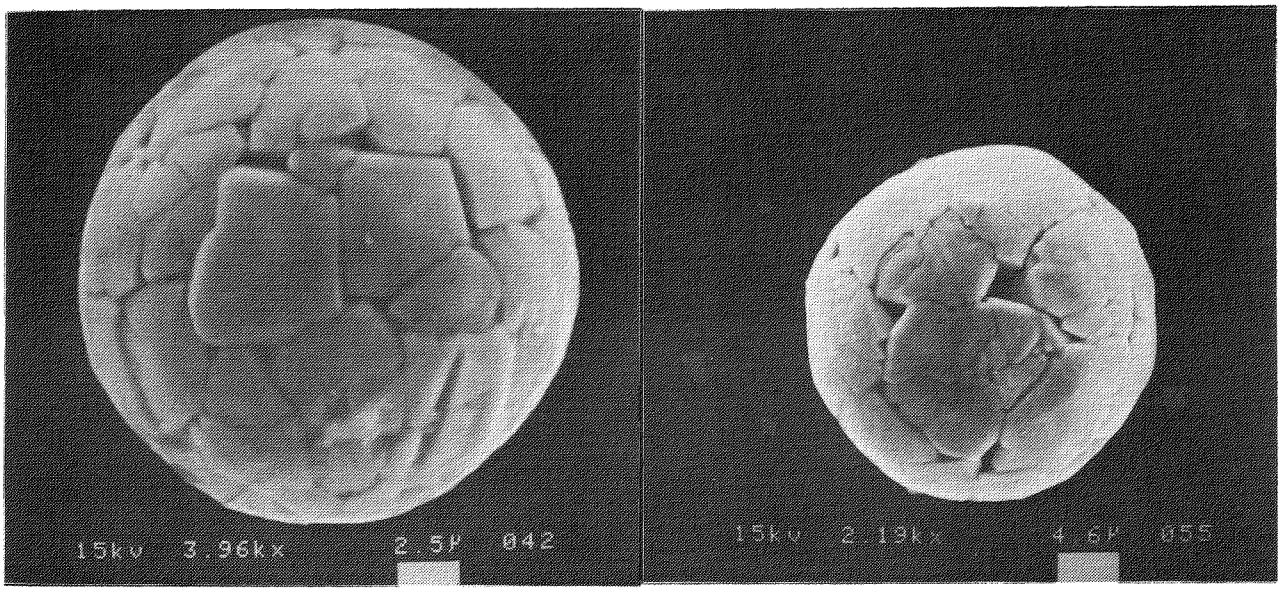

Fig.2 The "soccer ball shape microspherules" collected from bedded chert. They are conjectured the perovskite, $CaTiO_3$.

References.

1)S.Miono *et al.* Nuclear Instruments and Methods in Physics Research, 1992, North-Holland, in press.

2)K.Notsu *et al.* Geochimica Cosmochimica Acta, Vol.42, 903-907,1978.

Weathering of a Chondrite, Tsarev, L5

M. Honda[1], H. Nagai[1], K. Nishiizumi[2] and M. Ebihara[3]
1.Deptment of Chem.,Nihon University, Setagaya,Tokyo,156
2·Deptment of Chem., Univ. Calif.,San Diego, La Jolla, CA92093, U.S.A.
3.Deptment of Chem.,Tokyo Metropolitan Univ.,Hachioji,Tokyo

This study started on determinations of cosmogenic nuclides distributed in various fragments of Tsarev. In the course of our work, it is realized that we have to treat as many as samples of different locations in the meteorite. However, for determinations of some products we met difficulties because the available fragments are not equally fresh, but weathered samples had to be treated as other unweathered samples.

The Tsarev chondrite, L5, fell in Dec.1922 near the Tsarev village, in the region of Volgograd. Presumably due to unstable social atmosphere at that time, this event was not taken seriously. A systematic recovery started very late, since 1968 [1]. Even for only the 50 years terrestrial history, some fragments have been weathered as a whole at significant degrees. Among those fragments some of metallic iron have been lost, and metallic Ni disappeared [2]. Because this meteorite has been realized to be one of the largest chondrites, the distributions of cosmogenic nuclides have been studied in several laboratories. The fragments are distributed mainly in more than 10 large pieces of 280-50 kg sizes; total 1.5 tons have been recovered within a area of 6 km. According to our estimates the preatmospheric size was more than 10 tons most probably 30 tons. The cosmic ray exposures were for 10 m.y. to the first stage larger body and for 0.3 m.y. to the second stage. In such a large object, a search for neutron capture products like ^{60}Co, ^{41}Ca and ^{36}Cl is useful because they may be produced at the maximum at certain depth in the body. We started to measure ^{36}Cl in the target Cl, in their non magnetic fractions.

In this study, we surveyed the Cl contents in the fragments. However, some of them, 6 out of total 11 fragments contain more than 1000 ppmCl, whereas remaining fresh samples contain constantly 160 ppmCl. For determinations of Cl, neutron activation method by alkaline fusion for total Cl or after leaching with solutions. By a wet chemical colorimetry applying Hg(II) thiocyanate and Fe(III) in a dilute nitric acid was also used conveniently in ordinary laboratory [2].

We found first that the samples of highly contaminated with terrestrial Cl have been weathered at various extents. The other group, which contains a low level of Cl, had also to be examined for the nature of their Cl. In less extents but significant fractions of Cl have been found in the leached solutions starting with water. With some typical samples,

leaching experiments were performed and the specific activities of Cl-36 in Cl have been examined. The water (and citrate) soluble parts were found to be essentially terrestrial, and that of meteoritic Cl, which can be recovered finally in a dil. acid, is smaller than the total; 160-40=120 ppmCl is an averaged estimate as the meteorite proper (Table 1 and Fig.1). Only #15385 contains both Cl and metal at their highest levels. In other words, this unique sample seems to be just before the loss of metal, or at a beginning of weathering. Although the weathering cannot be expressed quantitatively, we apply their metal contents as the measure (Fig.2).

Besides Cl and metal, we also found some alterations to sulfide mineral in this chondrite. According to measurements of total sulfides by a full oxidation to sulfate, by fusion or by wet oxidation with aqua regia, the same contents of sulfides can be indicated. However, this is not reflecting that ordinary ferrous sulfide, troilite, remains in weathered chondrites. With dilute mineral acids, 0.1 -- 6 N sulfuric acids, all weathered samples do not react readily as unweathered members (Fig.2). The experiments were performed at room temperature standing for a few days.The formation of less soluble sulfides seems to be related to non-metallic Ni. The evolutions of H_2S in dilute acids can be observed colorimetrically again using mercuric thiocyanate, which forms HgS precipitate and leaving free thiocyanate anion.

As a conclusion, most probably weathering in Tsarev started with chloride contamination. Metallic iron was then lost most likely by an electrochemical mechanism in the presence of chlorides. During these steps alterations of troilite occurred. Other components such as phosphate and silicates have not been affected.

Table 1. Cl and ^{36}Cl found in leached solutions, at 70-80 °C.

Leach. Step	NAA	Colorimetry	AMS
#15390.6	ppm Cl	ppm Cl	dpm^{36}Cl/gCl
1). water 15 min.	27	23	4.3±0.2
2). 0.7m nitric acid	115	150	60.8±1.3
total	142	173	
bulk	165±4%		
#15383.5 No.3			
1). water 30min.	38	43	?
2).0.7m nitric acid	125	140	67.1±1.4
total	163	183	
bulk	132±4% (No.3)		
	159±4% (No.1)		

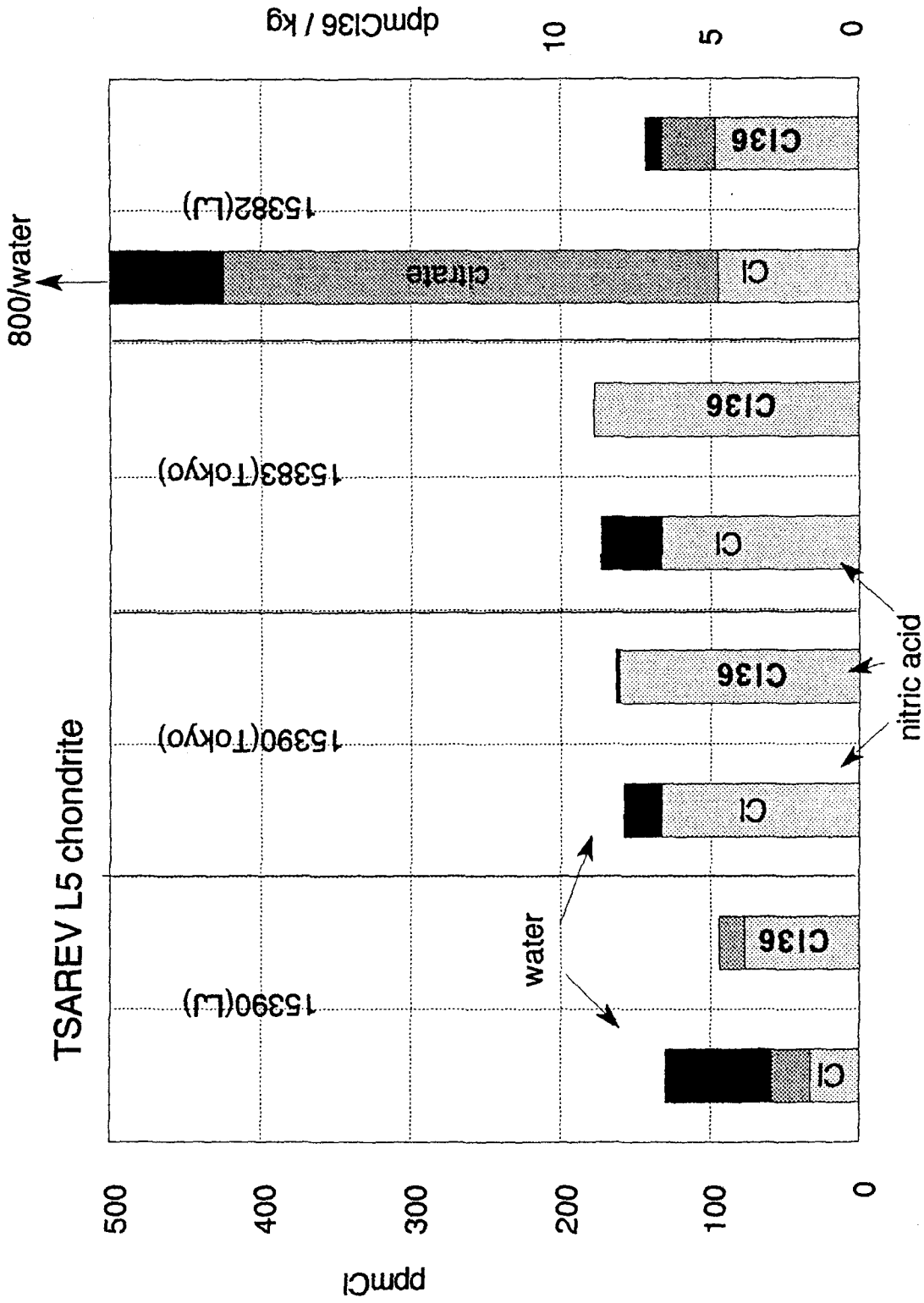

Fig.1 ^{36}Cl and Cl recovered in leached solutions.
water(black),citrate(gray), and nitric acid(pale)

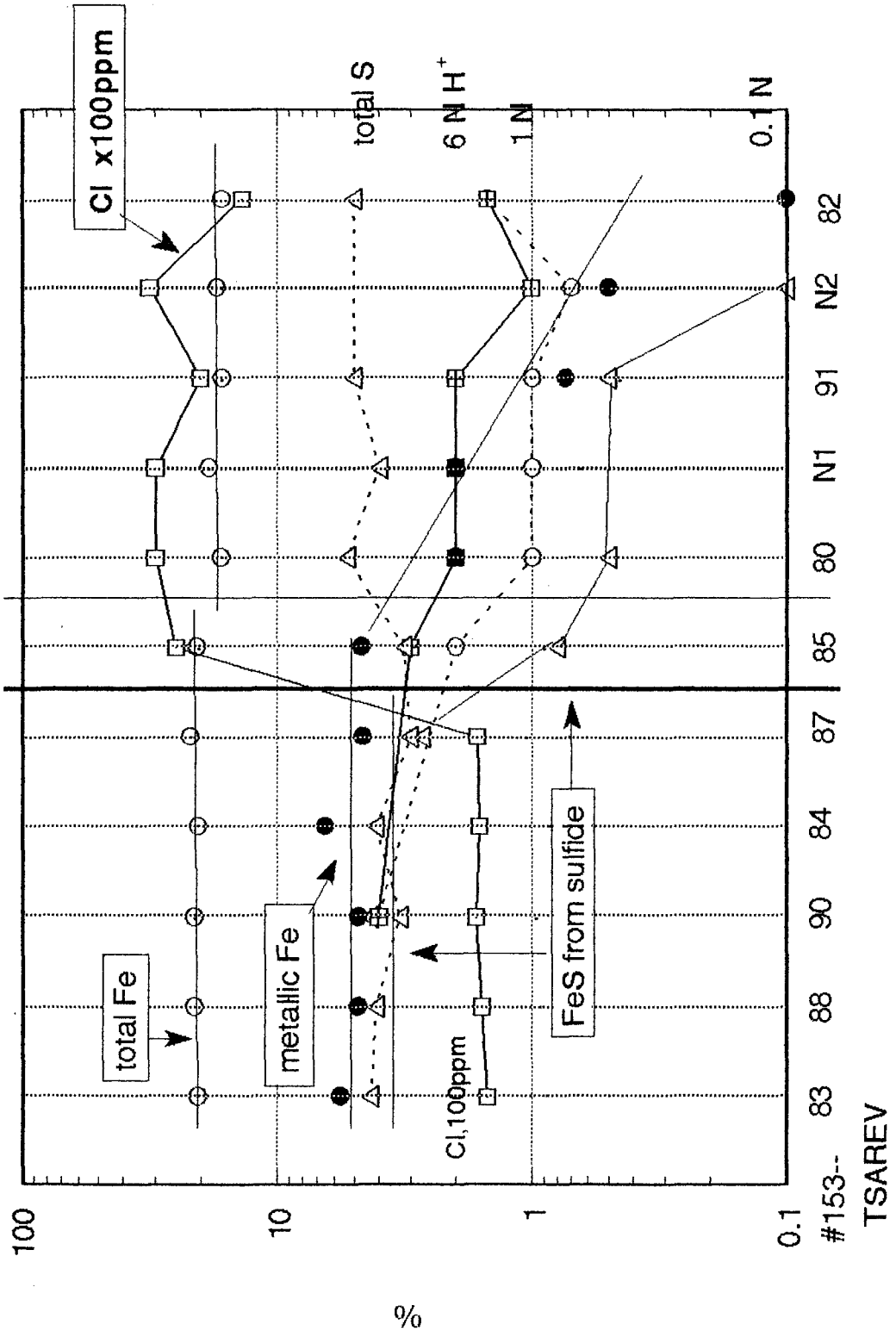

Fig.2 Variations of Cl, metal, and sulfide due to weathering.

Reference. 1. M. Petaev (1991) priv.commun., 2. L.L.Barushukova et al (1982) Meteoritika, 41, 41-43, in Russian, 3. Utsumi (1952), J. Chem. Soc. Japan, 73, 835;838 and A.Tomonari(1962) ibid,83, 693, in Japanese

63 — 1

TERRESTRIAL AGES OF ANTARCTIC METEORITES MEASURED BY THERMOLUMINESCENCE OF THE FUSION CRUST II

S. MIONO and A. NAKANISHI*

Department of Physics, Osaka City University, Osaka 558

*Department of Physics, Shiga University of Medical Science, Shiga 520-21

In previous paper[1], we measured the thermoluminescence(TL) intensities of fusion crust of 14 Antarctic meteorites and estimated acquried doses of these fusion crusts. Several of these meteorites have known terrestrial ages which were previously obtained by abundance of cosmogenic radioactive nuclides with accelerator mass spectrometry. A plot of acquried doses against terrestrial ages shows that the terrestrial ages were correlated well with the acquired doses. In present work, 9 meteorites were added to the result. Results are shown in fig.1.

In one meteorite(ALH76009), 3 sections of fusion crust were measured. 2 parts of those showed almost the same TL intensities, but another showed very high TL intensity. It seems that the sample of that fusion crust contained some of the interior of the meteorite at the sample preparation since the thickness of that part was thinner than the other parts.

There is the other method to estimate the terrestrial ages of the meteorites by TL technique. This method measure a ratio of the peak TL intensity at low temperature(LT) to that at high temperature(HT) in the glow curve for the interior sample[2]. We also measured TL intensities of the interior sample . A plot of LT/HT ratios against terrestrial ages is shown in fig. 2, and there is no correlation between terrestrial ages and LT/HT ratios.

References

1) S.MIONO *et al.*(1990),
Proc. NIPR Symp. Antarct. Meteorites, **3**, 240-243.
2) F.A.HASAN *et al.*(1987),
J. Geophy. Res., **92**, E703-E706.

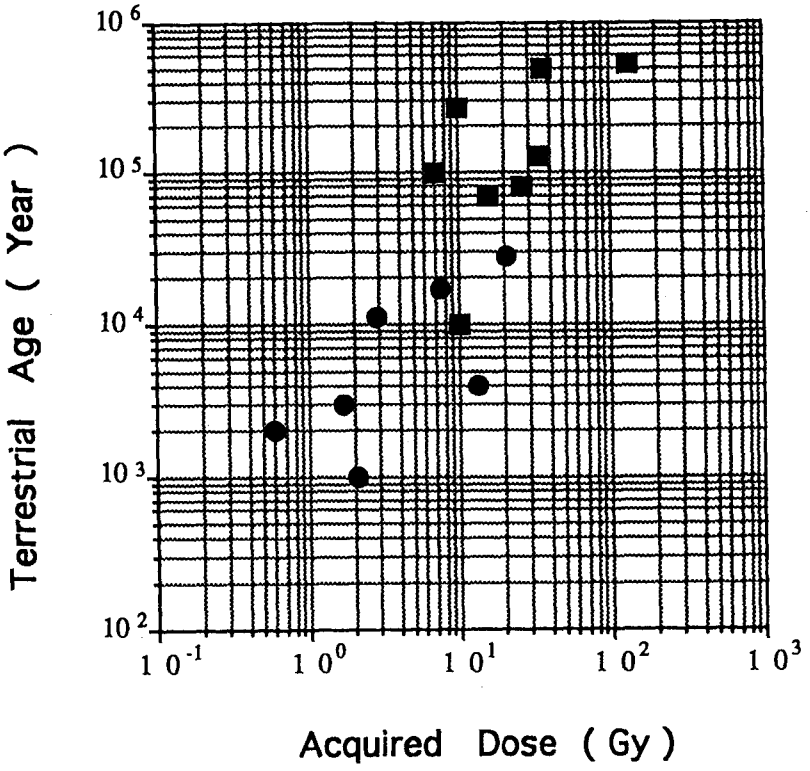

Fig. 1 A plot of terrestrial age against acquired dose.

● ; Yamato meteorites
■ ; Allan Hills and Meteorite Hills meteorites

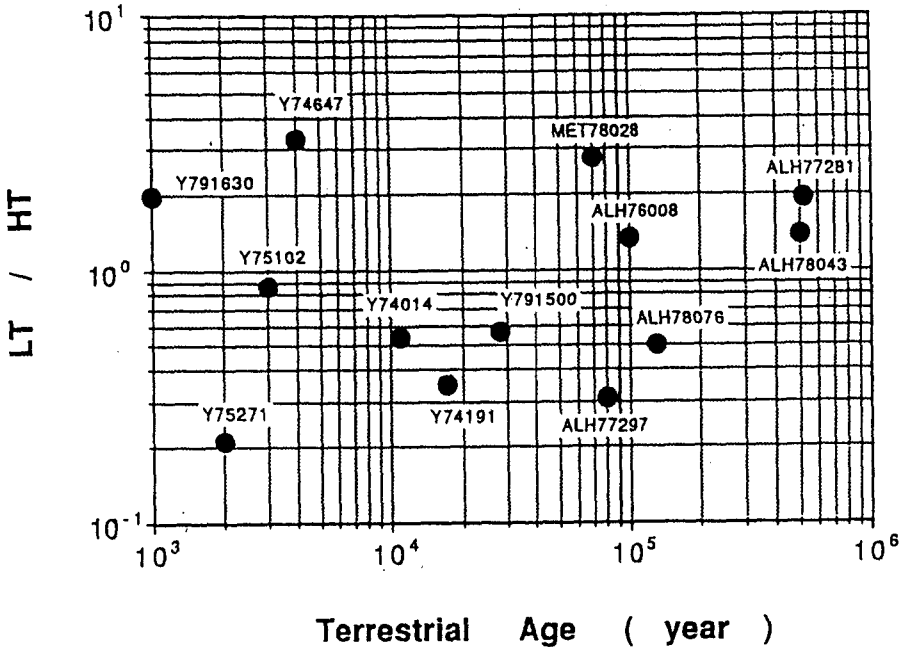

Fig. 2 A plot of LT/HT ratios against terrestrial ages

^{81}Kr-Kr EXPOSURE AGES AND NOBLE GAS ISOTOPIC COMPOSITIONS OF THREE NON-ANTARCTIC EUCRITES MILLBILLILLIE, CAMEL DONGA AND JUVINAS

Yayoi MIURA[1], Naoji SUGIURA[1] and Keisuke NAGAO[2]
1)Dep. of Earth and Planetary Physics, University of Tokyo, Tokyo 113.
2)Inst. for Study of the Earth's Interior, Okayama University,Tottori 682-01.

Introduction Eucrites belong to one of the differentiated meteorite groups. They are suitable for obtaining information about secondary events using radiogenic, fissiogenic and cosmogenic noble gases because 1)the abundance of trapped noble gases is relatively low, and 2)some target elements which produce fissiogenic or cosmogenic heavy noble gases are concentrated in eucrite. In this study, cosmogenic radioactive nuclide ^{81}Kr ($T_{1/2}$=2.5x10^{5}year) as well as all stable noble gases have been measured for three non-Antarctic eucrites: namely, Millbillillie, Camel Donga and Juvinas. We report here 1)the concentrations and isotopic ratios of noble gases, 2)the cosmic-ray exposure ages determined by ^{81}Kr-Kr method, 3)K-Ar ages, and 4)the estimated amounts of extinct nuclide ^{244}Pu using the concentrations of fissiogenic ^{136}Xe.

Samples

Millbillillie

Millbillillie fell into Western Australia in 1960. This meteorite is a partly brecciated, and is homogenized eucrite composed of several types of lithologies (Yamaguchi and Takeda, 1991). ^{81}Kr-Kr exposure age determined by Michel *et al.* (1991) is 22±3 and 26±4 Ma. Several pieces from the brecciated and unbrecciated parts ("b" and "u" in Table 1 designate brecciated and unbrecciated, respectively) were used for noble gas measurements.

Camel Donga

Camel Donga was recovered from Western Australia in 1984. Light noble gases (He-Ar) and bulk chemical compositions are reported by Palme *et al.* (1988). This meteorite has a high content (2 wt.%) of metallic iron.

Juvinas

Juvinas which weighs over 91kg fell into France in 1821. ^{81}Kr-Kr age of this meteorite has been reported to be 9.54±0.62 Ma (Freundel *et al.*, 1986).

Experiments Noble gases were measured using a mass spectrometrical system at Okayama University. The experimental procedure is the same as typical one described in Miura and Nagao (1992) and Miura *et al.* (1993). The samples weighting (0.1 - 1.1)g were melted at 1700°C in a ultra-high vacuum line. The extracted gases from the sample were purified using Ti, Zr-getters. The noble gases were then separated into four fractions (He-Ne, Ar, Kr and Xe) and measured using the mass spectrometer. The ranges of hot blanks at 1700°C are (6-21)x10^{-10}, (2-3)x10^{-11}, (1-10)x10^{-9}, (2-7)x10^{-13} and (N.D.-5)x10^{-14} cm^{3}STP for ^{4}He, ^{20}Ne, ^{40}Ar, ^{84}Kr and ^{132}Xe, respectively. Since the contribution of blank noble gases to each measured value was small, we will show uncorrected data.

Results and discussion

(1)The concentrations and isotopic ratios of He, Ne and Ar, and the concentrations of Kr and Xe are summarized in Table 1. Light noble gases of He, Ne and Ar are mostly cosmogenic except for radiogenic ^{4}He and ^{40}Ar. Alternatively, heavy noble gases (Kr and Xe) are mixtures of cosmogenic,

fissiogenic and trapped noble gases. To discuss each component in detail, the measured values have to be separated into individual component. For this calculation, we assumed that the isotopic compositions of trapped Kr and Xe in the eucrites are similar to those of atmospheric.
(2)Table 2 gives the concentrations of cosmogenic noble gases and the cosmic-ray exposure ages (T_{81}) calculated based on ^{81}Kr-Kr method (Eugster *et al.*, 1967; Marti 1967). Reproducibility of T_{81} is high. The average values of T_{81} are calculated to be 20.8±0.8 and 37.5±2.8 Ma (2σ error) for Millbillillie and Camel Donga, respectively. T_{81} of Juvinas obtained by single analysis is 11.2±0.9 Ma. Though the exposure age for Millbillillie agrees with the ages reported by Michel *et al.* (1991) within experimental errors, it is slightly younger. On the other hand, the age for Juvinas is about 15% older then that by Freundel *et al.* (1986). The cosmic-ray exposure ages of eucrites reported before are from a few Ma to 70 Ma with peak value of (10-20) Ma (Heymann *et al.*, 1968). The production rates of stable noble gases ^{3}He, ^{21}Ne, ^{38}Ar, ^{83}Kr and ^{126}Xe are calculated using their concentrations and T_{81}. P_3 of Camel Donga is significantly low compared with those for Millbillillie and Juvinas. Since the bulk chemical compositions between Camel Donga and Millbillillie are not so different, the variation in production rate of ^{3}He may be caused by a different shielding depth in meteoroid or loss of He from Camel Donga.
(3)Preliminary K-Ar ages were calculated as 3.2±0.3, 3.3±0.2 and 3.1±0.2 Ga for Millbillillie, Camel Donga and Juvinas using the average values of ^{40}Ar concentrations and K contents of 400, 400 and 300ppm with 10% error, respectively.
(4)The concentrations of trapped Kr and Xe of Juvinas are lower than those of Millbillillie, Camel Donga and other eucrites already reported (Freundel *et al.*, 1986; Miura *et al.*, 1993). The origin of the trapped Kr and Xe in eucrites may be the same as that in diogenites, *i.e.* adsorbed atmospheric Kr and Xe (Michel *et al.*, 1990). Since the abundance of trapped and cosmogenic Xe are low in Juvinas, high ^{134}Xe/^{130}Xe and ^{136}Xe/^{130}Xe ratios of 20.6±5.3 and 21.6±5.5 are observed after correcting contribution of cosmogenic ^{130}Xe. For other two eucrites, the values (2.9-3.3) and (2.4-3.0) for ^{134}Xe/^{130}Xe and ^{136}Xe/^{130}Xe, respectively, were observed. In the plot of ^{134}Xe/^{130}Xe versus ^{136}Xe/^{130}Xe, all data obtained for this work fall on a mixing line between atmospheric and ^{244}Pu-derived Xe. The excess ^{136}Xe concentrations are calculated to be (3.4-6.6), (3.6-4.9) and 5.4 x 10^{-12}cm^{3}STP/g for Millbillillie, Camel Donga and Juvinas, respectively. After subtracting ^{238}U-derived ^{136}Xe, excess ^{136}Xe concentrations are (2.9-6.1), (3.3-4.6) and 4.9 x 10^{-12}cm^{3}STP/g, which must derived from ^{244}Pu fission. These values correspond to (0.5-0.9), (0.5-0.7) and 0.8 ppb ^{244}Pu.

Acknowledgements We are grateful to Dr. P. Pellas and Dr. B. Zanda of Muséum National d'Histoire Naturelle, Paris for providing a sample (Juvinas).

[Reference] Eugster O., Eberhardt P. and Geiss J. (1967): E.P.S.L. 2, 77-82.; Freundel M., Schultz L. and Reedy C. (1986): G.C.A 50, 2663-2673; Heymann D., Mazor E. and Anders E. (1968): G.C.A. 32, 1241-1268.; Marti K. (1967): Phy. Rev. Lett. 18, 264-266.; Michel Th., Eugster O., Lehmann B., Thonnard N. and Willis R.D. (1990): Meteoritics 25, 387.; Miura Y. and Nagao K. (1992): Proc. NIPR Symp. on Ant. Met. 5, 298-309.; Miura Y., Nagao K. and Fujitani T. (1993): G.C.A. (in press); Palme H., Wlotzka F., Spettel B., Dreibus G. and Weber H. (1988): Meteoritics 23, 49-57; Yamaguchi A. and Takeda H. (1993): LPSC. XXIV, 148-152.

Table 1. Concentrations and isotopic ratios of noble gases in three eucrites Millbillillie, Camel Donga and Juvinas.

	^{3}He	^{4}He	$^{3}He/^{4}He$	^{20}Ne	^{21}Ne	^{22}Ne	$^{20}Ne/^{22}Ne$	$^{21}Ne/^{22}Ne$	^{36}Ar	^{38}Ar	^{40}Ar	$^{38}Ar/^{36}Ar$	$^{40}Ar/^{36}Ar$	^{84}Kr	^{130}Xe
Millbillillie -1	251	43500	0.005770	38.0	40.3	48.1	0.7896	0.8380	21.3	32.1	13900	1.5112	653.8	26.1	4.88
(b) 1.039g			±.000055				±.0011	±.0098				±.0080	±2.5		
-2	227	37000	0.006130	38.0	40.4	48.4	0.7859	0.8359	21.3	32.1	15600	1.5102	733.7	31.8	9.79
(u) 1.131g			±.000058				±.0016	±.0097				±.0092	±9.2		
-3	249	44700	0.005572	29.9	32.1	38.3	0.7816	0.8390	21.4	32.4	14800	1.5135	690.9	31.6	5.52
(b) 1.086g			±.000053				±.0022	±.0101				±.0077	±3.2		
-4	229	42300	0.005405	35.4	37.5	45.0	0.7861	0.8336	20.8	31.4	16300	1.5120	784.5	29.9	5.46
(u) 1.253g			±.000051				±.0021	±.0097				±.0076	±2.8		
-5	220	37200	0.005934	42.6	46.0	54.3	0.7852	0.8475	23.5	35.1	11700	1.4964	498.92	45.9	5.64
(u) 0.6400g			±.000027				±.0013	±.0066				±.0018	±.31		
-6	208	31000	0.006709	40.9	44.1	52.4	0.7807	0.8424	24.1	35.9	13000	1.4923	540.08	52.0	7.29
(u) 0.1319g			±.000031				±.0014	±.0065				±.0020	±.38		
-7	226	32200	0.007023	44.0	47.5	55.8	0.7879	0.8510	23.1	34.4	11400	1.4877	493.18	58.3	6.94
(u) 0.1314g			±.000039				±.0013	±.0060				±.0022	±.31		
Camel Donga -1	214	30300	0.007162	45.3	48.6	56.2	0.8064	0.8656	37.4	55.2	15800	1.4746	422.31	73.2	18.6
0.6639g			±.000031				±.0013	±.0067				±.0021	±.33		
-2	162	22900	0.007082	46.2	47.7	55.4	0.8335	0.8607	37.4	52.8	15300	1.4122	409.44	120	9.84
0.6536g			±.000032				±.0012	±.0067				±.0018	±.24		
-3	208	25900	0.008049	46.5	49.9	58.1	0.8003	0.8594	32.6	48.3	13500	1.4821	414.35	78.3	10.8
0.1619g			±.000055				±.0079	±.0067				±.0016	±.30		
-4	221	27100	0.008152	45.4	48.7	56.2	0.8082	0.8662	32.2	46.7	13600	1.4520	423.01	82.7	11.5
0.1529g			±.000037				±.0013	±.0068				±.0072	±.33		
-5	194	26500	0.007337	43.2	45.9	52.6	0.8208	0.8717	32.0	48.0	14200	1.5013	444.40	66.7	9.53
0.1369g			±.000058				±.0032	±.0034				±.0011	±.32		
Juvinas -1	121	27700	0.004384	17.1	17.3	20.7	0.8264	0.8366	9.34	13.8	12600	1.4825	1349.40	13.8	0.855
0.2953g			±.000048				±.0019	±.0031				±.0021	±.75		

Concentrations of He, Ne and Ar are given in unit of $10^{-9}cm^{3}STP/g$, and those of ^{84}Kr and ^{130}Xe are $10^{-12}cm^{3}STP/g$.
Error for concentration is estimated to be less than 10%, and that for isotopic ratio is 1σ. Blank correcton has not been applied.
"b" and "u" in Millbillillie designate brecciated and unbrecciated sample, respectively.

Table 2. Concentrations of cosmogenic ^{3}He, ^{21}Ne, ^{38}Ar, ^{81}Kr, ^{83}Kr and ^{126}Xe, ^{81}Kr-Kr exposure ages (T_{81}), and calculated production rates using the concentrations and ^{81}Kr-Kr exposure age.

Sample	$(^{3}He)_c$	$(^{21}Ne)_c$	$(^{38}Ar)_c$	$(^{81}Kr)_c$	$(^{83}Kr)_c$	$(^{126}Xe)_c$	T_{81}	P_3	P_{21}	P_{38}	P_{83}	P_{126}
	$10^{-9}cm^3STP/g$			$10^{-12}cm^3STP/g$			Ma	$10^{-9}cm^3STP/gMa$			$10^{-12}cm^3STP/gMa$	
Millbillillie -1	251	40.1	31.8	0.155	17.5	0.984	20.6±2.0	12.1	1.93	1.53	0.841	0.0473
-2	227	40.3	31.8	0.167	18.9	1.01	20.5±2.1	10.9	1.94	1.53	0.909	0.0486
-3	249	32.0	32.2	0.161	18.5	1.10	21.0±2.2	12.0	1.54	1.55	0.889	0.0529
-4	229	37.4	31.2	0.176	19.8	1.14	20.2±2.0	11.0	1.80	1.50	0.952	0.0458
-5	220	46.0	35.1	0.132	15.5	1.04	21.2±1.0	10.6	2.22	1.69	0.745	0.0500
-6	208	44.1	35.8	0.153	17.9	1.31	21.4±2.4	10.0	2.13	1.72	0.865	0.0633
-7	226	47.5	34.2	0.142	16.3	1.14	20.4±3.6	10.9	2.29	1.64	0.787	0.0551
Average of T_{81}							20.8±0.9 (2σ)					
Camel Donga -1	214	48.6	54.8	0.153	30.7	2.65	36.2±2.8	5.71	1.30	1.46	0.819	0.0707
-2	162	47.7	52.1	0.148	31.0	2.53	37.9±2.6	4.32	1.27	1.39	0.827	0.0675
-3	208	49.9	48.0	0.116	24.8	1.81	38.9±4.4	5.55	1.33	1.28	0.661	0.0483
-4	221	48.7	46.3	0.124	24.5	1.84	35.7±5.3	5.89	1.30	1.23	0.653	0.0491
-5	194	45.9	47.8	0.117	25.0	2.00	38.6±7.3	5.17	1.22	1.27	0.667	0.0533
Average of T_{81}							37.5±2.8 (2σ)					
Juvinas -1	121	17.3	13.8	0.158	9.20	0.578	11.2±0.9	10.8	1.54	1.23	0.821	0.0516

MÖSSBAUER SPECTROSCOPY STUDY OF THE METALLIC PARTICLES OF THE ANTARCTIC L6 CHONDRITE ALLAN HILLS 769

R.B. Scorzelli, I. Souza Azevedo, R.A. Pereira, C.A.C. Perez and A.A.R. Fernandes* Centro Brasileiro de Pesquisas Físicas, Rua Xavier Sigaud, 150 - CEP 22290-180, Rio de Janeiro, Brazil, * Instituto Militar de Engenharia, Rio de Janeiro, Brazil.

INTRODUCTION The Fe-Ni ordered phase with $L1_0$ superstructure (AuCu) has been first produced only by neutrons or electrons irradiation of the disordered alloy [1,2], because the diffusion process of the metallic atoms is very slow at the ordering temperature Tc=320 C.
Since 1977 it has been known that an ordered alloy occurs in slow-cooled meteorites that contain taenite (f.c.c. iron-nickel alloy). Some years later this naturally occurring compound has been given the name *Tetrataenite* [3]. In many meteorites it is a common accessory mineral and in some it is more abundant than taenite.
The Fe-Ni ordered phase has been detected by Mössbauer spectroscopy (MS) and X-ray diffraction (XRD) in the taenite lamellae of octahedrites [4], Ni-rich ataxites [5] and metal particles of chondrites [6].
The identification of the $L1_0$ superstructure in Fe-Ni alloys by MS is based on the fact that the ordered phase exhibits an asymmetric 6-line spectrum due to a quadrupole splitting arising from the non-cubic environment of the atoms in this structure.
We report here MS, XRD and Scanning Electron Microscopy (SEM) measurements on the ALLAN HILLS 769 (ALH-769) L6 chondrite. The ALH-769 was found in January 1977 in Allan Hills, South Victoria Land, Antarctica [7].

EXPERIMENTAL The transmission ^{57}Fe Mössbauer spectra were obtained at room temperature using a Co/Rh source in a conventional Mössbauer spectrometer. The MS has been performed with the metal particles of the chondrite obtained after magnetic and chemical separation. In magnetically enriched samples relatively large amounts of silicates and troilite still remain attached to the metallic phase. A complete separation is only achieved by HF treatment [6].
The lattice parameters were determined by refinement with the Rietveld method [8] applied to X-ray diffraction patterns obtained in a powder diffractometer with Bragg-Brentano focalization geometry operating in a step by step mode. The counting time per step was 10s in an angular range $20° \leq 2\theta \leq 100°$ using Cu radiation (λ = 1.5418 Å) and a quartz monocromator plane $(10\bar{1}1)$.
The metalic particles were studied using a scanning electron microscope (SEM) JEOL JSM-U3 working at 20KV coupled to a Tracor Northern (model 5500) energy dispersive X-ray spectrometer (EDS). Sample compositions were determined using a computer program in the EDS software package based on ZAF technique.

RESULTS AND DISCUSSION We investigate the presence of tetrataenite in metal particles of ALH-769 using magnetically separated fractions which have been purified from troilite and iron silicates. The Mössbauer spectrum of the magnetically enriched sample before chemical treatment is rather complex and exhibits a partial overlapping of lines which arise from the superposition of : iron silicates, α-phase (kamacite) or α_2- phase (martensite), γ-phase (taenite) and troilite. Due to the presence of silicates and troilite in the sample, it is very difficult to identify the presence of tetrataenite. Only after a complete separation of the metals it

is possible to detect the Fe-Ni 50/50 ordered phase with $L1_0$ superstructure . The Mössbauer spectrum of the metal enriched sample shows the coexistence of Fe-Ni γ-phases with different composition; the ordered 50/50 (tetrataenite), the disordered 50/50 taenite and a Ni-poor taenite with less than 30% Ni.

In figure 1 we can see an overlap of: a) a magnetic phase with a quadrupole splitting corresponding to the ordered Fe-Ni 50/50; b) a magnetic phase without quadrupole splitting corresponding to a ferromagnetic disordered Fe-Ni 50/50 in lower proportion; c) a paramagnetic γ-phase due to the Ni-poor taenite. The corresponding hyperfine parameters are listed in Table I.

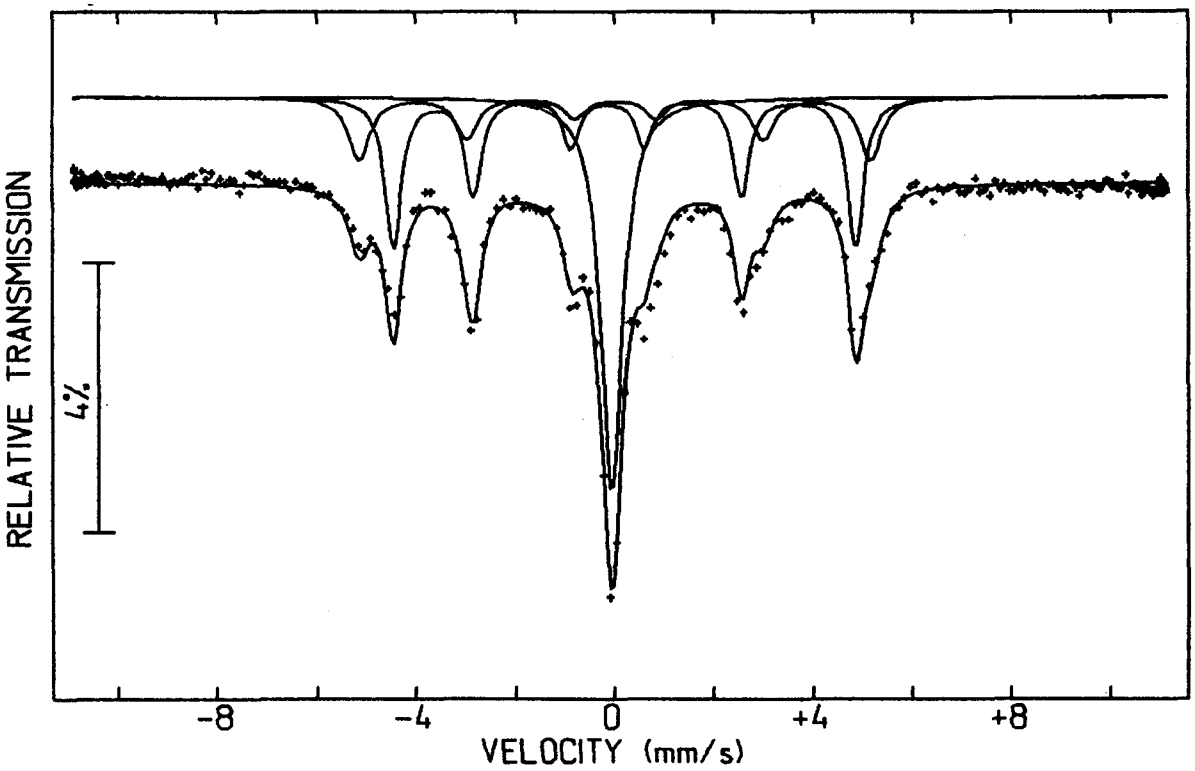

Figure 1. Mössbauer spectrum of the metal enriched sample

Table I. Mössbauer hyperfine parameters of metal enriched particles of ALH-769 L6 chondrite; Γ = linewidth at half height (∓ 0.03 mm/s), IS = isomer shift relative to ^{57}Co/Rh source (∓ 0.01 mm/s), ΔEq = quadrupole splitting (∓ 0.005 mm/s), HF = internal hyperfine field (∓ 5 kOe) and A = relative spectral area (∓ 5%).

FeNi phases	Γ(mm/s)	IS (mm/s)	ΔEq (mm/s)	HF (kOe)	A (%)
ordered Fe-Ni	0.37	-0.075	0.18	288	39
disordered Fe-Ni	0.55	-0.10	0.0	318	25
paramag. γ-phase	0.52	-0.17	----	----	36

In the above Table we can see the hyperfine parameters derived from the Mössbauer spectra in which the tetrataenite phase has been observed, as well as the proportion of the Fe-Ni alloys in this meteorite. The hyperfine field (HF) and the quadrupolar interaction (ΔEq) are similar to those observed for the ordered phases in irradiated iron-nickel alloys and in metal particles of LL and L non-Antarctic chondrites.

The lattice parameter $a_0 = 3.586 \pm 0.001$ Å obtained by XRD is in agreement with that reported for the ordered phase [9] and is smaller than that of the disordered alloy $a_0 = 3.596 \pm 0.001$ Å. The (001), (110), (021),(112), and (221,003) weak superstructure lines were detected.
The preliminary results obtained by SEM show two assemblies of particles. The larger ones have a quite homogeneous composition of ~ 50% Ni and the smaller ones have a low Ni concentration < 30% Ni. The particles are irregular in shape and exhibits a spongelike or foamlike aspect.
The proportion of tetrataenite in this L-chondrite is smaller than the ones already observed in some LL, since the relatively large Ni/Fe ratio found in the metallic phase of LL chondrites favours the formation of the $L1_0$ superstructure. which is also common in the L chondites, although in smaller proportions. The value of ΔEq of tetratenite in this chondrite is smaller than that observed with others L and LL chondites which presents little evidence of shock (for example the LL6 Chondrite St. Séverin). It is remarkable the presence of a considerable proportion of the 50/50 disordered phase coexisting with the superstructure.
The cooling rate, shock and reheating can influence the tetrataenite degree of ordering, modifying the hyperfine parameters values. The ΔEq values may vary from 0.25 mm/s for the Fe-Ni phase with a high degree of ordering, down to zero for the disordered phase. The hyperfine field and the width of the absorption lines tend to increase with increasing disordering.
A systematic Mössbauer study of several chondrites with different shock history [6] showed that the disordering process due to shock or re-heating leads to changes in the hyperfine parameters of the ordered phase.
To a better understand of the order-disorder process in this meteorite it is important to obtain more detailed information about the shock history occurred during primary cooling or during secondary processes. Other experiments are currently under investigation in order to correlate the Mössbauer results with the cooling and shock history recorded by the metallic phases of chondrites.

REFERENCES 1. Paulevé J. (1962) C.R.Acad. Sci. Paris 254, 965-968. 2. Néel L., Paulevé J., Pauthenet R., R. Laugier, J and Dautreppe D.J. (1964) J. Appl. Phys. 35, 873-876. 3. Clark R.S.Jr. and Scott E.R.D. (1980) Am. Miner. 65,624-630. 4. Petersen J. F., Aydin M. and Knudsen J.M. (1977) Phys. Lett. 6A, 192-194. 5. Danon J., Scorzelli R.B., Souza Azevedo I., Curvello W., Albertsen J.F. and Knudsen J.M. (1979) Nature 277,283-284. 6. Danon J., Scorzelli R.B., Souza Azevedo I. and Christophe-Michel-Lévy M. (1979) Nature 281, 469-471. 7. Yanai K. (1979) Catalog of Yamato meteorites, NIPR, Tokyo. 8. Young R.A. and Wiles D.B., (1981) Adv. X-ray Anal., 24, 1-23. 9. Scorzelli R.B. and Danon J., (1985) Physica Scripta 32,143-148; Chamberod A., Laugier J. and Penisson J.H. (1979) J. Magn. Mag. Mat. 10, 139-144.

Fe-Ni ALLOYS IN AN UNIQUE ANTARCTIC METEORITE YAMATO 791694

R.B. Scorzelli and A.A.R. Fernandes*, Centro Brasileiro de Pesquisas Físicas, Rua Xavier Sigaud 150, - CEP 22290-180, *Instituto Militar de Engenharia, Rio de Janeiro, Brazil.

INTRODUCTION Yamato 791694 (Y-791694) is an Antarctic iron meteorite classified as an ataxite [1] which uniqueness is due to its composition. The high concentration of Ni (35%) and other elements as Cu, In, Sn, Sb,Pb and Bi [2] is almost the highest among those of all known iron meteorites. The average Ni composition similar to Santa Catharina and Twin City meteorites is the same in which Fe-Ni alloys present the structural and magnetic Invar anomalies. Due to the slow cooling in their asteroidal bodies, iron meteorites are important as indicators of the phase transformations which occur in Fe-Ni-alloys. In the Invar composition range, Fe-Ni alloys can undergo segregation and /or ordering (depending upon Ni content) provided that the conditions favor atomic diffusion. Since the discovery of the ordered phase obtained by irradiation [3] it has been observed that alloys in the Invar region (30% -50% Ni), when subjected to irradiation separate into two phases, one ferromagnetic and the other paramagnetic, both with fcc structure. The ordered phase with $L1_0$ superstructure has been observed for the first time in 1962 in neutron irradiated Fe-Ni alloys. The tetragonal distortion of the superstructure $L1_0$ has its origin in an electric field gradient at the level of the iron atoms of the alloy. This gives rise to a Mösssbauer spectra that is singular between the Fe-Ni alloys, because it presents a typical asymmetry, that results from a relatively small quadrupolar interaction with the ^{57}Fe nucleus, superimposed on a large magnetic interaction of the ferromagnetic alloys.
Investigations by Mössbauer spectroscopy of taenite fields from meteorites of different chemical groups have disclosed differences in the state of order of tetrataenite (ordered Fe-Ni 50/50 alloy with superstructure $L1_0$) which are attributed to different cooling histories below ~ 350° C. Since taenite fields containing tetrataenite occur in the majority of the meteorites, including ordinary chondrites, pallasites, mesosiderites and iron meteorites, Mössbauer spectroscopy turns out to be a very powerful method to study cooling rates of meteorites below ~ 350° C. This cooling rates might give important information about genetic relations between the meteorites and provide new information upon their origin.
This paper presents preliminary results of our investigation on phase composition and structure of iron-nickel alloys in Y-791694 compared with previous results obtained with non-Antarctic Ni-rich ataxites on the basis of Mössbauer spectroscopy (MS), scanning electron microscopy (SEM), energy dispersive X-ray analysis (EDS) and X-ray diffraction (XRD) results.

EXPERIMENTAL Thin slices of the bulk of the Y-791694 meteorite were cut with a precision saw, carefully avoiding thermal stresses in the sample. Absorbers for Mössbauer measurements were prepared by polishing the slices to a thickness of about 70μm. The spectra were recorded with a $^{57}CO/Rh$ source in a conventional spectrometer.
The lattice parameters were determined by refinement with the Rietveld method applied to X-ray diffraction patterns obtained in a powder diffractometer with Bragg-Brentano focalization geometry operating in a step by step mode. The counting time per step was 10s in an angular range $20° \leq 2\theta \leq 100°$ using Cu radiation (λ = 1.5418 Å) and a quartz monocromator plane $(10\bar{1}1)$.
Scanning electron microscopy (SEM) was performed using a JEOL JSM-U3 working at 20KV coupled to a Tracor Northern (model 5500) energy dispersive X-ray spectrometer (EDS). Sample compositions were determined using a computer program in the EDS software package based on ZAF technique.

RESULTS AND DISCUSSION The Mössbauer spectrum at room temperature of a thin slice of the Y-791694 indicates the presence of at least two Fe-Ni alloy phases, a major one corresponding to a Ni-rich disordered taenite and a small amount of α or α_2-bcc alloy (fig.1). However, due to the broad linewidths typical of the disordered alloy, the best fit of the spectra was obtained using a distribution of hyperfine fields, with a maximum of the distribution curve at ~300 kOe with hyperfine parameters typical of a ~40% Ni disordered taenite.

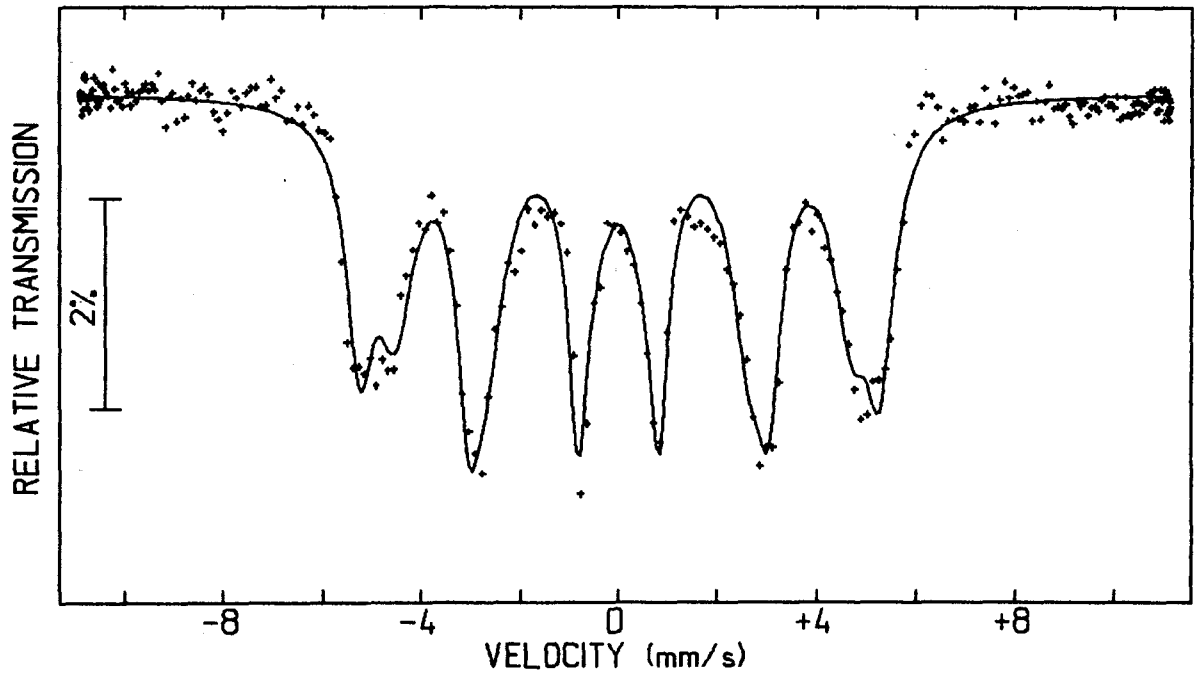

Figure 1. Mössbauer spectrum of a thin slice of the Y-79694 meteorite

X-ray diffraction pattern indicates the presence of a fcc Fe-Ni alloy with lattice parameter $a_0 = 3.5998 \pm 0.001$ corresponding to the disordered taenite and a bcc Fe-Ni alloy with $a_0 = 2.8618 \pm 0.003$ in a very low proportion.

The EDS analysis showed a quite inhomogeneous Ni distribution ~40% Ni and local enrichment of P in some regions, probably due to the presence of schreibersite. EDS mapping of the components is in progress to determine the influence of P in the Ni distribution.

In the Invar composition range, the slow cooled iron meteorites contain a cloudy zone structure composed of an ordered tetrataenite phase and a surrounding honeycomb phase poorer in Ni either of a γ or α-phase. This microstructure results from a spinoidal reaction below 350° C [4] and has been characterized by optical microscopy, SEM, XRD and MS [5,6] in the non-Antarctic Ni-rich ataxites Santa Catharina (~35% Ni) , Twin City (~30% Ni) and cannot be excluded in San Cristobal (~25% Ni) [7]. Lime Creek (~29% Ni) and Tishomingo (~32% Ni) have also been studied. Although the Ni content is similar in these meteorites, important differences were noticed between Lime Creek, Tishomingo and the others.

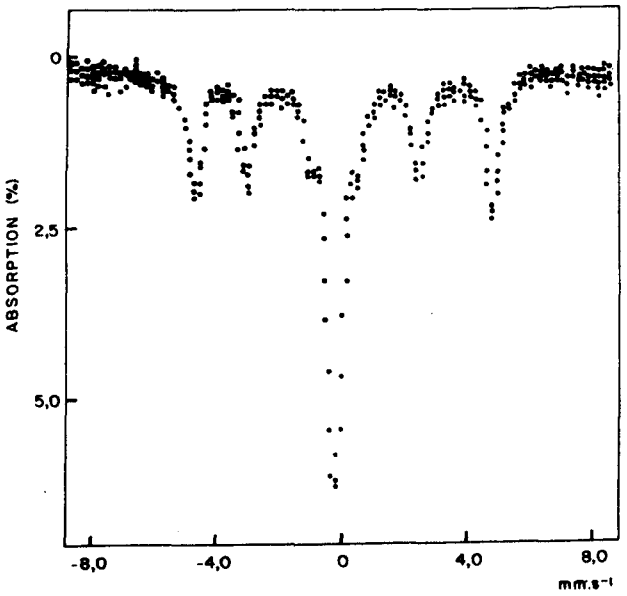

Fig.2. Mössbauer spectrum of a thin slice of the Santa Catharina meteorite.

The presence of the ordered phase Fe-Ni 50/50 with $L1_0$ superstructure in S. Catharina (fig.2), Twin City and San Cristobal indicates that phase decomposition has occurred at low temperatures since the ordering reaction proceeds below ~320° C. The different proportions of the ordered phases between them is probably related to their Ni content and to different cooling rates of these meteorites.

The Mössbauer spectra of Lime Creek and Tishomingo shows the absence of the quadrupole splitting typical of the ordered phase indicating that the Fe-Ni 50-50 is not ordered. The presence of the disordered ferromagnetic taenite can be attributed to a destruction of the ordered superstructure in these meteorites

Both Lime Creek and Tishomingo show metallographic evidences of a shock event , whereas no evidence for shock has been reported for San Cristobal, Twin City and S. Catharina.

In the case of the Antarctic Ni-rich ataxite Y-791694, in spite of the high nickel content, the Mössbauer spectrum showed a complete different phase composition. The results obtained up to now suggest that the main component corresponds to a fully disordered Fe-Ni alloy with ~ 40% Ni indicating a fast cooling rate for this meteorite. If more time was available for cooling, this meteorite would probably contain the cloudy zone structure. More detailed investigation are in progress.

REFERENCES 1.Yanai K. (1979) Catalog of Yamato meteorites, NIPR, Tokyo. 2.Shimamura T., Hinda M., Nagai H. and Yoshioka Y. (1979) Proc. 16th Symposium on Antarctic Meteorites ,79-81. 3.Paulevé J., Dautreppe D., Laugier J. and Néel L. (1962) C.R. Acad. Sci. Paris 254,965; J. Phys. Radium 23, 841. 4.Goldstein J.I., Williams D.B., Zhang J. and Clarke R.S. (1990) Physical Metallurgy of Controlled Expansion Invar-type Alloys, 67-83. 5.Scorzelli R.B. and Danon J. (1990) Physical Metallurgy of Controlled Expansion Invar-type Alloys, 85-100. 6.Scorzelli R.B. and Danon J. (1985) Phys. Scripta 32, 143-148. 7. Danon J., Scorzelli R.B. and Galvão da Silva E. (1985) Meteoritics, 20,632.

DIFFRACTION STUDY OF OLIVINES IN THIN SECTIONS BY MICRO-REGION LAUE METHOD USING SYNCHROTRON RADIATION. K.Ohsumi, M.Miyamoto*, T.Takase*, Photon Factory, KEK, (*)Mineralogical Institute, Univ.Tokyo.

Introduction A micro-region of a sample such as in a thin section has been observed and analyzed by an optical microscope(OM) for identification of included minerals or for texture analysis, and by an electron probe micro analyzer(EPMA) for chemical compositions. A structure image or its mutual relation to other minerals in a micro-region has been also observed by transmission electron microscopy(TEM). TEM has played an important role in the field of material science as well as earth science. However, TEM has not provided quantitative crystallographic information of these crystals. Much precise structural information of crystals has been obtained by the X-ray diffraction method and accumulated as the data base.

It is essential in the case of a thin section to analyze or refine the structure of minerals, and the mutual relationship between these minerals found in almost the same region, to the same limit as OM or EPMA. A system for this purpose has been developed based on that used to analyze a submicrometer-sized single crystal, by making use of synchrotron radiation(SR) with the Laue method at beamline 4B(BL-4B) of the Photon Factory(PF), KEK[1]. And then it was applied to profile analysis of olivines in ordinary chondrites.

Equipment It is most important in obtaining the diffraction data from a very small region to reduce the background to as low a level as possible. The diffraction equipment is placed in a vacuum chamber to avoid air scattering. The micro-region in a thin section should be kept stationary in the incident X-ray beam while data collection is carried out, otherwise the micro-region which is irradiated by the SR beam changes. Because of the long time needed for collection of diffracted intensities and diffraction geometry required for stationary thin sections, the Laue method with an imaging plate(IP;Fuji Co., Ltd), a storage phosphor detector, was employed. Taking into account the limited space around BL-4B, a micro-beam at the sample position is made by using an optical system installed in the beamline and diffraction appratus[1], in addition to a micro-pinhole set just after the optical system. Two micro-pinholes with diameters of 5 and 10μm were prepared. The micro-region in a thin section is observed and adjusted to the beam position by OM with CCD

mounted on the diffraction equipment. A schematic diagram of the experimental layout is shown in the figure.

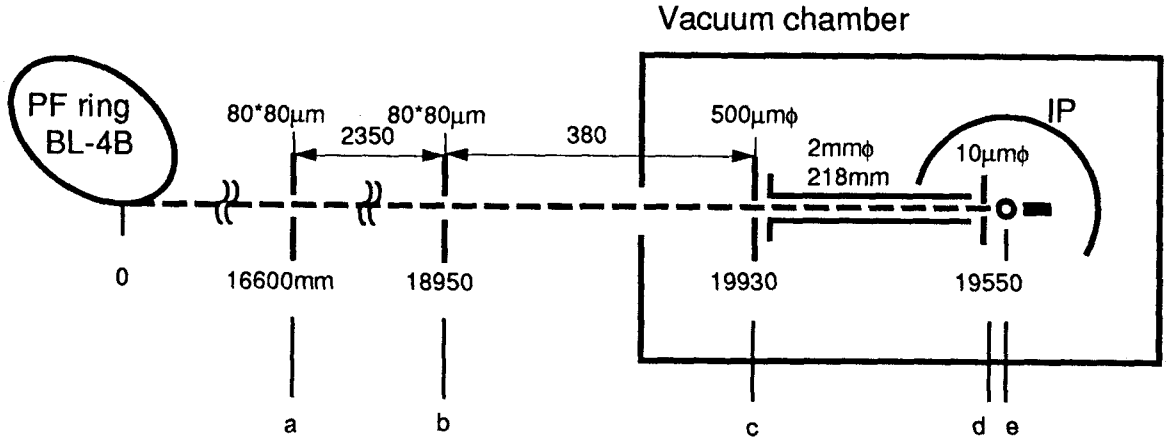

Software A software system which was developed for analysis of submicrometer-sized single crystals has been revised and used for data reduction of Laue patterns obtained using polychromatic SR, and structure refinement based on the intensities of Laue spots.

Experimental and Result Diffraction profiles of olivines included in L6 chondrites, Y7304 and Y7305, were examined by the method with 10μm micro-pinhole mentioned above at BL-4B in PF. The storage ring is always operated at an energy of 2.5GeV with its current from 350 to 200mA for 24hrs.

Y7304

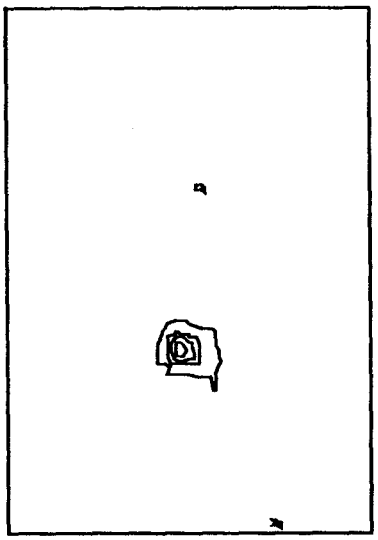

Y7305

Both of Laue patterns were taken over twenty five minutes with the ring current at around 250mA. Typical Laue spots obtained from each olivine are shown below in contour maps. FWHM of diffraction profiles is estimated in a form of solid angle shown in the table. That of Y7304 is more than a hundred times

	Y7304	Y7305
FWHM(solid angle) (steradi.)	$5.3 \cdot 10^{-4}$	$3.0 \cdot 10^{-6}$

greater than that of Y7305, which probably corresponds to the degree of wavy extinction ob- served by OM.

The authors would like to thank Drs.K.Yanai and H.Kojima for providing samples and discussion.

References

1.Ohsumi K.,Hagiya K. and Ohmasa M.(1991)Joun.Appl.Cryst.24,340-348.

Red Thermoluminescence from Enstatite

K. NINAGAWA[1], M. NAKAGAWA[1], A. MATOBA[1], H. YAMAGUCHI[1], I. YAMAMOTO[1], T. WADA[2], Y. YAMASHITA[2], S. HUANG[3], D. W. G. SEARS[3], S. MATSUNAMI[4] and H. NISHIMURA[5]

[1]*Okayama University of Science, 1-1, Ridai-cho, Okayama 700*
[2]*Okayama University, 1-1, Tsushimanaka 3-chome, Okayama 700*
[3]*University of Arkansas, Fayetteville, Arkansas 72701, USA*
[4]*Miyagi University of Education, Aramaki Aza Aoba, Sendai, Miyagi 980*
[5]*Naruto University of Education, Takashima, Naruto, Tokushima 772*

Introduction A mineral responsible for the thermoluminescence [TL] in meteorites is interpreted to be mainly feldspars[1]. The TL sensitivity of chondrites increases by a factor of 10^5 with metamorphism due to the crystallization of feldspar and TL sensitivity is an effective means of classifying the type 3 ordinary chondrites and CO chondrites[2,3,4,5]. In this classification the TL detection wavelength has been limited in a wavelength region between 320 and 480 nm, using an EMI 9635 photomultiplier tube with Corning 7-59 and 4-69 filters[4]. However, last year we found the intense TL at a spectral peak ~570 nm from anorthite-normative mesostases in primitive ordinary chondrites, Semarkona and Bishunpur. We also observed yellow cathodoluminescence [CL] from them[6,7].

Moreover, this time we found red TL from enstatite in an ordinary chondrite, Chainpur (LL3.4). GREER measured the TL from the enstatite of Enstatite chondrites and Aubrites, and has reported that the total TL output of meteoritic enstatite was inversely proportional to the amount of iron[8]. However the TL emission spectra and a TL image from enstatite have not been observed so far. In this paper TL emission spectra and TL images of a specimen of the Chainpur are reported, comparing with Cathodoluminescence [CL] images.

Petrography of the Specimen One of 3 fragments of the Chainpur (BM1915, 86 112.53 mg) was cut by a wire saw and ground to ~1 mm thickness with alumina and polished with diamond paste. However, petrographic characteristics of the specimen is not representative of Chainpur. There are some regions similar to this in Bishunpur. It shows a granular texture and consists of an assemblage of enstatite and lesser forsteric olivine with minor interstitial matrix (Fig. 1). Opaque minerals embedded in the matrix are kamacite and troilite. Ca-rich pyroxene and calcic plagioclase commonly occur as the interstitial phases. Euhedral enstatite crystals contain fine granular olivine inclusions. The enstatite and olivine are almost homogeneous in composition. Enstatite is mostly iron-free ($En_{98.4\text{-}99.4}Fs_{0.1\text{-}0.5}Wo_{0.4\text{-}1.2}$). The FeO and CaO contents of olivine are ranging from 3.18 to 5.30 wt% ($Fa_{3.2\text{-}5.5}$) and from < 0.03 to 0.16 wt%, respectively. Al and Na contents are variable in interstitial Ca-rich pyroxene ($En_{47.0\text{-}60.3}Fs_{0.3\text{-}0.5}Wo_{39.2\text{-}52.7}$) and calcic plagioclase, respectively. The Al_2O_3 concentration in Ca-rich pyroxene ranges between 3.2 and 13.8 wt%. The Na_2O content in calcic plagioclase ranges from 1.3 to 3.7 wt% ($An_{67.1\text{-}88.2}$).

TL Emission Spectra The specimen was irradiated to a dose of 13.2 kGy by Co-60 γ-rays. Figure 2 shows TL emission spectra of the specimen measured by a time-resolving spectroscopy system: (a) Distribution of the TL intensity as a function of both wavelength and temperature. (b) Spectra, obtained by averaging the TL intensity between 100 and 180 °C and between 180 to 320 °C, respectively. (c) Glow curves, obtained by averaging the TL intensity between 410 and 500 nm and between 600 and 700 nm, respectively. The TL of the specimen has spectral peaks at wavelengths of ~650 nm and ~450 nm. This was the first time that the red TL of

~650 nm was measured in meteorites. What minerals are responsible for the red TL ?

TL Images A TL spatial distribution readout system was arranged to measure red (~650 nm) and blue (~450 nm) TL images. The red TL image in a wavelength region of 580-880 nm was measured using a photon imaging head with a multialkali photocathode through a long pass filter, R-60. The blue TL image in a wavelength region of 400-580 nm was measured using a photon imaging head with a bialkali photocathode through a band pass filter, Corning 4-96.

The specimen was irradiated again to a dose of 13.2 kGy. The TL measurements were made by heating at 0.25°C/sec in nitrogen atmosphere. Figures 3 (a) and (b) show a induced red image in a 40-300 °C range and a blue TL image in a 40-150 °C range, respectively. The position with high TL intensity is expressed by concentration of black points. The portions of the red TL are different from those of the blue TL. The compositional analysis by a EPMA revealed that iron-free enstatite (< 1wt%) was responsible for the red TL and interstitial calcic plagioclase was responsible for the blue TL.

The induced TL glow curves of them were analyzed and are shown in Figs. 4. The red TL has three glow peaks at 140, 190 and 270 °C. The glow peak at 270 °C would correspond to that at 290 °C of two major peaks at 290 and 380 °C, reported by GREER[8]. The induced glow curve of this red TL from enstatite would be available to the classification (formation and/or metamorphism) and paring for enstatite chondrites and Aubrites. The blue TL has a glow peak at 100 °C with narrow width, which is usually shown in anorthite-normative mesostasis of ordinary chondrites[9].

CL Images The iron-free enstatite is known as a mineral responsible for the red CL in primitive ordinary chondrites[10]. The CL images were also measured for the same specimen by a Luminoscope, using a ECTAR 1000 film. Figures 5 show the CL images taken with long (50 sec) and short (1/15 sec) exposure times. The red and blue TL portions corresponds to red and blue CL portions, respectively. The colors of the CL coincide those of the TL. No CL portion corresponds to forsteric olivine (FeO >1 wt%).

Summary

1) Red TL with a 650 nm spectral peak was found in a specimen of Chainpur (LL3.4).
2) This red TL is due to iron-free enstatite.
3) The colors of the CL coincide those of the TL.

References

1) LALOU, C. et al. (1970): C. R. Acad. Sci., Ser.B, **270**, 1706-1708.
2) SEARS, D. W. et al. (1980): Nature, **287**, 791-795.
3) SEARS, D. W. (1988): Nucl. Tracks Radiat. Meas., **14**, 5-17
4) SEARS, D. W. et al. (1990): Proc. 21th Lunar Planet. Sci. Conf., 493-512.
5) SEARS, D. W. et al. (1991): Proc. NIPR Symp. Antarct. Meteorites, **4**, 319-343.
6) NINAGAWA, K. et al. (1992): Proc. NIPR Symp. Antarct. Meteorites, **5**, 281-289.
7) NINAGAWA, K. et al. (1992): Meteoritics, **27**, 269.
8) GREER, R. T. (1970): Mat. Res. Bull., **5**, 765-770.
9) NINAGAWA, K. et al. (1991): Proc. NIPR Symp. Antarct. Meteorites, **4**, 344-351.
10) SEARS, D. W. et al. (1992): Nature, **357**, 207-210.

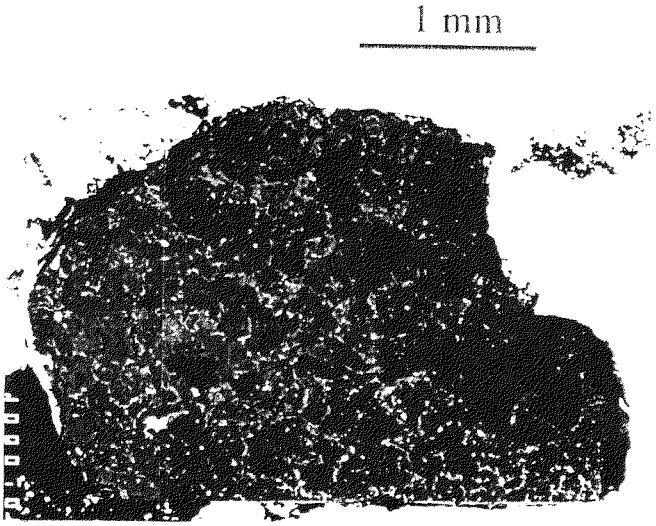

Fig.1 BSE image of a specimen of Chainpur (LL3.4).

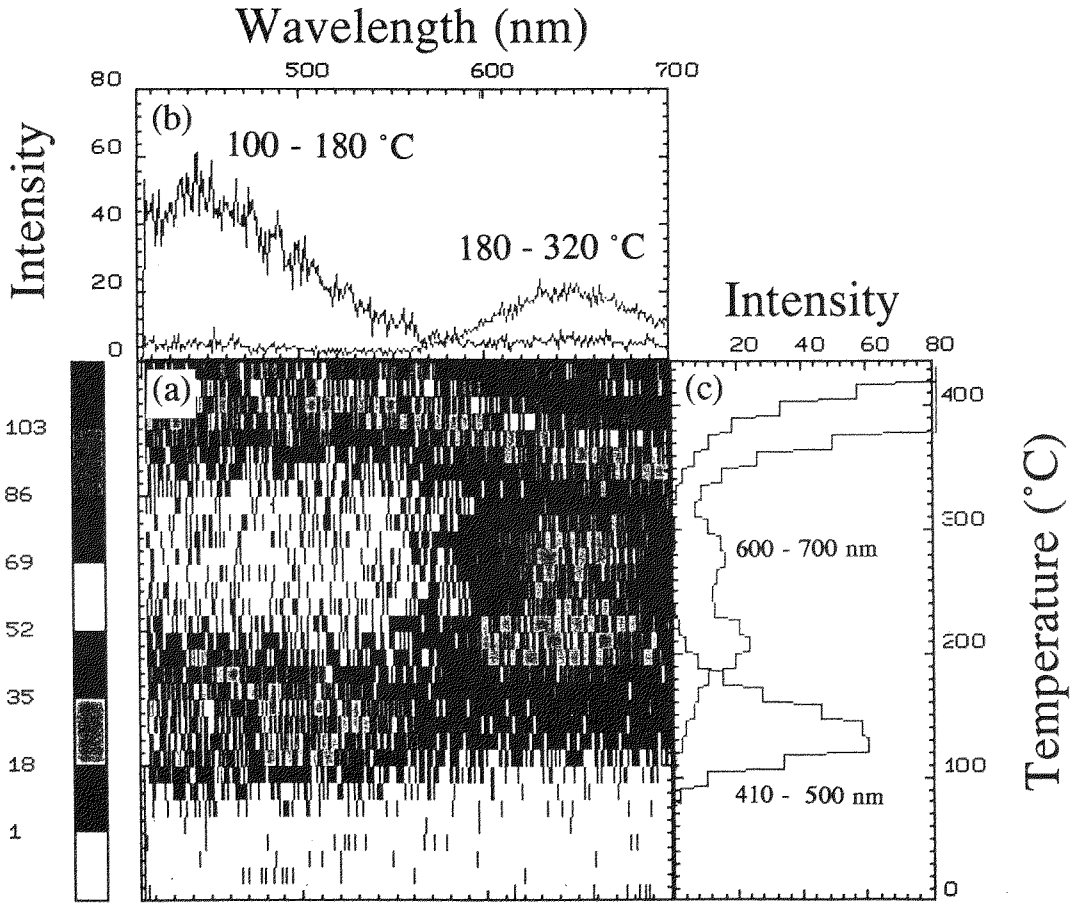

Fig. 2 TL emission spectra.

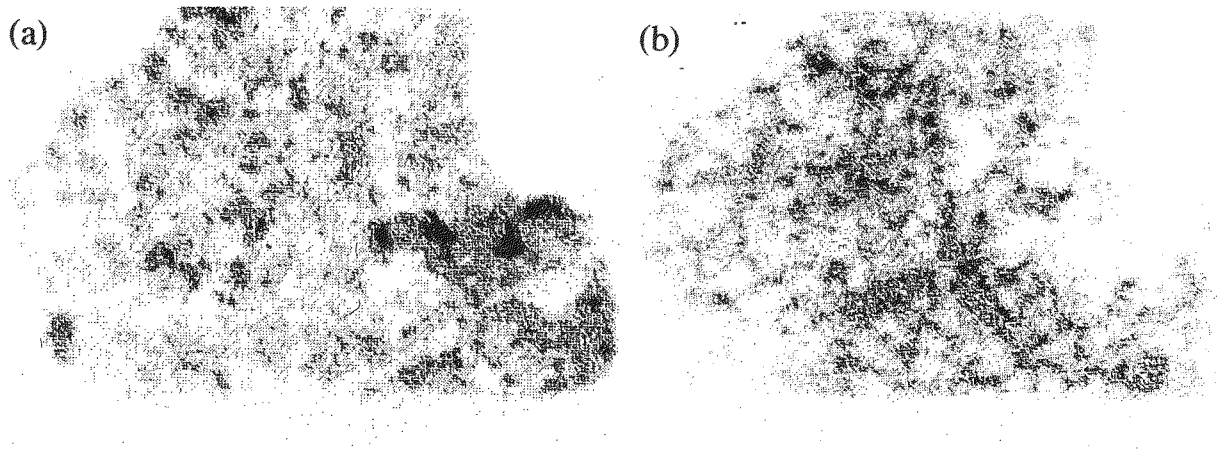

Fig. 3 TL images; (a) red TL image and (b) blue TL image.

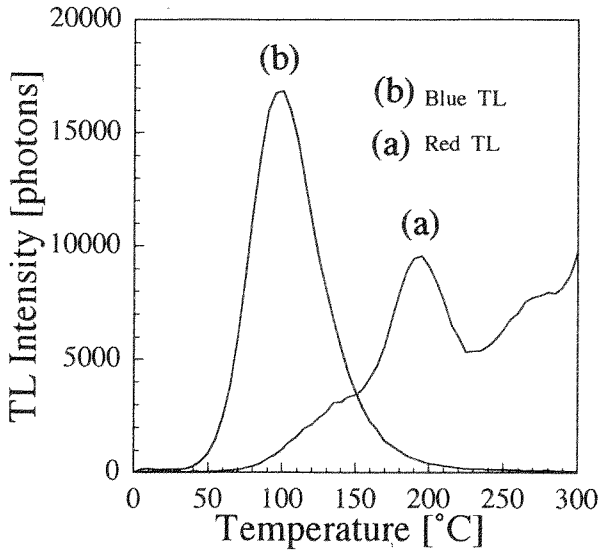

Fig.4 Glow curves; (a) red glow curve and (b) blue glow curve.

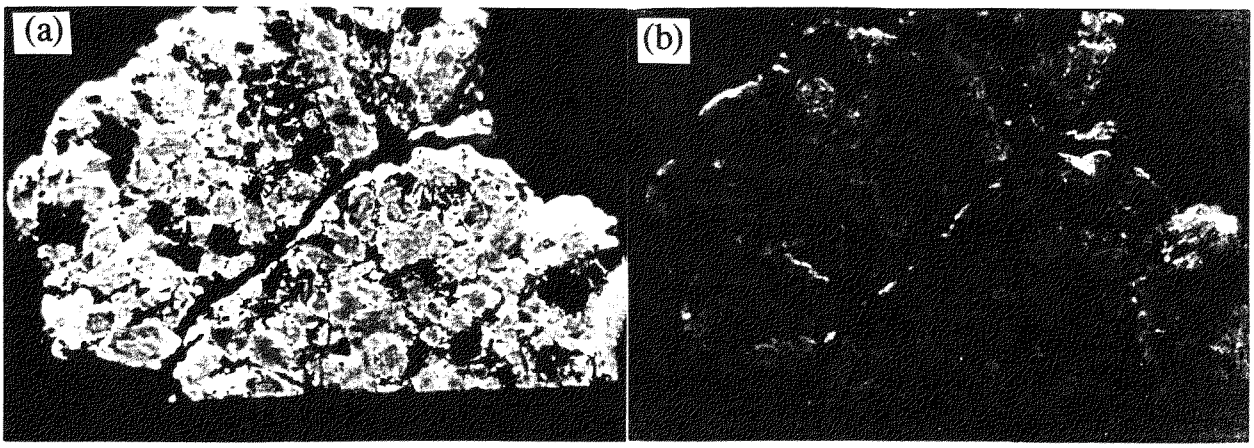

Fig. 5 CL images; (a) long exposure time (50 sec) and (b) short exposure time (1/15 sec).

Shock effects experiments of serpentine, and thermal metamorphic conditions in Antaractic Carbonaceous Chondrite.

Junji Akai[*1] and Toshimori Sekine[*2] [*1]:Dept.Geol. & Min. Fac. Sci., Niigata Univ.[*2]:Natl.Inst.Res. Inorg.Materi.

Antarctic carbonaceous chondrites, B-7904, Y-86720, Y-82162, Y-793321 , are unique in their petrographic features (Tomeoka et al, 1989a,b; Zolensky et al.,1989; Ikeda, 1991), and also in their experienced thermal metamorphism (Akai,1984, 1988,1990;) which has not been found from non-Antarctic carbonaceous chondrites. The following characteristics of the thermal metamorphism can be summarized : 1: Thermal transformation of serpentine type phyllosilicates to olivine or some intermediate structure is the evidence of thermal metamorphism ; 2; Voids structures were found and are described (Akai, 1992b). However, the origin of this structure is not clear,although following possibilities were suggested ; thermal metamorphism, irradiation, shock effects (or shock induced heating), radiation by fixed star (or the sun) ,alteration and so on.

T-T-T diagram were obtained by heating hexperiments for estimation of the thermal metamorphism (Akai,1992a). Comparing these experimental results and the observed data on meteorites, the degrees of thermal metamorphism were estimated to be in the following order : B-7904$\geq$Y-86720$>$ Y82162 $>$ Y793321 .

However, the causes of these change are not yet clear .Some phenomena relating the causes may be suggested ; internal thermal metamorphism in parent body of the meteorites , irradiation by some reason , shock effects (or shock induced heating for short time), radiation by fixed star (or the sun), alteration . Kimura et al .(1992) suggested that shock event ($<$ 45 GPa) may be the most plausible mechanism for heating of constituent minerals in B-7904 for short duration. He refered the results of Lange et al. (1985) in which antigorite shocked up to 45 GPa lacks petrographically observable shock indicators , although significant amount of H_2O was driven out of antigorite . These results seem to be consistent with the results of observation of thermally metamorphosed Antarctic carbonaceous chondrite. However , there are no direct observations and confirmation of the change of phyllosilicates by HRTEM yet. On the other hand, Miyamoto (1990) preliminarily pointed out that the suggested metamorphic temperature is theoretically possible when assuming that the process is the internal heating by thermal gradient in the parent body of some sizes. So, for the first time , shock experiments were carried out.

Shock experiments : Specimens of Murchison meteorite (#304,#316)and Lizardite (#302,#303 ,#314,#315) from Lizard although composition of the latter one is not always similar to those in meteorites but Mg rich type. The experiments were carried out

in Natl. Inst.Res. Inorg. Materials by one of the authors (T.S.) . Specimens were prepared as follows: specimen disks were mounted in stainless steel ring of 6 mm in inner diameter. The both sides of the ring were sandwiched stainless steel disk . planar shock wave were transmitted to the specimen through this design. Hugoniot of serpentine from J.G.R.,vol.96, 18011-18027(1991) were used. Flyers were Al- alloy for #314-316. The followings are the shock conditions :

	Impact velocity	First pressure	The last equilibrium pressure
# 302	1.215km/s	13.2 GPa	26.3GPa
#303	1.714	19.5	39.6
#304	1.439		32.1
#314	0.859	5.2	10.0
#315	1.305	8.3	16.1
#316	1.057		12.7

Examinig the shocked specimens the followings were found:phyllosilicates in the shocked specimens of # 304,#305 and #306 changed almost to amorphous substances although some exceptions are present probably because of heterogeniety in shock effects to the serpentine. Fig.1 shows TEM image of such serpentine mineral grain in # 304 suggesting slightly remaining layer structures. On the other hand, the phyllosilicates in shocked specimens of #314, #315 and #316 were still crystalline and not damaged by shock pressures. Fig.2a and 2b show TEM images of #316 , in which crystalline serpentine and a little damaged crystalline state are found. Some void-like textures were observed in some minerals (Fig.3), but the other minerals seem to be little affected by shock. The other textural features for shock were not clear. Furthermore, transitional structure in transformation of serpentine to olivine structure was not clearly found but amorphous state is observed. These facts do not always seem to coincide completely with the observed results on Antarctic carbonaceous chondrites although some resemblance is surely present. However, if the process to form observed mineral structures and textures is the shock event the corresponding pressure of Y-793321 for example , may be between 18 GPa and 32 GPa.

References: Akai,J.(1984) Pap.9th NIPR Symp.Ant.Met.59, — (1988) GCA,52,1593, — (1990) Proc.NIPR Symp.Ant.Met., 3,55, — (1992a) Pap.9th NIPR Symp.Ant.Met., — (1992b) Proc.NIPR Symp.Ant.Met.,5,120 Ikeda, Y. (1991) Proc.NIPR Symp.Ant.Met., 4,187; Kimura,M. et al.(1992) Proc.NIPR Symp.Ant.Met.5,74: Lange et al.(1985) GCA, 49, 1715; Miyamoto,M. (1990) Pap.15th NIPR Symp.Ant.Met.89; Tomeoka,K. (1989a) Proc. NIPR Symp.Ant.Met. , 2,36, — (1989b) Proc.NIPR Symp.Ant.Met.2,55 ; Zolensky, et al. (1989) Pap.14th NIPR Symp.Ant.Met.24.

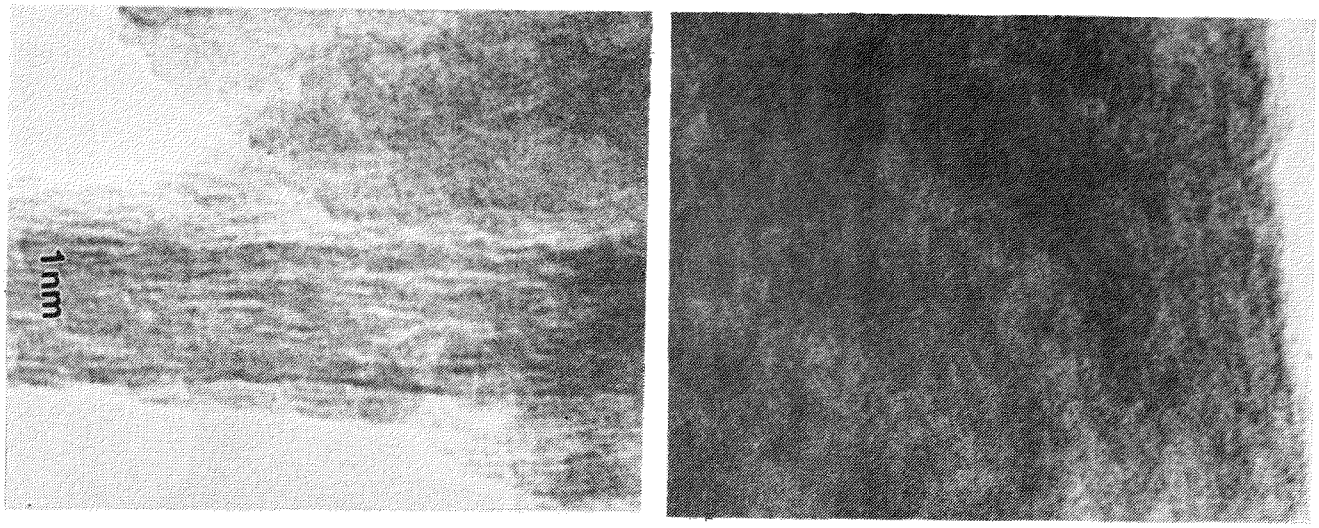

Fig. 1 TEM image of rare serpentine grains suggesting crystalline structure still broadly remaining. (Sp. #304)

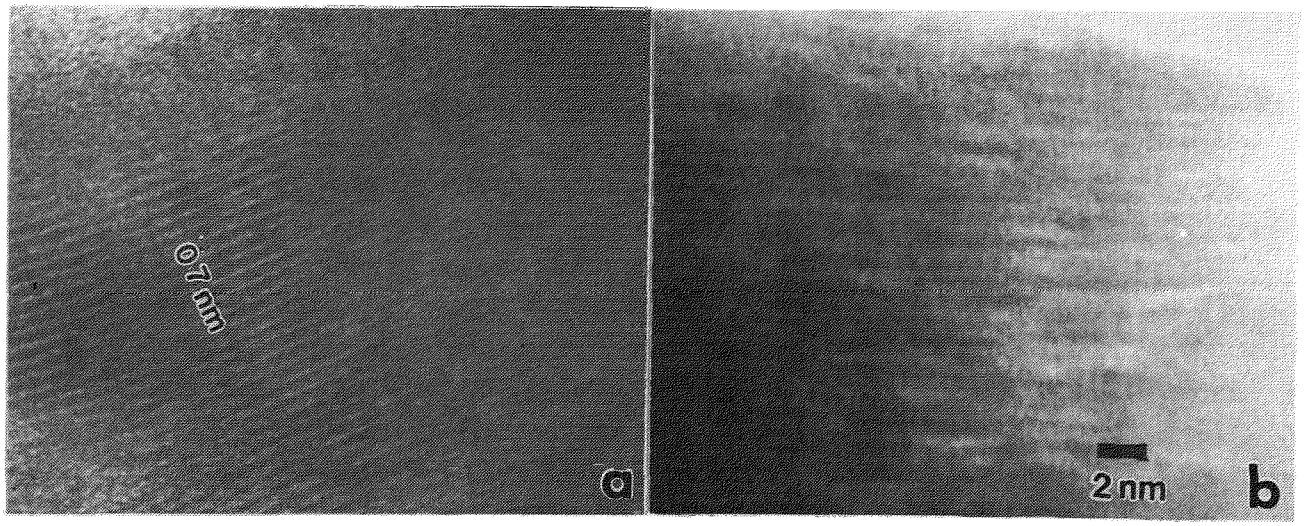

Fig. 2 HRTEM images of phyllosilicates of serpentine grains. (Sp. #316)

a : Crystalline serpentine structure without damage.

b : Damaged serpentine lattice image.

Fig. 3 TEM image of void-like structure found in #304.

Special Lecture (II)

Prof. Stuart Ross Taylor

The Australian National University, Canberra, Australia

The Planetesimal Hypothesis and the Early Solar System

Stuart Ross Taylor
Australian National University

Formation of planets from giant gaseous protoplanet precursors, or from dust, predict that their compositions should be uniform, with solar-type abundances. These are not observed and planetary compositions are diverse. Evidence in favor of the planetesimal hypothesis, involving the accretion of the planets from a hierarchical swarm of planetesimals, includes the heavily cratered ancient surfaces of the Moon, Mars and Mercury, the obliquities of the planets and compositional variations among the planets. In addition, the low density of the Moon and the high density of Mercury, are both probably due to large collisional events.

The initial stage of the formation of the solar system was the separation of a fragment, that became the solar nebula, from a molecular cloud. This fragment had relatively low angular momentum, which led to condensation in the center and a single stellar system rather than the very common (>80%) formation of a double star system. As the proto-Sun. moved toward the Main Sequence, early violent T Tauri and FU Orionis stages of stellar evolution swept water and other uncondensed volatile elements in the nebula out to a "snow line" at 5 A.U. Condensation in this region increased the local particle density. As a result of this, a 15-20 Earth-mass core formed quickly at 5 A. U. while the gaseous portion of the nebula was still present. This core collected a hydrogen and helium envelope by gravitational attraction before the gaseous nebula had totally dispersed.

Jupiter, however, has about 10 times the solar rock+ice/gas ratio, so that that the gaseous portion of the nebula was already partially dispersed by the time Jupiter had formed. Clearly the formation of a gas giant such as Jupiter requires fine timing, so that Jupiter-type planets may not necessarily be formed in other planetary systems. This early formation of Jupiter depleted the region around Mars (which is 3000 times less massive than Jupiter) and the asteroid belt (which now contains only 5% of the mass of the Moon). This present mass distribution indicates that the formation of Mars, and by inference that of the other terrestrial planets occurred after the formation of Jupiter and after the gaseous nebula had been dispersed.

The evidence from the chondritic meteorites indicates that chondrules formed in the nebula very close to T_0 (4560 m.y.) from pre-existing silicate dust. Volatile element depletion had already occurred before the chondrule-forming event. Separate silicate, metal and sulfide phases were present.

The chondrites appear to have formed quickly from local regions of the nebula, perhaps only 0.1 A.U. wide. Very little mixing among groups appears to have taken place. The wide variation in oxygen isotopes, in chondrite compositions, and the lack of mixing among different classes

implies considerable heterogeneity in the nebula. This seems to be unrelated to heliocentric distance. The K/U ratios, that are indexes of volatile/refractory element separation, for Earth, Mars and Venus indicate that depletion of the volatile elements extended throughout the inner solar nebula. Mars at 1.5 A.U. appears to contain about 50% more volatile elements than the Earth or Venus, as shown by the K/U ratios in the SNC meteorites.

The proportion of "igneous" asteroids in the main belt (nearly 100% at 2 A.U.) decreases rapidly with increasing heliocentric distance. The source of heating seems to be related to heliocentric distance, but is not clearly established. The preponderance of "igneous" asteroids in the inner portions of the asteroid belt leads to the inference that all bodies in the inner solar system (sunwards of the asteroid belt) from which the terrestrial planets were assembled, were melted and differentiated. The accretion of the terrestrial planets from bodies with iron cores and silicate mantles means that metallic core formation in the terrestrial planets would be essentially coeval with the accretion of such bodies.

Timescales for the accretion of the terrestrial planets from those rocky planetesimals which survived the early violent solar activity in the inner nebula were of the order of 10-50 m.y. Venus and the Earth (separated by 0.3 A.U.) probably have a similar bulk composition for the major elements, judging from the similarity in uncompressed densities and in K/U ratios for the two planets. This would indicate that the inner planets accreted from zones at least 0.3 A U. wide. Mars, 0.5 A.U distant from the Earth, has a different composition and thus accreted from a different population of planetesimals. Addition of material to the inner solar system during planetary formation from the asteroid belt beyond 2 A.U. was probably minimal, since the composition of meteorites mostly differs from that of the terrestrial planets.

During the final stages of the accretion of the inner planets, a large differentiated body about 0.15 Earth-mass collided with the Earth. This body was disintegrated and its silicate mantle was spun out into Earth orbit. The metallic core of the impactor was accreted to the Earth. A Moon-sized object formed, in Earth orbit, mostly from the silicate mantle of the impactor. Along with other compositional differences, the Moon contains 50% more FeO than the terrestrial mantle, consistent with derivation from a different body. The energy involved in this event is sufficient to melt the Earth completely.

However melting is a probable consequence of the accretion of the Earth from a hierarchical suite of planetesimals, even without the Moon-forming collision. The terrestrial mantle siderophile elements, water and noble gases may be derived from late cometary or asteroidal impacts, but evidence for such late veneers is not apparent on the Moon.

Taylor, S. R. (1992) *Solar System Evolution: A New Perspective* Cambridge University Press, 307 pp.

Abstract Only

PROPOSAL FOR SCATTERING /HALO/ OBSERVATIONS OF ARTIFICIALLY GENERATED OUTER SOLAR SYSTEM TYPE CRYSTAL CLOUDS IN THE LOW TEMPERATURE CONDITIONS OF ANTARCTIC ATMOSPHERE. Szaniszló BÉRCZI, Eötvös University, Dept.G.Technology, Budapest, Rákóczi ut 5.and József A. University, Dept.Climatology, Szeged, Hungary /H-1088/

INTRODUCTION Observations and chemical-model-calculations suggest a considerable amount of different type volatile condensates /especially various ice and clathrate crystalline materials: gas-hydrates/ in the Outer Solar System. In suitable conditions - i.e. in atmospheres, in rings or in the L_4 and L_5 Lagrangian Points of Outer Planets - these crystalline materials may form clouds: we call them Outer Solar System Type Crystal Clouds /OSSTCC/.

THE PROPOSED EXPERIMENT Scattering of the light coming from an intensive light source may reveal the existence and the composition of an OSSTCC. Light rays penetrating crystal particles suffer refraction. This refraction is determined by the refraction coefficient of the crystal and the characteristical face-angles of refracting crystal forms. Of the randomly oriented and dispersed crystals in the cloud the direction of the light-flux /i.e. the light source -- observer line/ selects those ones, which have a similar position according to the light source -- observer axis. These crystals are arranged according to the cylindrical symmetry of the whole system, and so they form a huge lens. This hypothetical lens of randomly scattered crystals produce a characteristical refraction phenomenon around the light source: a halo or ring. Such phenomenon should be studied in the low temperature Antarctic atmospheric conditions. In these atmospheric experiments and observations the intensive light soure should be our Moon or the Sun, which both rather frequently produce such halo phenomena. In terrestrial halo phenomena the ice crystals are the crystal-particles of the clouds. In the proposed experiments thse water-ice-crystals should be substituted by other OSSTCC. Such studies may serve as preliminary tests for spce-probe instruments, too, which should be sent to the Outer Solar System to detect OSSTCC during encounters with planetary bodies./The more low-temperature experiments has been proposed for Space Shuttle expeditions, also as preparations for the observations of OSSTCC for Pluto Fast Flyby, NASA./

CANDIDATES FOR COMPONENTS OF OSSTCC According to current chemical models and observations the most probable candidates for components of OSSTCC are different gas-hydrates. There are two important types of gas-hydrate crystals./Berecz, Balla-Achs 1980/ Both of them have cubic crystal structure, but with different unit-cell distances. The one with $6M.46H_2O$ /M for hydrate forming molecule/ stochiometric composition has unit-cell with 1.2 nanometers, the other one with $24M.136H_2O$ stochiometric composition has unit-cell with 1.7 nanometers.

THE EXPECTED HALO FOR OSSTCC CONSISTING OF GAS-HYDRATE CRYSTS The main factor in determining the characteristical refraction angle for crystals in the OSSTCC is the angle between the faces of the crystal. A cubis crystal - the characteristical form of

gas-hydrate crystals - has two important types of refracting angles /Greenler, 1980;/. One is the rightangle between two faces meeting at adges of the cube. This edge region of the cubis crystal can be considered as a prism with rightangle. The halo which is produced by such refraction type prisms /in the case of water-ice crystals/ is known from the literature: a huge 46 degrees radius ring on the sky /Greenler, 1980./.

The other type of refracting angle is at the pyramidal vertex at any of crystals. Pyramidal vertex refraction does not give new case for cubic crystals. In order to see it let us substitute an edge of the cube with a truncated face /as shown on fig.1./. The angle between the original cubic faces and the truncated faces is again a rightangle /fig.1./ so refraction at pyramidal regions give again a 46 degrees halo. There are no smaller prism-angles on cubic crystals, so in the case of gas-hydrate crystal components a 46 degrees halo may be expected in the experiments. This is a very large ring on the sky and has been observed very rarely in the case of special forms of ice-crystals /Greenler, 1980./.

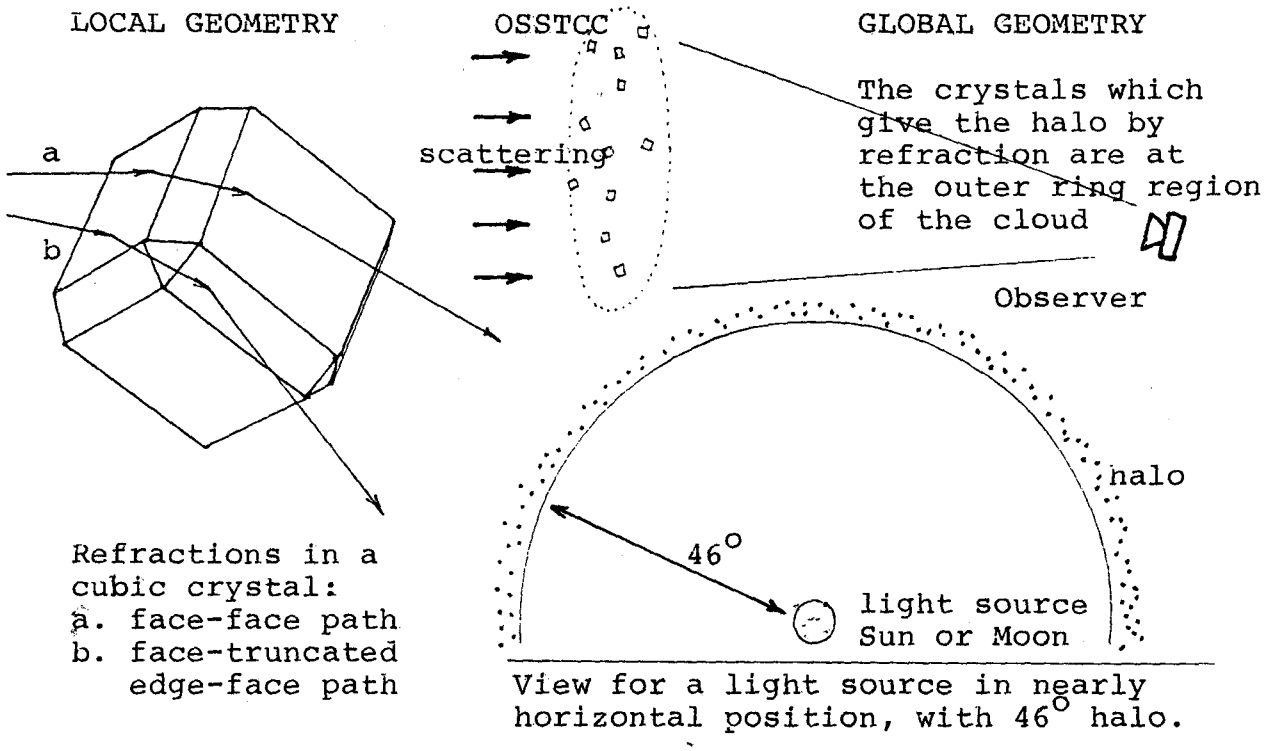

fig.1. Local and global geometry of the halo formation in an OSSTCC. Cubic crystal refractions show the two main types of path which contribute to the 46° halo formation.

SUMMARY An Outer Solar System Type Crystal Cloud /OSSTCC/ generating and measuring experiment /and principle/ has been proposed in cold Antarctic atmospheric conditions. According to the current knowledge about the Solar System chemistry /Lewis, Barshay, 1974./ gas-hydrates are the main constituents of the OSSTC clouds. On the basis of the crystal forms of gas-hydrates - cubic structure - a 46 degrees halo can be expected as the main scattering phenomenon visible for an observer /around a light source, where the cloud-iluminating and crystal-refracted light comes from/. The proposed experiments can be carried out with more low-temperature components /NH_3, CH_4/ in orbit /for example as a Space Shuttle experiment/, too. All these experiments may be preparations for the observations of OSSTCC by space probes to be sent in the near future to the outer Solar System planets.

REFERENCES

Barshay, S.S., Lewis, J.S. /1975/: Chemistry of solar material.In: The Dusty Universe. /Eds.: Field, G.B., Cameron, A.G.W./ Neale Watson Acad. Publ.

Berecz, E., Balla-Achs, M. /1980/: Gázhidrátok./Gas-Hydrates/. Akadémiai Kiadó, Budapest,/in Hungarian/

Bérczi, Sz. /1991/: Kristályoktól Bolygótestekig./From Crystals to Planetary Bodies/. Akadémiai Kiadó, Budapest, /in Hungarian/

Bérczi, Sz. /1993/: Short summary about the Planetary Light Halo through Lagrangian Point Crystal Cloud /PLH-t-LPCC/ proposal to the Pluto Fast Flyby /PFF/ Mission observations. Notice of Int. to the NASA Research Announcement 93 OSSA-5.

Bérczi Sz. /1993/: Preparations for the measurements of Gas-Hydrate Crystal Clouds in the Outer Solar System. Acta Climatologica, Szeged. Tom. XXVII. /in press/

Greenler, R. /1980/: Rainbows, Halos, and Glories. Cambridge University Press, Cambridge

Chemical fractionations in impact-melted L-chondrites: Point of Rocks and Chico

Toshiki Fujiwara and Noboru Nakamura
Department of Science of Material Differentiation, Graduate School of Science and Technology, Kobe University, Nada, Kobe 657, Japan

A considerable fraction of L-chondrites have been shocked. Intense shock events significantly affected the chemical compositions, primarily for rare gases, of these chondrites. The K-Ar and U-He ages of intensly shocked chondrites are much younger than those of unshocked chondrites. Other elements can be redistributed as well by shock. Actually, the Rb volatilization is suggested for shocked chondrites[1]. In addition, variation of Fe and S in ordinary chondrites is partly caused by shock melting[2]. Therefore, it is important to clarify more details of chemical fractionation during shock melting of chondrites. Previously, we have carried out Rb-Sr isotopic analysis for impact-melted L-chondrites, Point of Rocks and Chico, and obtained age of ~460Ma[3]. This age agrees with the Ar-Ar ages around 500Ma reported in [4]. In order to examine shock induced chemical changes, we have performed chemical analysis of these meteorites.

Samples were taken from the same chips analysed in our previous Rb-Sr study. For Chico, we analysed two specimens(Chico-1 and Chico-2) with different morphological features. Chico-1 is somewhat contaminated by unmelted materials. Abundances of K and Rb were determined by isotope dilution mass spectrometry. Abundances of Ca, Mg, Fe, Al, Cr, Mn, Ni and Co were obtained by inductively coupled plasma atomic emmision spectrometry, and that of Na was determined by atomic absorption spectrometry.

Figure 1 shows the L-chodrite[5] normalized(re-normalized to Mg=1) lithophile and siderophile element abundances. The elements are arranged in the order of increasing volatility from left to right. In the diagram, the following fractionation features are pointed out; (1)lithophile/siderophile element fractionation, (2)positive correlation between Al and Na, (3)fractionations among alkali metals and among siderophiles. It is important that these fractionations are not consistent with elemental volatilities but with ionic radii. This implies that abundances of these elements may not be established by gas/liquid nor gas/solid fractionation processes during impact event. The

lithophile and siderophile element abundances are suggested to reflect the solid/melt partitioning and silicate/metal melts fractionation, respectively.

Al correlates positively with Na, and is enriched relative to other normal L-chondrites. It is considered that the albitic melts formed by intense impact event on a L-chondrite parent body and were added to the source region of these meteorites. Pottasium has a positive correlation with Rb for most samples, and Point of Rocks and Chico-2 are depleted in these two elements relative to other L-chondrites. On the contrary, Chico-1 is enriched in these elements as a whole and show heterogeneous distribution. This heterogeneity may be partly due to a intrinsic chemical feature of the target material, and have been preserved because of incomplete melting of the specimen.

Most samples are depleted in siderophile elements relative to L-chondrite, and fractionated, with increasing order of Ni, Co and Fe. The Co correlates positively with Ni. Co/Ni ratio of each sample is rather higher than that of normal L-chondrites. This fractionation trend can not explained by volatilization losses of these elements during the shock melting. The most plausible explanation may be that the metal-sulfide phases are extracted as immisible melts during impact melting. If the partitioning of siderophile elements between silicate and metal-sulfide melts occurred and followed by drain of metal-sulfide melt during the impact melting event, silicate melt may have been depleted in these elements. Partition coefficient of silicate/metal liquids for Co is much larger than that of Ni[6]. Then, silicate melt will have a high Co/Ni ratio.

REFERENCES

[1] Minster J. F. and Allégre C. J. (1979) Meteoritics **14**, 235-248.
[2] Dodd R. T. (1981) Meteorites. Cambrige Univ. Press, 77-132.
[3] Nakamura N., Fujiwara T. and Nohda S. (1990) Nature **345**, 51-52.
[4] Bogard D. D., Garrison D. H., Scott E. R. D., Keil K., Taylor G. J., Vogt S., Herzog G. F. and Klein J. (1990) Lunar Planet. Sci. **XXI**, 103-104.
[5] Wasson J. T. and Kallemeyn G. W. (1988) Phil. Trans.R. Soc. Lond. A **325**, 535-544.
[6] Jones J. H. and Drake M. J. (1986) Nature **322**, 221-228.

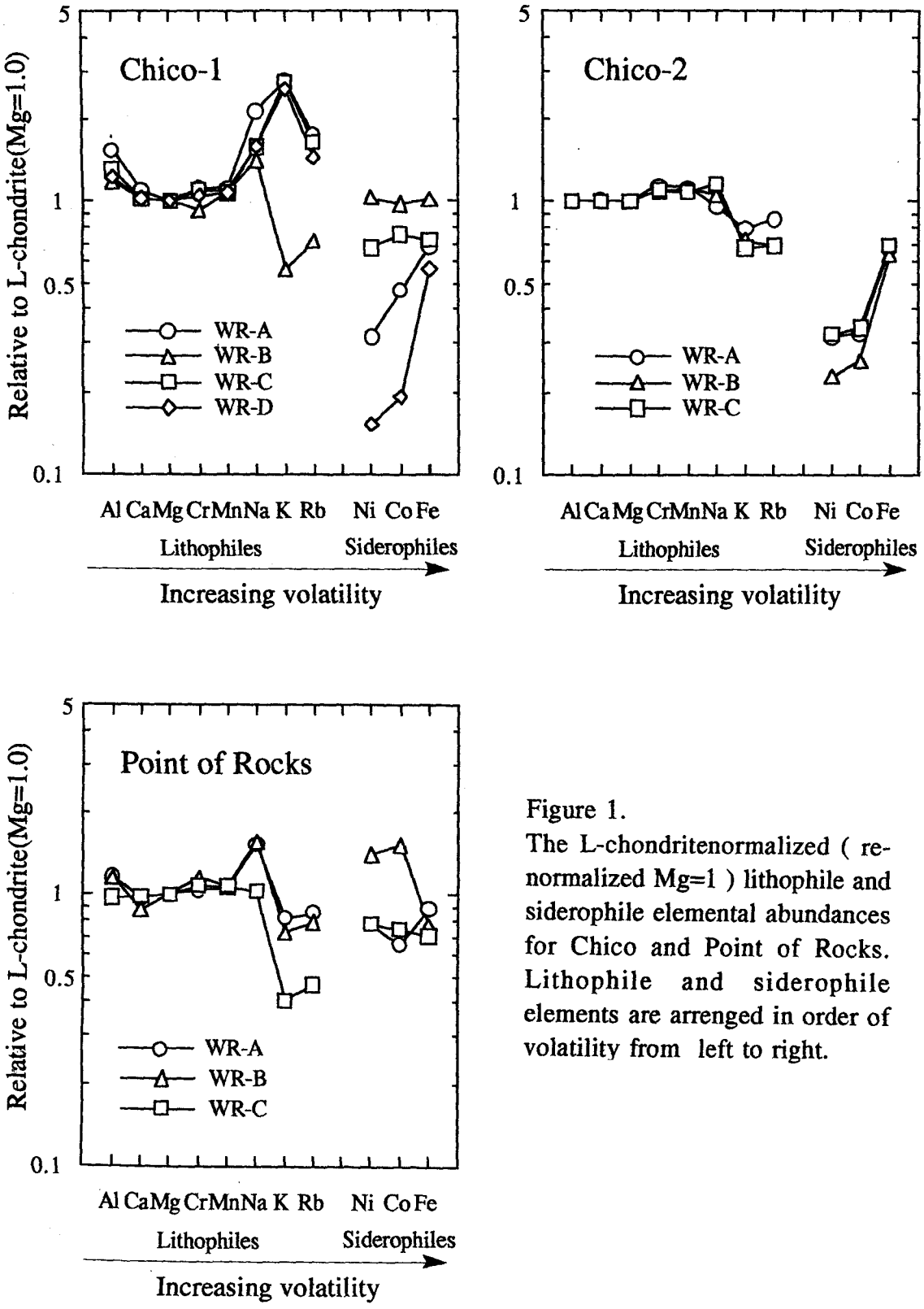

Figure 1.
The L-chondritenormalized (re-normalized Mg=1) lithophile and siderophile elemental abundances for Chico and Point of Rocks. Lithophile and siderophile elements are arrenged in order of volatility from left to right.

REE abundances in chondrules, inclusion and mineral fragments from Yamato-793321(CM) chondrite

Mutsuo Inoue[1], Noboru Nakamura[1,2] and Hideyasu Kojima[3]

[1]Department of Science of Material Differentiation, Graduate School of Science and Technology, [2]Department of Earth Sciences, Faculty of Science, Kobe University, Nada, Kobe 657, [3]National Institute of Polar Reseach, Kaga, Itabashi, Tokyo 173, Japan.

Introduction

Except for a few cases, REE abundance data of individual CM chondrules have rarely been reported until today. This is mainly due to analytical difficulty owing to their scarcity and small sizes. We have initiated precise determination of REE abundances in Murchison(CM) chondrules by dilect-loading isotope dilution mass spectrometry (DL-IDSM) method(1) and obtained interesting results(2). Extending our detailed REE search of CM chondrites, we analysed REE and other lithophiles for chondrules from Yamato (Y)-793321(CM) chondrite.

Samples and analytical procedures

Y-793321 is a weakly altered CM chondrite(3). The 3-5 chondrules, one inclusion and 2 olivine fragments were separated from the chondrite by hand-picking through freeze-thaw processing. Each sample was broken into two parts; One half was used for a polished thin section preparation and the other half was for precise analysis of lithophile elements. Petrographic textures, constituent minerals and the effect of aqueous alteration in each sample were examined by EPMA. On the other hand, abundances of REE, Ba, Sr, Rb, K, Ca and Mg were determined by DL-IDMS(1).

Results

Except for two samples, the textural and major chemical features of each specimen were characterized, as shown in Table 1. Although YC-9, -11 were not examined for the texture, lithophile element abundances suggest that they are chondrules.

The chondrule YC-7 shows an almost flat REE pattern and lower alkali abundances relative to refractory elements. The chondrule YC-11 indicates a smoothly fractionated REE pattern with negative Eu anomaly and lower alkali earths (Sr, Ba) together with the depletion of alkali metals (K, Rb). YC-8 and -9 appear to have similar pattern (Fig. 1a).

For YI-5, irregular light/heavy REE fractionation with LREE depletion are observed in REE pattern (Fig. 1b).

Two olivine spherules YO-1, -2 show the similar lithophile abundance features and the large discontinuity is not recognized except Mg (Fig. 2a).

Discussion

In general, refractory precursors of chondrules and CAIs are thought to have formed through gas/solid (or liquid) process and anomalous REE patterns are consistent with such nebula setting model(4). Lithophile element abundances in chondrule YC-7 and olivine spherules from Y-793321 also show no large discontinuity against volatility, which may suggest that these REE fractionations were (at least partly) controlled by elemental volatilities during the formation process. The YI-5 and YC-8, -9, -11 seem to show LREE depletions. These patterns are similar to those of Murchison chondrules. Such a REE fractionation is more consistent with solid/liquid fractionation. Alkali depletion of altered chondrules is probably due to leaching in aqueous alteration process. On the other hand, olivine spherules, including little metal balls and showing similar Fo (99.7) values to olivine phenocrysts, may be isolated olivines from porphyritic chondrules, and the origin through the condensation and melting process can not be ruled out.

Reference

(1) Nakamura N., Yamamoto K., Noda S., Nishikawa Y., Komi H., Nakagawa T. and Misawa K.(1989) Anal.chem, 61, 755-762.
(2) Inoue M. and Nakamura N.(1992) Papers presented to the 16th Symposium on Antarctic meteorites(Abstr.), 82-85.
(3) Kojima H., Ikeda Y. and Yanai K.(1984) Mem. Natl Inst. Polar Res., Spec. Issue 35,184-199.
(4) Misawa K. and Nakamura N.(1988) Geochim. Cosmochim. Acta 52, 1699-1710.

Table 1. Descriptions of analysed samples from Y-793321.

	wt(mg)	description	alteration
YO- 1	0.228	Olivine(Fo:99.7) fragment including spherical metal.	unaltered
YO- 2	0.160	Olivine(Fo:99.7) fragment including spherical metal.	unaltered
YI- 5	0.063	Ca,Al-rich inclusion(CAI): Forsterite -fassaite including euhedral spinel.	unaltered
YC- 7	0.099	Porphiritic olivine chondrule.	unaltered
YC- 8	0.059	Porphyritic olivine chondrule.	altered*
YC- 9	0.116	---	---
YC-10	0.089	Porphyritic olivine pyroxene chondrule.	altered*
YC-11	2.066	---	---

*Mesostasis was altered to Fe-rich phyllosilicate.

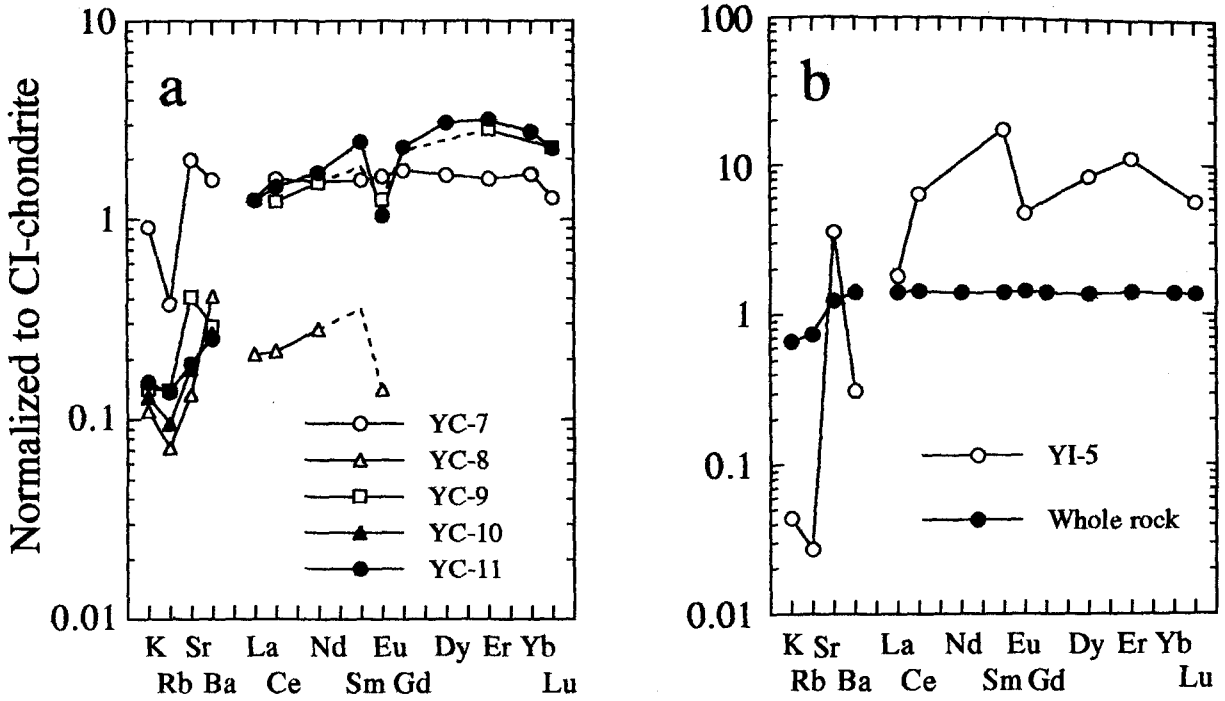

Fig. 1. CI-normalized REE patterns of a)chondrules, b)CAI and whole rock of Y-793321. Heavy REE of YC-8 and all REE of YC-10 were not determined.

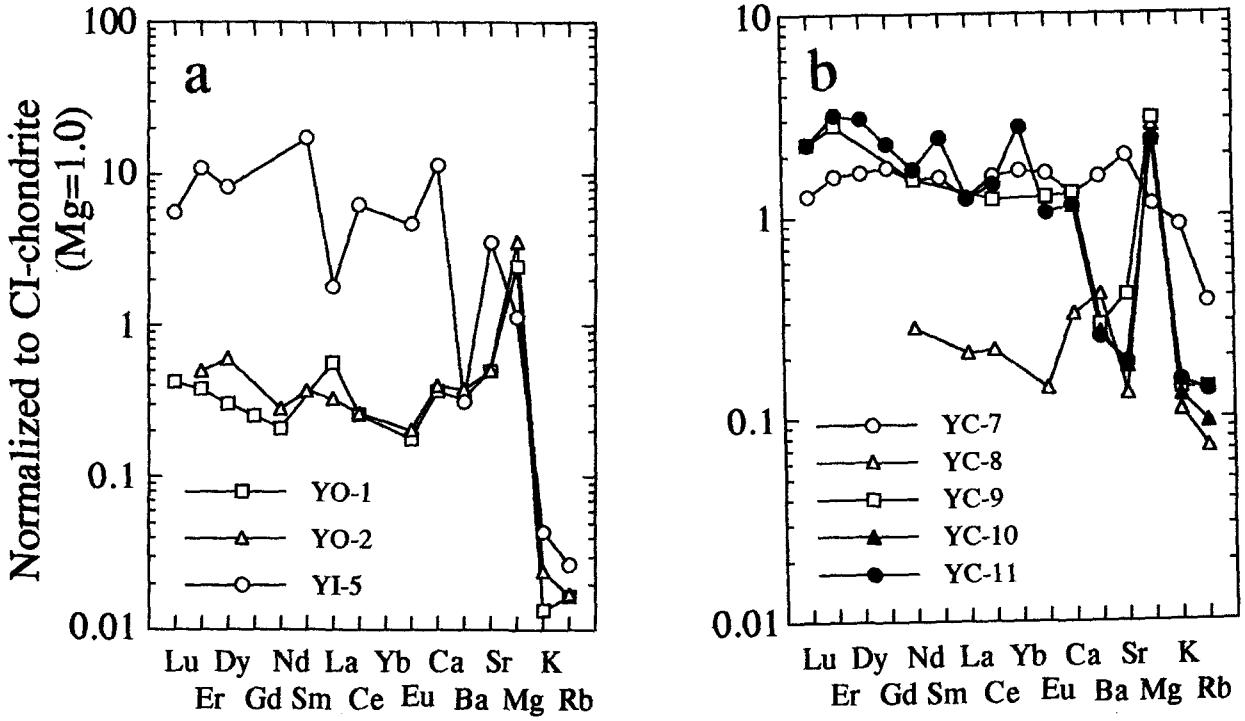

Fig. 2. CI-normalized abundances of lithophile elements of spherules from Y-793321; a)olivine and CAI and b)chondrules. Elements are arranged in order of increasing volatility from the left to the right.

Lunar basaltic meteorites Yamato-793169 and Asuka-881757: Samples of the same low-Ti mare-lava?

BRADLEY L. JOLLIFF, RANDY L. KOROTEV, and LARRY A. HASKIN

Department of Earth and Planetary Sciences, Washington University, St. Louis, MO 63130 USA

Meteorites Yamato-793169 and Asuka-881757 are basalts from the lunar maria. They are dissimilar in detail to any mare basalts returned by the Apollo or Luna missions, but they are compositionally so similar to each other that they almost certainly are related. Although Y793169 is relatively fine grained and A881757 is coarse grained [11,5,12,13,10], bulk compositional similarities are such that the two rocks can be related by containing slightly different proportions of plagioclase, Fe-Ti oxide, and mesostasis. We suggest that these are related as members of the same thick mare-basaltic pile and were probably ejected by a single impact. This is consistent with their similar ages and exposure histories.

Analysis and Results. We have studied by electron microprobe analysis of fused beads (FB-EMPA, Table 1) [e.g., 2] and instrumental neutron activation analysis (INAA, Tables 2 and 3) splits of the powders prepared for consortium study [13]. For INAA, three 70–80-mg subsamples of the A881757 powder were analyzed in one experiment. These analyses indicate that the powder is uniform in composition for samples ~75 mg in mass (Table 2). In a separate experiment, a single 19-mg sample each of the two meteorites was analyzed by INAA. The composition of the 19-mg subsample of A881757 agrees well with the average of the three 70–80-mg subsamples, except for Cr, which is 2.3% greater in the 19-mg subsample. In Table 3, the mass-weighted mean composition of the four analyzed subsamples of A881757 is presented .

For FB-EMPA, two beads ("A" and "B") were prepared of each meteorite from 10–15 mg of powder. For Y793169, the neutron irradiated powder was used; for A881757, unirradiated material was fused. For elements determined in common by the two techniques, results agree within analytical uncertainty, except that concentrations of Na obtained by FB-EMPA are ~0.93× those obtained by INAA; this is presumably the result of volatilization of Na during fusion.

For A881757, concentrations of some elements obtained for the two beads differ by an amount greater than expected from analytical uncertainty. Bead A has greater concentrations of TiO_2, FeO, and MgO and a lesser concentration of Al_2O_3 than does bead B. These differences correspond to a greater proportion of mafic minerals in bead A, suggesting slight heterogeneity of the powder in the 10-mg mass range.

Table 1. Mean results of electron microprobe analysis of two each (A and B) "fused beads" prepared from powdered meteorites. N = number of analyses averaged.

		Asuka-881757		Yamato-793169	
		A	B	A	B
N		5	4	4	4
SiO_2	%	45.96	46.31	45.89	46.95
TiO_2	%	2.49	2.28	2.08	2.14
Al_2O_3	%	9.68	10.22	11.79	11.71
Cr_2O_3	%	0.31	0.30	0.21	0.23
FeO	%	23.11	22.17	20.96	20.46
MnO	%	0.34	0.34	0.32	0.28
MgO	%	6.11	5.98	5.57	5.59
CaO	%	11.50	11.50	12.01	12.00
Na_2O	%	0.25	0.22	0.26	0.27
K_2O	%	0.037	0.033	0.054	0.055
P_2O_5	%	0.048	0.029	0.055	0.042
Sum	%	99.82	99.38	99.20	99.74

Approximate mass of fused powders: 10–15 mg

Discussion. Compositional similarities between the two meteorites have been noted, particularly the similarity of their unusual TiO_2 concentrations [10,13]. We obtained TiO_2 concentrations of 2.4% for A881757 and 2.1% for Y793169 and an average Ti/Fe ratio of 0.080±0.004 for the four beads (Table 1). Most Apollo mare basalts have Ti/Fe ratios either substantially higher or somewhat lower than this. Samples with similar Ti/Fe ratios (e.g., Apollo 15 pigeonite basalt 15597 with Ti/Fe=0.070) differ in other respects (e.g., 15597 is more magnesian and has different relative REE abundances [see 8]). Of the eight mare basins overflown by the Apollos 15 and 16 orbiting gamma-ray experiments, only two, Cognitum (Ti/Fe: 0.09±0.07) and Crisium (Ti/Fe: 0.03±0.09), have Ti/Fe ratios as low as, and within uncertainty of, the ratio in the meteorites [1]. This comparison speaks to the commonness of high-Ti basalts among near-equatorial mare basins. It also suggests a possible source for A881757 and Y793169, Mare Cognitum, as the VLT (very-low-Ti) basalt from Mare Crisium is compositionally distinct from the two meteorites (e.g., Ti/Fe: 0.041±0.004; [3,7]).

Might these two meteorites be petrogenetically related and, if so, how? They have similar bulk compositions and similar mineral compositions [9], and no isotopic differences are known yet that would preclude a relationship. The small bulk-compositional differences between the two meteorites can be explained by small variations in modal proportions of plagioclase, ulvöspinel, and mesostasis. We can model the composition of Y793169 as consisting of 86–90% material having the composition of bulk A881757, minus ~0.7% ulvöspinel, plus 7.5% plagioclase (mainly An_{96}), plus ~4–8% mesostasis. For these calculations, we use compositions of minerals given by [11] for A881757 and an estimated mesostasis composition from the ITE concentrations of the two meteorites. The slight differences between their compositions could have arisen from slightly different proportions of minerals and different proportions of mesostasis caused by short-range mineral and mesostasis liquid separations during crystallization within a cooling lava (i.e., "short-range unmixing" as discussed by [4]).

Table 2. Relative sample standard deviations (RSD, in %) for some elements determined with high-precision by INAA in three 70–80 mg samples of Asuka-881757 powder.

	RSD
Na	0.79
Sc	0.22
Fe	0.25
Cr	0.28
Co	0.24
La	2.5
Sm	1.2
Eu	3.1
Yb	1.6
Hf	3.8

Can A881757 and Y793169 be members of a differentiation sequence? Because of the coarse-grained texture of A881757 and the finer-grained texture of Y793169, it might be tempting to speculate that the more mafic A881757 is a pyroxene-rich mare cumulate, and Y793169 a corresponding liquid or a slightly more evolved differentiate of a common parent melt. We have considered the compositions of the two meteorites in terms of low-pressure equilibrium liquidus relations using methods developed by [6] and it appears that, in agreement with [9], the coarser-grained A881757 is not a cumulate. Rather, A881757 has a composition nearly that of a low-pressure liquid multiply saturated with plagioclase, pigeonite, augite, and olivine (Fig. 1). The composition of the Y793169 appears to have a small excess quantity of plagioclase relative to the low-P liquidus (Fig. 1). The simplest explanation is that these rocks originated in different levels of a single mare lava, but that they incorporated slightly different proportions of minerals and mesostasis. The compositional differences between the two rocks cannot result from a fractional crystallization mechanism; however, in this scenario, we must presume that the

proximity of the A881757 composition to the low-pressure liquidus was either a fortuity or resulted from prior, partial crystallization of its parent melt at low pressure; i.e., it did not originate as a low pressure partial melt.

As an alternative model, we consider relationships that might exist if one of these basalts, presumably the finer-grained Y793169, faithfully records a high pressure composition, unaffected by low-pressure fractionation. Based upon liquidus parameterizations from [6 and previous works], it appears that at intermediate pressures of 5–8 kb, the Y793169 composition is saturated with low-Ca pyroxene and plagioclase. At 10 kb, it is saturated with low-Ca pyroxene and augite. If such a liquid was brought to the surface rapidly, it would have been supersaturated with plagioclase because of expansion of the plagioclase field at low pressure (Fig. 1a). In this model, there is no simple explanation for A881757 as a differentiate of such a liquid, but it is conceivable that deeper in the mare flow, a small amount of early crystallizing (supersaturated) plagioclase might physically have separated (e.g., migrated upward, presumably leading to another, more aluminous basalt layer), at least on a small scale, before the liquid reached low pressure multiple saturation. The lower, more mafic assemblage would then have to expel a small amount of a mesostasis component (residual liquid), as discussed above.

Table 3. Results of instrumental neutron activation analysis, with 1-standard-deviation estimates of analytical uncertainty (±).

		Asuka-881757		Yamato-793169	
		conc.	±	conc.	±
Na_2O	%	0.254	0.003	0.280	0.003
CaO	%	11.9	0.4	12.2	0.4
Sc	µg/g	93.9	0.9	80.7	0.8
Cr_2O_3	%	0.302	0.003	0.231	0.003
FeO(t)	%	23.0	0.2	21.0	0.2
Co	µg/g	24.1	0.2	19.7	0.2
Ni	µg/g	<150		<100	
Rb	µg/g	<15		<7	
Sr	µg/g	140	40	170	40
Zr	µg/g	<150	50	70	30
Cs	µg/g	<0.5		<0.5	
Ba	µg/g	<120		101	10
La	µg/g	3.31	0.05	4.75	0.05
Ce	µg/g	9.1	0.3	13.2	0.3
Nd	µg/g	<30		12	2
Sm	µg/g	3.00	0.03	4.19	0.04
Eu	µg/g	1.02	0.03	1.22	0.02
Tb	µg/g	0.85	0.03	1.10	0.03
Yb	µg/g	3.57	0.05	4.56	0.05
Lu	µg/g	0.534	0.010	0.663	0.008
Hf	µg/g	2.53	0.08	3.19	0.07
Ta	µg/g	0.32	0.04	0.40	0.02
Ir	ng/g	<10		<5	2.1
Au	ng/g	<7		<3	1.2
Th	µg/g	0.45	0.04	0.74	0.04
U	µg/g	<0.5		0.13	0.05
mass	mg	246.3		19.03	

We conclude on compositional and petrologic grounds that these two meteorites could be samples of a single mare lava. Their small compositional differences can be explained by their having incorporated slightly different proportions of very similar mineral and mesostasis components. Whereas they may be related by a high pressure origin and subsequent separation of components during low-pressure crystallization, a simple crystal-fractionation relationship at low pressure, deriving Y793169 from A881757, is not indicated.

Acknowledgments. We are grateful to the National Institute of Polar Research for providing the powdered samples of Asuka-881757 and Yamato-793169 which led to this study. We thank John Longhi for the use of his phase-equilibria computer programs and Kaylynn Rockow for preparing the fused beads. This work was funded by NASA grant NAGW-3343.

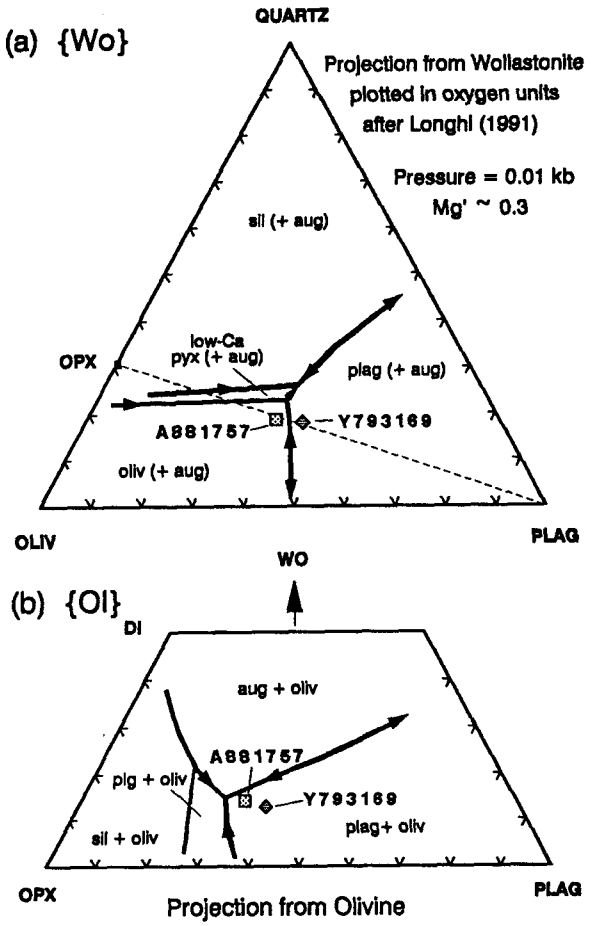

Figure 1. Liquidus surfaces in the pseudoquaternary system olivine-plagioclase-quartz-wollastonite projected onto (a) Oliv-Plag-Quartz and (b) Opx-Plag-Wo planes for conditions relevant to compositions of A881757 and Y793169. Liquidus relationships in proximity to the compositions of A881757 and Y793169 were determined using the computer program MAGPOX (Longhi, 1991), and the general shapes of liquidus projections away from these compositions were inferred from Longhi (1991), esp. his Figs. 3 and 4. Note that although the composition of A881757 apparently lies within the olivine field (a), it is on the pyroxene-plagioclase join, so its major mineralogy, as well as that of Y793169, is dominated by pyroxene and plagioclase.

References

[1] Davis P. A. (1980) Iron and titanium distribution on the moon from orbital gamma ray spectrometry with implications for crustal evolutionary models. *J. Geophys. Res.* **85**, 3209-3224.

[2] Jolliff B. L., Korotev R. L., and Haskin L. A. (1991) A ferroan region of the lunar highlands as recorded in meteorites MAC88104 and MAC88105. *Geochim. Cosmochim. Acta* **55**, 3051–3071.

[3] Laul J. C., Vaniman D. T., and Papike J. J. (1978) Chemistry, mineralogy and petrology of seven >1 mm fragments from Mare Crisium. *Mare Crisium: The View from Luna 24* (R. B. Merrill and J. J. Papike, eds.), p. 537-568, Pergamon.

[4] Lindstrom M. M. and Haskin L. A. (1981) Compositional inhomogeneities in a single Icelandic tholeite flow. *Geochim. Cosmochim. Acta* **45**, 15–31.

[5] Lindstrom M. M., Mittlefehldt D. W., and Martinez R. R. (1991) Geochemistry of Asuka-31: Comparison to basaltic lunar meteorites and mare basalts. In *Abstracts, 16th Symp. Antarct. Meteorites*, pp. 102–105, Natl. Inst. Polar Res., Tokyo.

[6] Longhi J. (1991) Comparative liquidus equilibria of hypersthene-normative basalts at low pressure. *Amer. Mineral.* **76**, 785-800.

[7] Ma M.-S., Schmitt R. A., Taylor G. J., Warner R. D., Lange D. E., and Keil K. (1978) Chemistry and petrology of Luna 24 lithic fragments and <250 μm soils: Constraints on the origin of VLT mare basalts. *Mare Crisium: The View from Luna 24* (R. B. Merrill and J. J. Papike, eds.), p. 569-592, Pergamon.

[8] Ryder G. (1985) *Catalog of Apollo 15 Rocks*. JSC 20787, NASA Johnson Space Center.

[9] Takeda H., Arai T., and Saiki K. (1992) Mineralogical studies of lunar meteorite Y-793169, a crystalline basalt. In *Abstracts, 17th Symp. Antarctic Meteorites*, pp. 109–112, Natl. Inst. Polar Res., Tokyo.

[10] Warren P. H. and Lindstrom M. M. (1993) Consortium study of lunar meteorites Yamato-793169 and Asuka-881757: Geochemical evidence of mutual similarity, and dissimilarity vs. other mare basalts. In *Lunar and Planetary Science XXIV*, p. 1483–1484.

[11] Yanai K. (1991) Gabbroic meteorite Asuka-31: Preliminary examination of a new type of lunar meteorite in the Japanese collection of Antarctic meteorites. *Proc. Lunar Planet. Sci.* **21**, 317–324.

[12] Yanai K. and Kojima H. (1991) Varieties of lunar meteorites recovered from Antarctica. *Proc. NIPR Symp. Antarctic Meteorites* **4**, 70–90.

[13] Yanai K., Takeda H., Lindstrom M. M., Tatsumoto M., Torigoye N., Misawa K., Warren P. H., Kallemeyn G. W., Koeberl C., Kojima H., Takahashi K., Masuda A., Nishiizumi K. (1993) Consortium reports of lunar meteorites Yamato 793169 and Asuka 881757, a new type of mare basalt. In *Lunar and Planetary Science XXIV*, p. 1555–1556.

GEOCHEMISTRY OF BULK SAMPLES AND MINERALS SEPARATED FROM BASALTIC LUNAR METEORITES ASUKA 881757 AND YAMATO 793169. Marilyn M. Lindstrom[1], David W. Mittlefehldt[2], David J. Lindstrom[1], Ming-Sheng Wang[3] and Michael E. Lipschutz[3].
1) NASA, Johnson Space Center, Houston, TX 77058, USA 2) Lockheed Engineering & Sciences, Houston TX 77058 3) Purdue University, W. Lafayette, IN 47907.

Asuka 881757 and Yamato 793169 are coarse-grained igneous rocks from the lunar mare and the first unbrecciated lunar meteorites [1-3]. Both meteorites are low-Ti basalts (TiO_2 1.5-2.5% in homogenized samples) with low Mg/Fe ratios (bulk mg' 31-35). They represent a new type of mare basalt. Our geochemical studies compare them to other lunar basalts and examine their internal elemental distributions.

Samples and Procedures. Our first 250 mg split of A-881757 (,94) was highly enriched in opaque phases and was unrepresentative of the bulk sample [4]. We were allocated additional samples of homogenized powder (,83), and splits both rich in opaques (,107) and poor in opaques (,108). The powder was further subdivided to provide two splits for INAA, one for RNAA, and one for FB-EMP. The opaque-rich split was separated into pyroxene, opaques, a residual ilmenite-pyroxene mixture and fines. The opaque-poor split was separated into pyroxene and plagioclase. All bulk samples and composite mineral separates were analyzed by INAA at JSC using our usual procedures [5]. In addition several large individual grains of pyroxene and plagioclase were analyzed by micro-INAA at JSC using special procedures [6]. Our sample of Y-793169 was a small split of a homogenized powder. After completion of INAA, the A-881757 and Y-793169 bulk samples were analyzed by RNAA at Purdue using standard procedures [7]. Splits of A-881757 bulk samples were analyzed for major elements at JSC by microprobe analysis of fused glass beads (FB-EMP). Because the FeO content of the fused bead from ,94 was different from that of the INAA sample of ,94, we also fused the INAA split and analyzed it.

Results. Analyses are presented in Table 1 (INAA), Table 2 (FB-EMP), and Table 3 (RNAA). Our INAA results on homogenized samples of A-881757 and Y-793169 are nearly identical to analyses of the same samples by other investigators. [8,9,10]. Our major element analysis of A-881757 powder (,83) is consistent with the INAA of that split, in contrast with our INAA and FB-EMP splits of ,94. Our analysis of the powder is similar to Yanai's wet chemical analysis of A-881757 [1] and very different from our earlier analysis of a TiO2-enriched sample (,94). Comparison of the compositions of A-881757 and Y-793169 shows that the two rocks are similar to each other, but distinct in composition. A-881757 is richer in compatible transition metals Fe, Ti, Sc, Cr, Co and poorer in incompatible elements REE, Hf, Ta, Th than Y-793169. Figure 1 uses the variation in TiO2 with mg' to compare these meteorites to other mare basalts. A-881757 and Y-793169 are the boxes at mg' 31-35. They plot close together, except for the unrepresentative high-Ti sample, and well apart from the lunar meteorite basaltic breccias EET87521 and Y-793274 which are the boxes at mg' 40 and 50-55. A-881757 and Y-793169 have higher TiO2 than the usual upper limit for VLT basalts (1-1.5%), but have very low mg' and fall at the boundary between Luna 24 VLT basalts and Apollo 15 low-Ti basalts. Although they are officially classified as low-Ti basalts, they seem to be intermediate between low-Ti and VLT basalts.

Trace element concentrations distinguish these two meteorites from all other mare basalts. Figure 2 is a plot of Sc vs. FeO for mare basalts (diamonds) and volcanic glasses (small squares) [11]. The volcanic glasses and low-Ti and VLT basalts form a low Sc trend, while the high-Al and high-Ti basalts form a high Sc trend. A-881757 and Y-793169 plot at the end of the high Sc trend. Their Sc concentrations (83-112 ppm) are only a little higher than those of the high-Ti mare

basalts, but are more than a factor of two higher than those of low-Ti and VLT basalts. Breccias EET87521 and Y-793274 plot along the low-Sc glass trend or at the intersection of the two trends. Our mineral analyses show that Sc is located mainly in pyroxene where concentrations range from 87-140 ppm. Differences in concentration between the separates are due in part to the inhomogeneous mineral compositions and in part to the uncertainty in composition of the individual pyroxene grains because actual weights were not measured and data were normalized to assumed FeO concentrations. Sc is also located in ulvospinel and ilmenite, although at lower concentrations than in pyroxene. The ilmenite/pyroxene and fines fractions appear to be dominated by pyroxene based on the high FeO and moderately high CaO contents, with minor opaque and other accessory phases. The presence of Sc in pyroxene, the most abundant phase, shows that accumulation of excess pyroxene cannot account for the factor of two enrichment in Sc over low-Ti basalts. A-881757 does not contain 1.5 -2 times the pyroxene of typical basalts as would be required to account for Sc enrichment. Among other trace transition metals, Cr is strongly concentrated in chromian ulvospinel, while Co is dispersed among pyroxene and opaque phases.

REE patterns of bulk samples of A-881757 and Y-793169 are plotted in Figure 3a. REE concentrations are higher than those of VLT basalts, but in the range of low-Ti basalts. However, the flat pattern in the middle to heavy REE is unusual, as most low-Ti basalts peak in the middle and fall off on both light and heavy REE. The REE patterns of basaltic breccias EET87521 and Y-793274 are light REE-enriched and suggest that they contain a small KREEP component. Distribution of REE among minerals in A-881757 are shown in Figure 3b. The REE pattern of the pyroxene composite is typical of clinopyroxene. The similarity between the pyroxene and whole rock REE patterns for all but the lightest REE, and the fact that pyroxene is the most abundant mineral in A-881757, suggest that the bulk of the REE reside in pyroxene. The plagioclase composite has a high Sr abundance and low REE concentrations. The REE pattern is light REE-enriched with a large positive Eu anomaly as is expected for plagioclase. The ulvospinel pattern is strongly enriched in heavy REE as well as Zr, Hf, and Ta which substitute for Ti. However, the ulvospinel has unexpectedly high REE concentrations, especially for light REE. Since ulvospinel occurs mainly in association with a symplectic intergrowth of late-stage minerals, we attribute the high REE concentrations to inclusion of accessory phases. The residual fines and ilmenite/pyroxene fractions have the highest concentrations of REE, Ba and Th. The REE patterns are similar to that of phosphate and we attribute the REE concentrations of these fractions to phosphate in the symplectite.

Discussion. Our geochemical studies of homogenized samples of A-881757 and Y-793169 have shown that they are very similar to each other and distinct from other mare basalts. They are low-Ti basalts with very low mg' and affinities to both low-Ti and VLT basalts. They have very high Sc concentrations compared to low-Ti and VLT basalts and have REE patterns that are distinct from other basalts. Studies of elemental distributions show that Sc and REE are concentrated in major minerals and that differences from other basalts are not due to cumulate processes. Studies by other consortium members also conclude that the two meteorites are similar basalts. Petrographic studies [1,2,13] show that they have similar mineral compositions, but different textures. Y-793169 is significantly finer-grained than A-881757. Radiogenic isotope studies [14] show that they have similar isotopic characteristics and crystallization ages and are distinct from other mare basalts. Studies of exposure histories [15,16] show that they have similar cosmic ray exposure ages and terrestrial ages, but that they do not represent the same meteorite.

In summary, A-881757 and Y-793169 are coarse-grained mare basalts that are very similar to each other, but are not paired meteorites. They are different from all other types of mare basalts in major and trace element composition, in crystallization ages, and isotopic characteristics. They do indeed represent a new type of basalt from an unknown area of the moon as suggested by Yanai [1].

Acknowledgments. We thank NIPR, Dr. K. Yanai and Dr. H. Takeda for including us in the consortium study, and R. Martinez, S. Field, and B. Bansal for assistance with INAA and mineral separations.
References. [1] Yanai K. (1991) PLPSC 21, 317-324. [2] Yanai K. and Kojima H. (1991) NIPR Ant Met 4, 70-90. [3] Yanai K. et al (1993) LPS XXIV, 1555-1556. [4] Lindstrom M.M. et al (1991) Abs NIPR 16, 102-105. [5] Mittlefehldt D.W. and Lindstrom M.M. (1991) GCA 55, 77-87. [6] Lindstrom D.J. (1990) Nuc. Instr. Meth. Phys. Rev. A299, 584-588. [7] Wang M-S. and Lipschutz M.E. (1990) NIPR Ant Met 3, 19-26...[8] Fukuoka T. (1992) Abs NIPR 17, 251-253. [9] Koeberl C. et al (1992) Abs NIPR 17, 219-222. [10] Warren P.H. and Kallemeyn G.W. (1992) Abs NIPR 17, 113. [11] Delano J.W. (1990) Lunar Volc. Glass., LPI, 30-31. [12] Warren P.H. and Lindstrom M.M. (1993) LPS XXIV, 1483-1484. [13] Takeda H. et al (1992) Abs NIPR 17, 109-112. [14] Torigoye N. et al (1993) LPS XXIV, 1437-1438. [15] Eugster O. (1992) Abs NIPR 17, 208-210. [16] Nishiizumi K. et al (1992) Abs NIPR 17, 129-132.

Table 1. INAA of Yamato 793169 and Asuka 881757 Bulk Samples and Mineral Separates

Sample	Y793169	A881757	A881757	A881757	A881757	A881757	A881757	A881757	A881757	A881757
Split	,81 bulk	,94 bulk	,83 pow	comp pyx	ind pyx	comp plg	ind plg	usp	ilm-pyx	fines
Weight	20.1mg	113.1mg	98.0mg	66.8mg	17ug**	15.6mg	74ug**	19.0mg	17.1mg	6.1mg
Na2O	0.30	0.14	0.254	0.037		0.78	1.01	0.007	0.071	0.092
CaO	11.9	6.80	11.5	9.9	9.6	18.5	19.0**	<0.8	8.9	6.1
FeO	20.9	27.0	22.6	28.1	28.1**	0.80	0.531	57.9	35.9	37.3
Sc	83.2	112	94.2	140	87	1.85	0.574	38.6	112.4	94.7
Cr	1590	1850	2100	2450	655	27.0	2.26	30,500	4050	5770
Co	19.8	27.8	24.5	30.9	22.3	0.72	0.312	31.9	30.0	38.5
Sr	140	84	160	100	82	410	415	<32		
Ba	87	90	60	<80	82	65	35	<48	200	130
La	4.84	2.44	3.32	2.21	2.34	1.07	0.252	2.80	11.4	9.87
Ce	14.5	7.5	9.8	7.7	7.6	2.40	0.63		32.6	27.7
Sm	4.20	2.48	3.08	2.66	3.31	0.51	0.257	1.73	9.98	8.35
Eu	1.24	0.60	1.01	0.32	1.4	2.12	2.43	0.175	1.29	1.04
Tb	1.07	0.75	0.87	0.80	1.06	0.10	0.019	0.43	2.41	1.95
Yb	4.65	3.34	3.70	3.63	6.88	0.29	0.052	3.94	8.98	7.60
Lu	0.65	0.51	0.53	0.55	1.15	0.031	0.010	0.588	1.25	1.06
Zr	180		<210		100	<60		290		
Hf	3.35	2.12	2.40	1.45	2.27	0.27	0.03	10.0	5.4	6.7
Ta	0.37	0.43	0.30	0.080	0.40	0.025	<0.013	1.73	0.53	0.96
Th	0.75	0.33	0.37	0.23	0.27	0.15	0.017	0.33	1.65	1.40

** Data normalized to FeO or Al2O3 in absence of actual sample weights.

Table 2. Major Element Analyses by FB-EMP

Sample	Y793169	A881757	A881757	A881757	A881757
Split	Yanai	Yanai	,94 FB	,94 INAA	,83 pow
Weight	639mg	3.5g	47.5mg	113mg	5.9g
SiO2	43.6	45.4	39.7	42.3	45.4
TiO2	1.52	1.66	5.62	6.1	2.34
Al2O3	12.9	11.5	10.9	6.31	10.5
Cr2O3	0.11	0.17	0.25	0.24	0.29
FeO	21.2	21.6	24.8	27.0	22.5
MnO	0.18	0.25	0.35	0.39	0.33
MgO	5.75	6.41	6.36	6.79	6.11
CaO	13.3	12.0	9.53	9.95	11.6
Na2O	0.40	0.50	0.14	0.14	0.25
K2O	0.13	0.04	0.02	0.03	0.04
P2O5	0.29	0.05	0.02	0.03	0.04

Table 3 RNAA of Bulk Samples

Sample	A881757	Y793169
Split	,83 pow	,81 bulk
Au	0.286	0.168
Sb	3.11	3.14
Se	280	611
Te	4.8+-1.9	<13
Bi	1.63+-0.17	2.7+-0.4
Ag	64.0	7.66
In	1.88+-0.03	0.72+-0.26
Tl	9.66	4.26
Zn	1.44	8.59
Cd	12.3	4.6+-0.3
Rb	662	1120
Cs	187	60.8
Ga	3.26	5.14
U	124	217

Fig 1.

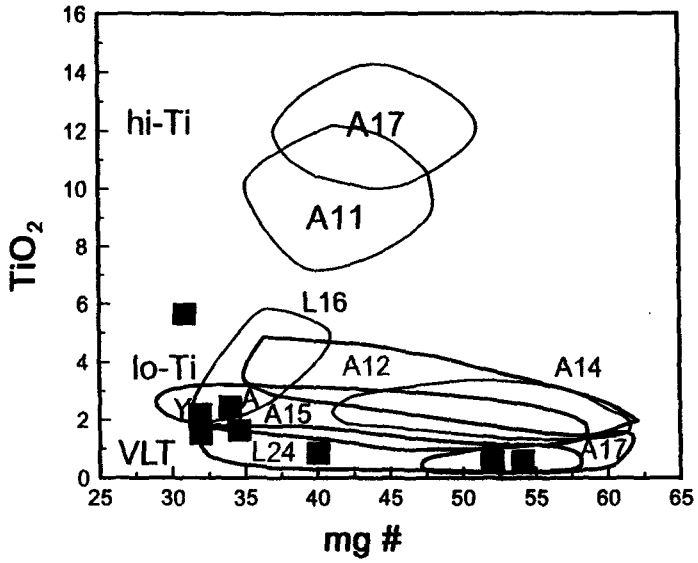

Fig 2.

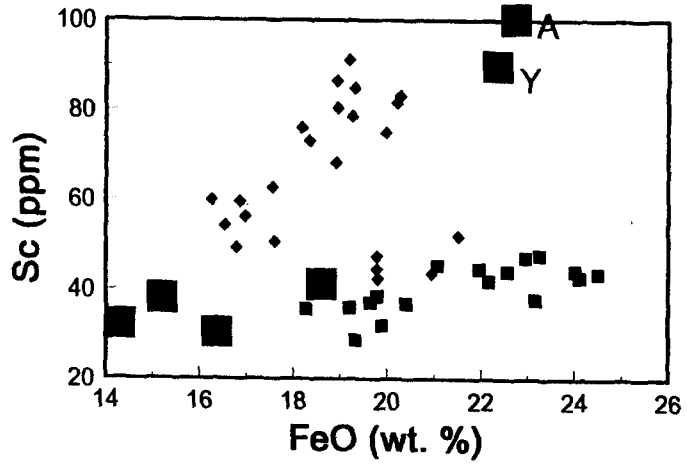

Fig 3

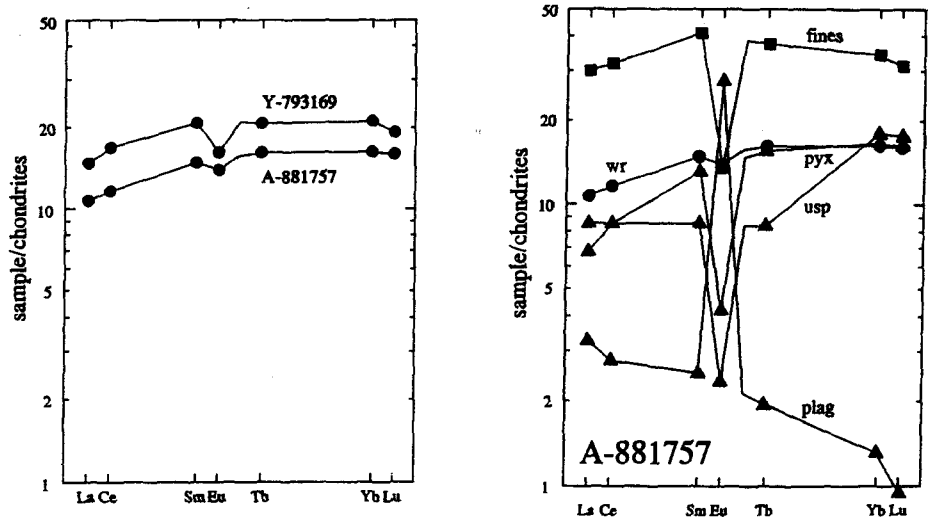

a. b.

THE RELATIONSHIP BETWEEN CHONDRULES AND ACHRONDRITES.

Marakushev A.A., Granovsky L.V., Zinovyeva N.G., Mitreikina O.B.
Moscow State University, 119899, Moscow, USSR.

The results of the detailed microprobe analyses of Efremovka (C3) chondrite are shown on the petrochemical diagram (Fig.1). On this diagram we distinguish magnesium (I), calcium - magnesium (II), aluminium (III) and calcium (IV) chondrules which are embedded in an iron enriched matrix. We can see on the diagram that the composition of main achondrite types are very close to those of the chondrules and matrix in Efremovka chondrite: ureilites and obrites (chondrule type I); diogenites, howardites, eucrites, shergottites and angrites (III and IV); and mesosiderites (matrix M). Similarity between the mineral compositions and the sequence of crystallisation also suggested connections between the origins of these groups of meteoric substance. Consequently the formation of achondrites may be analogous to the separation of magma into matrix and chondrules as found in chondrites. We can understand this process by studying Efremovka (C3), Saratov (L3), Ohansk (H) and Indarch (E) chondrites. These separations are shown by arrows on Fig.1. At the first stage the separation of melt took place and the result of this process was the formation of matrix and chondrule melts. Second follows a further separation of chondrule melt, exposing in the chondrites a "chondrule in chondrule" structure. The tendency of concentric zone separation is found in some chondrules, where the more refractory part of the melt (corresponding to calcium type) crystallises in the outer zone, and the more magnesium - iron rich part crystallises in the inner zone (Fig.2). Characteristically, as temperature decreases, such iron enriched inner chondrules lose equilibrium and disintegrate into two phases. This produces droplets of metal rich phases (troilite, kamacite) in the silicate chondrule matrix. The same separation of metallic melt as small droplets is observed in the Fe - silicate matrix of the chondrite. These separation processes of the first and second type are clearly revealed in the chondrites owing to gradual solidification within the cooling melt. Similar processes of differentiation occur in the parent body of achondrites as the iron - pallasite core and the silicate shell separate. However, occasionally, droplet differentiation of silicate melt (usually found in chondrites) can be observed in achondrites. So, in the Yurtuk howardite (Fig.3) drop-like zones in the concentric-zone structure are distinguished in the coarse-grained plagioclase - pyroxenic mass, where an inner zone is much enriched in iron. Iron is isolated as the smallest droplets in a silicate matrix. It is necessary to supplement this comparison of chondrules and chondrite matrix with achondrites by considering the isotopic characterisation of the minerals. Chondrites form a sequence LL-L-H-C3 of decreasing $\delta^{18}O$ measured by isotopic analysis of oxygen in pyroxens. The oxygen isotopic composition of mesosiderites, eucrites, howardites, diogenites places them in the middle of this sequence between H and C3. Therefore we consider that these achondrites result from a chondrite melt with symbol HH. Thus the whole chondrite sequence is regarded as: LL-L-H-HH-C3. Another group of meteorites E-chondrites, obrites and ureilites do not fit in this sequence. The origin of ureilites

is probably connected with the separarion of fassaite and spinel chondrules from C3-melts. These chondrules are anomalously enriched in light oxygen isotope (160). Eucrites, howardites, mesosiderites, nucklites and shergottites are kept within the single crystallisation trend of isotopic fractionation.

Fig.1 The petrochemical diagram of Efremovka chondrite and achondrites. 1 - The matrix composition (M) and chondrules (I- magnesium type, II- magnesium-calcium, III- aluminium, IV-V- calcium types) chondrite Efremovka; 2 - achondrites composition.

Fig.2 Chondrule concentric-zone structure with the metallic drop separation in the inner zone (Efremovka chondrite).

Fig.3 Concentric-zone separation in the Yurtuk howardite.

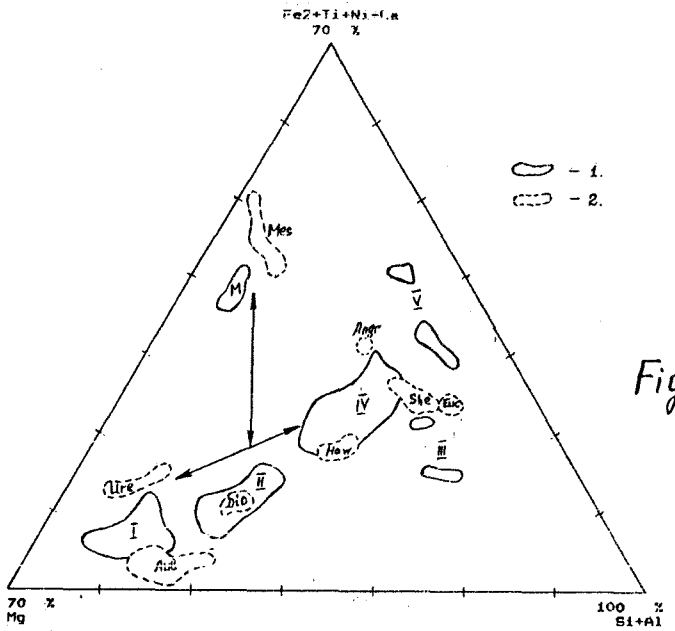

Fig.1

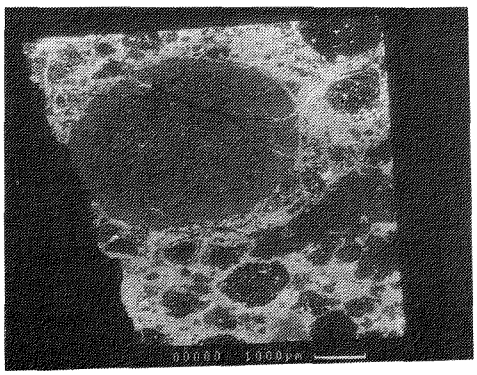

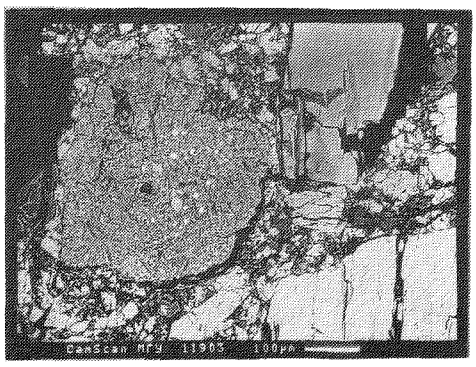

Catastrophe by Ocean and Continental Impacts from Shock Metamorphism

Yasunori MIURA[1], O.G.IANCU[1] and Keizo YANAI[2]

[1] Faculty of Science, Yamaguchi University, Yoshida, Yamaguchi 753, Japan.

[2] Department of Meteorites, National Institute of Polar Research, Kaga, Itabashi-ku, Tokyo, 173, Japan.

Almost all investigations of impact craters on the Earth are reported on dry continental rocks which show only excavated crater feature without major high shock metamorphism on fine ejecta. In order to get fine ejecta with high shock metamorphism, an artificial impact experiment in laboratory is inevitable to get all ejecta of shock metamorphism. Problem of global catastrophe of the Earth has to discuss on giant ocean-impact as well as dry land-impact, because sea covers 71 % of the crust surface. The main purpose of this study is to discuss global catastrophe from shock metamorphic data (mainly on formation of shocked quartz and its density-deviation) on various target rocks at the continents and ocean-floors [1,2,3].

1. Density-deviations at continental impact craters.

Shock metamorphism (mainly by density-deviation) of shocked silica materials is discussed in terrestrial continental impact craters of Canada, U.S.A., Australia and Germany, as listed in Table 1 [3].

Table 1. Samples from terrestrial continental impact craters used in this study.

Impact craters (Sample No.)	Diameter(km)	Target rock	Age (m.y.)
1) Barringer meteor crater, U.S.A. (13)	1.2	Sandstone	0.05
2) Sudbury, Ontario, Canada (31)	~140	Gneiss et al.	ca. 1850
3) Manicouagan, Quebec (21)	~100	Anorthosite	ca. 212
4) Charlevoix, Quebec (14)	~ 46	Granitic	ca. 360
5) Clearwater Lakes, Quebec (5)	~ 32(W)	Gneiss et al.	ca. 290
6) Mistastin, Nfl. (4)	~ 28	Anorthosite	ca. 38
7) Haughton, Nothern Ter. (2)	~ 20	Gneiss et al.	ca. 22
8) Teague Ring, W. Australia (5)	~ 28	Granite	1685
9) Gosses Bluff, NT (10)	~ 22	Sandstone	133
10) Connolly Basin, WA (5)	~ 9	Sandstone	60
11) Wolf Creek, WA (5)	~840(m)	Sandstone	0.5
12) Henbury, NT (10)	~157(m)	Sandstone	0.0042
13) Veevers, WA (5)	~ 80(m)	Sandstone	0.004
14) Dalgaranga, WA (5)	~ 24(m)	Sandstone	0.0003
15) Ries, Germany (5)	~ 24	Granite	14.8

Shocked quartz aggregates with mixed high-, normal- and low-density are co-existed with silica (or feldspar) glass materials by dynamic mixing process of terrestrial continetal impact craters. Shocked quartz with high density can be always formed in well-reserved terrestrial impact craters. Shocked silica polymorphic materials of stishovite, coesite and quartz with high density can be also obtained only at dynamic quenched process of shock metamorphism (Table 2). Coarse-grained (shocked) quartz formed by shock metamorphic evolution can be found at ejecta from large-size impact crater or along wall-rock of impact crater.

Table 2. List of shocked silica materials in terrestrial impact process including artificial impact craters [2].

Sample	Density ρ	$\Delta\rho$ (%)	Formation condition (P/T)
α-quartz	2.649	(0)	(Standard)
*Shocked quartz SQ	2.667	+0.8	Shock pressure (P)
*Shocked quartz LQ	2.638	-0.4	Shock temperature (T)
β-quartz	2.532	- 4.4	Temperature (T)
Tridymite	2.197	-17.1	Temperature (T)
Cristobalite	2.156	-18.6	Temperature (T)
Coesite	2.896	+ 9.3	Pressure (P)
*Shocked coesite	2.920	+ 9.8	Shock pressure (P)
Stishovite	4.290	+61.9	Pressure (P)
*Shocked stishovite	4.292	+62.1	Shock pressure (P)

* Shocked silica materials.

High values of density-deviation of shocked quartz (SQ) in the continental impact craters are summarized as follows (Table 3):

1) Shocked quartz aggregates at impact craters are very fine-grained (compared with hydrostatic and magmatic quartz crystal).
2) The lowest value of shocked quartz (LQ) is found at wall-rocks of Charlevoix impact structure ($\Delta\rho$=-0.4±0.1%).
3) The highest value of shocked quartz (SQ) is obtained at fine ejecta of the rim of the Barringer crater ($\Delta\rho$=+0.7±0.1%), which is not consistent with the size or age of the continental impact craters.
4) The density-deviation of the SQ grain does not show large value at old and large impact craters of Sudbury, Manicouagan, Acraman, Connolly and Ries. The main reason of difference in density-deviation of the SQ at impact craters is mainly due to different the sampling sites and weathering process of these impact craters.

2. Formation of fine shocked quartz by impact experiment

In order to elucidate formation of shocked quartz (SQ) by all types of impact, various samples of shocked quartz are collected at various sampling size and sampling site of impact experiments, which are summarized as follows (Table 4).

Table 3. High values of X-ray density-deviation of shocked quartz grains in representative terrestrial continental impact craters.

Sample	ρ (g/cm^3)	$\Delta\rho$	Shock Pressure(P)/ShockTemperature(T)
Standard			
Quartz(RC)	2.645(3)*	(Standard)	-
Barringer crater (U.S.A.)			
B-3W	2.664(6)	+0.7(2)	P
Clearwater lakes (Canada)			
DCW16429	2.656(0)	+0.4(1)	P
Lake Mistastin (Canada)			
LM-20-69	2.656(1)	+0.4(1)	P
Charlevoix (Canada)			
CH-11	2.655(1)	+0.4(1)	P
Sudbury impact structure (Canada)			
SBH144-1	2.653(1)	+0.3(1)	P
Dolgaranga meteorite crater (Australia)			
DR-43	2.653(2)	+0.3(1)	P
Gosses Bluff impact crater (Australia)			
GB-4MS	2.653(2)	+0.3(1)	P
Veevers impact crater(Australai)			
VR-23S	2.653(1)	+0.3(1)	P
Wolf Creek impact crater(Australia)			
WC-R-5S	2.654(3)	+0.3(1)	P
Henbury impact crater(Australia)			
HC-71-P	2.654(1)	+0.3(1)	P
Connolly Basin crater (Australia)			
CB-1WP	2.652(1)	+0.2(1)	P
Manicouagan impact crater (Canada)			
DMM (B)	2.648(2)	+0.1(1)	P
Lake Acraman impact crater(Australia)			
AC-7R	2.650(1)	+0.1(1)	P
Ries crater (Germany)			
R-2SV	2.651(1)	+0.1(1)	P

* Numbers in parentheses are standard deviation refering to the last decimal place of the data used for discussion.

1) The largest density-deviation of shocked quartz (SQ) is found only at fine ejecta (not wall-rock of impact crater).
2) All types of target-rocks can be formed shocked quartz (SQ) with high-density by impact experiments (Table 4).
3) It is found in this study that **silica-free rock** of basalt, gabbro and anorthosite can make fine shocked quartz (SQ) by impact (Table 4).

Table 4. Formation of shocked quartz from ocean-floor rocks of basalt, gabbroic anorthosite and some granite by steel projectile.

Target rocks	Density	Density-deviation	Ratio SQ/SF
1. **Basalt** (Ocean floor or Mantle rock)			
Original (before impact)	2.642(2)	(std.)	0.01
Fine ejecta (after impact)	2.646(2)	+0.16(6)	2.70
2. **Gabbroic anorthosite** (Silica-poor ocean or continetal rock)			
Original (before impact)	2.642(8)	(std.)	0.02
Fine ejecta (after impact)	2.651(2)	+0.33(6)	5.60
3. **Granite** (Continental or some ocean floor rock)			
Original (before impact)	2.640(1)	(std.)	1.6
Fine ejecta (after impact)	2.645(1)	+0.19(5)	3.0
4. **Sandstone** (Ocean sedimental or continental rock)			
Original (before impact)	2.645(1)	(std.)	(no SF)
Fine ejecta (after impact)	2.656(5)	+0.41(8)	-

3. Evidence of giant ocean-impact

Although Alvarez et al. (1980) [4] proposed that an asteroid (about 10km across) hitts the Earth 65 million years ago to result in global catastrophe bya titanic explosion and climate change, which is mainly discussed by high iridium contents from iron meteorite.

Bohor et al. (1984)[5] concluded that shocked quartz grains found in the K/T boundary layer come from **crystalline continental rocks**, because **sea-floor rock** has free silica and low-calcium type rocks.

The present result as listed in Table 4 indicates that shocked quartz can be formed at all types of target rocks including sea-floor rocks. Therefore, experimental results of synthesized shocked quartz from gabbroic, basaltic and anorthositic target rocks strongly suggest that feldspar-rich sea-floor rocks can make shocked quartz materials by titanic impact. The present result of formation of shocked quartz from sea-floor target rocks is consistent with the finding of ocean-impact crater at the K/T boundary near at Chicxulub, Yucatan by Hildebrand et al (1991) [6].

Moreover, global catastrophe at the end of Cretaceous period (K/T boundary) is analyzed by shock metamorphism of asteroid penetrating thin sea-floor probably until the upper mantle. Titanic explosion of asteroid disintegrated in a mass of exploding steam and vaporizing soil can be explained by " Phreatomagmatic (magmatic vapor) explosion" which create by abrupt boiling between high-temperature magma and cold sea-water after abrupt giant impact of asteroid to the ocean. The detailed study of magmatic vapor explosion by ocean impact is discussed the coming paper.

Main References:

[1] Miura Y. (1991): Shock Waves, 1, 35-41.
[2] Miura Y, Takayama K, Kato T, Kawashima N and Yamori A (1992): Proc. Shock Waves (Springer-Verlag), 18, 403-408.
[3] Miura Y and Takayama K (1993): Symp. Shock Waves (Japan), 2, 193-196.
[4] Alvarez LW, Alvarez W, Asaro F, Michel HV (1980): Science, 208, 1095-1108.
[5] Bohor BF, Foord EE, Modreski PJ and Triplehorn DM (1984): Science, 224, 867-869.
[6] Hildebrand AR, Penfield GT, Kring DA, Pilkington M, Camargo AZ, Jacobsen SB, and Boynton WV (1991): Geology, 19, 867-871.

Ejection Process from Shock Metamorphism of the Lunar and Martian Meteorites

Yasunori MIURA[1], Keizo YANAI[2] and O.G.IANCU[1]
[1]Faculty of Science, Yamaguchi University, Yoshida, Yamaguchi 753, Japan.
[2]Department of Meteorites, National Institute of Polar Research, Kaga, Itabashi-ku, Tokyo, 173, Japan.

Meteorite samples from the Moon, Mars and Asteroid belts have been found on the Earth's lands. But the detailed ejection process from the Moon or Mars is not known clearly so far. The main purposes in this study are to describe the shocked minerals of quartz, feldspar and graphite with high density in planetary materials, and to elucidate the probable ejection process of meteorites from the shock metamorphic investigation.

1. Shocked minerals on the Earth

Shocked silica aggregates with high density are one of the direct indicator of shock metamorphism [1]. The detailed investigation of shocked quartz in the terrestrial impact craters indicates the following results which can be used as standard data for planetary impact process (Table 1).

1) The value of density-deviation of shocked quartz is not correspond to the size of impact crater, if the samples are collected only from coarse-grained breccias or recrystallized rocks of the crater-wall.
2) The largest value of density-deviation of shocked quartz can be found in fine-grained ejecta of impact crater and K/T boundary samples.

Shocked plagioclases show almost diaplectic glassy without high-density phase though chemical composition of plagiocalse is easily changed after impact. This is the main reason why high density-values of crystalline parts of shocked plagioclase after impact event are greatly difficult to obtain in a single grain. The detailed data will be discussed the coming paper.

Shocked graphite which has not been previously reported can be found in Barringer crater and artificial impact craters as a state of fine-grained feature with complete mixing of iron metals [2,3]. But if the melted iron from iron meteorite is mixed at impact event, shocked carbon minerals of chaoite, lonsdaleite, and diamond can be remained by coating with iron-rich materials (as abrupt quenching materials) [2]. However as the weak structure of pure graphite (without mixing with any metals) can be easily broken after progressive weathering, shocked graphites are mostly difficult to use as standard shock metamorphism of ejection process.

Table 1. Density data of shocked quartz, plagioclase and graphite materials from Earth, Zagami SNC meteorites.

Sample	ρ (g/cm^3)	$\Delta\rho$	Locality	Others
1. Shocked quartz				
Quartz(RC)	2.645(3)*	[Standard]	Gifu, Japan	Rock Crystal
Earth B7	2.664(6)	+0.7(2)	Barringer, USA	On sandstone
Earth KT22	2.667(4)	+0.8(2)	CCN (USA)	Colorado
Mars ZQ-7	2.689(9)	+1.7(3)	Zagami SNC	Mars rock(?)
Moon	-	-		(Glassy)
2. Shocked coesite				
Earth B2W	2.920(10)	+0.5(3)	Barringer(USA)	Fine ejecta
3. Shocked plagioclase				
Mars ZP-6	2.77(4)	+2.4(4)	Zagami SNC	Mars Rock (?)
Moon Y86032	-	-		(Glassy)
4. Shocked graphite				
Earth BG2	2.459(1)	+0.6(1)	Barringer(USA)	Graphite+iron

* Numbers in parentheses are standard deviation refering to the last decimal place of the data used for discussion.

2. Ejection process of Martian rocks

There are two major formation processes of Martian SNC meteorites of (a) the same time of shock metamorphism and ejection from Martian surface (180 m.y.) and following collisions in space and cosmic ray exposure (0.6-11 m.y.), and (b) shock metamorphism by impact with extra-Martian bodies (180 m.y.) and ejection - cosmic ray exposure (0.6-11 m.y.).

From the following reasons obtained in terrestrial impact rocks, the formation process of Martian SNC meteorites is considered to be mainly by the above (a) process from maskelynite data, and the above (b) process from shocked quartz data.

1) The SNC meteorites are not the fine-grained aggregates but the coarse-grained meteorites (which can be found at terrestrial crater-walls).
2) High density-deviation of shocked quartz in Zagami achondrite could not be found in terrestrial impact craters. The anomalous high data of glassy shocked quartz grains indicate that primary Zagami meteorite are collided with other fragments in cosmic space (abrupt quenched condition after imapct).
3) Large maskelynite (i.e diaplectic plagioclase-like grains) can be found near at crater-wall of terrestrial impact craters. The anomalous data of SNC shocked plagioclases (in diaplectic maskelynite) indicate that large main maskelynite grains are formed by the primary impact of extra-Martian bodies at the Martian surface.

Thus it requires the following large impacts to excavate and eject as coarse-grained blocks (without major change of texture). The most probable ejection process of Zagamic SNC meteorites from Martian surface is summarized from the present shock metamorphic study as follows:

Table 2. Ejection process of Zagami SNC achondrite from Mars.

Main event	Age (m.y.)	Shocked metamorphism	Evidence
1) Major impact (excavation)	ca.180	Large maskelynite	Glassy plagioclase Large mass along wall
2) Ejection (excavation)	~ca.11	Less shock	Excavation by impact (as large mass)
3) Collision in space	~0.6	Shocked quartz	Abrupt quenching (in cold space)

3. Ejection process of the Lunar meteorites.

Lunar meteorite of Y-86032 shows typical breccia texture (as 73215, 63355, 15455 etc.) which reveals contains crystalline plagioclase in glassy plagioclase with different plagioclase-like matrix (i.e. breccia-in-breccia texture; Fig.1).

The following data indicate that the lunar meteorites are considered to be ejected by the large impact event from impact crater-wall.

1) Coarse-grained lunar meteorite is not direct high-speed ejecta from the center of impact crater. This is mainly because it contains few fine-grained shocked quartz from high-speed fine ejecta.
2) Coarse-grained diaplectic plagioclases (i.e. maskelynite) in the lunar meteorite are found near at crater-wall of terrestrial impact crater (not in fine-grained ejecta).
3) Breccia-in-breccia texture indicates two major stage of impact and mixting event (cf. Fig.1).
4) In order to get escape velocity from the lunar surafce at the impact event two major steps of impact events are required as listed in Table 3.

Table 3. Probable ejection process of lunar meteorite Y-86032.

Impact event	Shock metamorphism	Evidence
1) Large impact	Coarse diaplectic plagioclase	Breccia (plagioclase+ glassy plagio.)
2) Mixing of ejecta	Glassy matrix (of plagioclase-composition) with mafic minerals	Breccia-in-breccia texture
3) Small impact (with high speed and oblique impact)	Less shock feature	Coarse-grained breccias

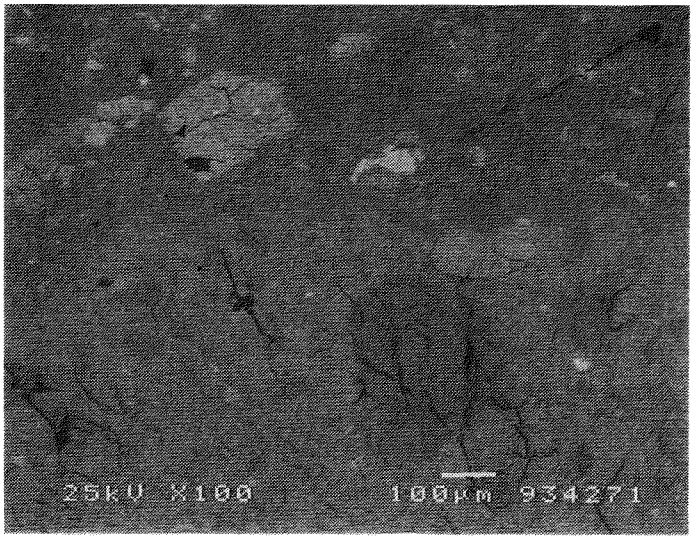

Fig. 1. Breccia-in-breccia texture of Y-86032 lunar meteorite. It contains crystalline plagioclase in maskelynite matrix which is surrounded by pyroxene mafic minerals in the maskelynite matrix.

Main References:

[1] Miura Y (1991): Shock Waves, 1, 35-41.
[2] Miura Y. (1992): Proc. Shock Waves (Japan), 2, 54-57.
[3] Miura Y et al. (1993): 18-NIPR Symposium (in this volume).

AMS C-14 AGES OF VARIOUS ANTARCTIC CHONDRITIC METEORITES

Y. MIURA[1], R.E. CRESSWELL[2], R.P.BEUKENS[2] and J.C. RUCKLIDGE[2]

[1] Faculty of Science, Yamaguchi University, Yoshida, Yamaguchi 753, Japan.
[2] IsoTrace Laboratory, University of Toronto, Toronto, M5S1A7, Canada

In order to discuss terrestrial age and terrestrial history of Antarctic meteorites, ^{14}C AMS terrestrial and weathering ages of various Antarctic chondrites will be reported in the 18th NIPR Symposium.

1. Experimental

Samples of 0.5g were crushed and measured using the ^{14}C sensitivity of the accelerator mass spectrometry (AMS) in Toronto. Carbon species of CO and CO_2 are separated at different temperatures, easpecially from a low temperature (500 to 900℃) to high temperature (~1600℃).

The zero age in this study is determined from saturated activity of ^{14}C in the Bruderheim L-6 chondrite, of mean value 54.6±0.5 dpm/kg.

2. Samples

The samples used in this study are eighteen chondrites : Y-74014 (H6), Y-74191(L3), Y-74647(H5), Y-75271(L5), Y-751500(H3), Y-790448(LL3), Y-791630(L4), Y-791717(CO3), Y-8011(L6), Y-81132(H5), Y-82095(L3), ALH-77231(L6), ALH-77232(H4), ALH-78112(L6), ALH-78130(L&), BTN-78002(L6), MET-78028(L6), and RKP-78002(H4).

Nine more Antarctic chondrite samples of Y-80, -81, -82, -84, and -86 series will be also added in this year.

3. Discussion

We will discuss the following questions in the 18th NIPR meeting, and compared with our results to earlier measurements of Antarctic chondrites [1,2].

Do the ^{14}C ages measured on eighteen chondrites (and 9 in preparation) show any differences?

(a) Are terrestrial ages of Yamato chondrites (1, 2, 3, 6, 11, 17, 24, 28 ka) older than Allan Hills chondrites (29, 30, 31, 34 ka), Bates Nunatak (15 ka), Meteorite Hills (24 ka), or Reckling Peak (22 ka)?
(b) What is the wide variation of terrestrial ages in Yamato chondrites?
(c) Are weathering and atmospheric exhanges in chondrites estimated from low temperature components?
(c) What is wide variation of ages in low temperature componenets of Yamato and Allan Hills chondrites?

References:

[1] Beukens R.P., Rucklidge J.C., and Miura Y. (1988): Proc. NIPR Symp. Antarctic Meteorites, 1, 229-230.
[2] Cresswell R.G., Miura Y., Beukens R.P., and Rucklidge J.C. (1993): Proc. NIPR Symp. Antarctic Meteorites (in press).

AMS C-14 AGES OF VARIOUS ANTARCTIC ACHONDRITIC METEORITES

Y. MIURA[1], A.J.T. JULL[2], E. CIELASZYK[2], D.J. DONAHUE[2], and K. YANAI[3]

[1] Faculty of Science, Yamaguchi University, Yoshida, Yamaguchi 753, Japan.
[2] NSF Arizona AMS Facility, University of Arizona, Tucson, AZ 85721, USA.
[3] National Institute of Polar Research, Kaga 1-9-10, Itabashi, Tokyo 173, Japan.

In order to discuss pairing problem and terrestrial history of Antarctic meteorites, ^{14}C AMS terrestrial and weathering ages of Antarctic achondrites will be reported in the 18th NIPR Symposium.

1. Experimental

Samples of 0.2-1.0g were crushed and measured using the ^{14}C sensitivity of the accelerator mass spectrometry (AMS) in Tucson. For heavily weathered samples, the carbonates are removed with an acid etch. For cosmogenic ^{14}C, the sample is melted with iron, in a flow of oxygen.

The zero age is determined from saturated activity of ^{14}C in the Bruderheim L-6 chondrite, of mean value 51.1±1.4 dpm/kg.

2. Samples

The samples used in this study are seven eucrites: Y-790007,72; Y-791186,51; Y-791960,52; Y-791962,50; Y-790260,90; Y-792510,95 and Y-82082,64; three diogenites: Y-74037,88, Y-74010,81 and ALH-77256,93. Nine more achondrite samples will be added in this research project.

3. Discussion

We will discuss the following questions in the 18th NIPR meeting, and compared with our results to earlier measurements of Antarctic achondrites [1].

Do the ^{14}C ages measured on 7 (and 6 in preparation) eucrites and 3 (and 4 in preparation) diogenites show any differences?

(a) Are Eucrites (5, 20, 25, 30, 35ky) older than diogenites (10, 15ky)?
(b) What are the pairing groups of eucrites ? (5, 20, 25, 30, 35ky)?
(c) What is the depth profile in an eucrite (ca. 2ky high in 5mm deeper inside)?
(d) Are AMS ages of A and B type diogenites the same ?

We will discuss the following questions of other Antarctic achondrites:

(a) Do the ^{14}C AMS ages of Antarctic howardites and Ureilites show any difference?
(b) The proposed samples are 7 howardites (Y-7308, Y-790727, Y-82091, Y-793497, Y-82052, Y-791448, Y-791492) and 2 Ureilites (Y-790981, Y-791538).
(c) New data of pairing and planetesimals structure are discussed by new AMS ages from Y-73 to Y-82 samples.

References:

[1] Jull A.J.T., Miura Y., Cielaszyk E., Donahue D.J. and Yanai K. (1993): Proc. NIPR Symposium (in press).

NOBLE GASES IN YAMATO-75097, -793241 AND -794046 CHONDRITES WITH IGNEOUS INCLUSIONS

Keisuke NAGAO
Institute for Study of the Earth's Interior, Okayama University, Misasa, Tottori-ken 682-01, Japan.

Noble gas isotopic compositions were measured for host and clast materials taken from Y-75097(L6), Y-793241(L6) and Y-794046(H5), which have igneous inclusions. Cosmic-ray exposure ages were calculated using the formula by Eugster (1988) and Schultz et al. (1991). The production rates for Y-793241 and Y-794046 were corrected using the chemical compositions by Fukuoka (1993) and Nakamura (1993). Ca concentration by Nakamura (1993) was used to calculate P38 for the clast of Y-75097 (Table 2). K-Ar ages were calculated based on the K concentrations by Fukuoka (1993) and Nakamura (1993). The ages were concordant between the host and clast of each meteorite, i.e., 0.49-0.60, 4.3-4.4 and 1.9-2.0 Ga for Y-75097, Y-793241 and Y-794046, respectively (Table 2).

Y-75097 and Y-793241 Similar cosmic-ray exposure ages (23-25 Ma) are obtained for both the hosts and clasts from Y-75097 and Y-793241 (Table 2), which imply close relationship between the two meteorites in respect to the history of cosmic-ray exposure. Unusually high $^{129}Xe/^{132}Xe$ ratios of 49.7 and 47.2 were observed in the clasts from Y-75097 and Y-793241, respectively. Excess ^{80}Kr, ^{82}Kr and ^{128}Xe produced by neutron capture reaction of Br and I were found in both the clasts. Fissiogenic ^{136}Xe ($2.6 \times 10^{-12} cm^3 STP/g$) was found only in the clast from Y-75097. Since U concentration of this inclusion has not be determined, the progenitor of the fission Xe is not clear at present. The results suggest that both the inclusions were closely related genetically with each other and might have been in a common parent body. The parent body was heavily fractionated and degassed before extinction of ^{129}I, resulted in low concentrations in noble gases, metals and Ca (Fukuoka, 1993) and in enrichments in halogens. Concordant K-Ar ages between host and clast for each meteorite indicate that thermal events resetting K-Ar system were occurred on the host meteorite parent body (or bodies) after emplacement of the inclusions in the host materials. Accordingly, the parent body of the inclusions must have broken up and ejected fragments until 4.3 Ga ago, or the parent body impacted L6 asteroid at that time. Short K-Ar ages (0.49-0.60 Ga) for Y-75097 correspond to the second thermal event, which did not affect the K-Ar system of Y-793241. If the two thermal events occurred on separate parent bodies, the identical exposure ages for two meteorites are hard to expect. Alternatively, if the meteorites were ejected from a single parent body by an impact event, the L6 parent body seems to be heterogeneous with respect to the thermal history.

Y-794046 Cosmic-ray exposure ages of about 3 Ma were calculated based on the cosmogenic ^{21}Ne and ^{38}Ar. Short exposure ages (1.1 and 1.0 Ma) obtained from the cosmogenic ^{3}He indicate a He loss from the meteorite. The Xe isotopic compositions in the clast are similar to the atmospheric values, and no fissiogenic Xe is observed. Cosmogenic ^{21}Ne concentration is higher than the value expected from chondritic chemical compositions, which implies an enrichment in Mg. This is confirmed by the chemical compositions for the clast by Fukuoka (1993). Although the noble gas compositions in the clast suggest material similar to diogenites, the high K content (Table 2) and other elemental concentrations (Fukuoka, 1993) do not agree with the chemical compositions of diogenites.

Table 1. Noble gas isotopic compositions of Y-75097, Y-793241 and Y-794046.

Sample	$^{4}He^{1)}$	$^{3}He/^{4}He$ (10^{-4})	$^{20}Ne^{1)}$	$^{20}Ne/^{22}Ne$	$^{22}Ne/^{21}Ne$	$^{36}Ar^{1)}$	$^{40}Ar^{1)}$	$^{38}Ar/^{36}Ar$	$^{40}Ar/^{36}Ar$	$^{84}Kr^{2)}$	$^{132}Xe^{2)}$	$^{129}Xe/^{132}Xe$
Y-75097												
Host	338	1083	8.01	0.8431	1.0743	2.32	240	0.5032	103.45	61.4	56.0	1.19
(113.1mg)		± 9		±.0018	±.0035			±.0005	± .08			± .02
Clast	271	1407	9.43	0.8435	1.0601	0.645	205	1.0175	317.69	16.2	7.5	49.7
(56.5mg)		±14		±.0016	±.0037			±.0017	± .32			±1.3
Y-793241												
Host	1750	227	5.99	0.8158	1.1945	1.30	6110	0.7158	4711	62.9	50.2	1.14
(86.3mg)		± 2		±.0016	±.0043			±.0014	±10			± .02
Clast	268	1457	7.06	0.8252	1.1972	0.390	3550	1.3264	9105	36.6	14.3	47.2
(113.2mg)		±12		±.0016	±.0043			±.0051	±60			± .7
Y-794046												
Host	33.1	529	0.891	0.8583	1.0853	0.500	577	0.3722	1154.0	57.6	87.9	1.34
(133.0mg)		± 5		±.0023	±.0047			±.0004	± 1.2			± .01
Clast	18.3	953	1.48	1.0164	1.1064	0.220	2280	0.7265	10350	73.1	22.5	0.99
(185.9mg)		± 8		±.0030	±.0039			±.0048	±100			± .02

1) $10^{-8}cm^{3}STP/g$, 2) $10^{-12}cm^{3}STP/g$.

Table 2. Cosmic-ray exposure and K-Ar ages.

	^{3}He	^{21}Ne	^{38}Ar	P3[1]	P21[1]	P38[2]	T3	T21	T38	K	K-Ar age
	$10^{-8}cm^{3}STP/g$			$10^{-8}cm^{3}STP/g/Ma$			Ma			ppm	Ga
Y-75097											
Host (L6)[3]	36.6	8.84	0.834	1.63[4]	0.396[4]	0.0414[4]	22.5	22.3	20.1	863$	0.60
Clast	38.1	10.55	0.610	1.60[5]	0.398[5]	0.0457[5]	23.8	26.5	13.4	938$	0.49
						(0.0251)[7]			(24.3)		
Y-793241											
Host (L6)[3]	39.8	6.15	0.782	1.57[6]	0.239[6]	0.0350[6]	25.4	25.8	22.4	870#	4.3
Clast	39.1	7.15	0.506	1.58[6]	0.270[6]	0.0231[6]	24.7	26.5	21.9	520$	4.3
						0.0200[7]			25.3	490#	4.4
Y-794046											
Host (H5)[3]	1.75	0.957	0.105	1.57[6]	0.333[6]	0.0411[6]	1.11	2.87	2.56	400#	2.0
Clast	1.75	1.32	0.135	1.68[6]	0.369[6]	0.0462[6]	1.04	3.58	2.92	1783$	1.9
										1760#	1.9

1) Production rates by Eugster (1988); 2) Production rate by Schuitz et al. (1991); 3) Hutchison (1993); 4) Chemical compositions of L-chondrite were assumed; 5) Chemical compositions of H-chondrite were assumed; 6) Chemical compositions by Fukuoka (1993) were used; 7) Ca concentration by Nakamura (1993) was used; $ Nakamura (1993); # Fukuoka (1993).

NOBLE GASES IN YAMATO-75097 INCLUSION: SIMILARITIES TO BRACHINITES (ONLY?). U. Ott, H.P. Löhr and F. Begemann. Max-Planck-Institut für Chemie, Saarstraße 23, D-6500 Mainz, F.R.G..

Because of our interest in Brachina and its relatives [1,2], we obtained from NIPR for noble gas analysis a sample from an inclusion in the L6 chondrite Y 75097 that, based on textural and mineralogical observations, had been described as being Brachina-like [3].

Results of our analysis are given below (Tables 1 and 2), together with data from a re-analysis of Brachina that we performed because of problems with Kr and Xe in our first analysis [1]. Also listed are the data for ALH 84025 [2].

Table 1. He, Ne and Ar in Yamato 75097 inclusion and brachinites. Concentrations in units of 10^{-8} cm³ STP/g.

Temp.	^{3}He	^{4}He	^{21}Ne	$\frac{^{20}Ne}{^{22}Ne}$	$\frac{^{21}Ne}{^{22}Ne}$	^{36}Ar	$\frac{^{38}Ar}{^{36}Ar}$	^{40}Ar
Y75097 inclusion I-1 (54 mg)								
800°C	5.23	84.2	0.248	1.042	0.908	0.0369	0.523	12.2
	±.21	±3.0	±.006	±.012	±.006	±.0034	±.033	±1.3
1800°C	32.4	267	10.5	0.847	0.947	1.61	0.376	111
	±1.3	±10	±.3	±.004	±.006	±.11	±.009	±8
total	37.6	351	10.7	0.851	0.946	1.65	0.379	124
	±1.3	±10	±.3	±.004	±.006	±.11	±.009	±9
Brachina B-1 (94 mg)								
800°C	1.97	146	0.0511	0.952	0.655	0.246	0.211	1033
	±.08	±4	±.0020	±.072	±.008	±.013	±.017	±83
1800°C	2.61	103	0.805	0.879	0.848	4.78	0.2054	1244
	±.11	±3	±.030	±.006	±.007	±.09	±.0015	±25
total	4.58	249	0.856	0.885	0.834	5.03	0.2057	2277
	±.14	±4	±.030	±.008	±.007	±.09	±.0017	±91
ALH 84025-P1 (32 mg)								
800°C	1.97	39.7	0.0107	2.5	0.643	0.113	0.29	26.8
	±.09	±1.7	±.0003	±1.4	±.038	±.019	±.14	±1.8
1800°C	16.6	159	3.84	0.893	0.919	2.71	0.492	47.5
	±.7	±7	±.07	±.008	±.009	±.18	±.012	±3.1
total	18.6	199	3.85	0.900	0.918	2.82	0.484	74.2
	.8	±7	±.07	±.009	±.009	±.18	±.012	±3.6

The ^{21}Ne cosmic ray exposure age of the Y 75097 inclusion, based on the production rate of Eugster [4], is 25 Ma, which is ca. 8 and 3 times longer than the exposure ages of Brachina and ALH 84025, respectively. Note that in this calculation we have applied no correction for chemical composition and that the ratio of cosmogenic ^{22}Ne to ^{21}Ne (1.06) is at the lower end of what is found in meteorites so that the empirical, $(^{22}Ne/^{21}Ne)_c$-based, shielding correction is uncertain and the ^{21}Ne exposure age may be too low. The close agreement with the corresponding exposure age based on ^{3}He (23 Ma) suggests, however, that such effects are

only minor. The abundance of ^{40}Ar falls far short (≤ 3%) of what will be produced within 4.5 Ga from a K content of ca. 700 ppm ([5]; cf. also [3]). Possibly the event that disturbed the Ar-Ar system in the host meteorite about 490 Ma or less ago [6] also significantly affected the inclusion, possibly leading to virtually complete loss of all radiogenic ^{40}Ar produced previously. A feature shared with ALH84025 but very few other stone meteorites is that $^{40}Ar/^{4}He_{rad}<1$.

Table 2. Krypton and xenon in Yamato 75097 inclusion and brachinites. Gas abundances in units of 10^{-12} cm³ STP/g.

Temp.	^{84}Kr	$\frac{^{80}Kr}{^{84}Kr}$	$\frac{^{82}Kr}{^{84}Kr}$	^{132}Xe	$\frac{^{128}Xe}{^{132}Xe}$	$\frac{^{129}Xe}{^{132}Xe}$	$\frac{^{136}Xe}{^{132}Xe}$
Y75097 inclusion - I1							
800°C	1.31	0.0839	0.227	0.889	0.090	1.183	0.322
	±.26	±.0132	±.020	±.143	±.044	±.068	±.017
1800°C	8.18	2.169	1.130	4.06	0.468	84.9	0.474
	±.45	±.064	±.033	±.34	±.025	±5.0	±.015
total	9.49	1.881	1.005	4.95	0.400	69.8	0.447
	±.52	±.075	±.036	±.37	±.024	±4.7	±.013
Brachina B-1							
800°C	54.6	0.0442	0.2066	5.25	0.0792	1.730	0.324
	±1.6	±.0011	±.0025	±.33	±.0045	±.037	±.009
1800°C	165	0.0439	0.2072	49.3	0.0854	7.489	0.318
	±5	±.0010	±.0020	±2.5	±.0011	±.057	±.002
total	220	0.0440	0.2070	54.5	0.0848	6.935	0.318
	±5	±.0008	±.0016	±2.5	±.0011	±.066	±.002
ALH 84025-P1							
800°C	31.4	0.0432	0.2102	4.08	0.084	1.030	0.324
	±1.5	±.0027	±.0070	±.50	±.020	±.026	±.014
1800°C	58.2	0.2499	0.2828	31.3	0.1286	7.048	0.3159
	±3.1	±.0051	±.0070	±.9	±.0033	±.113	±.0030
total	89.6	0.1774	0.2573	35.4	0.1235	6.354	0.3169
	±3.5	±.0048	±.0053	±.9	±.0037	.126	±.0032

The trapped gases are exceedingly low in abundance. Kr and Xe are even lower than in chondrites of type 6 such as the H6 Estacado [7]. We do not believe that this is due to a loss of trapped gases, however, together with ^{4}He and ^{40}Ar because, first, trapped gases appear always to be rather tightly bound and, second, because radiogenic $^{129}Xe^{*}$ occurs at an abundance of $\sim 3.4\times10^{-10}$ cm³STP/g, similar to Brachina (3.2×10^{-10}) and ALH 84025 (1.9×10^{-10}). Accordingly, the ratio $^{129}Xe/^{132}Xe$ is extremely high, reaching 85 in the second (1800°C) extraction step. Because of the low abundance of trapped gases, fissiogenic contributions to ^{136}Xe also clearly show up in the Y 75097 inclusion (Table 2). The inferred ratio $^{129}Xe^{*}/^{136}Xe_{f}$ of ~500 is compatible with the lower limit of 300 inferred for Brachina ([1]; cf. Table 2).

The low abundance of trapped gases is also responsible for the clear signature ehibited by the products of neutron capture on bromine and iodine that show up as excesses in the Kr isotopes 80 and 82 as well as in ^{128}Xe, leading to such extreme values as $^{80}Kr/^{84}Kr \approx 2.2$, ca. 55 times higher than the normal trapped value (Table 2). Concentrations of the neutron capture products are similar in the Yamato 75097 inclusion to what is observed in ALH 84025, but similar values are also found in some chondrites [8]. In Brachina they are smaller, but if production occurred during the recent exposure to cosmic rays as a meteoroid, the difference can be explained by differences in exposure age, shielding and Br and I concentrations. An attempt to determine Br and I in the inclusion is underway.

The elemental abundance pattern of Ar, Kr, Xe (Tables 1,2; cf. discussion in [1]) of the Y 75097 inclusion is similar to that of the brachinites. This conclusion rests primarily on the $^{84}Kr/^{132}Xe$ ratio, however, because $^{36}Ar/^{132}Xe$ (nominal value, ie. corrected for spallogenic contributions only:~2900) may be enhanced due to an (unknown) contribution to ^{36}Ar from neutron capture on ^{35}Cl, similar to the case of $^{80,82}Kr$ and ^{128}Xe.

The Yamato 75097 inclusion exhibits, relative to Brachina and its sibling ALH 84025, similarities based on textural, mineralogical and chemical grounds [3,5]. The noble gas data indicate similar abundance of radiogenic $^{129}Xe^*$, similar $^{129}Xe^*/^{136}Xe_f$ ratio and similar elemental abundance pattern of the heavy rare gases. While not conclusive, the noble gas data thus certainly do not contradict an association with the brachinites. On the other hand, the systematics of oxygen isotopes appears to suggest that it is clearly distinct [9,10]. An association with H chondrites as suggested by the oxygen isotopes seems, however, extremely difficult to reconcile with the noble gas data, at least if a similarity to <u>bulk</u> H chondrites is sought. While L- and LL-chondrites often show $^{84}Kr/^{132}Xe$ high compared to the normal planetary ratio of ~1, H chondrites usually are at the lower end of the planetary range [7,11,12]. Nor do bulk ordinary chondrites show such high ratios $^{129}Xe/^{132}Xe$, because, as noticed in [12], radiogenic $^{129}Xe^*$ and trapped ^{132}Xe seem to have been lost to almost equal extent during metamorphism so that there is very little variation of their ratio among the different chondrite groups.

The situation may be different if the Y 75097 inclusion is compared to individual <u>constituents</u> of the chondrites, such as chondrules. Hutchison and coworkers have found a 'pebble' of H-chondritic composition within the Bärwell L chondrite [13] and suggest that the formation of this clast may be related to the formation of chondrules. They also point out other cases of H-chondritic material in L chondrite meteorites including the case of the Y 75097 inclusion of interest here. It is certainly interesting to consider a possible relation to chondrules also in this case, based on a comparison of noble gas patterns. It turns out that, based on what little data there are available, such a

connection would appear to be possible. Quite similar to the Y 75097 inclusion, chondrules are usually characterized by low abundances of trapped xenon and high $^{129}Xe/^{132}Xe$, and the concentration of radiogenic $^{129}Xe^*$ found in the Y 75097 inclusion falls well within the range of what has been observed in chondrules (e.g. [14,15]). The same is true for Brachina and ALH 84025. Unfortunately, to the best of our knowledge, there are no data reported in the literature for chondrules that would allow to check for similarities in the elemental abundance pattern.

Such a connection appears not necessarily in contradiction to the oxygen isotopes which show Y 75097 plotting close to the H chondrites and Brachina removed from them, since oxygen isotopes in OC chondrules show a complex behaviour [16] and the position of the Brachina points appears not inconsistent with a position at the lower left end of the OC chondrule field. Further work trying to establish (or disprove) the possibility of a link between the brachinites (including the Y 75097 inclusion) and the chondrules is certainly worth of being pursued.

References 1. Ott U., Löhr H.-P. and Begemann F. (1985) Meteoritics 20, 69-78. 2. Ott U., Löhr H.P. and Begemann F. (1987) Meteoritics 22, 476-477. 3. Yanai K., Matsumoto Y. and Kojima H. (1984) Proc. 8th Symp. Antarct. Meteor. 1983, 29-35. 4. Eugster O. (1988) GCA 52, 1649-1662. 5. Warren P.H. and Kallemeyn G.W. (1987) LPS XVIII, 1056-1057. 6. Kaneoka I., Takaoka N. and Yanai K. (1987) Proc. NIPR Symp. Antarct. Meteor. 1, 206-214. 7. Moniot R.K. GCA 44, 253-271. 8. Eugster O., Michel Th., Niedermann S., Wang D. and Yi W. (1993) GCA 57, 1115-1142. 9. Mayeda T.K., Clayton R.N. and Yanai K. (1987) Proc. 11th Symp. Antarct. Meteor. 1986, 144-150. 10. Clayton R.N., Mayeda T.K., Goswami J.N. and Olsen E.J. (1991) GCA 55, 2317-2337. 11. Schelhaas N., Ott U. and Begemann F. (1990) GCA 54, 2869-2882. 12. Schultz L., Weber H.W. and Begemann F. (1990) Meteoritics 25, 405-406. 13. Hutchison R., Williams C.T., Din V.K., Clayton R.N., Kirschbaum C., Paul R.L. and Lipschutz M.E. (1988) EPSL 90, 105-118. 14. Caffee M.W., Hohenberg C.M. and Swindle T.D. (1982) Proc. 13th Lunar Planet. Sci. Conf., JGR 87 Suppl., A303-A317. 15. Swindle T.D., Caffee M.W. and Hohenberg C.M. (1988) GCA 52, 2215-2227. 16. Grossman J.N., Rubin A.E., Nagahara H. and King E.A. (1988) In: Meteorites and the Early Solar Sstem (eds. J.F. Kerridge and M.S. Matthews), pp. 619-659. University of Arizona Press, Tucson.

NITROGEN ISOTOPIC COMPOSITION OF THE LUNAR METEORITE ASUKA-31, Naoji Sugiura, Department of Geophysics, Univ. of Tokyo, Tokyo, Japan.

Introduction: Nitrogen isotopic composition is quite variable among solid bodies in the solar system, and therefore is a useful tracer of formation histories of planets, satellites and asteroids. The relationship between the Earth and the Moon has been debated for many years, and now the view that the moon was formed by an giant impact on the Earth is favored. Oxygen isotopic composition of the Moon and the Earth is identical and seems to be consistent with the giant impact hypothesis. Nitrogen isotopic composition of the moon, if determined accurately, will be a strict constraint on this issue. It is, however, quite difficult to make an accurate measurement of the nitrogen isotopic composition of lunar samples, because the nitrogen abundance is very small. A recent study [1] of lunar soil samples suggested that the lunar nitrogen is isotopically normal, i.e. close to the air nitrogen isotopic ratio. This nitrogen, however, is a surface correlated nitrogen and its origin seems debatable. It is desirable to make isotopic composition measurement of nitrogen which is trapped in rock forming minerals. Aiming at solving this problem, the nitrogen isotopic composition of Asuka-31 meteorite, which is a coarse-grained gabbro, was measured.

Results: The nitrogen abundance and the isotopic composition obtained by the stepped combustion method from plagioclase grains in Asuka-31, are shown in the figure. A large amount of nitrogen released at 500 C and below is most likely organic contamination. An isotopically heavy nitrogen, released at the highest temperatures are cosmogenic nitrogen mixed with some normal nitrogen. Thus if indigenous lunar nitrogen is present, its isotopic signature should be seen at an intermediate temperature range, from 700 C to 900 C. The nitrogen isotopic composition observed in this temperature range is identical to that of the terrestrial air nitrogen (within the uncertainty of our system).

Discussion: The result, at the face value, is consistent with a common origin of the Moon and the Earth. However, the abundance of nitrogen (0.02 ppm per step) is not far from the hot blank (0.005 ppm per step), and if a small amount of organic nitrogen with a nearly normal isotopic composition persisted to the 700 C to 900 C temperature range, it could well explain the measured value. Thus, my conclusion is that there is not abundant, isotopically anomalous nitrogen in the lunar meteorite Asuka-31.

Reference: 1. Kerridge J.F.,Eugster O.,Kim J.S. and Marti K. Proc. Lunar Planetary Sci. 21, 291-299.

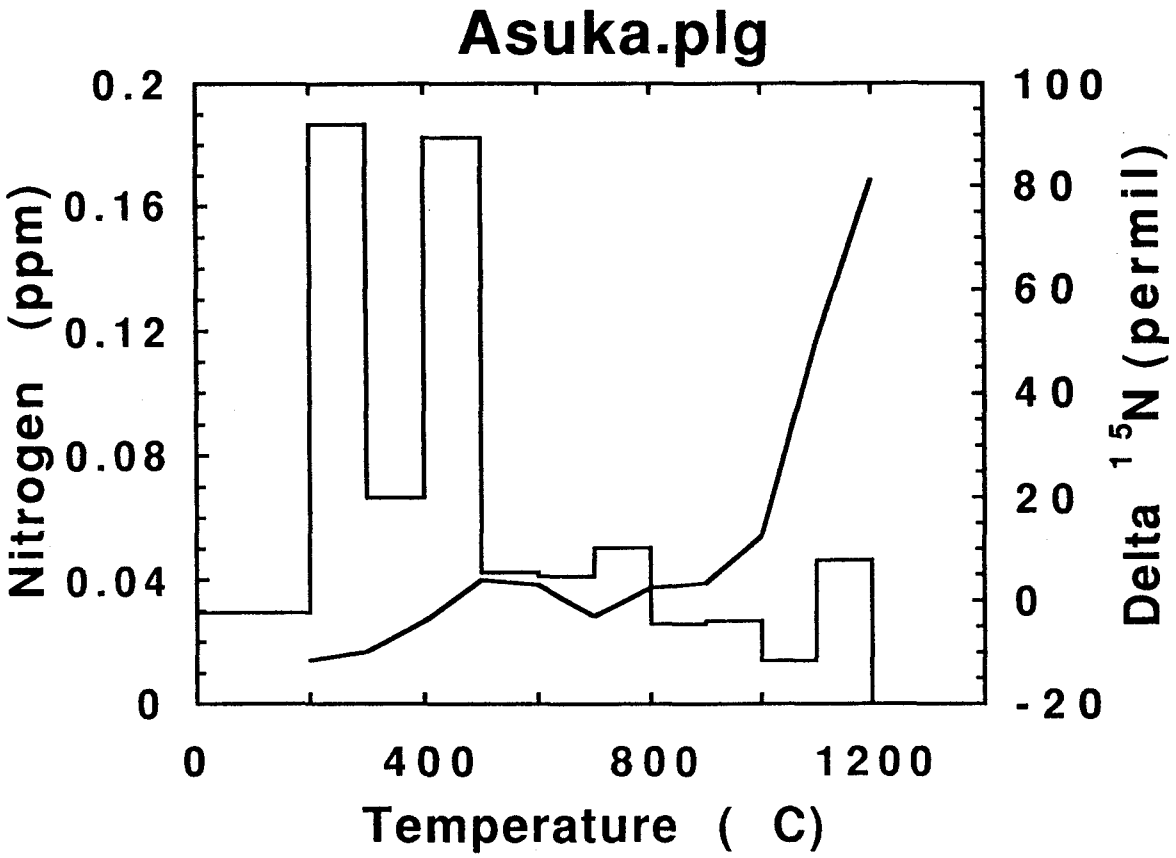
Asuka.plg
Nitrogen (ppm)
0.2
0.16
0.12
0.08
0.04
0
Delta ^{15}N (permil)
100
80
60
40
20
0
-20
0
400
800
1200
Temperature (C)

REE ABUNDANCES AND CHRONOLOGY OF ASUKA-881757 LUNAR METEORITE.

Kazuya Takahashi and Akimasa Masuda*. The Institute of Physical and Chemical Research Wako-shi, Saitama 351-01, Japan (*University of Electro-Communications, Chofu, Tokyo 182, Japan)

More than ten Antarctic meteorites have been recognized as the lunar meteorite. Many of them were classified anorthositic breccias and they are considered to have been originated from lunar highlands. Recently, several meteorites were identified as mare gabbros or basaltic breccias. Aska-31(Asuka-881757) is one of lunar meteorites with mare origin. According to Yanai and Kojima[1] and Lindstorm et al.[2], this meteorite is a new type of lunar sample (a very coarse-grained mare gabbro) and have the bulk chemical compositions and trace element abundances close to very-low-titanium mare basalt.

We were allocated Asuka-881757 SubNo.85 and SubNo.104 for REE (rare earth elements) measurements and Rb-Sr isotopic analyses. For SubNo.85, we analyzed REE abundances and Rb-Sr isotopic system as a whole rock sample and we separated SubNo.104 into mineral fractions by hand-picking under binocular. We have analyzed whole rock sample and each mineral separation.

Our results may be summarized as follows.

1. The Rb-Sr age of A-881757 is 3.75 ±0.07 Ga (I_{Sr}= 0.69912 ±0.00004). -----Fig. 1
2. The Sm-Nd age of A-881757 is 3.82 ±0.09 Ga (I_{Nd}= 0.50803 ±0.00009, ε_{Juv}(3.82Gyr.)=+7.5 ±0.2). -------Fig. 2
3. A-881757 has a smooth REE pattern and is L-REE depleted with a small Eu anomaly and no Ce anomaly). --------Fig. 3
4. The REE pattern can be explained by large scale (about 15 - 20%) partial melting process in the lunar lower mantle, and the calculated Sm/Nd ratio of source material is 0.45. -------Fig. 4
5. From Sm-Nd isotopic data, the assumed source material would also have L-REE depleted pattern (calculated Sm/Nd ratio is 0.49). This is consistent with the above estimation.

The REE abundance patterns of whole rock is consistent with the hypothesis that Asuka-881757 is mare origin. It is notable that no Ce anomalies are observed for Asuka-881757. For lunar highland samples and lunar meteorites with highland origin, various degrees of positive Ce anomalies have been found[3], [4]. The fact that Ce anomalies was not observed in Asuka-881757 could not become the evidence of mare origin, but it will give us suggestive data concerning the origin of Ce anomalies occurring in lunar highland samples.

According to previous studies by many workers for lunar mare samples, low titanium basalt yielded Rb-Sr ages around 3.2-3.6 Gyr. The above ages around 3.7-3.8 Gyr. is slightly older than the ages generally known for mare basalts. Therefore, there would remain some suspicion about the lunar mare origin for Asuka-881757 or it is possible that this lunar meteorite belongs to new type of mare samples.

References

[1]Yanai, K. and Kojima, H. (1991): Proc. NIPR 15th Sym. Ant. Met., 118-130.
[2]Lindstrom, M.M., Mittlefehldt, D.W. and Martinez, R.R.(1991): NIPR 16th Sym. Ant. Met., 102-105(abstract).
[3]Masuda, A., Nakamura, N., Kurasawa, H. and Tanaka, T.(1972) Proc. Lunar Sci. Conf., 3rd 1307-1313.
[4]Takahashi, K. and Masuda, A. (1987) Proc. NIPR 11th Sym. Ant. Met., 71-88.

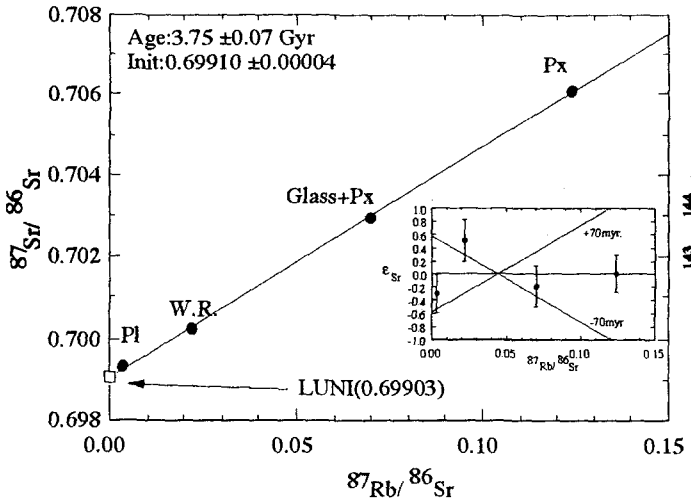

Fig.1 The Rb-Sr isochron plot for Asuka-881757

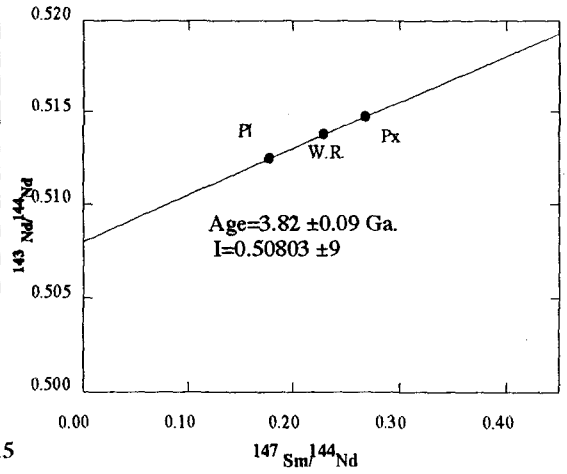

Fig.2 The Sm-Nd isochron plot for Asuka-881757

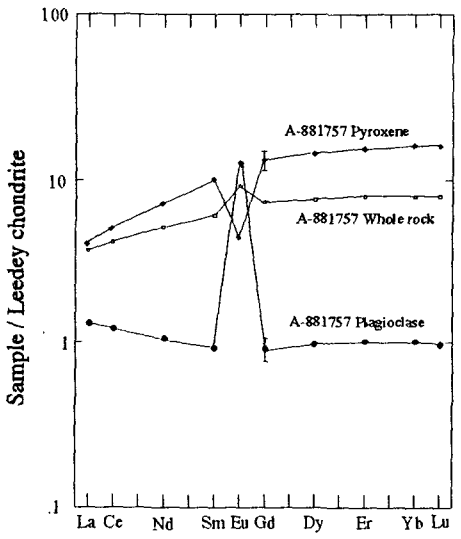

Fig. 3 REE abundance patterns for the samples from Asuka-881757

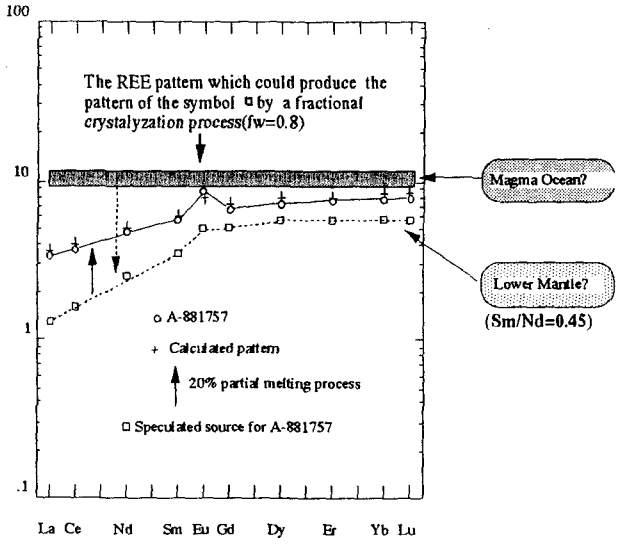

Fig. 4 The REE abundance pattern of the assumed source for Asuka-881757

THE ABLATION PRODUCTS OF THE METEORITE FUSION CRUST; POSSIBLY SOURCES OF MICROMETEORITES.

Marek ZBIK. South Australian Museum. North Terrace, Adelaide 5000 S. AUSTRALIA.

The interaction between a meteoric body and the atmosphere, which results in visible phenomena, occurs in the upper atmospheric layers. As the body penetrates to lower, and correspondingly denser layers of the air, lattice destruction increases as the surface layer of the meteor is heated up to many thousands of degrees, resulting in it being vaporized and melted. An envelope of hot gases and plasma surrounds the meteoritic body, accompanied by considerable compression of the air in front of it. Under pressure from the oncoming air stream the molten matter on the surface of the meteoritic body is constantly blown off (ablated) and sprayed into tiny droplets, some of which are immediately vaporized, while some solidify, forming tiny solid spherules. These spherules of various compositions accumulate in the soil layer at the planetary surface.

Most of a meteoroid's mass is ablated during its passage through the atmosphere and is transformed into small glassy spherules, irregular glassy fragments, and tiny mineral dust particles. Most investigations concentrate on the meteorite core material and treat the fusion crust as of minor importance but during its passage through the atmosphere 0.9 of a meteorite's mass is transformed into glassy fusion crust, blown off and spread over the planetary surface (1). From concentrations of nickel-iron particles in antarctic snows and deep-sea drill cores, it has been estimated that the Earth accumulates up to 200 tons per day of these micrometeoroids and meteoritic dust.

It is currently not clear what proportion of micrometeorites are the ablation products of larger meteoroids. It has been suggested some micrometeorites are interplanetary dust particles (IDPs), which are thought to be the most primitive of particles in the solar system, having not been altered by the processes of accretion since their formation at the beginning of the solar system. These are broken up into small fragments as they pass through the atmosphere, and, as they are very fragile and friable, soon decompose on the Earth's surface.

Recently a wide range of micrometeoritic material has been collected from the Antarctic and Greenland ice sheets (2,3,4,5,6,7) and analysis of this material has shed new light on the flux on extraterrestrial material reaching earth

To find the resolution of this problem, seven different meteorites were studied. Compositions of the silicate minerals were determined with a JEOL electron microprobe at the University of Adelaide Centre for Electron Microscopy and Microbeam Analysis. Analyses were made using an accelerating voltage of 15 kV, a sample current of 3 nA, and a beam width of 5 μm.

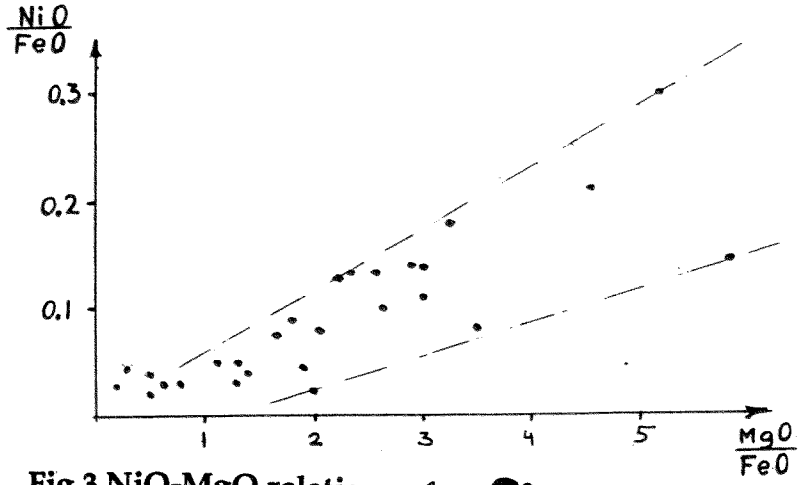

Fig 3 NiO-MgO relations of analyzed chondrites.

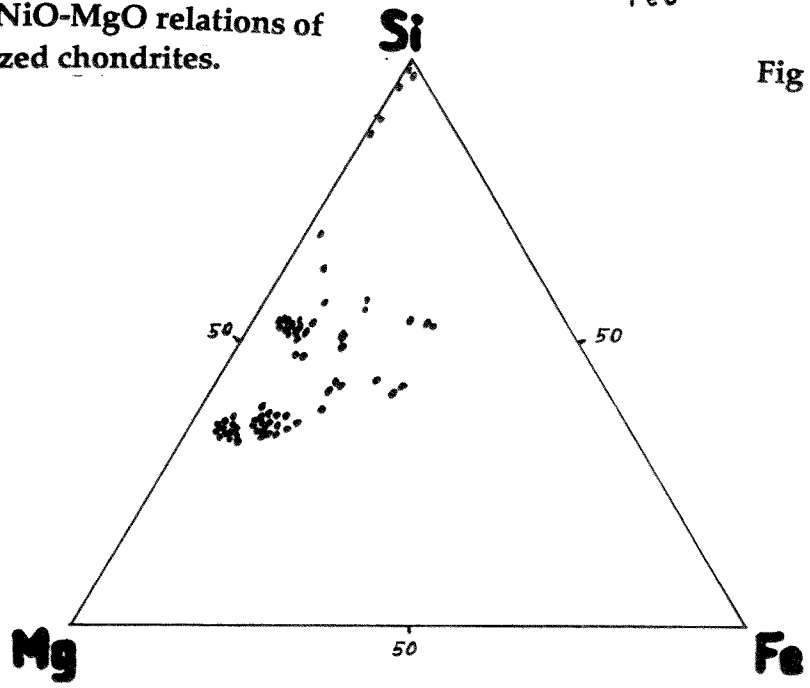

Fig 2 Atomic plotting Si-Fe-Mg for examined ordinary chondrites.

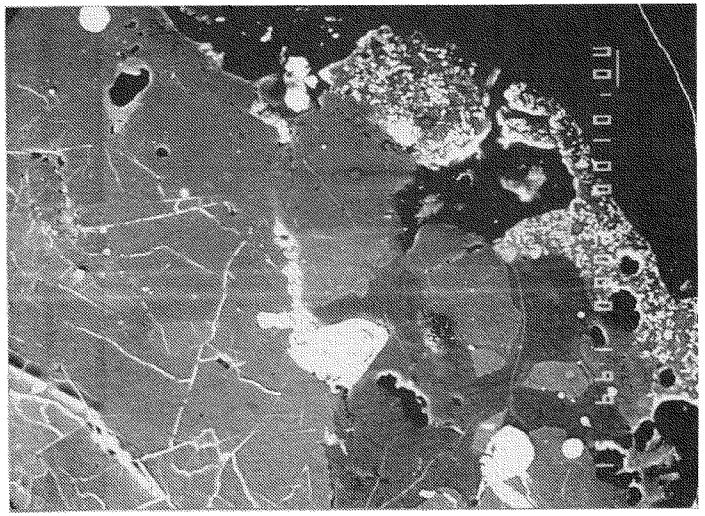

Fig 1 Scanning electron photographds of the fusion crust of:
A.-the Pultusk chondrite

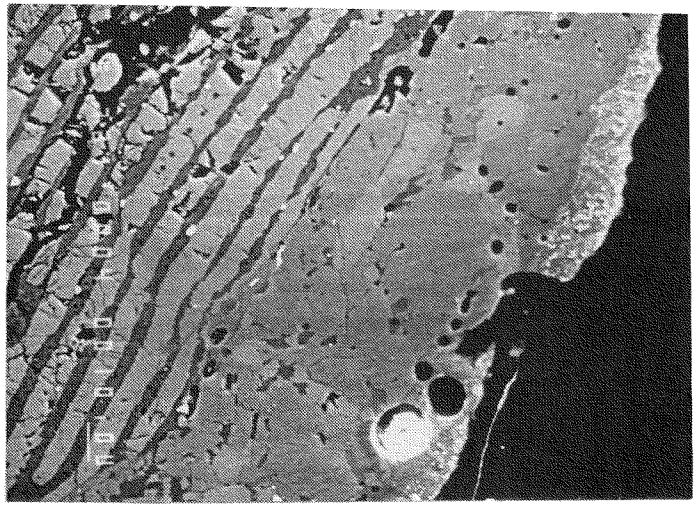

B.-the Pilawa Gorna chondrite

The scanning electron microscope microphotographs of the some meteorites have been shown in figure 1. Three different zones can be seen: (1) A bright zone heavily decorated by iron dendrites, (2) a zone full of bubbles and (3) a smooth glassy zone with bubbles. The presence of the dendrities in first zone is evidence of a rapid cooling process in the melted part of the fusion crust happening after the meteorite fell into the lower atmospheric layers. In the second zone there are numbers of bubbles of different size showing degasing processes being involved below melted and degased surface layer of the fusion crust. Mature large bubbles are opened into the surface. The third zone show glassy structure often with fractures (Fig. 1A) which occur as an effect of the cooling process. Many minerals being amorphed retain their shape and chemical composition in this zone. When a small bubble starts to expand in isolated areas of this layer and when the growing rate is so rapid, it can lead to splitting off the fragments of the fusion crust and spreading them in the atmosphere. Such fragments could be found in deep sea sediments and Antarctic ice sheets.

Representative chemical analyses are presented in triangle diagrams (Fig. 2) and the Ni/Mg correlation (Fig. 3). The results presented in Fig. 2 in general confirmed the differences of meteorite groups and show enrichment in Mg in the surface layer and enrichment of the fusion crust in Fe and Si in comparison to the bulk elements' content. The glass from the upper glassy fusion crust from the surface layer (melted showing dendrites) is depleted of Fe (this element concentrated in dendrire crystals) and enriched with Mg and Ni but lower layer with bubbles and below is enriched with Fe in comparison to the average mineral composition and makes the tail from left to the right direction on the triangle diagrams. In Fig. 3 the simple dependence between Ni and Mg in the glass of the fusion crust in first enriched in these elements and depleted in Fe zone can be seen.

The study of these specific glasses formed in an extremely high thermal gradient and pressure conditions, which can not be recreated in the laboratory, is the focus of our investigations.

References: /1/. Bronstern.V.A. Physics of the Meteorite Behaviour. Nauka, Moscow(1981). /2/. Maurette, M., Jehanno C. Robin E. and Hammer C. (1987) Nature, 328, 699-702. /3/. Maurette, M., Pourchet M., Bonny P., de Angelis M. and Siry P. (1989a) Lunar Planetary Science 20, 644-45. /4/. Maurette, M., Cragin, J., and Taylor, S., (1992) Meteoritics, 27, 257. /5/. Maurette, M., Hammer, C., Immel G., and Pourchet, M. (1992) Meteoritics, 27, 257-8 /6/. Flynn, G.J., Sutton, S.R., and Klöck, W. (1992) 17th Symposium on Antarctic meteorites, August 1992. paper 33 1 - 4 /7/. Beckerling, W., Bischoff, A., and Klock, W. (1992) Meteoritics, 27,200-1.